**Mechanical Reliability of Lead-Free Solder Paste Alloys in Surface Mount Applications with Different Surface Finishes**

By

George Kelly Winstead

A dissertation submitted to the Graduate Faculty of
Auburn University
in partial fulfillment of the
requirements for the Degree of
Doctor of Philosophy

Auburn, Alabama
December 13, 2025

Keywords: Lead-free solder, Fatigue, Shear, Reliability

Copyright 2025 by George Kelly Winstead

Approved by

Sa'd Hamasha, Chair, Associate Professor, Industrial and Systems Engineering
John Evans, Charles D. Miller Endowed Chair Professor, Industrial and Systems Engineering
Jia (Peter) Liu, Assistant Professor, Industrial and Systems Engineering
Michael Bozack, Professor Emeritus, Physics

Abstract

It has been a little more than 23 years since the European Parliament released the lead-free directives that piloted the electronics manufacturing industry to adopt lead-free solder alloys. During this time, there still doesn't exist a clearly identified lead-free solder alloy to replace the eutectic Sn63Pb37. Even the dominate use of SAC305 (Sn-3Ag-0.5Cu) is still being evaluated and tested with different surface finishes while introducing doping elements for various applications where shear, fatigue and creep continue to plague electronic assemblies.

This study takes the approach of utilizing different solder paste alloys in small quantities with SAC305 being used for the final assembly of components. The attempt of this approach is to provide data to support whether the use of a solder paste alloy with additional doping elements (Bi, Ni, and Sb) would improve the mechanical performance over a single SAC305 solder joint. The smaller quantities of the solder paste would provide cost savings over using a more expensive four-element or five-element alloy for all soldering locations for a given product. The study will also consider the effects of two different surface finishes, Organic Solderability Preservative (OSP) and Electroless Nickle Immersion Gold (ENIG).

Four different strain rates will be used to collect ultimate shear strength data while three different cyclic fatigue tests will be used to estimate reliability. These examinations will evaluate three different solder paste alloys with a SAC305 solder sphere on a single SMT mount: 1) SAC305, 2) SAC308-Bi-Ni, and 3) SAC347-Bi-Sb-Ni-x. These solder paste alloys are examined at 4 mil and 5 mil thicknesses over OSP and ENIG surface finishes.

## Artificial Intelligence (AI) Use Disclosure Statement

In the preparation of this dissertation, no Artificial Intelligence (AI) tools were used.

## Acknowledgments

First and foremost, I would like to thank Dr. Saad Hamasha, my advisor and PhD Committee Chair. When I began to consider pursuing a PhD, Auburn University was not a school I was considering due to the long distance from my home. I emailed Dr. Hamasha. He replied and we exchanged a few emails that led to a visit to the campus. During our meeting, Dr. Hamasha walked through his research and found an area that aligned with my interest, assisted in transferring previous graduate classes, and helped to establish a plan to satisfy the residency requirements. The way I saw it, he cared and that made the decision easy. I also want to thank all my PhD Committee members: Dr. John Evans, Co-Advisor, Dr. Jia (Peter) Liu, and Dr. Michael Bozack. A final Thank You to Dr. George Flowers for stepping in to be the University Reader. I sincerely thank you all. I also appreciate all the professors I have encountered while taking their classes at Auburn. Some I developed a solid relationship with whom have been very helpful in this endeavor: Dr. Tom Devall and Dr. Richard Sesek.

In thinking about all the people that I need to acknowledge in achieving this incredible honor, I realized that it extends far past those at Auburn. I would like to deeply thank the following people for educating me and contributing to whom I have become:

- Dr. Gary Langford (Naval Postgraduate School)
- Dr. David Jenn (Naval Postgraduate School)
- Dr. Michael Pecht (University of Maryland)
- Dr. Clement Kleinstreuer (North Carolina State University)
- Dr. Rich Gould (North Carolina State University)
- All my high school teachers at Southern Nash High School in Bailey, NC

This list is not all inclusive. There are so many others. So, to all those that have contributed to my education, from first grade on, my sincere and humble thank you. I hope that I have made you proud.

Table of Contents

List of Tables

List of Figures

List of Abbreviations

| | |
|---|---|
| °C | degrees Celsius |
| °F | degrees Fahrenheit |
| Ag | Silver |
| Al | aluminum |
| $Al_2O_3$ | alumina |
| AlN | aluminum nitride |
| ANOVA | analysis of variance |
| Au | gold |
| BGA | ball grid array |
| Bi | bismuth |
| CABGA | chip array ball grid array |
| Cd | cadmium |
| CTE | coefficient of thermal expansion |
| Cu | copper |
| DSC | differential scanning calorimetry |
| ENIG | electroless nickel/immersion gold |
| EPA | (U.S.) Environmental Protection Agency |
| Fe | iron |
| FE | finite element |
| FEA | finite element analysis |
| Ga | gallium |
| HASL | hot air solder leveling |

| | |
|---|---|
| HMC | hybrid microcircuit |
| In | indium |
| IMC | intermetallic compounds |
| IPC | *formerly* Institute for Interconnecting and Packaging Electronic Circuits |
| JEITA | Japan Electronics and Information Technology Industries Association |
| MLB | multilayer board |
| Mo | molybdenum |
| MTBF | mean time between failure |
| MTTF | mean time to failure |
| NEMA | (U.S.) National Electrical Manufacturers Association |
| Ni | nickel |
| NSMD | non-solder mask defined |
| OSP | organic solderability preservative |
| Pb | lead |
| PCB | printed circuit board |
| Pd | palladium |
| PET | polyethlylene terephthalate |
| ppm | parts per million |
| psi | pounds per square inch |
| Pt | Platinum |
| RoHS | Restriction of Hazardous Substances (short for Directive on the restriction of the use of certain hazardous substances in electrical and electronic equipment) |

| | |
|---|---|
| SAC305 | Sn-3.0Ag-0.5Cu |
| SAC (Sn-Ag-Cu) | silver-aluminum-copper |
| Sb | antimony |
| SMT | surface mount technology |
| Sb | antimony |
| $Sb_2O_3$ | antimony trioxide |
| SMIC | Senju Metal Industry Company |
| SMD | solder mask defined |
| Sn | tin |
| Sn-Pb | tin-lead |
| Sn63-Pb37 | tin (63%) – lead (37%) |
| SPI | solder paste inspection |
| $S_y$ | yield strength |
| $S_{y,0.2\%}$ | 0.2% offset yield strength |
| $S_u$ | ultimate strength |
| $T_d$ | decomposition temperature |
| $T_g$ | glass transition temperature |
| THT | through-hole technology |
| TMA | thermomechanical analyzer |
| WEEE | Waste electrical and electronic equipment |
| W/m·K | (watt/meter·Kelvin) unit of thermal conductivity |
| USS | Ultimate shear strength |

# Chapter 1 Introduction

## 1.1 Solder Technologies

Evolving trends in the development of electronics are constantly forcing technological advancements in the application of solder. The increase in the miniaturization of electronic assemblies, the increase in lead-free solder legislation and the harsher operational environments continue to add to design complexity. Manufacturing processes are also continuously being improved to satisfy these trends. Developing new solder alloys and bonding materials while enhancing assembly applications and soldering processes are just a few of the electronic technologies focused on solder and its application [1].

Solder is used to bond electrical component's leads (or pins) to printed circuit board (PCB)'s pads. Solder also provides mechanical strength for component assembly while simultaneously conducting electricity needed to complete each circuit [2]. Solder is constructed as a fusible metal alloy, and as with the nature of alloys, it doesn't have a single melting point. Solder must be heated to its liquidus temperature to be fully melted [3]. The liquidus temperature must be compatible with the materials of the mating parts to be soldered. The solder must flow to form a smooth and uniform coating between the component leads and surface pads. Once cooled, the solder joint must conduct electricity between mating parts and provide mechanical reliability in support of the final product's intended operational environment. The end-use environment may subject the solder joints to vibration, shock, humidity, and thermal cycling. With increasing utilization of lead-free solder, the solder industry offers a wide selection of solder alloys composed of three, four, five or more materials. Even though Sn-3Ag-0.5Cu (SAC305) is the leading lead-free choice, there is yet to exist an agreement on which lead-free solder alloy will be preeminently identified [2].

To help facilitate the flow and solidification of solder, solder flux and paste are used to promote the adhesion of solder to the mating components to be assembled. Oxidation occurs in all metals when in the presence of air. The oxides that develop on the solder, on the PCB pad, or both prevent the solder from flowing uninformedly between the joint. Flux is used to dissolve or disrupt these oxides to promote optimal bonding of the solder to the mating electrical components. Fluxes are formulated to work with the metals being joined at the processing temperature of the solder. Fluxes are composed of organic material, generally water soluble or acid core [4]. Solder paste is merely a mixture of solder powder, flux, and other material. Unlike using flux alone, solder paste creates a metallurgical bond to the applied surface [3].

Electrical components are assembled to a PCB via two leading process categories [5]:

1) Through-hole technology (THT); and
2) Surface mount technology (SMT)

THT describes the assembly of electrical components where the component's leads are inserted through holes on the PCB and solder is applied to secure it in place as shown in Fig. 1.1 [5].

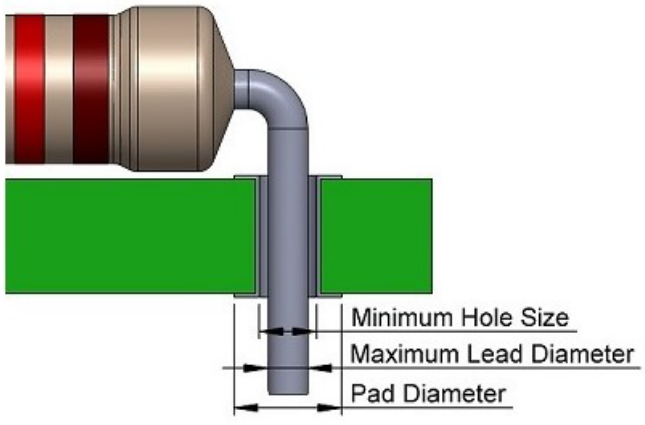


Fig. 1-1: Cross-section view of through-hole mount application.
Adapted from [6].

Through-hole mounting for PCB assembly has been around since the 1920s. It is still a prevalent assembly process because come components (i.e., high power components, connector plugs, switches) require the added strength of the leads soldered into a through-hole. It is also a very cost-effective approach when the production volume is low, and assembly can be done manually. One of the drawbacks of this assembly process is the low assembly densities that hinder miniaturization [5].

SMT depicts components that are soldered to pads built into the PCB as shown in Fig. 1.2 [5].

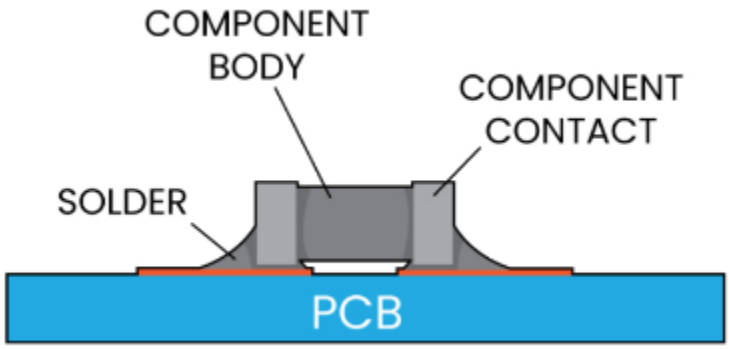


Fig. 1-2: Cross-section view of surface mount application.
Adapted from [7].

SMT started in the 1960s on ceramic substrates and the technology was adapted to accommodate laminate substrates in the 1980s. SMT was developed to assemble hybrid microcircuits (HMC) because of the difficulties in mounting extremely small components using through-hole mount technology. This makes SMT more suitable for miniaturization due to the reduction in size and height of the electrical components, which also contributes to reduced trace widths on the PCB [5].

The soldering process includes not only the processes of applying the solder but also the processes of applying a flux or solder paste. There are several ways for flux to be applied to a PCB. For SMT applications, solder paste is generally used. For THT applications, flux is applied as a mist to the

secondary (non-component) side of the board. For hand-soldering, the flux is integral to the solder wire and is applied during the soldering process [4]. Solder paste is primarily applied to SMT applications by screen printing or stencil printing. Applying the solder paste is the same for both processes with the difference being whether a screen or stencil is used as shown in Fig. 1.3 [8].

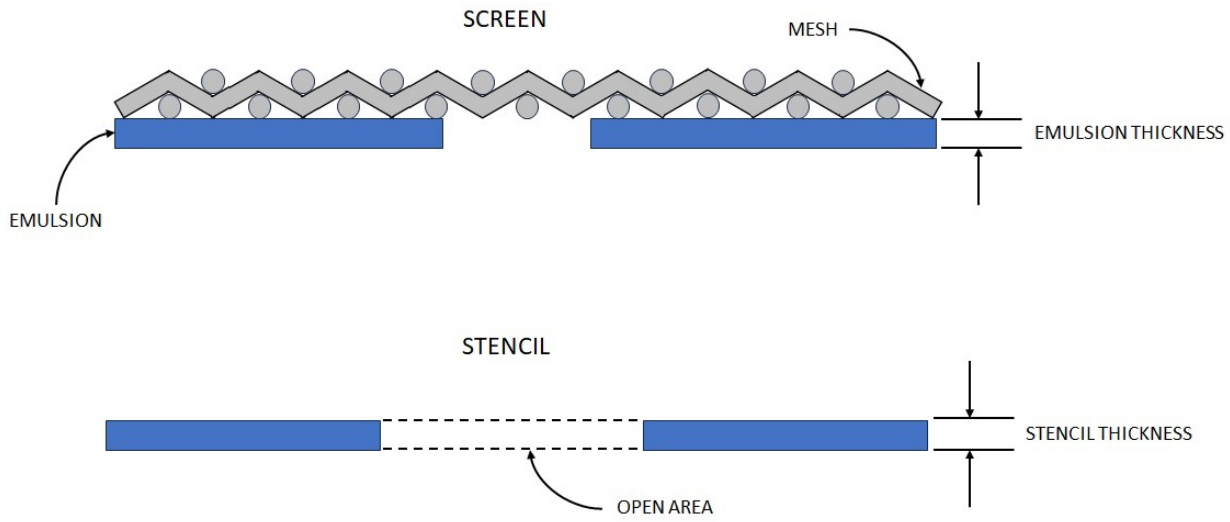


Fig. 1-3: Cross-sections of stencils and screens for solder paste printing.
Adapted from [8].

The solder paste is squeegeed across the face of the screen or stencil and forced into the desired position on the PCB [8].

The application of solder is accomplished in two ways: mass soldering; and directed-energy bonding. Mass soldering or flow (or reflow) techniques are characteristic of mass production volumes. The PCB is heated, and the entire populated circuit board is soldered concurrently. Oven reflow soldering and wave soldering are the most found production methods. Oven reflow is used extensively for SMT assemblies while wave soldering is used for SMT, THT and mixed assemblies [9].

## 1.2 Mechanical Properties of Solder

The mechanics of a material illustrate how it will behave in a particular temperature environment and how it will respond when subjected to loads. One of the ways to express load behavior is in terms of strain and stress depicted using a stress-strain curve as shown in Fig. 1.4 [10].

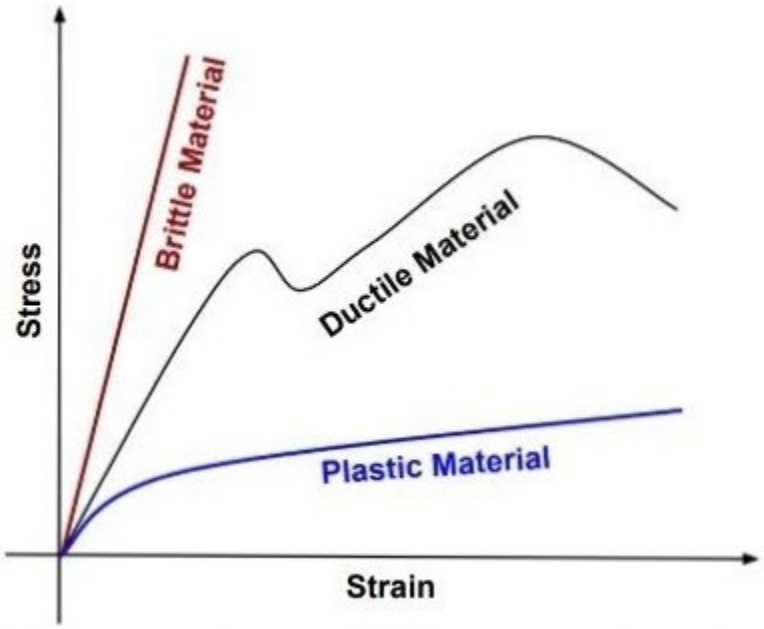


Fig. 1-4: Stress-strain curves.
Source: [11].

The stress-strain relationship of the solder material helps to determine the shear and pull strengths for a given solder joint [12].

A ductile material, such as low-carbon steel, is characterized by the stress-strain curve shown in Fig. 1.5 [13].

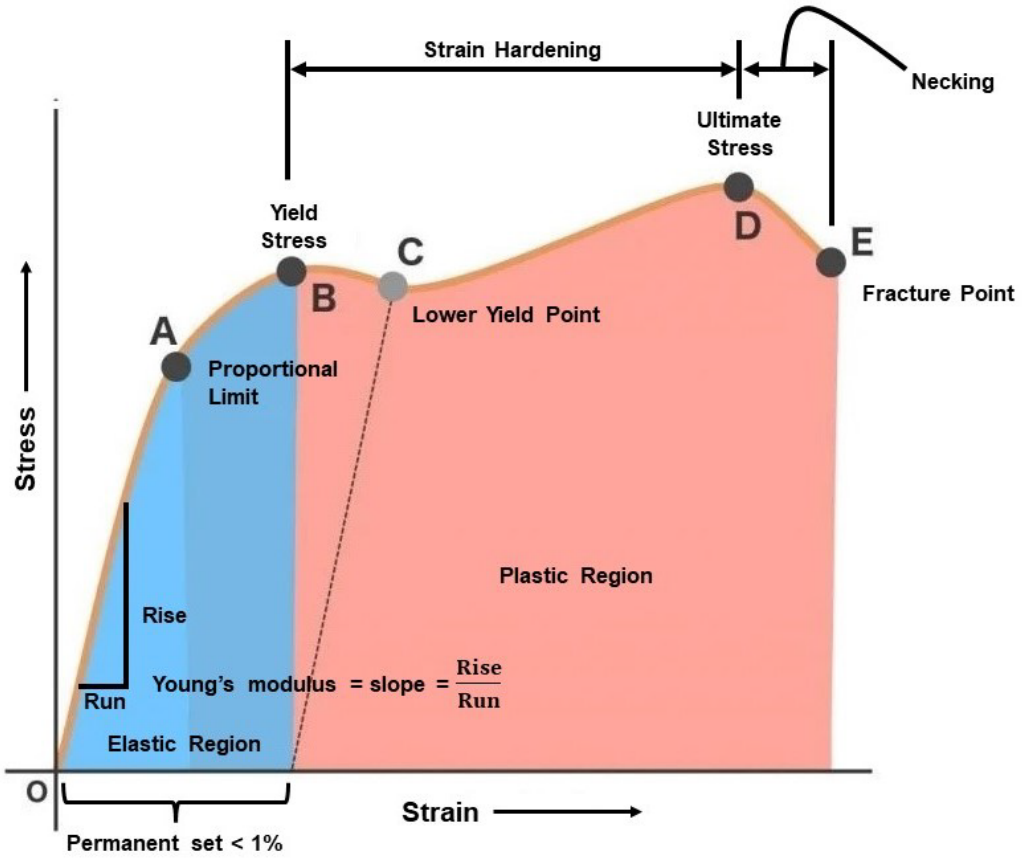


Fig. 1-5: Stress-strain curve of low-carbon steel.
Adapted from [14].

In the blue region, ductile material will have an elastic behavior. The curve will initially be linear, such that stress is proportionate to the strain until it reaches the proportional limit. As the load is increased, the stress curve flattens as it reaches the (upper) yield point. This point is considered the elastic limit. Following the yield point is a sudden drop in a material's load carrying ability to the lower yield point as the material enters the pink region known as the plastic region. This is the region where the material breaks down, and permanent deformation occurs. From this point the curve starts rising constantly until it flattens as it reaches the ultimate stress point. This part of the plastic region refers to the material experiencing strain hardening which refers to the material elongating as its cross-sectional area decreases. Beyond the ultimate

stress point, the material begins to have localized reduction in the cross-sectional area. This is due to slip planes forming in the material and the literal strains created are caused by shear stress [13].

Other metals or elements like low-carbon steel such as nickel and molybdenum exhibit the same type of stress-strain relationship. But as the physical ductility of a material increases, the yield point is not as distinct. For those ductile materials, it is procedural to define a yield strength using the offset method. A 0.2% strain (0.002 in./in.) is customarily chosen for this point as shown in Fig. 1.6 [13].

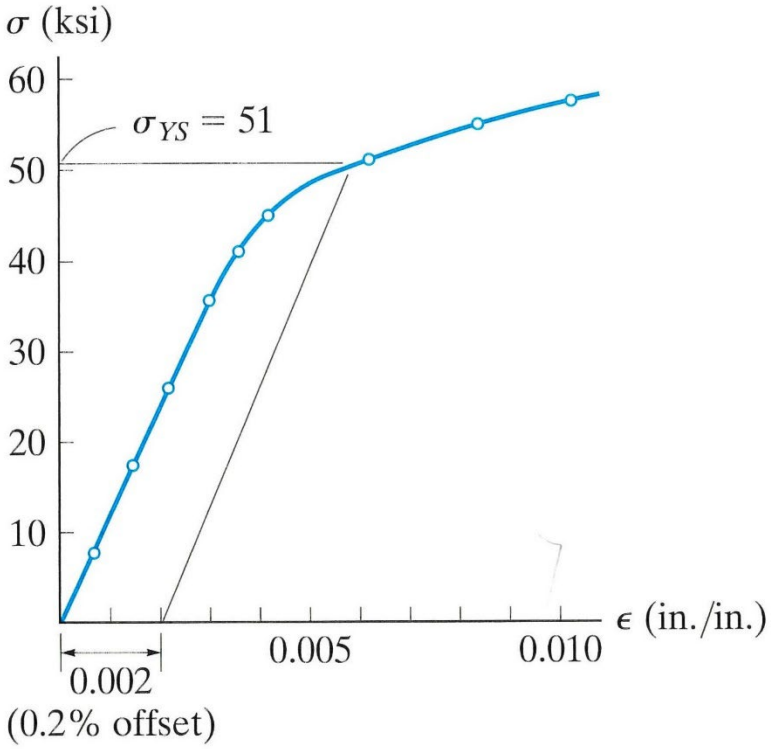


Fig. 1-6: Yield strength for an aluminum alloy.
Source: [13].

Tin-lead and SAC solder alloys are composed mainly of tin (Sn), lead (Pb), silver (Ag) and copper (Cu) [15]. These elements are considered as, if not more, ductile than aluminum as shown in Table I [16].

TABLE I
PHYSICAL DUCTILITY
ADAPTED FROM [17], [16].

| Element | Symbol | Poisson's ratio | Physical Ductility |
|---|---|---|---|
| Perfect Ductility | - | 0.5 | 1 |
| Gold | Au | 0.44 | 0.93 |
| Lead | Pb | 0.44 | 0.93 |
| Silver | Ag | 0.37 | 0.73 |
| Tin | Sn | 0.36 | 0.69 |
| Aluminum | Al | 0.35 | 0.65 |
| Copper | Cu | 0.34 | 0.62 |
| Molybdenum | Mo | 0.32 | |
| Nickel | Ni | 0.31 | 0.50 |
| Iron (low-carbon steel) | Fe | 0.29 | 0.43 |
| Bismuth | Bi | as low as -0.1; as high as 0.8 | (brittle) |
| Antimony | Sb | as low as -0.1; as high as 0.8 | (brittle) |
| Perfect Brittleness | - | 0 | 0 |

Bismuth (Bi) and antimony (Sb) are very anisotropic meaning that the material properties are dependent on the direction of the stress applied. Due to this behavior, the Poisson's ratio used to calculate physical ductility can exceed 0.5 but equally be negative depending on direction. This

generally renders the material to be considered brittle [16]. Bismuth and antimony are added to Sn-Ag-Cu (SAC) solder alloys to improve reliability but in very small quantities (<1%) [15].

A stress-strain relationship like that of aluminum or any material with a greater physical ductility is considered to exhibit elastic-plastic behavior. As the load is increased on a material of this nature, localized stresses will rapidly increase to the elastic limit before the bulk of the material. Increasing the load past the elastic limit will initiate plastic behavior in these localized areas which results in the shape of the stress-strain distribution exhibited by aluminum [18]. Tamin and Shaffiar show that SAC material does indeed exhibit the same stress-strain relationship characteristic of an elastic-plastic material as shown in Fig. 1.7 [10].

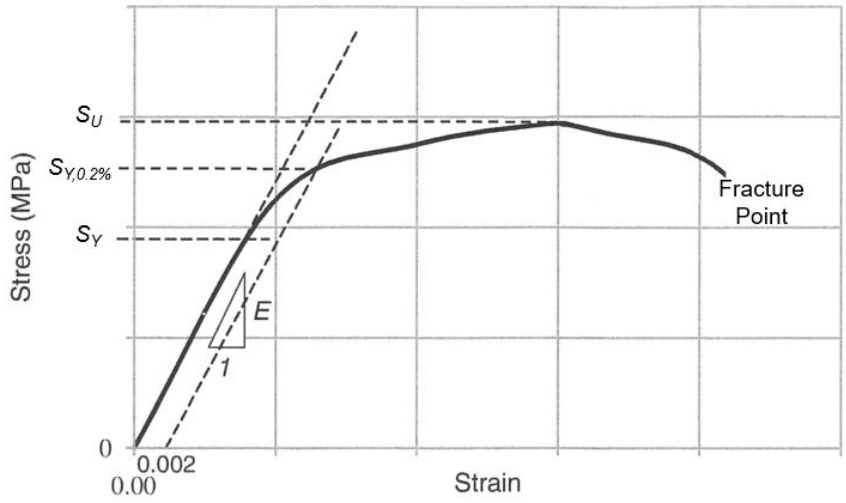


Fig. 1-7: Typical Sn-Ag-Cu solder alloy stress-strain curve.
Adapted from [10].

For the most part, SAC solder behaves as an isotropic, homogenous material. The yield strength for this curve, $S_Y$, is obtained from the data. It is determined at the point when the stress-strain relationship deviates from being linear. The 0.2 % offset yield strength, $S_{Y,0.2\%}$, is identified as typical for an elastic-plastic material. However, when modeling this type of curve for finite

element (FE) analysis, the 0.2 % offset yield strength is not used [10]. The ultimate strength, $S_U$, is the maximum stress obtained from the data. During the necking portion of the stress-strain relationship, the fracture point is considered the point at which the stress reduces to 70% of the ultimate strength if fracture has not occurred before that point.

Temperature, specifically the melting point, is another key mechanical parameter. A proper metallurgical bond is needed between the solder and the leads of the component to be assembled. Applying a good metallurgical bond requires understanding of the phase diagram of the alloys comprising the solder. The metallurgical phase diagrams show the limits of each metal dissolving into the others and the melting points depending on the composition of the alloy. An example of a binary, phase diagram of elements A and B is shown in Fig. 1.8 [8].

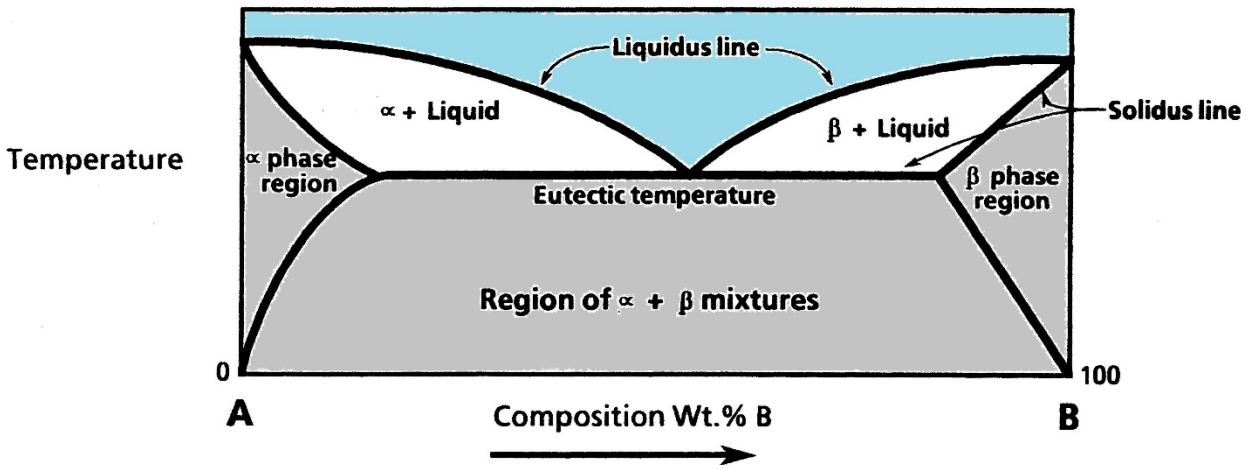


Fig. 1-8: Example of a binary eutectic system of elements A and B.
Adapted from [8].

At point A, the solder composition is entirely element A. At point B, the solder composition is entirely element B. The solid lines capture the equilibrium between the solid and liquid phases of the alloy. The light blue area above the liquidus line indicates the allow is completely a liquid. The light gray area below the solidus line indicates the allow is completely a solid. The light gray

area also depicts the solubility of each element into the other at varying temperatures. For this particular allow composition, it exhibits an eutectic temperature point. The eutectic temperature point represents a specific combination of each element that renders an exact melting point where the alloy transitions from solid to liguid. The eutectic melting point is lower than the individual melting points of either element A or B. If element A is changed to be lead (Pb) and element B is changed to be tin (Sn), the phase diagram can be updated to show melting temperatures at 0% composition of B, 100% composition of B and the eutectic temperature. The melting point of pure lead is 327 °C and the melting temperature of tin is 231 °C. The eutectic combination for this binary alloy is 63 % tin and 37 % lead. The eutectic melting point of this combination is 183 °C (361 °F) [8]. The phase diagram can be updated to show the specific attributes for a tin-lead (Sn-Pb) alloy as shown in Fig. 1.9 [8].

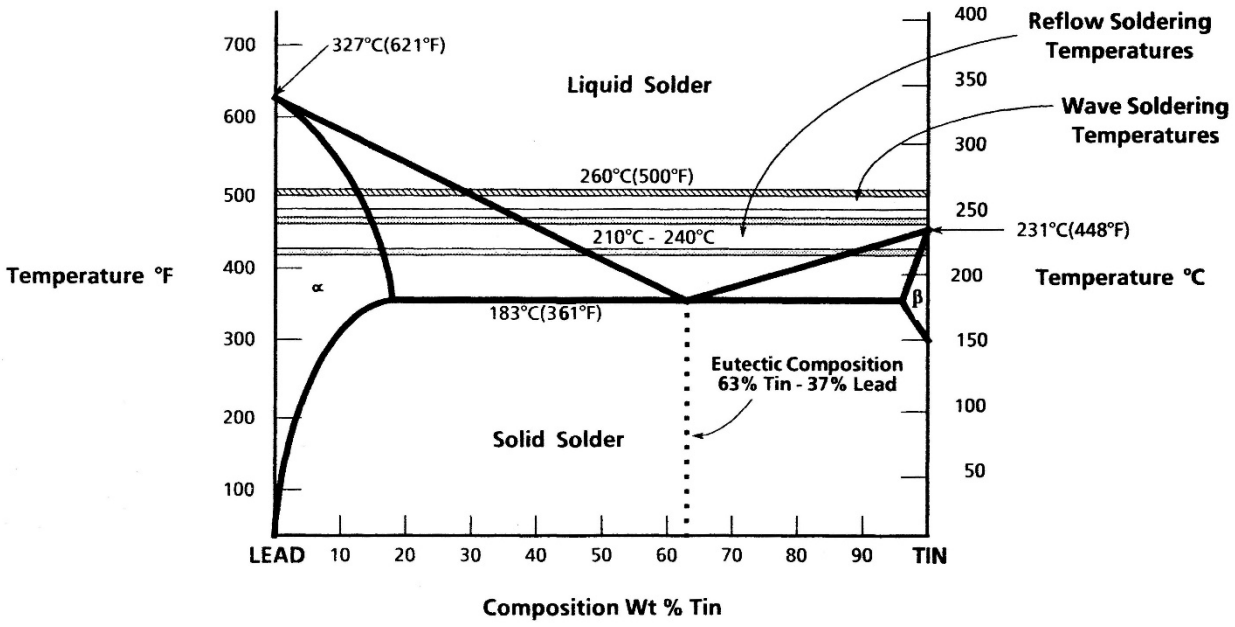


Fig. 1-9: The tin-lead phase diagram.
Source: [8].

The Sn-Pb phase diagram clearly shows how the melting point of a particular combination of each element of a binary allows effects the operational temperatures of reflow soldering and wave soldering processes. The general industry guidelines for reflow soldering temperatures are around 30 to 50 °C above the melting point while wave soldering temperatures are around 35 to 70 °C. The reason for these elevated temperatures is to ensure the solder has a low viscosity with the right amount of flow characteristics to promote recirculation of the solder in the solder pot. For noneutectic solder, the reflow soldering and wave soldering temperatures would need to be elevated above the liquidus temperature line for a given composition. Establishing reflow and wave soldering temperature parameters applies to lead-free solder alloys and solder alloys comprised of three or more elements that may or may not exhibit a eutectic temperature point [8].

### 1.3 Reliability of Lead-Free Solder Joints

In 2006, two directives issued by the European Parliament become effective. Those directives targeted to restrict the use of lead; as well as other substances deemed hazardous, in electrical and electronic equipment [19]:

1) Directive 2002/95/EC – on the restriction of the use of certain hazardous substances (RoHS) in electrical and electronic equipment; and
2) Directive 2002/96/EC – on waste electrical and electronic equipment (WEEE)

In Japan, the Home Appliance Recycling Law of 2001 requires the recycling of lead found in home products. Considering this law, many Japanese companies adopted practices to remove lead solder from each home product's as well as commercial product's design. In doing so, most Japanese companies have selected from a wide range of lead-free solder alloys as suitable replacement [3].

The Japanese law does not cover a broad range of products as identified in the WEEE Directive. The recycling goals are lower than the WEEE Directive and they do not expand over time. Also, the Home Appliance Recycling Law does not cover other hazardous materials as specified in RoHS Directive. Without the additional regulations, Japanese companies are known to be proactive in addressing concerns for the environment. And as the recycling law ages, it will expand to include other products and recycling goals [20].

A few lead laws and regulations have been passed in the United States over the last few decades. The laws focus on lead in household paints, lead in the environment, and lead in disposed waste. However, solder material containing lead is not treated as hazardous if recycled. In addition, products with less than 3% by weight are deemed lead-free and are not considered as hazardous [3]. The U.S. Environmental Protection Agency (EPA) has included lead as one of 17 chemicals that are hazardous. The Institute for Interconnecting and Packaging Electronic Circuits (IPC) has developed a process for transitioning from lead-based solder to lead-free in hopes of encouraging the use. But still, the United States has yet to specifically ban the use of lead solder in electronics [21].

In 1997, Prasad lists various products produced that utilize lead as part of the construction or assembly as shown in Table II [8].

TABLE II
LEAD CONSUMPTION BY PRODUCT
ADAPTED FROM [8].

| PRODUCT | CONSUMPTION (%) |
|---|---|
| Storage batteries | 80.81 |
| Other oxides (paint, glass and ceramic products, pigments, and chemicals) | 4.78 |
| Ammunition | 4.69 |

| PRODUCT | CONSUMPTION (%) |
|---|---|
| Sheet lead | 1.79 |
| Cable covering | 1.40 |
| Casting metals | 1.13 |
| Brass and bronze billets and ingots | 0.72 |
| Pipes, traps, other extruded products | 0.72 |
| Solder (excluding electronic solder) | 0.70 |
| Electronic solder | 0.49 |
| Miscellaneous | 2.77 |

Electronics only utilize 0.5% of the total lead available for product production. That number by itself would seem insignificant [8]. The U.S. Environmental Protection Agency projected as of 2005, approximately 130 million cell phones in the United States alone would be replaced yearly with a newer model. INFORM, Inc. estimated in addition to those cellphones retiring, there are 500 million cell phones lying unused around homes awaiting to be disposed. Of the millions of cellphones that are being replaced and not being used, less than 1% of those are recycled [22]. If those numbers are updated for 2024 and accounting for all electronics and not just cell phones, it becomes clear that the 0.5% can indeed be significant, which is contributing to continued legislation from governments to eliminate the use of lead solder in product design.

Up until the efforts to eliminate and restrict the use of lead in electronics, Sn-Pb based solder had a long, reliable history in the production of electronics. Introducing a new lead-free solder alloy didn’t change the assembly processes as much as it forced a reassessment of the production parameters surrounding those processes. There are two main considerations driving the establishment of new process parameters when using a lead-free solder. First, lead-free solder has

a much higher melting temperature. Second, lead-free solder has poor solderability when compared to established lead-based solder [5].

Intrinsic mechanical properties of each solder alloy contribute to the reliability of a solder joint, but it also relies heavily on the interface between the mount and component, the process of applying the solder connection and the service life conditions. Solder exhibits more complex behavior due to changes in temperature, time, and stress than the classic materials covered in strength of materials. For a given solder alloy and mounting application, the main factors contributing to the reliability of the solder joint are temperature, surface conditions of the mount, stress range, strain rate and inherent microscopic structure [3]. According to Hwang, the mechanical properties of a solder joint may not be the same as that of a bulk equivalent primarily for two reasons [3]:

1) During solidification, a high quantity of dissimilar nucleation sites would form in the presence of an extreme ratio of substrate's pad surface to the volume of solder; and
2) The formation of intermetallic compounds (IMC) when the solder reacts with the substrate's pad material.

## 1.4 Problem Statement

In 2019, roughly 70% of electronic devices malfunctioned due to defects introduced during the design and production processes with solder joint failures being the leading cause [23]. This issue is still prevalent today because the integrity of a lead-free solder joint is not solely dependent on the intrinsic properties of the solder alone. There are several properties or parameters that contribute to a solder joint's integrity [3]:

- Suitability of the mechanical properties of the solder alloy

- Compatibility of the substrate's pad with the solder alloy/paste
- Acceptable wetting of mating surfaces
- Form, fit, and function of the joint design
- Application method of applying the solder to the joint
- Internal stresses due to anisotropic behavior of alloy elements
- Formation of IMCs

But even if the reliability of a solder joint could be solely dependent on the mechanical properties of a particular solder alloy, which one would be chosen? SAC305 is the most popular choice primarily due to cost [24]. But, the IPC standard J-STD-006C, Requirements for Electronic Grade Solder Alloy and Fluxed and Non-Fluxed Solid Solders for Electronic Soldering Applications, list an additional 31 lead-free solder alloys frequently used by industry [25], [26]. This does not include the additional number of proprietary solder alloys that industry releases yearly in hopes of developing an alloy that helps to alleviate current solder joint reliability issues. To supplement the challenge of selecting a solder alloy, consideration must also be given to the use and application of solder flux and paste.

Cost is another driver in selecting a lead-free solder alloy. The cost varies by three main factors: 1) the number of elements comprising the alloy; 2) the quality of the alloy; and 3) the process by which the solder is applied. The material used to comprise a lead-free solder alloy are priced according to the market price of each element which can fluctuate and solder alloys containing a higher amount of silver will be more expensive. Higher quality lead-free solder alloys will be more expensive while lower quality equivalents will contain more impurities. Some lead-free solder alloys contain specific alloys to enhance performance which increase the cost. The more intricate the manufacturing processes to apply solder increases cost. How the raw material solder

is received can cost more. For example, solder purchased as a wire as opposed to paste will be more expensive. For wire, lead-free solders, as the diameter increases so does the cost [27].

Once the solder joint is assembled, it begins to age. Immediately, time, temperature and mechanical loading start reducing the solder joint's integrity. Thermal cycling can be caused by natural or induced environments including the cycling of power. This causes expansion and contraction of the solder joints which leads to crack formation that eventually results in open circuit situations. Shock to a product during transportation or mishandling can create mechanical loading situations that induce shear stress on solder joints. Normal and abnormal mechanical loading conditions that are cyclic can induce fatigue stress while cyclic temperature conditions induce creep [28].

The problem is not an absence of research or data of multiple combinations of lead-free solder alloys, solder fluxes, PCB's pad surface finishes and the processes used to construct the assembly. The research thus far identifies very similar issues and conditions distinctive to a lead-free solder joint. However, the research also demonstrates that the mechanical strength and reliability can vary significantly even when the same solder alloy is used across multiple solder joint assemblies. The use of design assessment tools, such as finite element analysis (FEA), are important in estimating reliability. The data currently available for determining the characteristics of lead-free solder joints needed in making reliability predictions is not extensive enough to be used to validate those predictions. Continued research and testing bring about new failure modes which need to be understood. As data is continuingly being generated, it will help to refine existing modeling and simulation models to improve reliability estimations of lead-free solder joints [28].

## 1.5 Research Objectives

The purpose of this research is to add to the data of lead-free solder joint testing. The testing performed by this research will add to the understanding of the mechanical behavior of lead-free solder joints. The additional data should help to design better formulas and models to predict lead-free solder joint reliability more accurately. The following objectives will be achieved in this research:

1) Create test cases to appropriately test solder joints under several mechanical loading situations for reliability predictions;
2) Assess mechanical properties of SAC305, solder joints using different solder paste alloys under as-assembled conditions;
3) Examine the effects of solder past volume on the shear properties of SAC305, solder joints under as-assembled conditions;
4) Determine the effects of different substrate's pad surface finishes on the mechanical properties of SAC305, solder joints with different solder paste under various strain rates and cycles;
5) Contribute to refining reliability models for predicting the fatigue life of SAC305 solder joints used in normal operating environments.

## 1.6 Proposed Dissertation Organization

Eight chapters comprise this dissertation. An introduction to the research identifying the problem statement and research objectives is covered in Chapter 1. Chapter 2 goes into detail about the SMT solder joint and the assembly characteristics of SMT solder joints. Research previously conducted on similar test articles under similar test conditions will be discussed in

Chapter 3 to anticipate results that would be forthcoming. Chapter 4 will identify the procedures of the experiment, the assembly of the test articles, the equipment used, and the test to be conducted. Chapter 5 presents the effect that different solder paste alloys and different volumes of solder paste alloys have on the shear properties of a SAC305 solder joint. Next, the effect that different solder paste alloys have on the fatigue properties of a SAC305 solder joint are given in Chapter 6. Chapter 7 will provide the effect that substrate's pad surface finish has on the shear and fatigue properties of different solder paste alloys of a SAC305 solder joint. Finally, Chapter 8 will provide a summary of results and identify continued areas of research to be conducted by others.

## Chapter 2 Surface Mount Technology and Reliability Testing

Today, surface mount technology (SMT) is the most widely used system for designing the assembly of PCBs. The key attribute is that all connections between the PCB and the components are a simple overlap joint to PCBs' pads. There are advantages and disadvantages to this style of PCB. One advantage is that trace spacing on the opposite side of the PCB is not limited due to not having through-holes needed for through-hole components. Another advantage is the SMT approach accommodates smaller components which leads to PCB being denser in component population. A main disadvantage is that there are no leads to SMT components to support the attachment of instruments or probes for testing purposes. This leads to designing test pads into the PCB to facilitate diagnostic work. Plus, the smaller component sizes make it more difficult to remove heat from the assembly compared to through-hole components [29].

The typical single-sided SMT PCB is the entry level circuit board. Its simple construction renders a low-cost choice for production. The simplicity of its design also lends it to very cost-effective manufacturing processes. The assembly of the SMT PCB is performed in one step of placing the components on the pads and soldering them in place usually be a reflow process. In applications where space consideration is minimal, a double-sided SMT PCB provides an advantage for having both sides being used to manufacture circuits. In this case, the assembly process is simply repeated for the opposite side. A single-sided SMT PCB is constructed of a substrate layered with conductive copper on one side and topped with a solder mask to prevent oxidation and solder bridging between close pads. Solder mask can be applied to the opposite side as well. For a double-sided SMT PCB, the opposite side of the substrate also gets a layer of copper beneath the solder mask [29]. Because of the copper layer on both sides, the double-sided PCB is the entry level circuit board for THT. The connection between the two layers of copper is

accomplished by installing vias which are plated, drilled holes in a double-sided PCB [30]. Models of a single-sided and double-sided SMT PCB are shown in Fig. 2-1 [31].

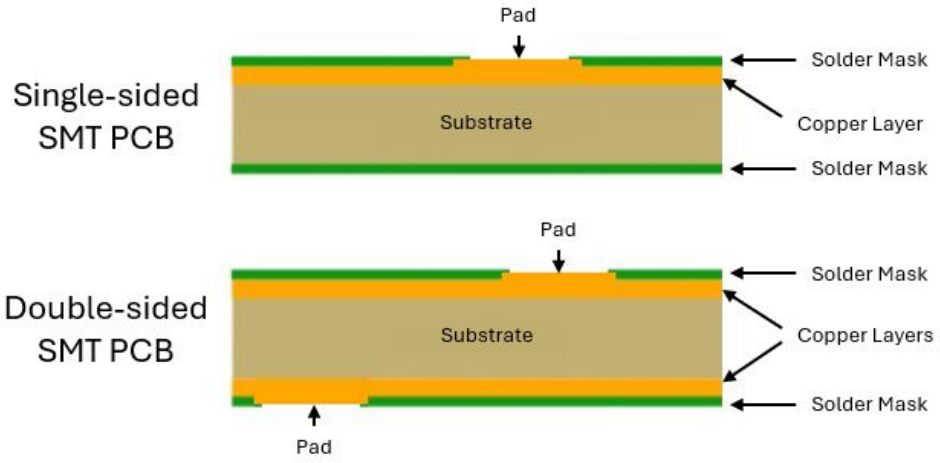


Fig. 2-1: Difference between single-sided and double-sided SMT PCBs. Adapted from [31].

Though, there are generally no holes needed for a SMT PCB assembly, when assembled to a double-sided PCB, through-holes may be added to allow the use of through-hole components. This permits a double-sided PCB to host more complicated circuits. Double-sided PCBs lead to multilayer boards (MLBs). These boards have three or more layers of copper. MLBs can have anywhere from 4 to 16 layers of different circuits. Buried or blind vias are used for layer-to-layer connections that involve connecting to inner layers. Along with the typical laminate substrate, MLBs incorporate a layer or more of prepreg. Pregreg is a fabric soaked in resin that is then rolled press and partially cured in an oven. Pregreg layers are not as structurally rigid as the laminates used for a substrate [30]. A model of a MLB is shown in Fig. 2-2 [32].

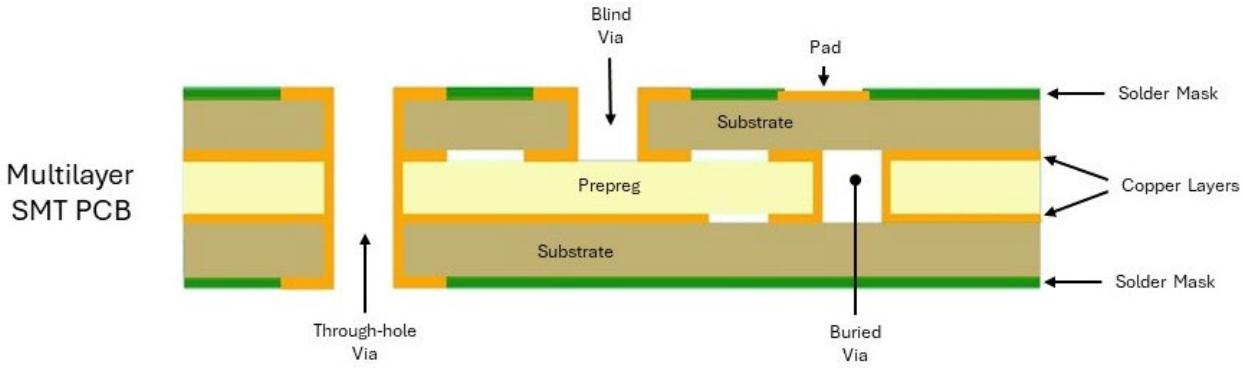


Fig. 2-2: Multilayer SMT PCB.
Adapted from [32].

With introducing through-hole components to SMT PCBs, three different types of double-sized, surface mounting arrangements have been established: 1) Type I; 2) Type II; and 3) Type III. Though these types are not necessarily instituted, they are the ones generally used in SMT designs [8]. Type I SMT assembly is only of SMT components placed on both sides of the PCB as shown in Fig. 2-1 [33].

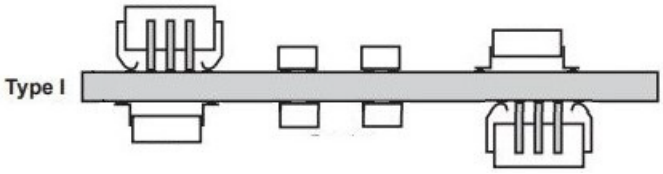


Fig. 2-3: Type I surface mounting.
Adapted from [8].

Type II consist of a mixture of SMT and THT components on the primary side of the PCB while only SMT components are placed on the other side as shown in Fig. 2-2 [33].

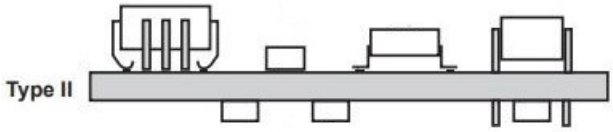


Fig. 2-4: Type II surface mounting.

Adapted from [8].

Type III places only THT components on the primary side of the PCB and only SMT components on the other side as shown in Fig. 2-3 [33].

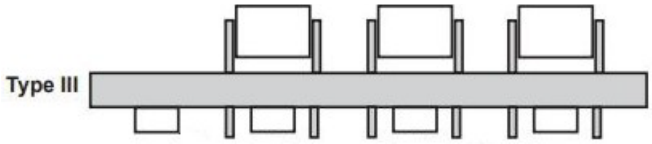


Fig. 2-5: Type III surface mounting.
Adapted from [8].

From single-sided to multilayer PCBs, this type of PCB board is considered a rigid PCB. The substrate is a solid or composite material that does not allow the PCB to bend or twist. A PCB of this type supports assemblies that require a very high level of reliability. Flexible PCBs also exist. Flexible PCBs use plastic such as a polyimide that is very flexible but has a high heat resistance. The PCB components are attached to the copper layer which is then encapsulated by the polymeric material as shown in Fig. 2-6 [34].

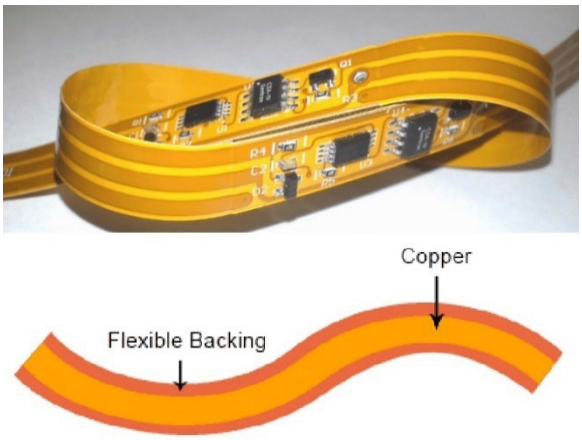


Fig. 2-6: Flexible PCB
Source [34].

## 2.1 Substrate

The supporting structure of the PCB is often referred to as the substrate. It provides the supporting surface for all the other materials used to assemble a PCB. It has a vital role in electrical and mechanical reliability of the PCB. The substrate is defined in two categories: 1) laminate substate, typically used in PCB assemblies; and 2) constraining substrate, selected to match the coefficient of thermal expansion (CTE) to that of the components assembled to it. Before choosing a substrate, it is best to identify the qualities needed by the material that supports the operational environment and the associated cost [8].

The materials used to construct a substrate are vast, which adds complexity to determining which substrate is best suited for the end product. The base material can range from polymeric laminates to ceramics and from supporting planes to constraining cores [8]. With laminates, the complexity increases with the choice of resins and state of cure of those resins. Laminates can also be strengthened with fillers from fiberglass to aramid paper to cotton. Consideration would also need to be given for the conductive foil, plated through-holes and SMT pads. The base material of the substrate is a very crucial part of the PCB due to its interaction with the manufacturing processes. So, not only are the mechanical and electrical performances of the PCB's substrate leading the decision-making process, but a substrate that complements the manufacturing processes is equally important [35].

### 2.1.1 Selecting the Base Material

Selecting the base material for the substrate can be very challenging. The base materials must first withstand the construction processes of the PCB. Following that, the PCB must survive the lead-free assembly processes without incurring defects and maintain the product's established

reliability. There are five parameters used to assess a substrate's ability to endure lead-free assembly processes [36]:

- Glass transition temperature ($T_g$)
- Coefficients of thermal expansion (CTEs)
- Moisture absorption
- Time to delamination
- Decomposition temperature ($T_d$)

Except for ceramic substrates, substrates are predominately constructed with plastics. Plastics, the resin part of the substrate, exhibit structural changes at particular temperatures. The glass transition temperature ($T_g$) is the temperature above which a sturdy and brittle laminate starts to become soft and very ductile and loses a significant measure of its mechanical strength [8]. Though $T_g$ is thought to be a specific temperature, this is not necessarily true. The $T_g$ is greatly affected by the thickness of the resin as well as the degree of the cure. Fully cured resins where all of the reactive sites have cross-linked exhibit higher $T_g$. Because of this relationship, $T_g$ can be used to ascertain the point to which the resin has been cured. The $T_g$ also impacts thermal expansion. The rate at which the resin expands is lower when the temperature is below $T_g$ than when it is above it and the higher $T_g$; the slower the onset of the rate of CTE [35]. Together with CTE, $T_g$ is a laminate property that is traditionally used to determine a suitable, substate material [8].

The coefficients of thermal expansion are the ratios of the change in the X, Y, and Z directions for a given change in temperature. The units of CTE are commonly expressed as ppm/°C. The effects of expansion are not the same in all directions. The changes in the X and Y directions can

be restricted by laminates constructed with glass or cotton fibers. Changes in the Z direction are not constrained but can be locally restricted by plated through-holes as shown in Fig. 2-7 [8].

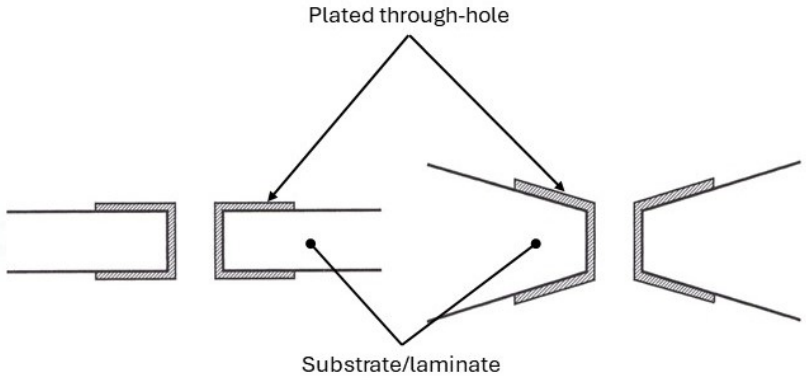


Fig. 2-7: The effects of thermal expansion on substrate in Z direction.
Adapted from [8].

Substrates of pure resin will have a higher CTE compared to composite laminates containing fiberglass or other material used for strengthening [37]. The CTE of a typical, epoxy resin board (FR-4) is nearly 15 ppm/°C. When compared to a ceramic carrier substrate with a CTE of 6 – 7 ppm/°C, the CTE of the epoxy resin board is close to double that its ceramic equivalent. With the CTE of solder falling in the range of 21 – 30 ppm/°C, the difference between the CTE of the substrate and the solder will subject the solder joint to distortion which will lead to failures under cyclic loading [3].

To examine the relationship between CTE and $T_g$ further, the $T_g$ versus CTE curves for three hypothetical resin laminates are plotted in Fig. 2-8 [35].

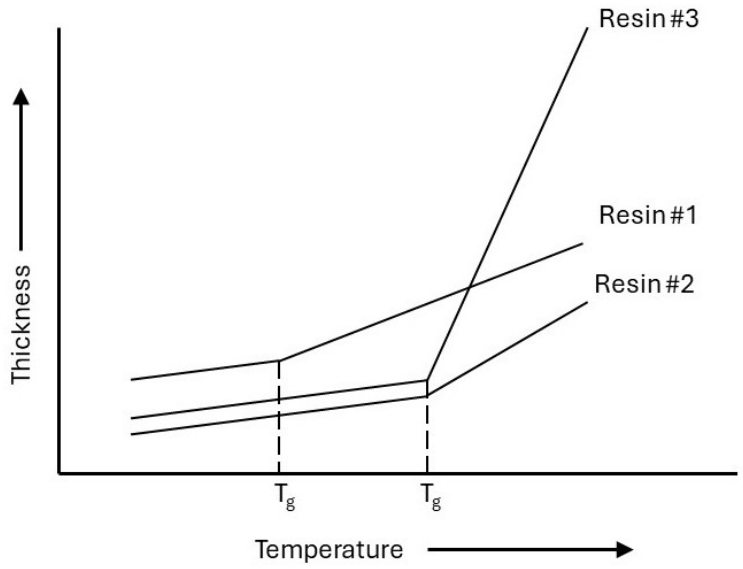


Fig. 2-8: $T_g$ versus thermal expansion for substrates of different resins.
Adapted from [35].

Resin #3 has a higher $T_g$ than Resin #1 but the same CTE. As the temperature is elevated to $T_g$ point of Resin #3, Resin #3 CTE is higher than Resin #1. Resin #1 and Resin #2 have equal CTEs up to Resin #1 $T_g$, but Resin #1 has a lower $T_g$ than Resin #2. From that point, Resin #1 CTE is higher than Resin #2. However, after the temperature passes Resin #2 $T_g$, The CTE of Resin #1 is lower than Resin #2 due to the increased laminate thickness of Resin #1. Lastly, Resin #2 and Resin #3 have equal $T_g$ values, but the rate of CTE after $T_g$ is lower for Resin #2 even though the laminate is thinner. Though there exist general relationships between $T_g$ and CTE, factors such as laminate thickness, resin type, filler material and state of cure can alter the relationship [35].

Moisture absorbed into the substrate during construction can impact PCB reliability during component assembly. The absorbed moisture has an even greater effect on lead-free PCB assemblies. The reason is the vapor pressure resulting from the moisture being exposed to the

temperatures associated with PCB assembly processes. A plot of vapor pressure to temperature is shown in Fig. 2-9 [36].

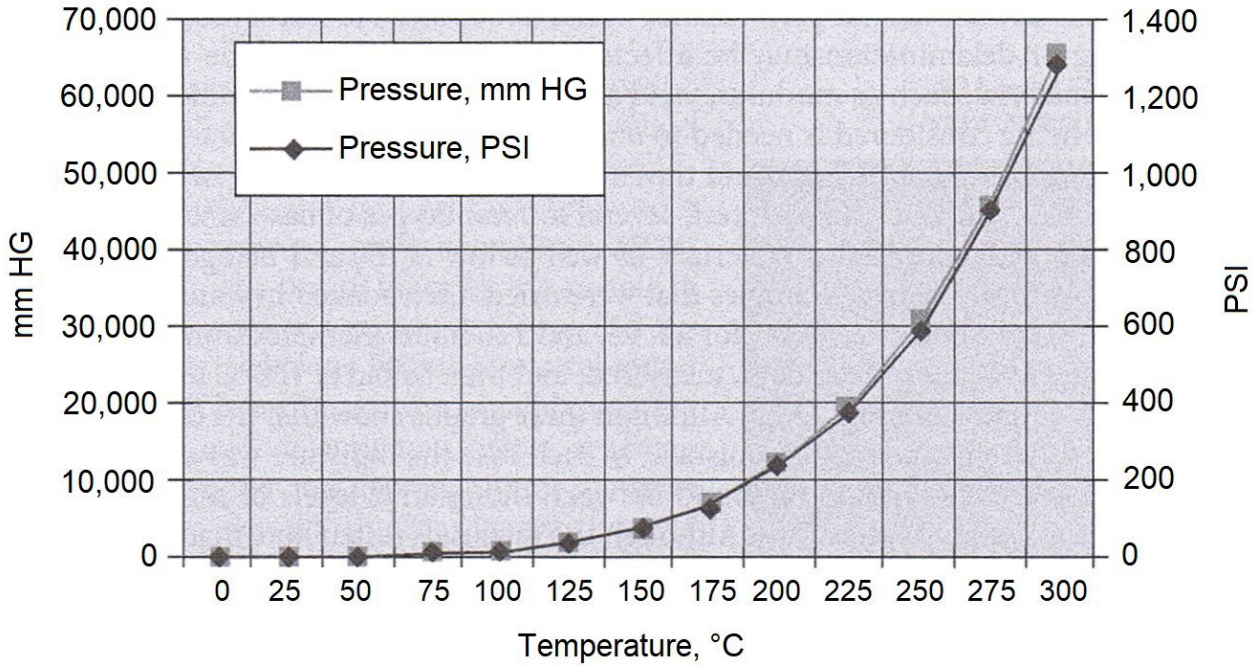


Fig. 2-9: Vapor pressure of water versus temperature.
Adapted from [36].

The water vapor pressure created at the reflow upper limit for lead-free SAC305 (260 °C) is greater than the vapor pressure at the reflow upper limit for Sn63-Pb37 (230 °C) [15] [36]. The vapor pressure at 260 °C is approximately 700 psi while the pressure at 230 °C is close to 400 psi. The greater the vapor pressure, the increased bond stresses between substrate components and the propagation of cracks in the laminate. The storage and fabrication of substrates and the storage and assembly of PCB must be understood to facilitate the proper selection of the base material. If needed, baking or drying steps can be added to the overall fabrication and assembly processes to help remove absorbed moisture [36].

The time to delamination is simply the time it takes a laminate or PCB to delaminate for a given isothermal temperature. Samples are placed in a thermomechanical analyzer (TMA) for testing.

The most familiar temperatures used for testing are 260 °C (T260) and 288 °C (T288) [36]. Delamination marks a prompt increase in laminate thickness when it occurs. Though time to delamination tests have received considerable interest as lead-free assemblies are becoming more prevalent, the relationship between reliability and time to delaminate has not been fully established. T260 and T288 tests independently do not indicate high reliability for those applications of lead-free solder assemblies. In contrast, some laminates that have demonstrated excellent reliability, the time to delamination was average [37].

As a substrate is heated beyond $T_g$ and delamination temperatures, the laminate will reach a point where the resin will decompose. The resin will chemically break down as by-product compounds are released resulting in the laminate weighing less. The decomposition temperature, $T_d$, is the temperature at which this occurs. Industry has defined the $T_d$ as the temperature at which 5 percent of the initial mass of the laminate has been lost. But a question that is commonly asked is if the lead-free assembly process upper temperature is approximately 260 °C and $T_d$ is at or above 300 °C, then why would decomposition of the laminate be a parameter of concern? The reason is that all laminates experience some level of decomposition when subjected to the PCB assembly processes. The onset and gradual decomposition of a laminate occur after $T_g$ and usually results in 1 percent to 3 percent mass loss due to the operational temperatures during PCB assembly. The higher the $T_d$, the less decomposition that will occur to the substrate when the PCB is assembled or reworked. However, there are laminates with $T_d$ below 340 °C that exhibit great reliability in lead-free applications while other resins with $T_d$ higher than 340 °C in lead-free applications are less reliable.

### 2.1.2 Glass Epoxy Substrates

Selecting the base material for the substrate can be difficult depending on the intricacy of the PCB design. It is very important to understand the operational environment of the end-product in helping to choose the best material. Data developed from material qualification testing has become very helpful to PCB manufacturers. The data pertaining to a particular base material can provide a performance characteristic that can be compared to the operational environment to which it is intended to operate. Though the focus of the base material properties for this research is centered on lead-free assembly and mechanical reliability research, electrical performance must also be taken into consideration when selecting materials [38].

Six categories of substrate core material: 1) epoxy; 2) phenolic; 3) polyester; 4) ceramic; 5) metal core; and 6) polyimide are compared in Table III.

TABLE III
SUBSTRATE CORE PROPERTIES

| Substrate Composition | $T_g$ (°C) | CTE (ppm/°C) | Moisture Absorption (%) | $T_d$ (°C) at 5% weight loss |
|---|---|---|---|---|
| Epoxy | 120 – 180 [g] | 45 - 65 [a] | 0.08 – 0.15 [a] | ≥ 361 [h] |
| Phenolic | 130 – 180 [g] | 68 [a] | 0.1 – 0.36 [a] | ≥ 263 [h] |
| Polyester (unsaturated) | 80 – 100 [g] | 55 – 100 [a] | 0.15 – 0.6 [a] | ≥ 340 [i] |
| Polyimide | 300 – 330 [g] | 15 - 50 [a] | 0.45 – 1.25 [a] | ≥ 514 [h] |
| Metal core | 150 – 200 (Al) [c]<br>200 (Cu) [j]<br>(max. service temp) | 23 (Al) [b]<br>17 (Cu) [b] | n/a [1] | 660 (Al) [c]<br>1083 (Cu) [j]<br>(melting) |
| Ceramic | 1000 - 2000 [d]<br>(sintering) | 2.5 – 6.8 [e] | negligible [f] | >> 2000 [d]<br>(melting) |

a – Source: [39]. b – Source: [41]. c – Source: [43]. d – Source: [45]. e – Source: [47].
f – Source: [40]. g – Source: [42]. h – Source: [44]. i – Source: [46]. j – Source: [48].
1 – Copper/aluminum do not absorb moisture; however, the outer layers are suspectable to oxidation. Source: [49].

Rigid polyimide and ceramic based substrates are used in high temperature applications based on their higher glass transition temperatures. The CTEs of polyimides are lower than the other thermoset resins and if the end application requires more restraint of the CTE, ceramics provide a solution to that need. This allows PCBs constructed with these compositions to retain their mechanical and electrical properties in operational environments of elevated temperatures. Polyimide and ceramic based substrates are also more expensive and require specialized manufacturing processes. Ceramic core substrates, such as alumina ($Al_2O_3$) and aluminum nitride (AlN), are extremely brittle [50].

When there is a requirement for flexible circuits, flexible polyimides and polyesters, such as polyethlylene terephthalate (PET), a saturated polyester, are used as PCB substate cores. Flexible polyimides are more commonly used but polyesters are more economical and are selected in applications of lower operational temperatures. If the end application requires more thermal and chemical stability, then flexible polyimides are chosen [50].

Metal core substrates, such as aluminum and copper, are used in high-power applications where a lot of heat is generated. In this situation, the substrate cores provide a means to transfer or conduct the heat away from the PCB components. Aluminum is the cost-effective choice while typically providing 1 W/m·K to 3 W/m·K of thermal conductivity. Copper provides a much greater thermal conductivity of around 400 W/m·K but comes at a greater cost. Copper's density is greater thereby rendering heavier sized PCBs than an aluminum equivalent [50].

Phenolic resins are judged as an entry-level or basic-purpose thermoset [51]. Phenolic resins exhibit good chemical resistance and excellent thermal resistance. Phenolic resins are low in cost with simplistic manufacturing processes and investment. They have intrinsic flame-retardance characteristics to prevent or slow the propagation of a flame [52]. Homogeneous mixtures are

brittle, so fillers and compounds are added to attain better mechanical and electrical characteristics [51].

Epoxy resins are considered the most successful for PCB substrates. They have low CTE comparable to other PCB thermoset substate core. Epoxy resins exhibit good adhesion to copper. It has good electrical and mechanical properties [53]. It is readily available from single to multilayer boards. Epoxy core can be strengthened with a filler material. This gives glass epoxy laminates structural stability while retaining ductile properties of the resin. The reinforcements are formed into yarn and then woven into patterns. The laminate can contain other chemicals such as curing agents, stabilizing agents, flame retardants and adhesion promoters. Adhesion promoters are used to prevent delamination. Curing agents are used to advance the cross-linking of the resin compounds while stabilizing agents are used to resist decomposition at elevated temperatures [8]. The US National Electrical Manufacturers Association (NEMA) was one of the first to establish a classification of PCB base material. Established NEMA grades are provided in Table IV [35].

TABLE IV
NEMA BASE MATERIAL GRADES
ADAPTED FROM [35].

| Grade | Resin | Reinforcement | Flame Retardant |
|---|---|---|---|
| FR-1, -2 | Phenolic | Cotton paper | Yes |
| FR-3, -4, -5 | Epoxy | Woven glass | Yes |
| FR-6 | Polyester | Mat glass | Yes |
| G-10 | Epoxy | Woven glass | No |
| CEM-1 | Epoxy | Cotton paper/woven glass | Yes |
| CEM-2 | Epoxy | Cotton paper/woven glass | No |
| CEM-3 | Epoxy | Woven glass/mat glass | Yes |
| CEM-4 | Epoxy | Woven glass/mat glass | No |
| CRM-5 | Polyester | Woven glass/mat glass | Yes |
| CRM-6 | Polyester | Woven glass/mat glass | No |

The most chosen PCB substrate core material is FR-4. It is used in a wide variety of applications from computers and computer accessories, telecommunication, manufacturing controls, aerospace, and automotive. But even the FR-4 designation can comprise different epoxy resins, reinforcements, fillers, curing agents and flame retardants. All these difference variations of FR-4 also affect $T_g$, CTE, $T_d$, and moisture absorption [35]. Table V provides a comparison of different FR-4 configurations [37]:

TABLE V
$T_g$, $T_d$, AND CTE VALUES FOR COMMON FR-4 MATERIAL
ADAPTED FROM [37].

| Material | $T_g$ (°C) | X/Y CTE (ppm/°C) | Z-axis Expansion (% from 50 – 260 °C) | $T_d$ (°C) at 5% weight loss |
|---|---|---|---|---|
| Standard $T_g$ FR-4 | 140 | 15 - 17 | 4.2 | 320 |
| Filled mid-$T_g$ FR-4 | 150 | 13 – 14 | 3.3 | 330 |
| Halogen free, filled mid-$T_g$ FR-4 | 155 | 13 – 14 | 3.1 | 390 |
| High-$T_g$ FR-4 | 170 | 13 – 14 | 3.5 | 300 |
| High-$T_g$/$T_d$ FR-4 | 175 | 13 – 14 | 3.5 | 340 |
| Filled high-$T_g$/$T_d$ FR-4 | 180 | 13 – 14 | 2.8 | 340 |
| Halogen-free high-$T_g$/$T_d$ FR-4 | 180 | 13 – 14 | 2.9 | 395 |

The components in constructing a FR-4 substrate core provide an excellent blend of cost, performance, and manufacturability. The range of fiber reinforcement styles makes it easy to control thickness and dielectric. The range of epoxy resins makes it straightforward to customize substrate properties to suit the end-use application [35]. This is why FR-4 was chosen to be the base material for this research.

## 2.2 Pad Design

The reliability of a solder joint is influenced significantly by the pad design. Both the size and shape have a considerable impact [28]. The size and shape of the solder pad on the substrate subjected to the solder joint is affected by the solder mask and is defined by one of two applications: 1) solder mask defined (SMD) and 2) non-solder mask defined (NSMD). The physical difference between the two applications is displayed in Fig.

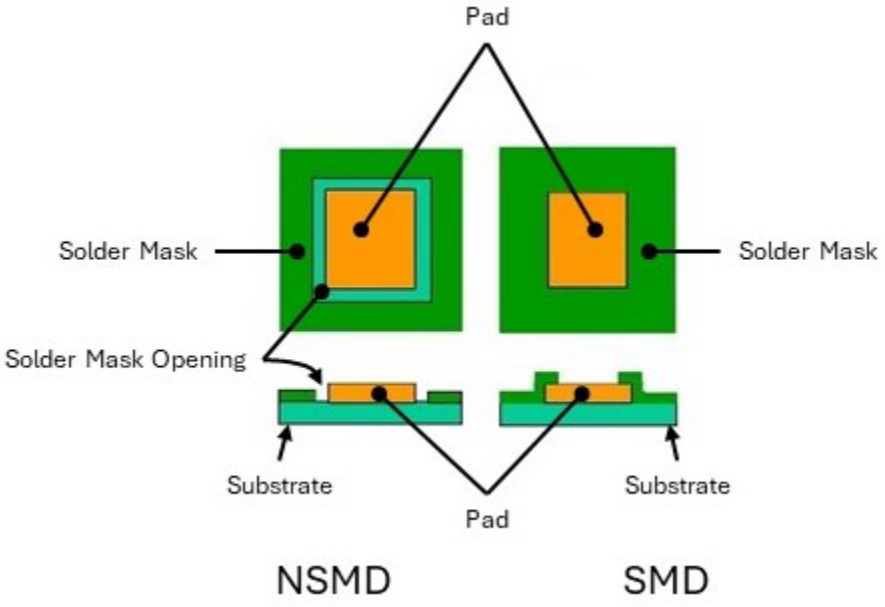


Fig. 2-10: Comparison of SMD and NSMD applications.
Adapted from [54].

The "finish" is a term that describes the treatment of the surface of the pads on the substrate. The purpose of the finish is to promote solder adhesion such that components will solder completely and present a reliable solder joint. There are metallic and nonmetallic finishes. Metallic finishes can be applied by a process called "plating." Finishes can be organic or inorganic. Organic finishes are frequently applied through an immersion process [55].

### 2.2.1 Solder Mask

Solder mask is a coating material applied to a PCB substrate core to prevent solder from adhering to selected areas of the substrate during soldering. The Institute for Printed Circuits (IPC) standardized the use of the term based on its wide use in industry. Its initial purpose was to eliminate short circuits due to soldering but has served to provide other functions. Solder mask also provides plating resistance for pad finishes and to increase dielectric strength [56].

There are three types of solder mask: 1) non-imageable; 2) imageable; and 3) temporary. Non-imageable is an older type of solder mask. They are applied in the desired final pattern via a patterned, nylon screen. However, this process cannot meet the fine features and tolerances of today's PCB designs. They are used today only for cheap, simply electronic products. Imageable is used for high-density PCB with tight tolerances and detail image requirements. This is accomplished with a photoimageable solder mask. Depending on the pitch, or distance, between pads, photoimageable solder mask can provide dams or "webs" as narrow as 0.001 inch to separate SMT pads in proximity. They are available in either dry-film or liquid form. Due to the lower cost, ease of use, simply assembly processing and availability, liquid form accounts for 98 percent of the products made. Dry-film applications tend to be thicker than the liquid alternative and thereby limiting its use. Temporary solder masks are for applications where the solder mask is not a permanent part of the PCB. They can be peeled away from the substrate or dissolved with a chemical solvent [56].

There are a number of assembly considerations that need to be accounted for when determining a new solder mask. The thickness, of course, is an assembly consideration. Some assembly processes tend to generate solder balls on the PCB. The surface finish of the solder mask can help eliminate them. The compatibility with soldering flux and paste, cleaning agents, adhesives,

and with the PCB substrate core material [56]. But one major assembly consideration that greatly affects reliability of the solder joint is the pad size and the nearness of the solder mask to it. SMD and NSMD pad construction are used for optimizing the solder joint with regards to the solder mask depending on the needs of the circuity of the PCB [28]. Pad construction of a SMD and NSMD solder joints is shown in Fig. 2-11 and Fig. 2-12.

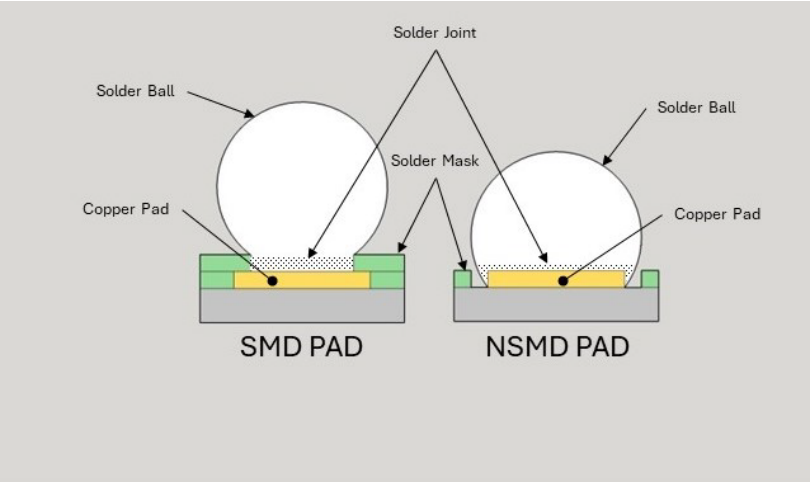


Fig. 2-11: Solder adherence to SMD and NSMD copper pads. Adapted from [57].

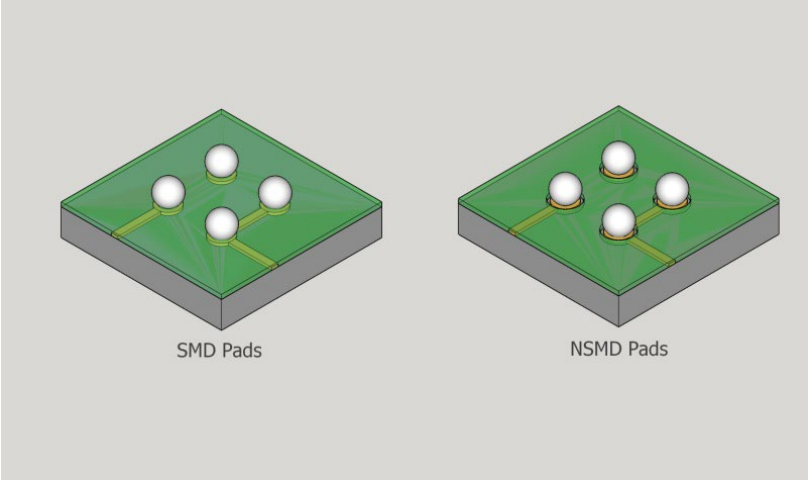


Fig. 2-12: Isometric view of SMD and NSMD Pad Styles. Source [58].

SMD pads are more tolerable of mechanical shock loads due to good adhesion, but they are susceptible to thermomechanical fatigue. By "resting" on the solder mask, as the substrate core material is exposed to cyclic temperatures, the CTE of the core material in the Z-axis imparts localized stresses to the solder joint. This contributes to fatigue and creep reliability issues of a lead-free solder joint on a SMD pad. During PCB assembly, the SMD pad promotes self-centering of the solder joint. SMD pads require tight tolerancing of the solder mask opening. NSMD pads have no stress concentration at the solder joint since they are not exposed to CTE mismatches with the PCB materials. Since the solder mask attached to the pad, it reduces the strength of adhesion between the copper pad to the PCB [59].

The selection of the solder mask also must take into consideration the surface finish of the pads. The reason is most finishes are administered after the solder mask has been applied to the PCB. Table VI provides details to the application of the finish and how that impacts the solder mask [56].

TABLE VI
SURFACE FINISH COMPATIBILITY WITH SOLDER MASK
ADAPTED FROM [56].

| Finish | Compatibility issues |
|---|---|
| Hot air solder leveling (HASL) | This is a quite common finish associated with leaded solder alloys. The PCB is treated with flux, plunged into flowing solder, and removed through air knives to eliminate excess solder. Lead-free solders require notably higher temperatures for this process. This places higher stress on the solder mask and poses post-HASL cleaning problems. |
| Electroless nickel/immersion gold (ENIG) | Each plating supplier has its own immersion bath and has a different level of assertiveness to the solder mask. Generally, the immersion chemistry and solder mask must be qualified together before use; otherwise, the PCB may experience breakdown of the solder mask. Thicker coatings may prevent the breakdown. Disproportionate micro-etching before plating will weaken the solder mask and cause tape test failure as the overhanging mask is fragmented. |
| Immersion tin | |
| Immersion silver | These two finishes are non-threatening to the solder mask and very few issues are known. |
| Organic solderability preservative (OSP) | |

### 2.2.2 Lead-Free PCB Finishes

The finish to the copper pad is a important element in establishing a reliable solder joint between the component and the PCB. Its main purpose is to protect the copper and retain relative ease of making the solder joint. Lead-free solder has altered surface finish specifications for PCBs. It has changed about every facet of applying surface finishes. With the reduction of lead solder alloys, HASL is becoming increasingly outdated though there are lead-free HASL alternatives. As the circuit density increased during the height of HASL, this led to the comeback of organic coatings, such as organic solderability preservatives (OSPs) and metallic layers such as immersion silver, electroless nickel/immersion gold, and immersion tin. In moving to establish no-clean operations in PCB assembly has led to a decline in OSP in favor of the metallic finishes [60].

Most of the familiar metallic finishes are applied via “plating.” Plating is categorized into different methods of deposition employed. The two most used for lead-free finishes are electroless plating and immersion plating. Electroless and immersion are very alike in that no external power is needed to force the deposition reaction. Electroless, or autocatalytic, plating process is nonstop until the substrate is pulled from the plating solution, or bath. This allows for a high thickness level [55]. Final thickness can be controlled by the temperature of the chemical bath, the pH of the solution along with the amount of time spent in the bath. Immersion, or displacement, plating is self-limiting due to the chemical reaction stops when the entire copper pad is fully coated or when the copper pad stops supplying electrons to the displacement reaction. Table VII displays the commonly used surface finishes and the typical thickness for lead-free solder [60].

TABLE VII
COMMON SURFACE FINISHES WITH TYPICAL THICKNESSES
ADAPTED FROM [60].

| PCB Surface Finish | | Typical Thickness |
|---|---|---|
| Electroless nickel/immersion gold (ENIG) | Nickel: | 3 – 6 μm (0.118 – 0.236 mil) |
| | Gold: | 0.04 – 0.12 μm (0.002 – 0.005 mil) |
| Immersion silver | | 0.1 – 0.4 μm (0.004 – 0.016 mil) |
| Immersion tin | | 0.6 – 1.2 μm (0.024 – 0.047 mil) |
| Organic solderability preservative (OSP) | | 0.1 – 0.6 μm (0.004 – 0.024 mil) |

Electroless nickel immersion gold (ENIG) is a universally used finish [55]. ENIG begins with an electroless layer of nickel topped with a thin layer of immersion gold. This surface finish serves many functions. It promotes soldering and wedge wire bonding with aluminum or copper. The gold layer provides oxidation protection to the nickel layer. The nickel layer makes diffusion of the underlying copper pad into the gold difficulty. Gold does not oxidize and dissolves easily into the solder when applied providing excellent wetting to the nickel layer [60]. ENIG finishes are seamlessly flat surfaces for soldering SMT components with exceptional solderability. The finish exhibits minimum handling issues and can withstand multiple processes. The solderability of the finish can last for at least 18 months in storage. The process for applying an ENIG finish is complicated, involving more than 20 process steps, each of which require detailed process control. One major reliability issue concerning ENIG finishes is termed “black nickel” which is caused by a interfacial fracture prompted by corrosion of the nickel layer initiated by the process of layering the gold. When soldering is attempted to these flawed finishes, the gold dissolves off the SMT pad and forms a weaker bond with the underlying nickel [55].

Immersion silver simply forms a thin layer of silver of the copper pad. This finish is multifunctional. The application process is also simple [60]. During assembly of a SMT PCB,

the silver dissolves rapidly when the solder is applied. It is more vigorous than an organic coating such as OSP. One main disadvantage is the finish can tarnish rather quickly when placed in storage. The use of immersion silver is still relatively "new" and the long-term reliability of its use is still being assessed. Immersion tin is like immersion silver in how the layer of tin is applied to the copper pad; however, unlike silver, tin relies on chemical reducing agents, or catalysts, to enhance the deposition of tin. In addition, the reducing agents or not ecological friendly and damage solder mask material. Also, immersion tin finishes are known to form intermetallic compounds (IMC) with the copper pad and develop growth of tin whiskers [55].

Organic solderability preservatives (OSP), on the other hand, are not metallic finishes. It is an organic finish applied to the copper pad. OSP is applied through an immersion process, but the mechanism is different from the metallic finishes. The process is more of a surface absorption rather than a deposition reaction. It provides short-term anticorrosion and anti-tarnish protection until it dissolves during soldering. Its main purpose is to provide solderability. This type of finish is very affordable [55]. The finish has at best a 12-month shelf life when applied. With the introduction and growing use of lead-free solder, newer products of OSPs are being developed to better withstand the SMT assembly temperatures associated with lead-free processes. Some of the limitations or disadvantages include difficulty inspecting thicknesses, nonconductive surface, copper is completely exposed after assembly and can be problematic for applying solder paste [60].

Other finishes exist but their use is extremely limited compared to the ones identified in Table VII. Electrolytic nickel/electrolytic gold is commonly used in applications of prominent levels of force applied to physical connections. Electroless palladium provides great oxidation protection but due to the elevated prices of palladium, immersion silver becomes a more viable option.

Electroless palladium/immersion gold (EPIG) was developed to provide a solution for high frequency and very fine pitch applications due to the degree of signal loss of nickel. But again, due the high prices of palladium combined with the high prices of gold, ENIG would be the better alternative if deemed suitable for that particular capability. Electroless gold and immersion gold provide very good wetting, solderability, and oxidation protection but the cost and process control methods prevent widespread use as a commonly used finish [60].

The solder mask does not seem to pose any significant bias towards reliability assessment of the solder joint with the exception of the solder mask's proximity to the copper pad and suitability with applying particular finishes. Since the SMD design places limitations and stresses on the solder joint, it is considered a more conservative choice over the NSMD design. When considering metallic surface finishes, ENIG is the prominent choice. For this research, solder joint reliability will be evaluated utilizing joints constructed with SMD pads and ENIG and OSP surface finishes.

## 2.3 Metallurgy and Application of Solder

The fundamental elements of a PCB are the substrate, typically an epoxy glass with copper traces, and a solder mask to insulate portions of the copper traces. The exposed portions of copper are available for soldering. Boards designed with THT components will have copper through-holes that may be coated with solder. SMT boards will have copper pads with an applied finish for soldering components. But all of these elements could not be chosen without taking into consideration the thermal assembly processes of applying the solder, the density of the components and their temperature limitations, the solder paste and flux qualities, and last but not least the solder alloy intent for the assembly [61].

The solder chosen for PCB assembly provides both the electrical and mechanical interfaces. For PCB designed with THT, the plated through-hole provides some mechanical strength due to component leads being inserted into the through-hole. But with SMT, the solder is solely responsible for providing the mechanical strength by the bond between the copper pad and the component. The strength of the solder joint's bond relies on the solderability of the surface finish, the formation of intermetallic compounds that may develop, and the phases, and temperatures associated with the phases, of a particular solder alloy [8].

Metallurgy is the field of study within mechanical engineering and materials science that focuses on the chemical and mechanical behavior of metals, intermetallic compounds, and alloys. It is in this area that the physical properties of a solder alloy are determined and evaluated. The phase diagrams are constructed to depict that phase of the alloy depending on the percentage of each element in the alloy and the temperature that the alloy is exposed to. Stress-strain relations are established and evaluated at different temperatures and strain rates. The mechanisms for fatigue and creep are discovered and documented [62].

### 2.3.1 Lead-Free Solder Alloys

Almost all solders are alloys of at least two or more metallic elements. When melted and cooled into a solder joint, the properties of that joint are dependent on the ratio of the elements to each other. Changes in the ratio within a solder alloy are made to provide different mechanical properties suited for specific purposes. Some of mechanical properties include adjusting the melting point, hardness, stress-strain behavior, and resistance to shock. However, changing the alloy ratio for a particular solder alloy in hopes of achieving a suitable melting point can cause other properties to lessen or degrade. This became keenly apparent with the move from the eutectic tin-lead (Sn-Pb; SN63 alloy) solder to lead-free solders. Lead-free solder alloys have higher melting temperatures and in hopes of developing a lead-free alloy with lower melting temperatures, other mechanical properties were affected negatively [15].

Solder alloys comprising of only two elements are termed binary alloys such as Sn-Pb or tin-bismuth (Sn-Bi). Solder alloys having three elements are termed ternary alloys such as the lead-free tin-silver-copper (Sn-Ag-Cu) which is commonly denoted as SAC. For example, the lead-free solder alloy SAC305 designation stands for 3.0 percent silver (A) and 0.5 percent copper (C) with the remaining balance being tin (S). Beyond an alloy having three elements, there is quaternary alloys having four elements, pentanary alloys having five elements, and so forth. Binary and ternary alloys are easier to formulate and control but when a fourth and fifth element is introduced at percentages significantly less than 0.5 percent, it becomes increasingly challenging to control the alloy ratios. In wave soldering, the solder is maintained in a molten state in a large pot. Over time, the materials from the PCB and components will dissolve into the solder causing the minor elements to be modified or even depleted [15].

Since the RoHS directive of 2006, manufacturers have steadily worked to identify a consensus, lead-free solder replaced for SN63. SAC305 is an industry leader but has yet to be acknowledged as the chosen replacement. The lead-free solder alloys predominantly used by industry are listed in Table VIII [15].

TABLE VIII
LEAD-FREE SOLDER ALLOYS AND THEIR TEMPERATURE RANGES
ADAPTED FROM [15].

| Alloy Family | Most Common Composition, Wt.% | Solidus Temperature, °C | Liquidus Temperature, °C |
|---|---|---|---|
| Lead Solder | | | |
| Sn-Pb | Sn-37Pb | 183 | 183 |
| Lead-Free Solders | | | |
| Sn-Cu | Sn-0.7Cu | 227 | 227 |
| Sn-Ag | Sn-3.5Ag | 221 | 221 |
| | Sn-5.0Ag | 221 | 240 |
| Sn-Ag-Cu | Sn-3.0Ag-0.5Cu | 217 | 221 |
| | Sn-3.5Ag-0.9Cu | 217 | 217 |
| | Sn-3.5Ag-0.7Cu | 217 | 220 |
| | Sn-3.8Ag-0.7Cu | 217 | 220 |
| | Sn-3.9Ag-0.6Cu | 217 | 223 |
| | Sn-4.0Ag-0.5Cu | 217 | 225 |
| Sn-Ag-Bi | Sn-1.0Ag-57Bi | 137 | 139 |
| | Sn-3.4Ag-4.8Bi | 200 | 216 |
| | Sn-3.5Ag-5.0Bi | 208 | 215 |
| | Sn-3.5Ag-1.0Bi | 219 | 220 |
| | Sn-2.0Ag-7.5Bi | 191 | 216 |
| Sn-Ag-Bi-Cu | Sn-2.5Ag-1.0Bi-0.5Cu | 214 | 221 |
| | Sn-2.0Ag-3.0Bi-0.75Cu | 207 | 218 |
| Sn-Bi | Sn-58Bi | 138 | 138 |
| Sn-Zn-Bi | Sn-8.0Zn-3.0Bi | 191 | 198 |
| Sn-Zn | Sn-9.0Zn | 199 | 199 |

There are 12 elements that are currently considered practical for developing lead-free solder alloys. Of those available, some have limitations or restrictions on their practical use. A list of elemental candidates is in Table IX [15].

TABLE IX
ELEMENTAL CANDIDATES FOR LEAD-FREE SOLDER
ADAPTED FROM [12], [63], [64], [65].

| Element | Symbol | Cost (per Troy ounce) (8/1/2024) | World Production (metric tons) (2023) | World Reserves (metric tons) (2023) |
|---|---|---|---|---|
| Antimony | Sb | $0.73 | 83,000 | 2,000,000 |
| Bismuth | Bi | $0.45 | 20,000 | Not available |
| Copper | Cu | $0.28 | 49,000,000 | 1,000,000,000 |
| Gallium | Ga | $10.41 | 610 | 1,100 |
| Gold | Au | $2,434.00 | 3,000 | 59,000 |
| Indium | In | $12.98 | 990 | Not available |
| Mercury | Hg | Not available | 1,200 | Not available |
| Palladium | Pd | $930.00 | 210 | 71,000 (PGM) [1] |
| Platinum | Pt | $974.00 | 180 | |
| Silver | Ag | $28.88 | 26,000 | 610,000 |
| Tin | Sn | $0.93 | 290,000 | 4,300,000 |
| Zinc | Zn | $0.08 | 12,000,000 | 220,000,000 |

1 – PGM stands for platinum group metals (palladium, platinum, iridium, osmium, rhodium, and ruthenium).

Copper, silver, tin, and zinc are the most used elements for lead-free solder alloys. Copper, tin, and zinc are very economical. However, due to the cost of silver, its ratio within a solder alloy is usually small. Gold, palladium, and platinum are considered too expensive for a common lead-free solder alloy element as well as their limited availability. Even though the cost of gallium and indium are well within the cost of silver, the limited availability of these elements prevents them from meeting the quantity needs of the PCB industry. Mercury (Hg) is a RoHS restricted element. The cost of antimony and bismuth are very attractive for consideration as a solder alloy element with world production quantities similar or better than silver. Antimony is used

sparingly to slightly improve physical properties of lead-free solder alloys. Bismuth, though used more commonly than antimony, has limitations that prevent its widespread use [15].

Antimony has been used in tin-lead solder alloys. When tin-lead solder alloys have included around 0.3% to 0.5% antimony, the solder demonstrates improved opposition to thermal fatigue than tin-lead solder alloys that are not doped with antimony. When added to lead-free solder alloys, antimony forms intermetallic compounds with silver and copper that increases the strength of the solder joint [66]. The general rule for adding antimony is no more than 6% of the tin concentration. There are concerns that antimony is a toxic substance, but it only relates to the soluble salts and gases formed with antimony [67]. For example, antinomy trioxide ($Sb_2O_3$), used as a flame retardant, is toxic at 0.5 mg/m³ of air but this compound is not created during the soldering or salvaging processes [66]. So, as an element in a solder alloy, antimony is not a toxic material that should be identified and monitored [67].

Bismuth has been more than a doping element for solder alloys; it's a major solder alloy element. It has a low melting point which makes it an advantageous element to add when trying to lower the liquidous or melting point of a particular lead or lead-free solder alloy. As shown in Table VIII, the lead-free solder alloy, Sn-58Bi, has an incredibly low eutectic melting point of 138 °C. However, without the presence of lead, large percentages of bismuth render a solder joint extremely brittle. For this reason, bismuth ratios are kept low in the range of 3% to 6% [67]. Bismuth expands when it freezes as opposed to tin that shrinks. This condition is termed "fillet lifting" but is mostly linked to ternary lead-free solder alloys in the alloy configuration of Sn-Cu-Bi and Sn-Ag-Bi [15]. Bismuth is considered low toxic and to be non-carcinogenic [67]. However, in large concentrations, bismuth is known to be contaminated with cadmium (Cd). In

those instances, special handling instructions and ventilation when soldering may be mandatory [15].

The Sn-Ag-Cu lead-free solder alloy family is the most predominate lead-free alloy used for PCB assemblies. It has far better tensile strength than Sn-Pb but considerable worse shear strength. Though it isn't eutectic, its liquidus temperature is approximately 35 °C higher than SN63. SAC solder alloys are compatible with most surface finishes and platings used for lead soldering. SAC solder alloys are double or triple the price of a comparable Sn-Pb alloy. The ability of a SAC solder joint to withstand mechanical shock decreases as the amount of silver increases. For example, SAC105 (Sn-1.0Ag-0.5Cu) is more shock resistant than SAC405 (Sn-4.0Ag-0.5Cu) [15].

Out of the family of Sn-Ag-Cu lead-free solder alloys, the favorite choice is SAC305 (Sn-3.0Ag-0.5CU). Initially after the RoHS directive, Sn-3.5Ag-0.9Cu and Sn-0.7Cu were the two choice materials because they were eutectic. The high cost of silver and the patent cost owed to Iowa State University for the two eutectic alloys drove the Japan Electronics and Information Technology Industries Association (JEITA, formerly JEIDA) to find an alternative. It was Senju Metal Industries' patented Sn-3.0Ag-0.5Cu that was finally approved. Though it was not eutectic, its melting temperature was lower than Sn-0.7Cu and it was comparably cheaper than the Sn-3.5Ag-0.9Cu while providing the same level of performance. In time, the IPC endorsed SAC305 as "the lead-free alloy of choice for the electronics industry" which pushed U.S. companies to incorporate it into their electronic product designs. This resulted in SAC305 displacing the two eutectic options and propelled other industry suppliers into developing SAC305 offerings. Due to the huge amount of utilization of SAC305 over time, industry and academia captured a large amount of reliability data which helped push it as the "go-to" lead-free

solder standard [24]. However, even though there is no clear consensus to which Sn-Ag-Cu alloy is the best, one approach being taken to improve the reliability of SAC305, ternary solder alloy is to add small amounts of "impurity" elements. This leads to developing quaternary and pentanary SAC alloys termed "SACX" solders [15].

### 2.3.2 Solder Fluxes and Pastes

Solder flux is a chemical compound that removes surface oxidation of the metals being joined when heated by the application of solder, but it also has other functions just as important. Solder flux must [61]:

- Boosts the formation of intermetallic layers at the solder interface
- Dissolves metallic salts that have formed due to metal oxide reactions
- Protects the surfaces from reoxidation before the solder is applied
- Evenly distributes the heat during soldering
- Enhances wetting by reducing the surface tension of the soldering interfaces

A solder flux performs its functions by being composed of four main ingredients: 1) vehicle; 2) solvent; 3) activators; and 4) additives. The vehicle is a soft solid or liquid that covers the surface to be soldered. It dissolves the metallic salts and evenly transfers the heat from the soldering operation. The solvent dissolves the other ingredients and evaporates during the soldering process. The activator's main role is to improve the flux's ability to remove the oxidation on the soldering surfaces. Additives can be any other ingredient that performs a special function such as increasing the wetting properties, lowering the surface tension of the mating surfaces, or providing better flux viscosity [61].

The IPC standard, Requirements for Soldering Fluxes (IPC J-STD-004D), classify fluxes into four general classifications: 1) inorganic acid; 2) organic acid; 3) rosin; and 4) resin. Each of the classifications are further broken down into flux type, flux designator, and flux activity level. The classifications and categories of fluxes are shown in Table X [8].

TABLE X
J-STD-004B FLUX CLASSIFICATION AND DESIGNATORS
ADAPTED FROM [8], [68].

| Flux Material | Symbol | Flux Activity Level (% Halide by weight) | Flux Type | Flux Designator | Characteristics |
|---|---|---|---|---|---|
| Rosin | RO | Low (<0.05%) | L0 | ROL0 | Natural product extracted from pine trees; inactive at room temperature; not soluble in water; leaves behind a residue |
| | | Low (≥0.05 and <0.5%) | L1 | ROL1 | |
| | | Moderate (<0.05%) | M0 | ROM0 | |
| | | Moderate (≥0.5 and <2.0%) | M1 | ROM1 | |
| | | High (<0.05%) | H0 | ROH0 | |
| | | High (≥2.0%) | H1 | ROH1 | |
| Resin | RE | Low (<0.05%) | L0 | REL0 | Synthesis or modified rosin; decomposes during soldering; low solubility in water; leaves behind very low residue |
| | | Low (≥0.05 and <0.5%) | L1 | REL1 | |
| | | Moderate (<0.05%) | M0 | REM0 | |
| | | Moderate (≥0.5 and <2.0%) | M1 | REM1 | |
| | | High (<0.05%) | H0 | REH0 | |
| | | High (≥2.0%) | H1 | REH1 | |
| Organic | OR | Low (<0.05%) | L0 | ORL0 | Stronger than rosin fluxes but weaker than inorganic fluxes; soluble in water; organic acids commonly found in foods |
| | | Low (≥0.05 and <0.5%) | L1 | ORL1 | |
| | | Moderate (<0.05%) | M0 | ORM0 | |
| | | Moderate (≥0.5 and <2.0%) | M1 | ORM1 | |
| | | High (<0.05%) | H0 | ORH0 | |
| | | High (≥2.0%) | H1 | ORH1 | |
| Inorganic | IN | Low (<0.05%) | L0 | INL0 | Highly corrosive; used to remove oxidation from ferrous and nonferrous metals which cannot be soldered with weaker fluxes; not used on electronic assemblies |
| | | Low (≥0.05 and <0.5%) | L1 | INL1 | |
| | | Moderate (<0.05%) | M0 | INM0 | |
| | | Moderate (≥0.5 and <2.0%) | M1 | INM1 | |
| | | High (<0.05%) | H0 | INH0 | |
| | | High (≥2.0%) | H1 | INH1 | |

Fluxes are applied to the PCB in several ways but are used specifically for THT. For SMT applications, solder paste is used. Solder paste is a combination of solder powder particles mixed into a flux with the addition of gelling agents [4]. Its main purpose is to temporarily hold components to the pads in preparation for soldering either reflow or wave processes. The fluxes used to produce solder pastes are still the same identified in IPC J-STD-004D (ISO 9454-1, DIN EN 29454-1, or DIN 8511 if flux selection is based on European or German standards) so the vehicle, activator, and solvent ingredients are covered. The other parameters of a solder paste needing control are the metal composition, metal content, and particle size and shape [8].

The metal composition is the same as that of any solder made available like the ones shown in Table VIII. If a particular lead-free solder alloy exists and is available, it can be used to construct a solder paste. Its applicability is the same as for the solder. Factors such as cost, strength, and compatibility with surface finishes need to be considered. An added consideration would be if the solder paste metal composition was different than the solder, then that addition compatibility would need to be assessed. The metal content of a solder paste is a percentage by weight of the metal to flux ratio. SMT assemblies generally use a solder paste containing 88 to 90% metal (this is approximately 50% by volume). The metal content has a great impact on the solder joint quality, specifically the reflow solder process. For example, a 10% difference in metal content for the same solder paste thickness can result in overflow and deficient reflow solder joints [8].

The size and shape of the solder particles determine the solder paste's printability and oxide content. Solder particles which are spherical in shape are preferred. Particles that are irregular in shape can clog printing screens and stencils. Irregular shaped particles have a higher surface area than the spherical ones which increase the oxide content. Also, solder paste power size is determined by the pitch and size of the PCB pads, the mesh designation, and the aperture size of

the printing screens and stencils. By not matching the solder powder type with the correct mesh designation and printing apertures can also result in clogging if the particles are too big and the formation of solder balls if particles are too small. Nominal powder size is established in the IPC standard, Requirements for Solder Paste (IPC J-STD-005B) as shown in Table XI [8].

TABLE XI
SOLDER POWDER TYPE BY WEIGHT PERCENTAGE AND SIZE
ADAPTED FROM [69].

| | By Weight | | | |
|---|---|---|---|---|
| | < 0.5% larger than | >/ 10% between | </ 80% between | >/ 10% smaller than |
| Type | (microns) | | | |
| 1 | 160 | 150-160 | 75-150 | 75 |
| 2 | 80 | 75-80 | 45-75 | 45 |
| 3 | 60 | 45-60 | 25-45 | 25 |
| 4 | 50 | 38-50 | 20-38 | 20 |
| 5 | 40 | 25-40 | 15-25 | 15 |
| 6 | 25 | 15-25 | 5-15 | 5 |
| 7 | 15 | 11-15 | 2-11 | 2 |
| 8 | 11 | 8-11 | 2-8 | 2 |

### 2.3.3 Solder Physical Properties

The mechanical properties of lead-free solder at room temperature and elevated temperatures are very dependent on the strain rate and the amount of time under strain. This makes it very challenging when designing PCB solder joints for high reliability. Most solder reliability prediction models are centered on high temperature conditions. Plastic flow that is thermally triggered (i.e. creep) dictates the stress-strain behavior at very rapid and very low strain rates. Strain rates, elastic and plastic, not involving thermal activation are small when compared to heat related plastic flow [62]. In spite of this, the research conducted will focus on elastic-plastic shear and fatigue loading under isothermal conditions at room temperature but the applicability of creep under those conditions will be evaluated.

Each lead-free solder alloy composed of a specific elemental composition has unique mechanical properties. Experimentation of these lead-free solder alloys to calculate mechanical properties for assessing reliability of electronic assemblies has been very challenging. As a solder joint cools and solidifies to an isothermal condition, it causes the growth of intermetallic compounds (IMCs). For example, when SAC405 is applied on a copper pad with an ENIG finish, $Ag_3Sn$ IMC forms in the bulk solder, $(Cu,Ni)_6Sn_5$ forms at the solder/pad interface, and $Ni_3Sn$, a smaller size IMC, forms at the solder/pad interface as well. Also, other elements may be present in the alloys as impurities. The growth of IMCs and impurities leads to statistical variation in measuring mechanical properties [10].

#### 2.3.3.1 Stress-Strain Relations

Taking the basic relationship between stress and strain as presented in Section 1.2, a solder joint's stress and strains are composed of a 3D Cartesian stress and strain components [10]. Hooke's Law represents a materials behavior in the elastic region of a stress-strain diagram as shown in Equation 2.1 [19].

$$\sigma_{elastic} = E\varepsilon_{elastic} \tag{2.1}$$

And both normal and shear stresses in the elastic region are expressed in Equation 2.2 [10].

$$\begin{Bmatrix} \sigma_x \\ \sigma_y \\ \sigma_z \\ \tau_{xy} \\ \tau_{xz} \\ \tau_{yz} \end{Bmatrix} = \frac{E}{(1+v)(1-2v)} \begin{bmatrix} 1-v & v & v & 0 & 0 & 0 \\ v & 1-v & v & 0 & 0 & 0 \\ v & v & 1-v & 0 & 0 & 0 \\ 0 & 0 & 0 & (1-2v)/2 & 0 & 0 \\ 0 & 0 & 0 & 0 & (1-2v)/2 & 0 \\ 0 & 0 & 0 & 0 & 0 & (1-2v)/2 \end{bmatrix} \begin{Bmatrix} \varepsilon_x \\ \varepsilon_y \\ \varepsilon_z \\ \gamma_{xy} \\ \gamma_{xz} \\ \gamma_{yz} \end{Bmatrix} \tag{2.2}$$

Where [10];

- $\sigma_x$, $\sigma_y$, $\sigma_z$ are normal stresses
- $\tau_{xy}$, $\tau_{xz}$, $\tau_{yz}$ are shear stresses

- $\varepsilon_x$, $\varepsilon_y$, $\varepsilon_z$ are normal strains
- $\gamma_{xy}$, $\gamma_{xz}$, $\gamma_{yz}$ are shear strains
- $E$ is the Young's (elasticity) modulus
- $v$ is the Poisson's ratio
- $G$, the Shear Modulus, is calculated from the Young's Modulus and Poisson's ratio as shown in Equation 2.3 [10].

$$G = E/\big(2(1+v)\big) \tag{2.3}$$

This simplifies the shear stress-strain relationship in the elastic region in all directions to Equation 2.4 [10].

$$\tau = G\gamma \tag{2.4}$$

The yield point is the point at which the elastic region ends, and the plastic region begins. The plastic region is when the solder alloy experiences plastic flow. This is also the point that the uniaxially load portion of the solder joint reaches a maximum shear stress that corresponds to the solder joint's shear yield strength level. The relationship between the maximum shear stress and the yield strength is represented by the Maximum-shear-stress theory developed by Henri Tresca. The Maximum-shear-stress theory is only applicable to ductile material which makes its use suitable for evaluating solder joint behavior under load. Constructed on Mohr's circle for the uniaxial stressed component, the maximum shear stress at yield is expressed in Equation 2.5 [10].

$$(\tau_{max})_Y = G(\gamma_{max})_Y = S_Y/2 \tag{2.5}$$

But shear occurs in a multi-axial state when a solder joint is subjected to multi-axial normal stresses and strains. This leads to the premise of using the Maximum-distortional-energy theory (von Mises) to understand the shear stresses at yield. The effective yield strength of a subjected to complex stresses is expressed in Equation 2.6 [19].

$$(S_Y)_{effective} = \frac{1}{\sqrt{2}}\left[\left(\sigma_x - \sigma_y\right)^2 + \left(\sigma_y - \sigma_z\right)^2 + (\sigma_z - \sigma_x)^2\right]^{\frac{1}{2}} \tag{2.6}$$

The corresponding effective strain at the onset of yield is expressed in Equation 2.7 [19].

$$(\varepsilon_Y)_{effective} = \frac{\sqrt{2}}{3}\left[\left(\varepsilon_x - \varepsilon_y\right)^2 + \left(\varepsilon_y - \varepsilon_z\right)^2 + (\varepsilon_z - \varepsilon_x)^2\right]^{\frac{1}{2}} \tag{2.7}$$

The corresponding shear stress to the von Mises stress is derived as shown in Equation 2.8 [19].

$$\tau_{effective} = \frac{1}{\sqrt{3}}(S_Y)_{effective} \tag{2.8}$$

And the corresponding shear strain to the von Mises strain is derived as shown in Equation 2.9 [19].

$$\gamma_{effective} = \sqrt{3}(\varepsilon_Y)_{effective} \tag{2.9}$$

But this theory only accounts for elastic behavior. When the solder joint is loaded past the yield strength, the solder joint begins to deform due to the combination of elastic and plastic straining. The plastic strain is a time-independent strain that is irreversible due to strain hardening. The plastic region of a ductile material does not follow Hooke's law as shown in Fig. 2-13 [19].

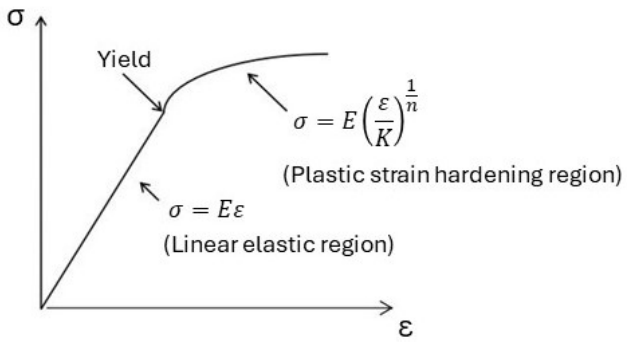


Fig. 2-13: Elastic plastic stress-strain curve plot.
Adapted from [19].

Therefore, derived from Fig. 2-13, the plastic strain follows the Ramberg-Osgood equation as shown in Equation 2.10 [70].

$$\varepsilon_{plastic} = K\left(\frac{\sigma_{plastic}}{E}\right)^{n} \tag{2.10}$$

The coefficient *K* is a material constant that can be dependent on temperature [10]. The exponent *n* is a material, strain hardening constant. By changing the value of *n*, the response of the Ramberg-Osgood stress-strain curve are shown in Fig. 2-14 [71].

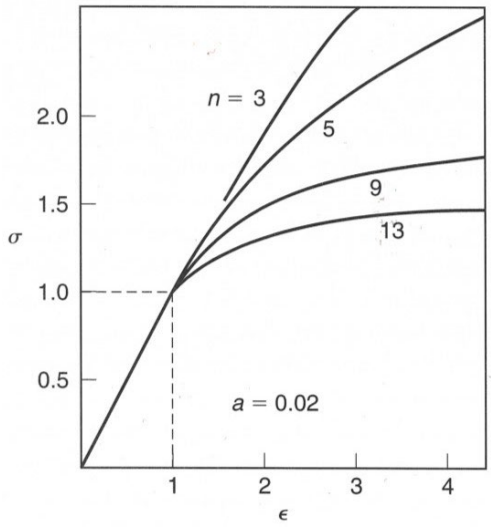


Fig. 2-14: Ramberg-Osgood stress-strain curves as exponent *n* changes.
Source [71].

Another contributor to the total strain of a solder joint is the time-dependent plastic strain or creep strain [62]. This captures both instances of creep and viscoplasticity. Whereas creep is the rearrangement of strain and stresses due to constant stress levels from high temperature environments, viscoplasticity is specifically time-dependent plastic strain. They are generally separated for analytical purposes but are physically the same. Creep becomes considerable when the homologous temperature is above 0.4. Homologous temperature is defined as the ratio of $T/T_m$ (°C/°C), where $T_m$ is the melting temperature of the solder alloy. There are a few models/equations for creep strain [10]. Pang presents the Creep Constitutive Model shown in Equation 2.11 [19].

$$\frac{d\varepsilon_{creep}}{dt} = A\sigma^n exp\left(-\frac{Q}{RT}\right) \tag{2.11}$$

Variables $A$ and $n$ are material constants and $Q$ is the energy needed to activate the creep process. The last two variables, $R$ and $T$, represent the universal gas constant and the absolute temperature (Kelvin) [10].

Summing the three components of strain represent the Elastic-Plastic-Creep model for analyzing a ductile material behavior such as solder joint as shown in Equation 2.12 [19].

$$\varepsilon_{total} = \varepsilon_{elastic} + \varepsilon_{plastic} + \varepsilon_{creep} \tag{2.12}$$

Another factor that affects the stress-strain relationship is the rate of strain. The strain rate can affect the stress-strain relationship. This behavior adds complexity when trying to determine the elastic and plastic regions for a given solder alloy. This condition is magnified when occurring under an elevated homologous temperature. Also, the creep and viscoplasticity strains decrease as the strain rate increases and become nonexistent when the strain rate comes near infinity. To

illustrate, three different stress-strain curves with different strain rates for a eutectic Sn-Ag alloy are displayed in Fig. 2.15 [62].

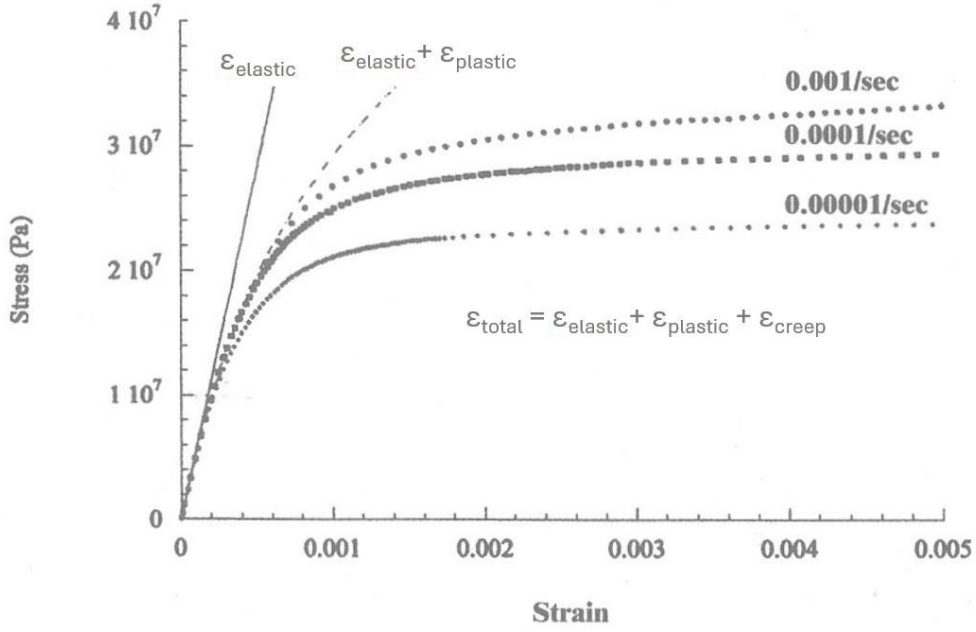


Fig. 2-15: Stress-strain curves at different strain rates for Sn-3.5Ag solder alloy. Adapted from [62].

The classic mechanical approach established in the elastic-plastic-creep model separates the time-independent and time-dependent plastic strain. Tamin et al indicates that this frequently leads to over-calculating the magnitude of the strain and irregularities in the data. This prompted the development of a unified inelastic strain theory. The purpose was to capture the plastic behavior into a single variable. Quite a few unified inelastic strain models have been proposed [10]. The viscoplastic constitutive model treats the dislocation caused by plastic and creep motion as a single, inelastic strain variable as shown in Equation 2.13 [19].

$$\varepsilon_{total} = \varepsilon_{elastic} + \varepsilon_{inelastic} \tag{2.13}$$

The most widely used model for calculating total inelastic strain is the Anand model. The Anand model does not use or identify specific yield conditions to determine inelastic strain. The inelastic strain is influenced by the current stress, temperature, and internal material variables. Also, the plastic flow is presumed to occur in all areas where stress is present [10]. The Anand model for calculating inelastic strain is shown in Equation 2.14 through 2.16 [19].

$$\frac{d\varepsilon_{inelastic}}{dt} = \dot{\varepsilon}_{inelastic} = A\, exp\left(-\frac{Q}{RT}\right)\left[\sin h\left(\xi\frac{\sigma}{s}\right)\right]^{\frac{1}{m}} \tag{2.14}$$

$$\dot{s} = \left\{h_0\left|1-\frac{s}{s^*}\right|^a * sgn\left(1-\frac{s}{s^*}\right)\right\} * \frac{d\varepsilon_{inelastic}}{dt} \tag{2.15}$$

$$s^* = \hat{s}\left[\frac{1}{A}\frac{d\varepsilon_{inelastic}}{dt} exp\left(-\frac{Q}{RT}\right)\right]^n \tag{2.16}$$

Where [19];

- $d\varepsilon_{inelastic}/dt$ (also expressed as $\dot{\varepsilon}_{inelastic}$) is the effective inelastic strain rate
- $\sigma$ is the effective true stress
- $s$ is the deformation resistance
- $\dot{s}$ is the rate of deformation
- $\xi$ is the stress multiplier
- $m$ is the strain rate sensitivity of stress
- $h_0$ is the hardening/softening constant
- $\hat{s}$ is the coefficient for deformation resistance saturation value
- $a$ is the strain-rate sensitivity of hardening or softening
- $n$ is the strain rate sensitivity of the saturation value

The viscoplastic stress associated with the inelastic strain is determined by Equation 2.17 through 2.19 [19].

$$\sigma = \sigma^* - \left[(\sigma^* - cs_0)^{(1-a)} + (a-1)ch_0\sigma^{*(-a)}\varepsilon_{inelastic}\right]^{\left(\frac{1}{1-a}\right)} \quad (2.17)$$

$$\sigma^* = \frac{\hat{s}}{\xi}\left(\frac{\dot{\varepsilon}_{inelastic}}{A}\exp\left(\frac{Q}{RT}\right)\right)^n * \sin h^{-1}\left[\left(\frac{\dot{\varepsilon}_{inelastic}}{A}exp\left(\frac{Q}{RT}\right)\right)^m\right] \quad (2.18)$$

$$c \equiv \frac{1}{\xi}\sin h^{-1}\left[\left(\frac{\dot{\varepsilon}_{inelastic}}{A}exp\left(\frac{Q}{RT}\right)\right)^m\right], c < 1 \quad (2.19)$$

Where:

- $\sigma^*$ is the saturation stress [19]
- $s_0$ is the initial internal state variable (temperature dependent) [10]
- $h_0$ is the initial hardening coefficient (temperature and strain rate dependent) [10]
- $c$ is a function of strain rate and temperature [19]

The Anand model was established to model the deformation of ductile material under high homologous temperatures [10]. Most of the parameters used to calculate the viscoplastic stress and inelastic strain are derived from curve-fitting processes of engineering data from creep tests under different strain rates and temperatures [19]. The research conducted will not include creep testing therefore the engineering data will not support curve-fitting efforts to define values for the parameters of the Anand model. In addition, the shear and fatigue testing conducted will occur at a homologous temperature in the range of 0.12. This is appreciably lower than the 0.4 value where creep is considered significant in a material's deformation under load. The presumption for this research will be that the basic elastic-plastic-creep model will support characterizing the solder joints behavior for the shear and fatigue testing performed at room temperature.

All the stress-strain data collected during testing is termed engineering stress-strain data. The stress is calculated from the force measured from instrumentation divided by the area of the cross-section of the solder joint. The strain is acquired from test instrumentation. But the engineering stress-strain data needs to be converted to true stress-strain values. The true stress accounts for constant reduction of the cross section during the loading of the solder joint under test. The engineering stress-strain data is converted to true stress-strain values with Equations 2.20 and 2.21 [10].

$$\sigma_{true} = \sigma_{engineering}\left(1 + \varepsilon_{engineering}\right) \tag{2.20}$$

$$\varepsilon_{true} = \ln\left(1 + \varepsilon_{engineering}\right) \tag{2.21}$$

The graphical relationship between the engineering and true stress-strain curves for testing SAC405 at a strain rate of 19.74 $s^{-1}$ is shown in Fig. 2-16 [19].

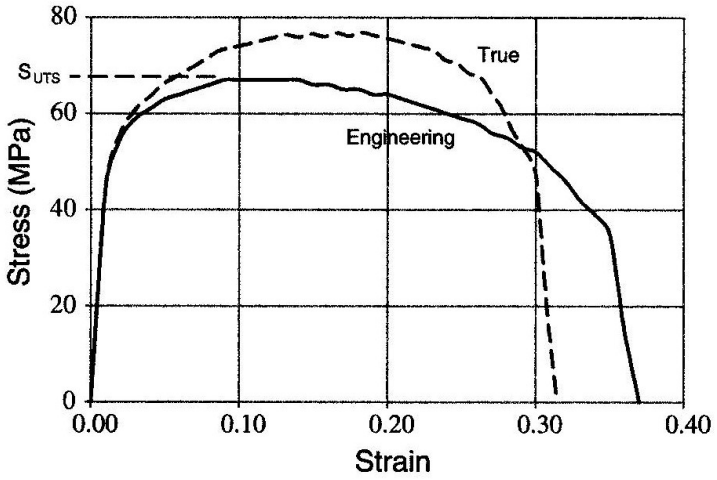


Fig. 2-16: Comparison of engineering and true stress-strain curves of SAC405. Source [19].

For a finite element analysis (FEA), the true stress-strain is needed to calculate the stresses and strains internally throughout the material. When necking occurs, the true stresses in the material continue to increase while undergoing sizable plastic strains. However, Pang indicates that localized necking from triaxial stresses causes the true stress-strain curve tends to be inaccurate when the solder joint is subjected to large plastic strain. But this inaccuracy is minimized since the magnitude of the inelastic strain during necking is very small. This is because at fracture the failure occurs due to a fatigue damage mechanism [19].

#### 2.3.3.2 Isometric Fatigue

When a solder joint is subjected to cyclic loads under a constant temperature, significantly below homologous temperature, the joint will fail after a number of cycles. The number of cycles to failure depends on the magnitude of the load and strain. The larger the strain the fewer cycles to failure. The lower the strain than the number of cycles increases before failure. If the magnitude of the cyclic load is low enough to not cause a failure, then this is generally termed the endurance limit. All metals do not exhibit this trait but if the cyclic load's magnitude is such that failure does not occur until after several million cycles then that value is typically referred to as the endurance limit. Isometric fatigue test is executed with constant amplitude with associated stress-strain and cycle-to-failure graphs. The cycles can incorporate pauses or dwell times between cyclic loads [62].

There are three stages to isometric fatigue failure at low homologous temperatures: 1) fatigue crack nucleation; 2) microcrack propagation and coalescence; and 3) macrocrack propagation. Microcracks fall into the submicron size range. Macrocracks are generally a couple millimeters or larger. Due to the size of PCB solder joints, the first two stages receive the most focus. And if there are preexisting cracks, then the focus is solely on the second stage [62].

When there are no preexisting cracks in the solder joint, fatigue failure initiates with stress concentrating around stress risers and flaws which are not considered cracks. These are areas in the solder joint that have sharp corners or notches that cause the stresses to be higher than the surrounding area. This also includes pores and other internal defects that develop when applying the solder to component on a PCB. Stress concentrators are unintentionally present at the interface of the solder joint, pad, and solder mask area due to the design [62].

The second stage of fatigue failure covers stable crack growth. This is best explained by Sanford's description of the plastic blunting model of Laird which describes slip (or shear) band motion and the formation of striation. A crack starting from no load is shown in Fig. 2-17 [71].

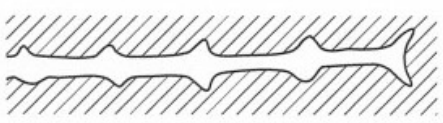

Fig. 2-17: Microcrack with no load.
Source [71].

The two small notches at the tip of the crack are at 45° slip zones as the load is applied as shown in Fig. 2-18 [71].

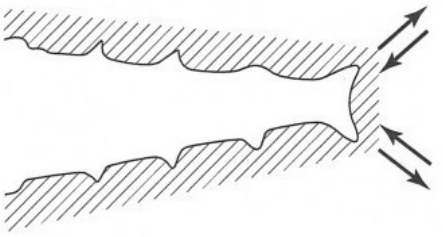

Fig. 2-18: Microcrack with tensile load applied.
Source [71].

As the crack reaches maximum strain, the slip zones at the tip of the crack begin to blunt or broaden as shown in Fig. 2-19 [71].

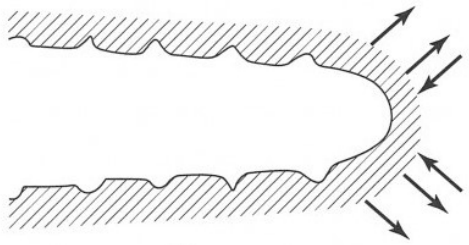

Fig. 2-19: Microcrack at maximum strain.
Source [71].

When the load and slip directions are reversed, the crack is pushed together which causes the blunt tip of the crack to buckle forming new notches as shown in Fig. 2.20 [71].

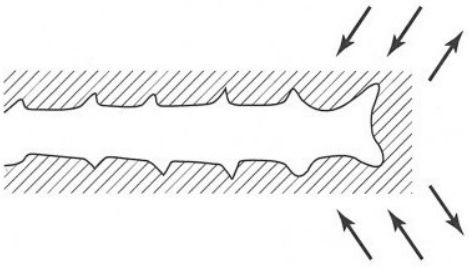

Fig. 2-20: Microcrack with load removed and new notches.
Source [71].

Now the crack is back to no load with additional striation marks waiting for the next load cycle as shown in Fig. 2-21 [71].

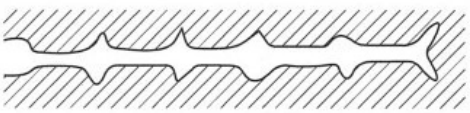

Fig. 2-21: Microcrack at no load with two new notches.
Source [71].

Eventually, the microcrack grows to a length of critical instability when the maximum stress is applied. At this point, the crack grows very rapidly and becomes a macrocrack. This is the third stage of fatigue failure. This is simply when the maximum stress intensity factor, $K_{max}$, of the stress intensity factor range, $\Delta K$, is greater than the critical stress intensity factor (or fracture toughness), $K_c$. It is during the third stage that the solder joint fails.

Fatigue behavior is mathematically expressed by the Coffin-Manson function. It relates the total strain per cycle in terms of elastic and plastic strain and number of cycles to failure as shown in Equation 2.22 [28].

$$\varepsilon_{total} = \varepsilon_{elastic} + \varepsilon_{plastic} = AN_f^{-c} + BN_f^{-m} \tag{2.22}$$

Whereas the variables $A$, $B$, $c$, and $m$ are constants extracted from test data [28]. This relationship is a hysteresis loop of the true stress-strain of the solder joint under cyclic loading. It is graphically presented in Fig. 2-22 [10].

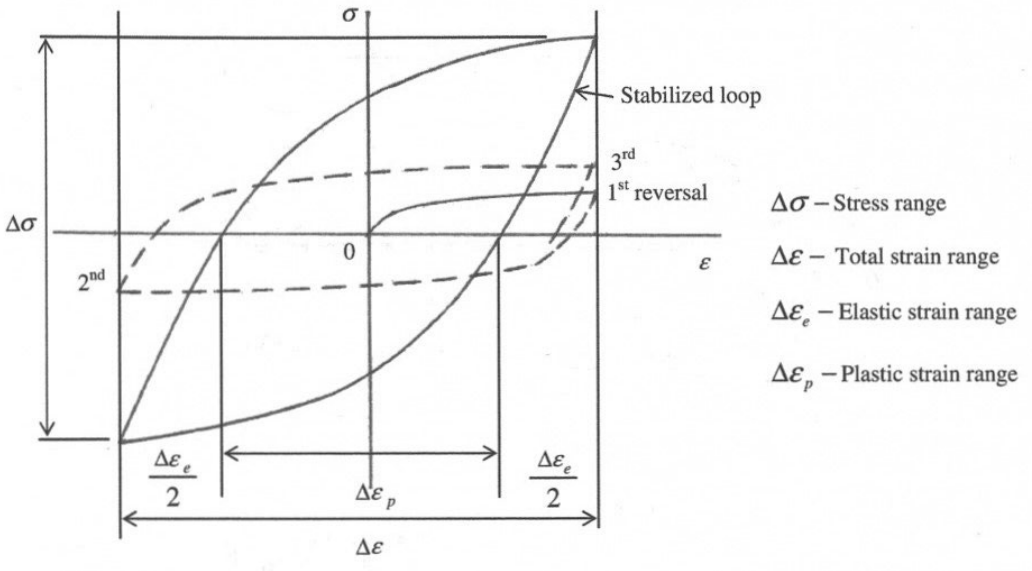


Fig. 2-22: Sketch of true stress-strain fatigue hysteresis loop with no dwell. Source [10].

Low cycle fatigue failure (generally 10,000 cycles or less) is mainly caused by plastic strain. Recalling that elastic strain is reversible and plastic strain is permanent, Equation 2.22 can be reduced and rearranged by deeming the elastic strain negligible as shown in Equation 2.23 [28].

$$N_f = \left(\frac{A}{\varepsilon_{plastic}}\right)^{\frac{1}{m}} \tag{2.23}$$

The Coffin-Manson expression can also be written in terms of inelastic shear strain range as shown in Equation 2.24 [10].

$$N_f = c(\Delta\gamma_{inelastic})^m \tag{2.24}$$

Whereas the variables *A*, *c* and *m* are constants determined with experimental data.

Ahmad and Brillhart indicate that when the solder joint's temperature is above a homologous temperature of 0.5 (This is slightly higher than 0.4 suggested by Tamin et al [10]), the temperature and the cyclic frequency becomes additional influencers to the number of cycles the solder joint can sustain before fatigue failure. This is due to the addition of creep strain. The Coffin-Manson expression is modified as shown in Equation 2.25 [28].

$$N_f = \left(\frac{A}{\varepsilon_{plastic}}\right)^{1.9} f^{\frac{1}{3}}\, exp\left(\frac{0.123}{kT_{max}}\right) \tag{2.25}$$

Whereas *k* is the Boltzmann's constant and variable *A* is a constant determined from experimental data [28].

The time to failure can be simply calculated from the number of failures by Equation 2.26 [62].

$$t_f = N_f(2t_r + t_h) \tag{2.26}$$

Whereas [62]:

- $t_r$ is the ramp time
- $t_h$ is the hold time
- $(2t_r + t_h)$ is the cycle time

Excluding the initial cycles for the onset of fatigue, there is a linear relationship between time-to-failure and hold time; $t_f = A + Bt_h$. For a given strain rate, as the frequency increases so does the number of cycles to failure. But this relationship levels at around 0.05 Hz. After this point, the number of cycles rapidly decreases as the frequency is increased [62].

Generally, the definition of fatigue failure is when a specimen completely separates. With regards to electronics, failure may occur sooner as electrical connections are intermittent or electrical resistance changes to a point the equipment becomes unreliable. Solder joint connection can be so small that failure occurs during the microcrack stage. Fine lists 4 criterion by which to determine a solder joint failure by fatigue [62].

1) Sudden reduction in maximum stress – An increase of dislocation (microscopic flaws in the crystal lattice of the solder joint) density due to plastic strain cycling causes work hardening. But when the load is removed the dislocation density reduces causing recovery. Quickly, the material will become balanced between work hardening and recovery cycles to establish a steady state, maximum stress curve. This can last for several cycles until there is an abrupt drop in maximum stress as shown in Fig. 2-23 [62].

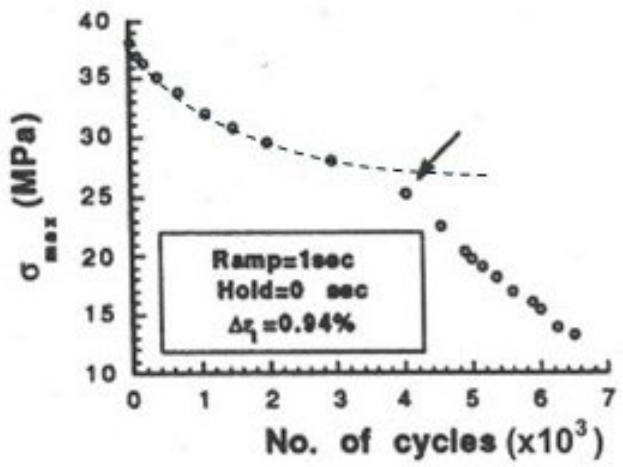


Fig. 2-23: Number of cycles to abrupt drop in maximum stress
Adapted from [62].

2) Sudden change in $\sigma_{max}/\sigma_{min}$ ratio – This ratio is almost constant but will suddenly drop when a significant change in a crack size occurs as shown in Fig. 2-24 [62].

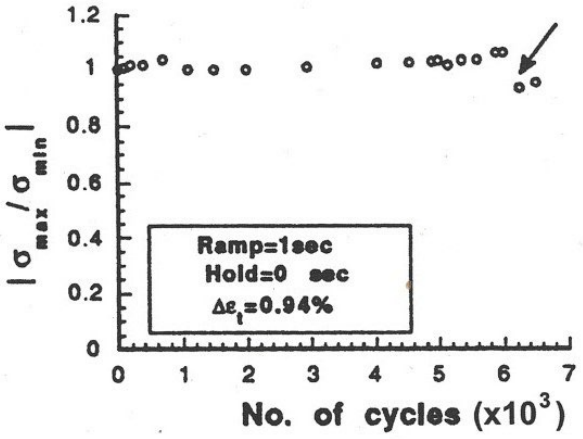


Fig. 2-24: Number of cycles to sudden change in max/min stress ratio
Adapted from [62].

3) Higher homologous temperatures – Higher temperatures promote crack nucleation sooner with the addition of creep strain.

4) Electrical resistance – Electrical resistance increases from crack nucleation and as microcracks lengthen. Establishing a criterion for unacceptable resistance would define a failure by this method.

#### 2.3.3.3 Intermetallic Compounds (IMC)

Intermetallic compounds (IMCs) are compounds introduced during soldering at the boundary of the liquid solder and the metal surfaces of the PCB which it comes into contact. IMCs are an absolute must because it is the formation of these compounds that provide the bond of the solder joint. They are composed of the elements present in the solder alloy, the copper of the SMT pad, and applicable elements of the surface finish. However, the mechanical properties of the IMCs greatly contrast with those of the solder alloy and the metals of the SMT pad. Solder, being considered soft with a reasonably low melting temperature, has very good electrical conductivity. IMCs are brittle with high melting temperatures with poor electrical conductivity. Immediately after soldering, the IMC layer is very thin, but the initial layer varies with solder liquidus temperature, contact intimacy with SMT pad, and time. Over time the IMC layer grows. As the IMC layer becomes thicker, the solder joint becomes more brittle [2]. Even before the solder is applied to a PCB during assembly, lead-free alloys can develop IMCs within bulk solder. Unlike Pb in Sn-Pb alloys, the Ag and Cu in Sn-Ag-Cu alloys form intermetallic compounds with Sn [72].

The most prevalent IMCs that form between Sn-Ag-Cu alloys at a copper pad are $Cu_6Sn_5$ and $Cu_3Sn$. These IMCs are seen in solder joints with copper pads having immersion silver, immersion tin, or OSP finishes. The $Cu_3Sn$ IMC layer forms adjacent to the copper pad while the $Cu_3Sn_5$ forms between the $Cu_3Sn$ IMC layer and the Sn-Ag-Cu solder alloy. These two IMC layers are similarly observed when a Pb-Sn alloy is applied to a copper pad with the same

finishes [72]. A scanning electron microscope (SEM) image of the two IMC layers are shown in Fig. 2-25 [73].

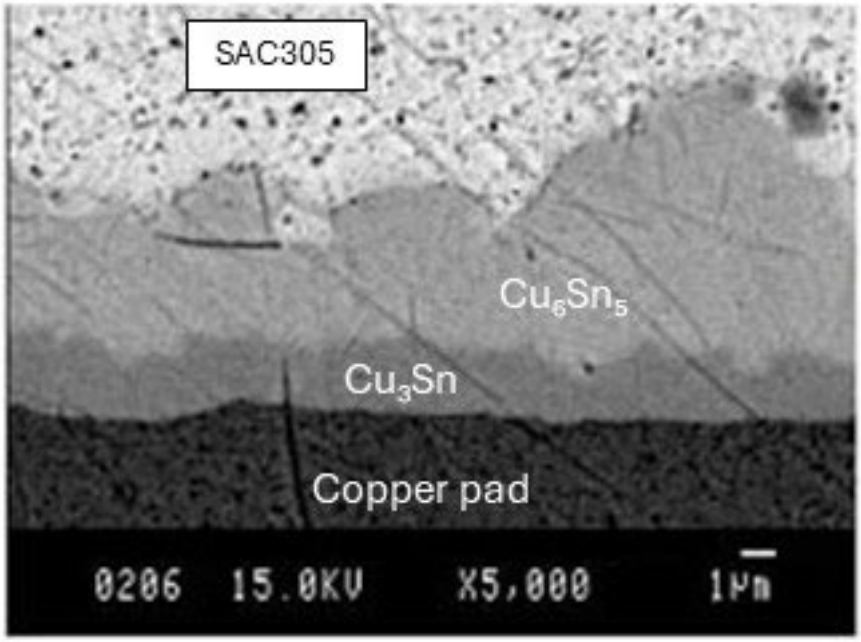


Fig. 2-25: $Cu_3Sn$ and $Cu_6Sn_5$ IMC layers on copper pad with SAC305 solder. Adapted from [73].

Copper pads finished with ENIG are considered for high-end applications. ENIG finishes renders excellent solder joint reliability but also introduces other IMCs that inadvertently cause reliability concerns [74]. The electroless plating of the nickel layer on a copper pad has limited amounts of phosphorus. The ENIG finishing process submerges PCBs in a bath of nickel-phosphorus alloy to deposit the layer of nickel on the copper pads. This process leaves small amounts (between 2% to 14%) of phosphorus being deposited into the nickel layer [75]. Depending on the concentration of phosphorus, $Ni_3P$ and $Ni_2$-P-Sn IMCs form on the nickel-plated surface finish [74]. One of the first and mostly widely observed IMCs to form when solder is applied to a Ni finish is $Ni_3Sn_4$ [72]. Some solder joints with Ni finishes have shown

$Ni_3Sn_2$ to form as well [74]. These IMCs are particularly found in Sn/Ni and Sn-Ag/Ni solder joints [72]. However, it is not uncommon for $Ni_3Sn_4$ to also form with Sn-Ag-Cu/Ni solder joints [76].

The formation of the Cu-Ni-Sn ternary IMCs have become the leading IMCs associated with Sn-Ag-Cu solder alloys when soldered to ENIG finished surfaces. The $(Cu,Ni)_6Sn_5$ and $(Ni,Cu)_3Sn_4$ IMCs are found to form along the Sn-Ag-Cu/Ni interface. Also, trace amounts of gold from the ENIG finish that dissolved during the soldering process can form $AuSn_4$ IMCs. The Cu-Ni-Sn ternary and $AuSn_4$ IMCs can be seen in Fig. 2-26 [72], [77]

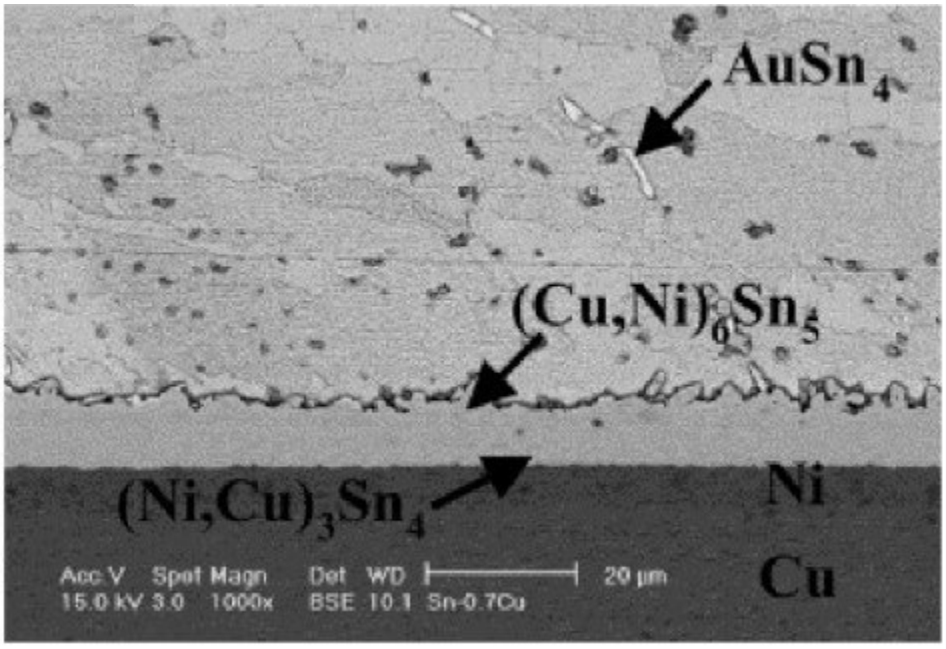


Fig. 2-26: Sn0.7Cu/Ni BGA solder joint SEM micrograph aged for 100 days at 170 °C. Adapted from [77].

One IMC that forms in bulk Sn-Ag-Cu solder is $Ag_3Sn$. It can be found frequently in SAC305 solder joints or other lead-free solder joints where the solder has a high level of silver in the alloy. Unlike most IMCs, the presence of $Ag_3Sn$ helps to prevent or lower crack growth which improves a solder joints' strength. Due to this characteristic, Sn-Ag-Cu solder joints with higher

silver content exhibit better thermal fatigue properties than SAC alloys with lower silver content [78]. However, $Ag_3Sn$ can also grow and coarsen like all IMCs which would counter its strength improving characteristics and render a solder joint less reliable [79]. The formation of $Ag_3Sn$ IMCs is shown in Fig. 2-27 [78].

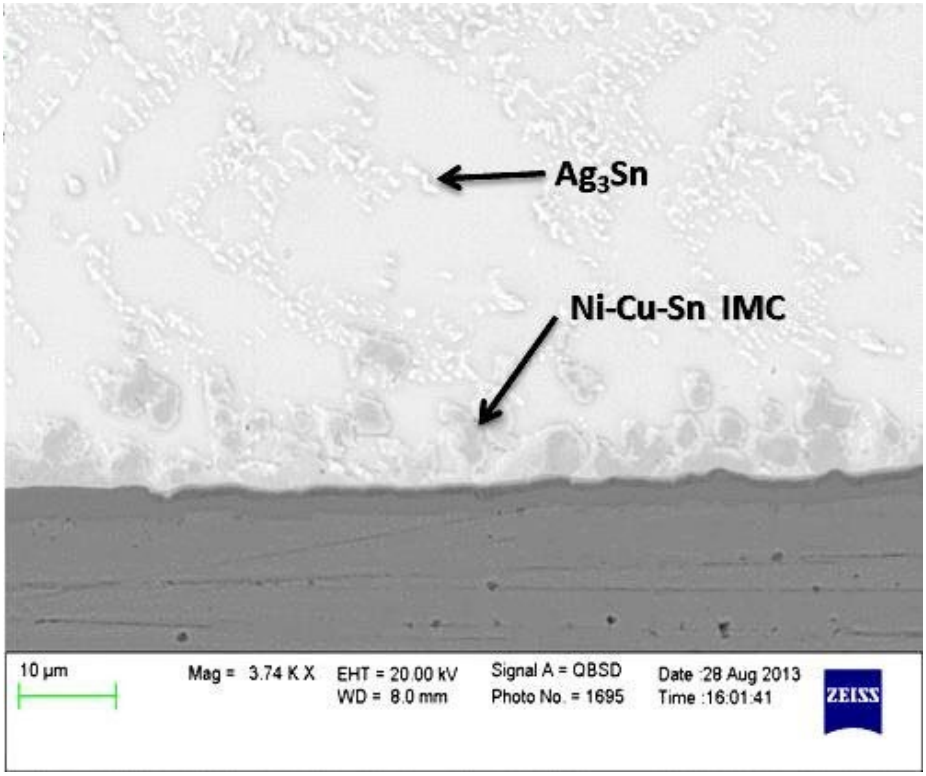


Fig. 2-27: SAC305 solder joint on ENIG, no aging.
Source [78].

The formation of IMCs starts during the liquid state when the solder is applied to an electronic assembly. Once the solder joint has solidified, the IMCs then exhibit growth that is temperature dependent. The rate of formation/growth of IMCs is dependent on the physical state of the solder, the level of elements within the solder alloy and copper pad finish, and the temperature at which the compounds are formed and exposed. For example, solder alloys with higher levels of Sn will have higher rates of interdiffusion. This suggests that SAC solder alloys will have higher

formation and growth rates of Cu-Sn and Ni-Sn IMCs that eutectic Sn-Pb solder alloys [80]. Additionally, the level of Cu in a SnAgCu solder alloy affects the IMC formations and shear reliability of the solder joint. Flip chip solder joints were tested with four different SnAg solder alloys with Cu content of 0%, 0.5%, 1%, and 2%. The shear testing results showed that although the solder joints presented equivalent shear strength, the location of the failure was different. At 0% copper, the failure site was either at the interface of the solder joint/PCB pad or the die of the flip chip cracked. At 0.5% copper, the failure site was either in the bulk solder joint or the interface with the PCB pad. At 1% copper, the failure site was at the interface of the solder joint/die. And at 2% copper, the failure was solely within the bulk solder joint. The failure locations are illustrated in Fig. 2-28 [12].

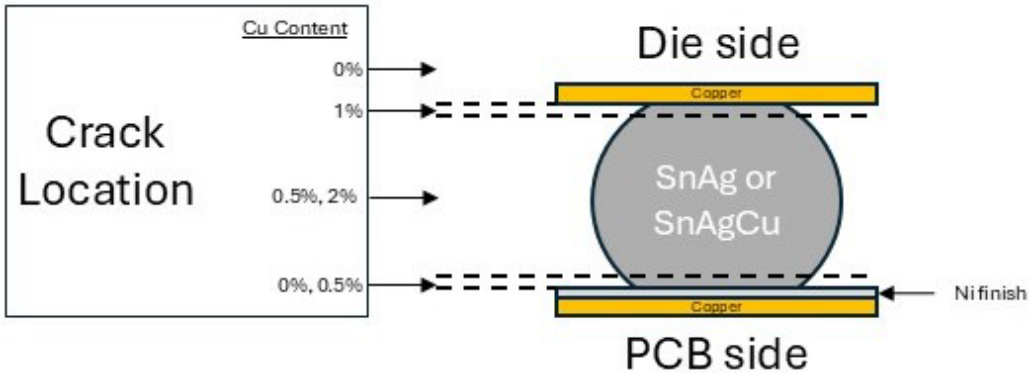


Fig. 2-28: Flip chip solder joint crack location relative to Cu content in solder. Adapted from [12].

The Cu content also affects IMC formations. At the Ni finish, as the copper concentration increased to 2%, the only IMC observed was $(Cu,Ni)_6Sn_5$. The formation and thickness of IMCs with Ni became more suppressed as the Cu concentration increased. Moreover, the predominate growth of CuSn IMCs, in turn promoted the growth of $Ag_3Sn$ IMCs within the bulk solder. The

formation of IMCs for the flip chip solder joints tested in regard to the level of Cu in the solder are presented in Table XII [12].

TABLE XII
EFFECTS OF CU CONTENT IN SOLDER ON NI IMC FORMATION
ADAPTED FROM [12].

| **Die Side** | | | |
|---|---|---|---|
| Cu | Cu | Cu | Cu |
| $(Cu,Ni)_6Sn_5$ | $(Cu,Ni)_6Sn_5$ | $(Cu,Ni)_6Sn_5$ | $(Cu,Ni)_6Sn_5$ |
| SnAg (0% Cu) | SAC305 (0.5% Cu) | SAC3010 (1% Cu) | SAC3020 (2% Cu) |
| $(Ni,Cu)_3Sn_4$ NiPSn (500 nm) $Ni_3(P,Sn)$ (300nm) | $(Cu,Ni)_6Sn_5$ NiSnP + $Ni_3(P,Sn)$ (250 nm) | $(Cu,Ni)_6Sn_5$ NiSnP (240 nm) | $(Cu,Ni)_6Sn_5$ |
| Ni finish | Ni finish | Ni finish | Ni finish |
| Cu | Cu | Cu | Cu |
| **PCB Side** | | | |

This simplifies the IMC structure in the solder joint. Multiple IMCs with layers and thicknesses having different CTEs introduce additional failure points. By having a single IMC, the IMC layer got stronger, forcing the point of failure to the more ductile part of the solder joint. Even though the shear strength of the solder joint remained unchanged due to the increased Cu content, the solder joint's reliability improved regarding drop shock due to relocating the failure point to the bulk solder [12].

There have been studies researching the use of solder alloy additives to help control the growth of IMCs. This generally involves converting a binary or ternary solder alloy into a ternary or quaternary alloy respectively by adding elements. Ramli et al summarized the effects of additives on IMC formation and growth as being "substantial." Noting that additives will alter the microstructure of the solder alloy (i.e. solidus and liquidus temperatures), the additional elements

can change the final IMC thicknesses, the rate of growth, and the formations of IMCs at the solder interface. A summary of alloy additives on IMC thickness captured by Ramli is shown in Table XIII [77].

TABLE XIII
LEAD-FREE SOLDER ADDITIVES' INFLUENCE ON IMC GROWTH
ADAPTED FROM [77].

| Solder Alloy | Alloy Additive | Effect on IMC Thickness |
|---|---|---|
| Sn-4Ag | Zn | Decrease |
| Sn-0.5Cu | Al | Decrease |
| Sn-0.7Cu | Al | Decrease |
| | Cr | Decrease |
| | In | Decrease |
| | Ni | Decrease |
| | P | Increase |
| Sn-0.5Ag-0.7Cu | Ga | Decrease |
| Sn-2.8Ag-0.5Cu | Bi | Unchanged |
| Sn-3.0Ag-0.5Cu | Sb | Unchanged |
| | Fe | Unchanged |
| | In | Unchanged |
| | Ge | Increase |
| | Co | Decrease |
| Sn-3.8Ag-0.7Cu | Nd | Decrease |
| | Mo | Decrease |
| | Co | Decrease |
| | Zn | Decrease |
| Sn-3.9Ag-0.7Cu | La | Decrease |
| Sn-0.7Cu-0.05Ni | Bi | Unchanged |
| Sn-0.7Cu-0.2Ni | In | Increased |

When electronic assemblies are aged at elevated temperatures, IMCs grow in thickness. For example, a SAC305 solder joint with an OSP finish exhibited formation of a very thin layer of $Cu_3Sn$ adjacent to the pad with a thick layer of $Cu_6Sn_5$ between the $Cu_3Sn$ IMC and SAC305 solder alloy shortly after assembly [81]. The energy needed to activate the growth of $Cu_6Sn_5$ is lower than what is needed for $Cu_3Sn$. This explains why the initial layer of $Cu_6Sn_5$ is larger than

the layer of $Cu_3Sn$ after soldering. After the soldering process, the IMCs layer begins to expand when exposed to elevated temperatures. The higher the temperature, the faster the layer expands [77]. When the same solder joint was exposed to 100 °C for 120 hours, the IMC layers both grew in thickness. This observation is shown in Fig. 2-28 [81].

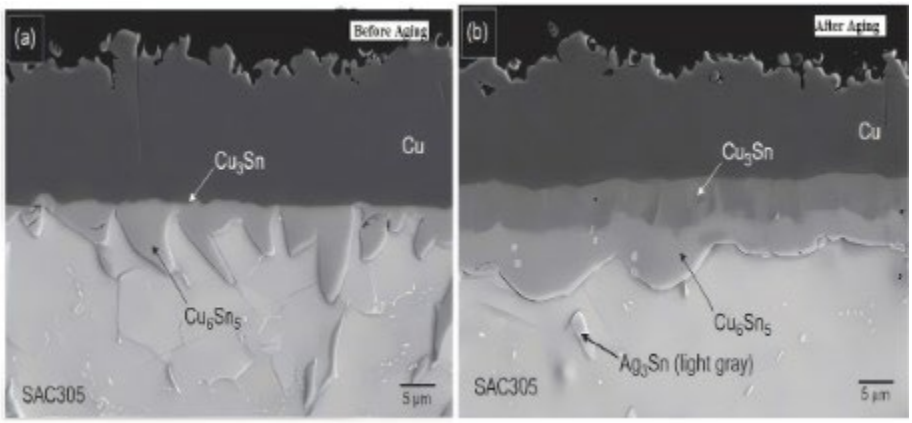


Fig. 2-29: IMC formation and growth to a SAC305 solder joint when aged. Source [81].

Not only do higher temperatures trigger the growth of IMCs but the way the elevated temperatures are applied contribute differently to the growth. Lau and Lee refer to a study that related IMC growth to the type and duration of heat exposure. The study tested samples exposed to thermal aging, thermal cycling, and thermal shock. The exposure time was the same for all three with the thermal aging being at 125 °C at 100% of the time while the thermal cycling and thermal shock were exposure to 125 °C less than 50% of the time. The initial thought was that isothermal aging would result with the most IMC growth since it was exposed to the maximum temperature the longest. Upon review, thermal shock and thermal cycling both had larger IMC layer growth than isothermal aging. It was concluded that the solder joint experienced greater levels of stress due to the changing temperatures. The stress of thermal cycling and thermal shock produced higher energy levels which act as a catalyst for IMC formation. The growth of

IMC thickness for a SAC387 solder joint with ENIG finish when exposed to thermal aging, thermal cycling, and thermal shock is shown in Fig. 2-30 [12].

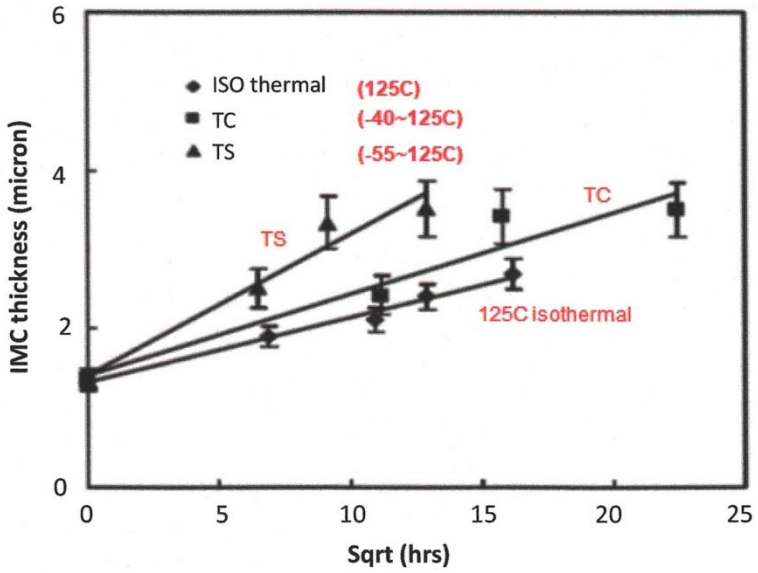


Fig. 2-30: The application of heat on IMC growth for SAC387 joint on NiAu finish. Source [12].

Research has discovered that the volume of solder can influence IMC thickness. Ramli referred to several studies of reflowing Sn-Ag-Cu solder of different size solder spheres to examine the formation of IMCs. The studies discovered that the smaller the solder sphere, the thicker the IMC layers. The rationale for this observation was that the concentration of Cu in the smaller spheres intensified faster than larger spheres for the same size copper pad with and without surface finishes [77].

## 2.4 Lead-Free Solder Joint Reliability

The mechanical and electrical attachments between the PCB and the components are accomplished by solder joints. The reliability of an electrical product depends heavily on the quality of the solder joints. Solder joint cracking due to stresses from thermal or mechanical loading can introduce intermittent or complete openings of electrical circuitry. The reliability of solder joints is expected to be greater than the reliability of the components and the PCB for the entire life of the product. This means that product failures during the functional life should not come from failed solder joints. Solder joint failures occur during infant mortality and wear-out life [82]. All three reliability periods of a product's life cycle are shown in Fig. 2-31 [83].

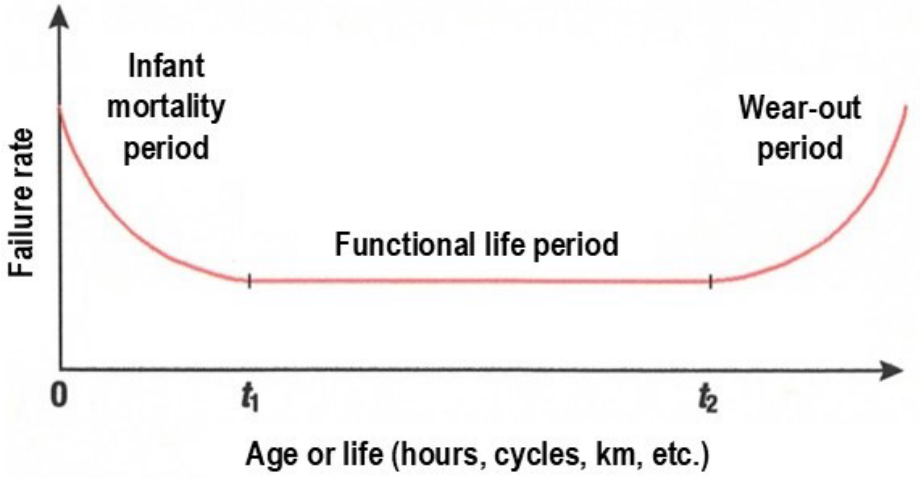


Fig. 2-31: Idealized bathtub failure rate curve.
Adapted from [83].

The three periods of failure outlined in the bathtub curve are described [83]:

1. Infant Mortality Period – The failure rate decreases rapidly during the initial release of a product. This time period is generally referred to as the "burn-in" or "debugging" period. Some companies will perform in-house burn-in testing to reduce or eliminate product failures during this period after the product is made available.

2. Functional Period – This is the period in which a product experiences a constant failure rate. This failure rate is usually the reliability established during the design of the product.
3. Wear Out Period – This period starts at the end of the useful life of a product. The failure rate increases. This is when replacement or major repair efforts are conducted.

The reliability and failure rate of a product is determined using the probability distribution function. An example of a probability distribution function, $f(t)$, is shown in Fig. 2-32 [83].

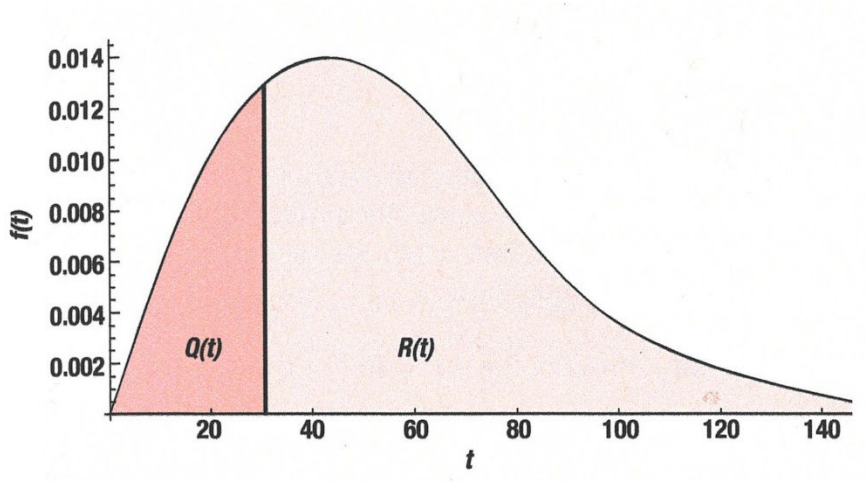


Fig. 2-32: Probability distribution function.
Source [83].

Whereas unreliability is [83]:

$$Q(t) = \int_0^t f(t)\, dt \tag{2.27}$$

Reliability is [83]:

$$R(t) = \int_t^\infty f(t)\, dt = 1 - Q(t) \tag{2.28}$$

Reliability can also be expressed in terms of percentiles of product life where the $B_\alpha$ life is the period it takes for a percentage, α, of the products to fail [83]:

$$R(B_\alpha) = 1 - \frac{\alpha}{100} \tag{2.29}$$

And because the integral of the probability distribution function must equal 1 [83]:

$$\int_0^\infty f\,(t)\,dt = 1 \tag{2.30}$$

The failure rate (or hazard rate), $h(t)$, is expressed as [83]:

$$h(t) = \frac{f(t)}{R(t)} \tag{2.31}$$

The mean time to failure, MTTF, is expressed as [83]:

$$MTTF = \int_0^\infty tf(t)\,dt = \int_0^\infty R(t)\,dt \tag{2.32}$$

The probability distribution functions follow two models: 1) discrete and 2) continuous. Reliability and failure rate are frequently modeled by two discrete and five continuous distributions. Binomial and Poisson are the discrete distributions while normal, lognormal, exponential, Weibull and gamma are the continuous distributions. The functions for discrete distributions are termed probability mass functions (pmf) and for continuous distributions are termed probability density functions (pdf) [83].

Discrete distributions are built around a distinct, random variable that is countable. The binomial distribution is a probability distribution where only two mutually exclusive results can occur for a given trial. For example, for 10 flips of a coin, the results would be heads/not-heads or tails/not-tails. For 10 rolls of a die, the results would be one/not-one, two/not-two, three/not-three and so forth. The pmf, $f(x)$, for a binomial distribution calculates the probability of $k$ results for a given number of trials $m$ with a probability of success $p$ as [83]:

$$f(k) = \left(\frac{m!}{k!(m-k)!}\right) p^k (1-p)^{m-k} \tag{2.33}$$

Where the binomial distribution mean, μ, is provided by [83]:

$$\mu = mp \tag{2.34}$$

And the variance provided by [83]:

$$\sigma^2 = mp(1-p) \tag{2.35}$$

Where the number of trials is very high (1,000) and the probability of success is very low (0.01), the Poisson distribution can be used in lieu of a binomial distribution [84], [83]. The pmf, *f*(*x*), for the Poisson distribution calculates the probability for *k* results as [83]:

$$f(k) = \frac{\mu^k}{k!} e^{-\mu} \tag{2.36}$$

Where the Poisson distribution mean and the variance are provided by [83]:

$$\mu = \sigma^2 = mp \tag{2.37}$$

Continuous distributions are characterized by having a random variable that extends over time (or a real number). Reliability of a product is categorized in time to failure. Being that continuous distributions are pdfs the distribution can't be summed. It must be integrated. Therefore, the generic pdf for a continuous distribution is given as [83]:

$$f(x) = \frac{d}{dx} F(x) \tag{2.38}$$

Where *F*(*x*) is the cumulative distribution function (cdf) representing a particular continuous distribution model. The generic means of a continuous distribution function is given as [83]:

$$\mu = \int_{-\infty}^{+\infty} x f(x)\, dx \tag{2.39}$$

With the generic variance of a continuous distribution function given as [83]:

$$\sigma^2 = \int_{-\infty}^{+\infty} x^2 f(x)\, dx - \mu^2 \tag{2.40}$$

### 2.4.1 Weibull Distribution

Due to the broad range of failure rate curves that can be model, the Weibull distribution is the most used distribution for reliability modeling. The Weibull distribution is based on three parameters that define the pdf as [83]:

$$f(t) = \beta\eta^{-\beta}(t-\gamma)^{\beta-1}e^{-\left(\frac{t-\gamma}{\eta}\right)^{\beta}} \tag{2.41}$$

Where $\gamma$ is the location (or time delay) parameter, $\beta$ is the shape parameter, and $\eta$ is the scale parameter [83]. If the pdf is integrated with $\beta > 0$ and $\eta > 0$, reliability is calculated as [83]:

$$R(t) = e^{-\left(\frac{t-\gamma}{\eta}\right)^{\beta}} \tag{2.42}$$

And the failure rate is given by [83]:

$$h(t) = \frac{\beta}{\eta}\left[\frac{t-\gamma}{\eta}\right]^{\beta-1} \tag{2.43}$$

The MTTF is calculated by [83]:

$$MTTF = \gamma + \eta + \Gamma\left(\frac{1}{\beta} + 1\right) \tag{2.44}$$

Where Γ(n) refers to the value referenced from the Gamma function table. And the standard deviation is calculated by [83]:

$$\sigma = \eta\sqrt{\Gamma\left(\frac{2}{\beta} + 1\right) - \Gamma^2\left(\frac{1}{\beta} + 1\right)} \tag{2.45}$$

The shape parameter controls the shape of the failure rate curve. When $\beta > 0$ and $\beta < 1$ for a given $\eta$ and $\gamma$, the failure rate decreases with time represented by curves of the infant mortality period. When $\beta = 1$, the failure rate becomes constant with time as represented during the functional life period. This is a distinct situation of a Weibull distribution that is examined under

the exponential distribution (discussed later). When $\beta > 1$, the failure rate increases with time represented by curves of the wear-out period. These relationships are shown in Fig. 2-33 [83].

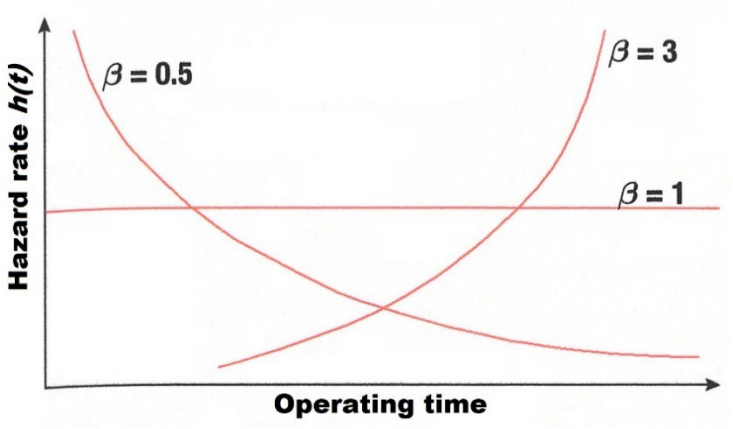


Fig. 2-33: Weibull shape parameter's effect on failure rate, where $\eta = 1$ and $\gamma = 0$. Adapted from [83].

The shape parameter also influences the pdf which is shown in Fig. 2-34 [83].

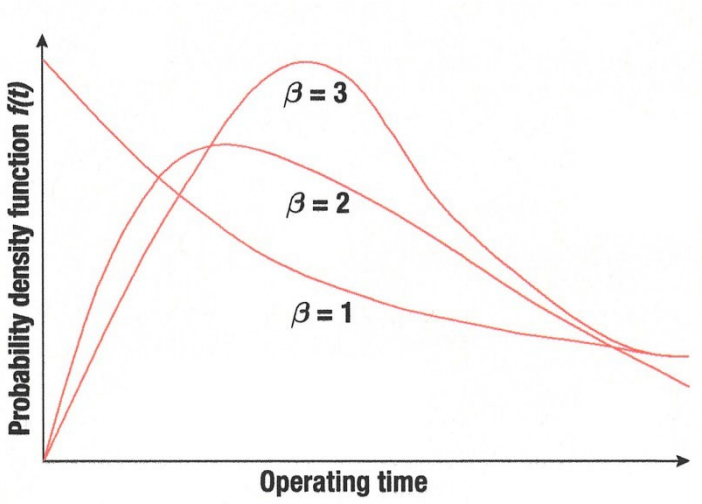


Fig. 2-34: Weibull shape parameter's effect on probability density function ($\eta = 1$; $\gamma = 0$). Source [83].

The scale parameter stretches or shrinks the pdf put maintains the original starting point and curve's outline as shown in Fig. 2-35 [83].

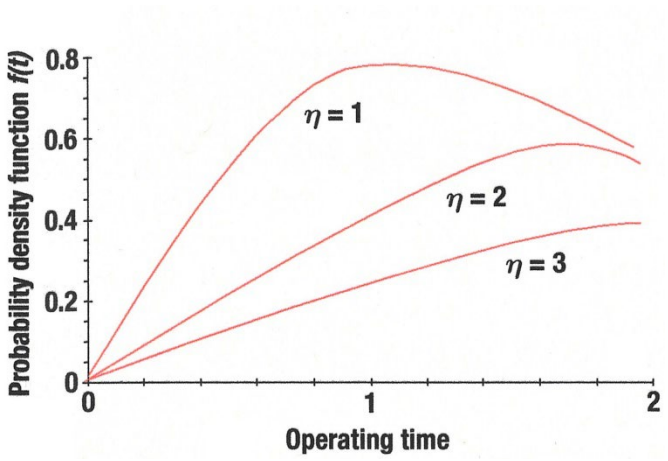


Fig. 2-35: Weibull scale parameter's effect on probability density function ($\beta = 2$; $\gamma = 0$). Source [83].

The location parameter simply moves the starting point along the time axis (operating time). When pdf starts at zero, $\gamma$ is equal to zero. When $\gamma > 0$, the starting point moves to the right of the time axis. However, when $\gamma < 0$, this puts the starting time to the left of time zero. This is viewed as failures occurring during storage or transport before the product is put into use. This is modeled by calculating a pmf value at t = 0 and starting the pdf from that point. This is illustrated in Fig. 2-36 [83].

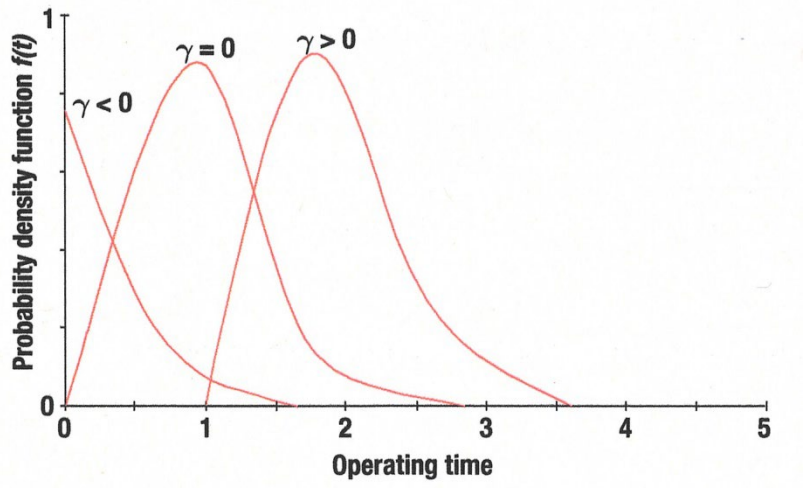


Fig. 2-36: Weibull location parameter's effect on probability density function ($\beta = 2$; $\eta = 1$). Source [83].

The three-parameter Weibull pdf is used in situations where the failure rates are increasing or decreasing for products being debugged or wearing out such as electronic parts or parts subjected to corrosion and fatigue strength [12]. When the location parameter, $\gamma$, is zero, this is referred to as the two-parameter Weibull. Simultaneously, when the shape parameter, $\beta$, equals 1, the Weibull simply becomes an exponential distribution which is used to determine constant failure rates during the useful life period [83].

### 2.4.2 Lognormal Distribution

The lognormal distribution applies to several engineering conditions. Strength of metals, dimensions of structural elements, biological parameters are some of the conditions. It has been applied in reliability modeling to describe fatigue failures and model time to repair [83]. The time-to-failure follows a lognormal distribution which would mean that the natural logarithm of the time-to-failure would follow a normal distribution. The pdf for a lognormal distribution is given by [12]:

$$f(t) = \frac{1}{\sigma t\sqrt{2\pi}} exp\left[\left(-\frac{1}{2}\right)\left(\frac{\ln t-\mu}{\sigma}\right)^2\right] \tag{2.46}$$

Whereas $\sigma$ (also referred as $\sigma'$) is the standard deviation (shape parameter) and $\mu$ (also referred as $\mu'$) is the mean (scale parameter) of the natural logarithm of $t$ which follows a normal distribution. So, the MTTF of the lognormal distribution is [12]:

$$MTTF = exp\left[\mu + \frac{\sigma^2}{2}\right] \tag{2.47}$$

And the variance is [12]:

$$\sigma^2_{lognormal} = \left(e^{\sigma^2} - 1\right)e^{2\mu+\sigma^2} \tag{2.48}$$

The reliability of a lognormal distribution is calculated by [12]:

$$R(t) = 1 - \frac{1}{\sigma\sqrt{2\pi}} \int_t^{\infty} exp\left[-\frac{(\ln t - \mu)^2}{2\sigma^2}\right] dt \tag{2.49}$$

With the failure rate being expressed as [12]:

$$h(t) = \frac{\frac{1}{\sigma t\sqrt{2\pi}} exp\left[-\frac{(\ln t - \mu)^2}{2\sigma^2}\right]}{1 - \frac{1}{\sigma\sqrt{2\pi}} \int_t^{\infty} exp\left[-\frac{(\ln t - \mu)^2}{2\sigma^2}\right]} \tag{2.50}$$

The scale parameter (also referred to as the location value) influences the location parameter, $e^{\mu}$. As $\mu'$ increases for a given $\sigma'$, the skewness of the pdf and failure rate decreases (goes from positive to negative) as shown in Fig. 2-37 and Fig. 2-38 [85].

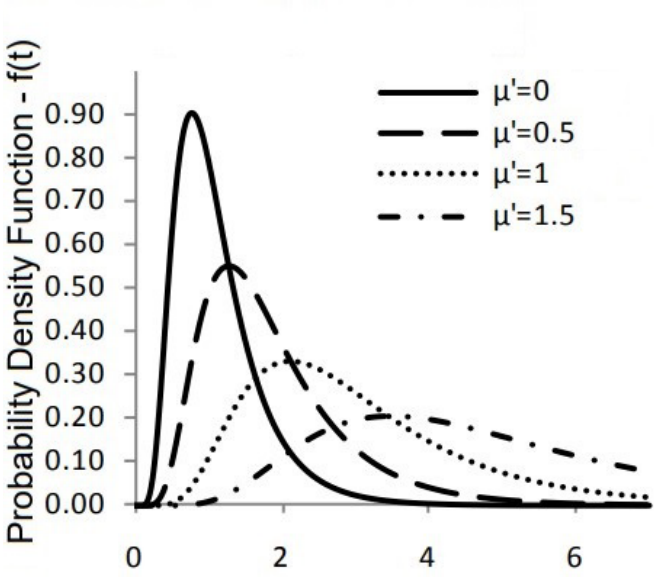


Fig. 2-37: Effects of $\mu'$ on lognormal pdfs ($\sigma' = 1$).
Adapted from [85].

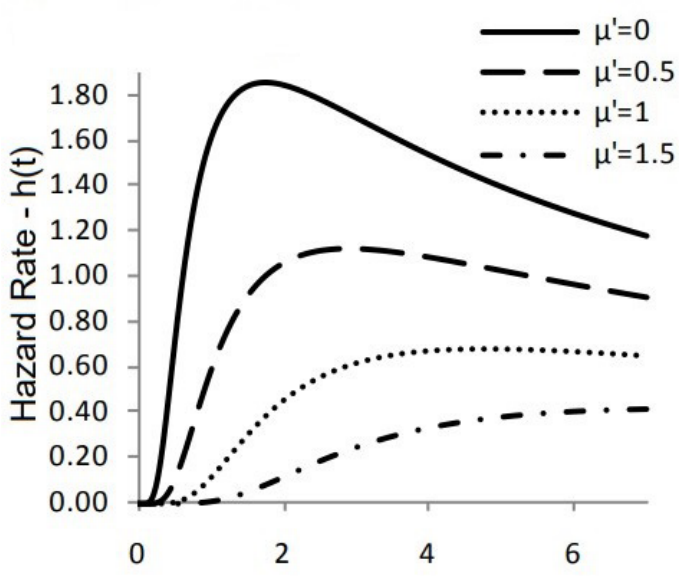


Fig. 2-38: Effects of $\mu'$ on lognormal hazard rates ($\sigma' = 1$).
Adapted from [85].

The shape parameter also affects the skewness of the lognormal pdf. As $\sigma'$ increases, the skewness increases (becoming more positive) for the pdf and failure rate as shown in Fig. 2-38 and Fig. 2-39 [85].

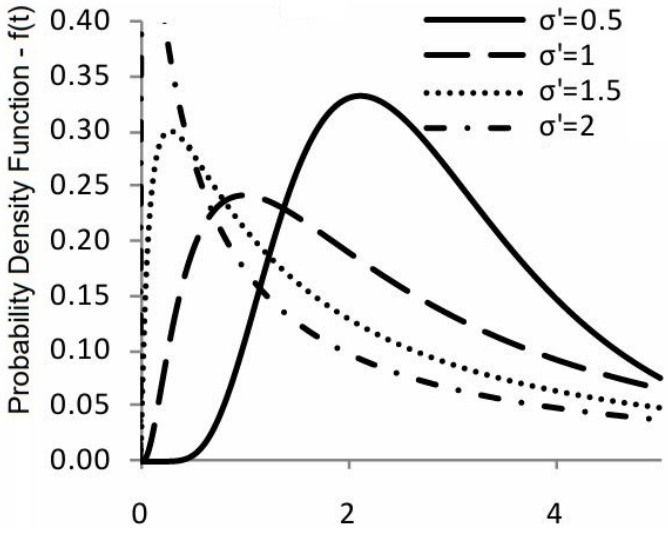


Fig. 2-39: Effects of $\sigma'$ on lognormal pdfs ($\mu' = 1$).
Adapted from [85].

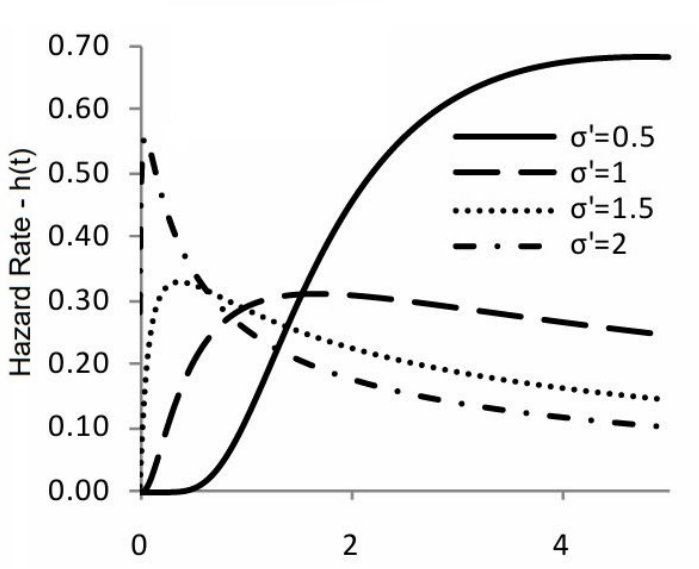


Fig. 2-40: Effects of $\sigma'$ on lognormal hazard rates ($\mu' = 1$).
Adapted from [85].

### 2.4.3 Probability Plots

By using probability plots, the failure data can be used to determine a probability density function for reliability. Computer software is typically used to hypothesize the distribution and calculate the distribution parameters. The time-to-failure (e.g., cycles-to-failure) are arranged from shortest to longest. A reliability estimate is selected. The data are plotted alongside a notional distribution with expectations that the data points will be linear to the hypothesized distribution. The plot is performed on probability plotting graphs with the x-axis representing the time-to-failure and the y-axis representing the unreliability percentage. A straight line is then drawn through the points that best captures a linear relationship of those points [83].

The time-to-failure points are pulled directly from testing or product in service. The unreliability estimate is determined from several techniques: 1) “midpoint plotting position”; 2) “expected plotting position”; 3) “median plotting position”; 4) “median rank”; and 5) Kaplan-Meier ranks

(software specific). An example of a list of these unreliability estimates for an unspecified cdf is shown in Fig. 2-41 [83].

| | Estimate of cumulative distribution function or unreliability | | | |
|---|---|---|---|---|
| Rank order (*i*) | Midpoint plotting position | Expected plotting position | Median plotting position | Median rank |
| 1 | 2.5 | 4.8 | 3.4 | 3.406 |
| 2 | 7.5 | 9.5 | 8.3 | 8.251 |
| 3 | 12.5 | 14.3 | 13.2 | 13.147 |
| 4 | 17.5 | 19.0 | 18.1 | 18.055 |
| 5 | 22.5 | 23.8 | 23.0 | 22.967 |
| 6 | 27.5 | 28.6 | 27.9 | 27.880 |
| 7 | 32.5 | 33.3 | 32.8 | 32.795 |
| 8 | 37.5 | 38.1 | 37.7 | 37.710 |
| 9 | 42.5 | 42.8 | 42.6 | 42.626 |
| 10 | 47.5 | 47.6 | 47.5 | 47.542 |
| 11 | 52.5 | 52.4 | 52.5 | 52.458 |
| 12 | 57.5 | 57.1 | 57.4 | 57.374 |
| 13 | 62.5 | 61.9 | 62.3 | 62.289 |
| 14 | 67.5 | 66.7 | 67.2 | 67.205 |
| 15 | 72.5 | 71.4 | 72.1 | 72.119 |
| 16 | 77.5 | 76.4 | 77.0 | 77.033 |
| 17 | 82.5 | 80.1 | 81.9 | 81.945 |
| 18 | 87.5 | 85.7 | 86.8 | 86.853 |
| 19 | 92.5 | 90.5 | 91.7 | 91.749 |
| 20 | 97.5 | 95.2 | 96.6 | 96.594 |

Fig. 2-41: Examples of cdf estimates per technique for sample sizes up to 20. Source [83].

After the probability plots have been constructed for different cumulative distribution functions, the "goodness" of the fit of those plots is part of deciding the best distribution that fits the data. The probability distributions are selected based on whether it fits the data and the physics of the failures. For example, both a lognormal and Weibull distribution may render very close fits to a particular set of data. Therefore, the specific nature of the failures can help determine which cdf would be best suited to proceed with analyzing the test data [83].

In contrast, all failures of a particular sample size can be caused by multiple failure mechanisms. This would make it difficult to identify a single cdf by which to model the unreliability even

when one or more distributions seem to fit the data well. This will lead to the distributions having poor predictability. In these cases, it would be better to separate the test data for each failure mode and then fit the distributions [83]. Data from a single sample size separated into two separate failure modes are fitted to two different Weibull distributions as shown in Fig. 2-42 [83].

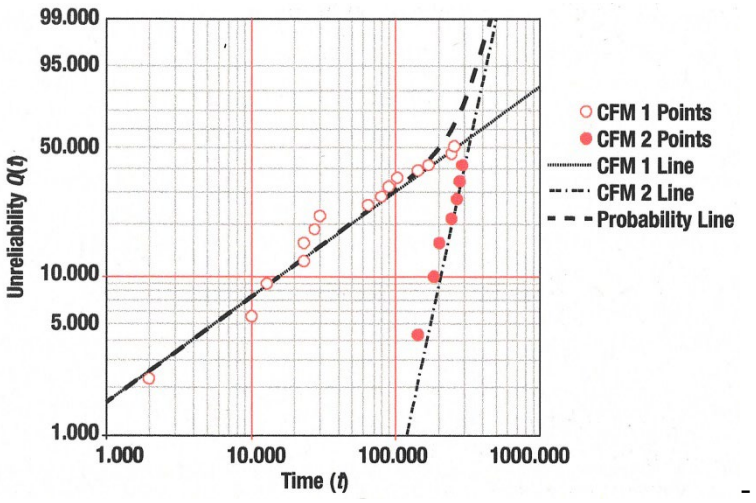


Fig. 2-42: Weibull probability plots for competing failure mechanisms.
Source [83].

Statistical analysis does not magically project the future. The results of analysis are highly dependent on the quality of defining the assumed distribution model and associated assumptions. Defining the modes of failure, validating the data, using the model correctly, and understanding the limits of extrapolation/interpolation are all part of the effort to establish the best distribution model. In the end, the cumulative distribution function (and probability distribution function) must be established by the test data. Guessing should not be used to determine the distribution [83].

# Chapter 3 Literature Review

A lot of research has been conducted in the areas discussed in Chapter 2. A large portion of research conducted has been around the use of SAC305. SAC305 has been tested and evaluated under a vast number of design considerations. SAC305 has been evaluated under shear and fatigue conditions. Some of those conditions included different surface finishes, different pad designs, and different solder joint configurations. Solder joint configurations ranged from individual solder balls on SMT pads to ball grid array (BGA) assemblies. Some of those test articles underwent accelerated aging while some were non-aged. Research has been conducted by expanding the SAC305 ternary composition to quaternary and pentanary compositions by adding "doping" elements such as Ni, Bi, and others in hopes of altering the mechanical and electrical properties to better suit the PCB assembly processes and end product applications.

The research identified in this chapter will be closely aligned to the research conducted in the follow-on chapters. The intent is to have previous test data that can be relatable to the data developed in this research. This will provide better analysis of the data obtained for drawing conclusions. It will also assist in determining possible errors made during the acquisition of the data. Previous research collected provides insight into what should or could be expected. In the minute areas that the previous research cannot be directly relatable to the research data generated herein, then areas of future research can be acknowledged.

## 3.1 Strength Testing

### 3.1.1 Effects of Bi on SAC Solder Joint Shear Properties

Belhadi et al conducted research on three different SAC solder alloys with different percentages of Bi. The test articles were constructed with a FR epoxy substrate comprising 121 individual SMT pads with an OSP finish with each having an 18 mil (0.46 mm) solder sphere. All the SMT pads were of a SMD design. The test articles were tested in as received and aged conditions. The composition of each solder alloy is shown in Table XIV [86].

TABLE XIV
SOLDER JOINT MAJOR CONSTITUENTS
ADAPTED FROM [86].

| Alloy name | Alloy composition | Melting temperature, °C |
|---|---|---|
| SAC305 | Sn, 3.0%Ag, 0.5%Cu | 217 |
| SAC-3Bi | Sn, 3.0%Ag, 0.5%Cu, 3.0%Bi | 205 |
| SAC-6Bi | Sn, 2.25%Ag, 0.5%Cu, 6.0%Bi | 205 |

The as received (unaged) test articles with the three different solder alloys were subjected to three different shear rates as outlined in Table XV [86].

TABLE XV
SUMMARIZES THE SHEAR TEST MATRIX
ADAPTED FROM [86].

| Solder alloy | Shear strain Rate $sec^{-1}$ | Sample size |
|---|---|---|
| SAC305 | 0.008<br>0.8<br>8 | 10<br>10<br>10 |
| SAC-3Bi | 0.008<br>0.8<br>8 | 10<br>10<br>10 |
| SAC-6Bi | 0.008<br>0.8<br>8 | 10<br>10<br>10 |

The testing showed that the average ultimate shear strength for the SAC alloys having Bi were higher than the SAC305 alloy across all three different strain rates. It was also noted that the average shear strength increased as the strain rate increased for all the alloys tested in an unaged condition. The results of these findings are illustrated in Fig. 3-1 [86].

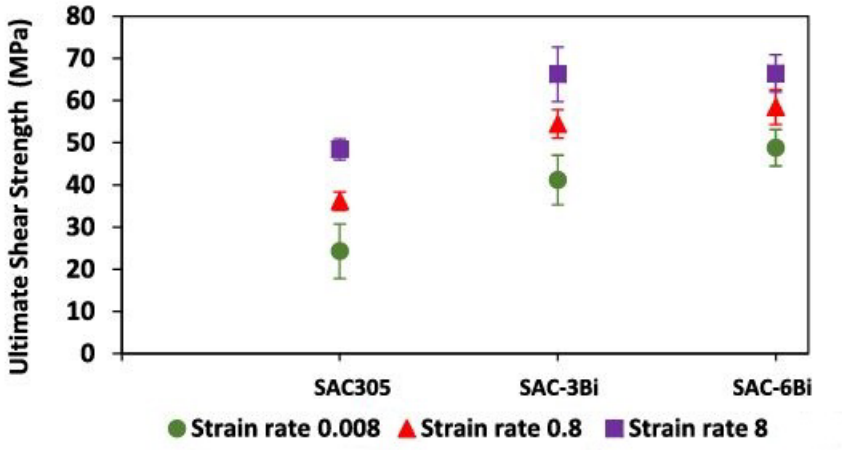


Fig. 3-1: Ultimate shear strength at different strain rates – 0 h.
Adapted from [86].

The presence of Bi in the alloy altered the solder joint microstructure by way of solid solution strengthening, the precipitate hardening, and the reducing the growth rate of the IMC layer. The research provided other observations. As the content of Bi increased, it correspondingly exhibits a decrease in fracture points. Also, as the Bi concentration increased, it rendered the solder joint more brittle. The brittle nature of the solder joints containing Bi was noted as becoming more brittle when aged [86].

### 3.1.2 Effects of Minor Ni Doping on SAC305 Performance

Fleshman et al tested SAC305 solder alloy against a SAC305 alloy doped with 0.1% Ni. Test articles were built with substrates comprising SMT pads with an OSP finish that was polished with $Al_2O_3$ particles no larger than 0.05 µm. Each SMT pad was soldered with an 11.8 mil (300

μm) solder sphere. All the SMT pads were of a SMD design. The test articles were tested in an as received condition. The test samples used two different solder alloys: 1) SAC305 and 2) SAC305-0.1Ni. All test articles were subject to a single, slow shear speed of 250 μm/sec. The sample size for all tests was 40. The peak shear forces (gram-force) of the unaged samples tested are shown in Fig. 3-2 [87].

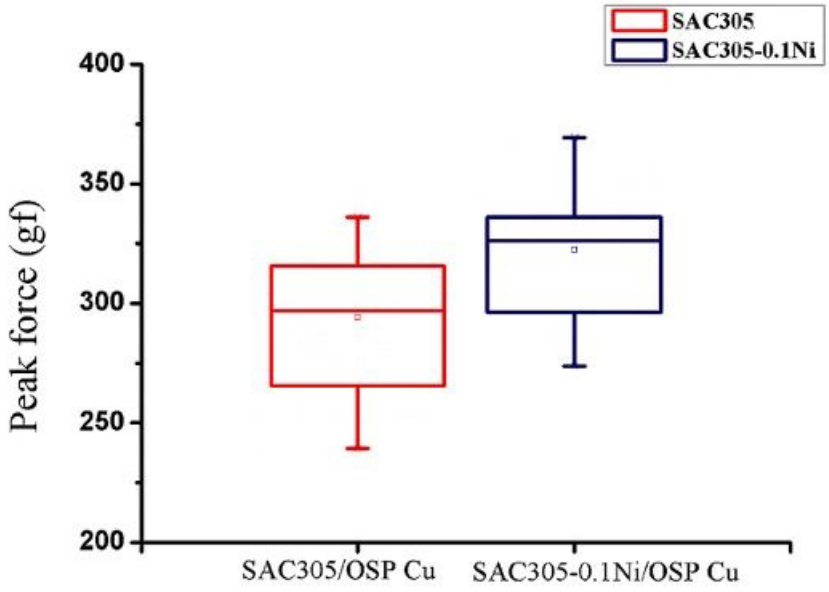


Fig. 3-2: Peak shear force of SAC305 and SAC305-0.1Ni
Adapted from [87].

When examining the grain structure of the solder joints, Ni contributed to the interlaced grain structure and finer IMCs precipitate of the SAC305 doped alloy leading to it having a higher shear strength. And with inducing a very slow speed of shear, failure occurred in the bulk solder instead of the IMC layer in both alloys. This type of failure is considered to fall into ductile fracture mode. The maximum, minimum, and average peak shear force and deviations recorded from the shear tests are shown in Table XVI [87].

TABLE XVI
AVERAGE SHEAR FORCE OF SAC305/SAC305-0.1Ni SOLDER JOINTS
ADAPTED FROM [87].

| | Peak Force (gf) | | | |
|---|---|---|---|---|
| **Alloy name** | **Maximum** | **Minimum** | **Average** | **Deviation** |
| SAC305 | 336.2 | 239.2 | 290.8 | 30.9 |
| SAC305-0.1Ni | 369.5 | 273.7 | 322.5 | 27.1 |

In a later study, Fleshman again tested the shear strength improvements of SAC305 solder, but this time lowered the Ni content of the SAC305 alloy to 0.05% [88]. Fleshman et al investigated shear property improvements that minor amounts of Ni would have on a SAC305 solder joint. Test articles were built with substrates comprising SMT pads with an OSP finish with each having an 11.8 mil (300 µm) solder sphere. All the SMT pads were of a SMD design. The test articles were tested in an as received and aged conditions. The test samples used three different solder alloys: 1) SAC305; 2) SAC305-0.05Ni; and 3) SAC305-0.1Ni. All test articles were subject to a single, slow shear speed of 250 µm/sec. The sample size for all tests was 50. The peak shear forces (gram-force) of the unaged samples tested are shown in Fig. 3-2 [88].

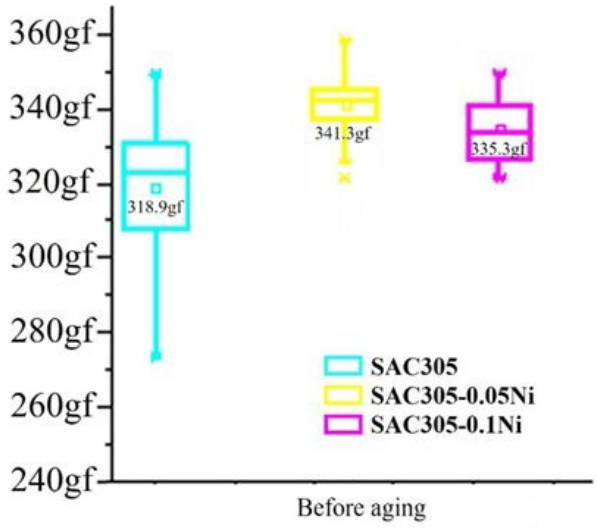


Fig. 3-3: Peak shear force of SAC305-xNi solder joints before aging.
Adapted from [88].

The addition of very small quantities of Ni in the SAC305 alloy improved the shear strength of the SAC305 solder joint. The testing did show that increasing the amount of Ni from .05% to 0.1% resulted in a slight decrease in shear strength from the SAC305-0.05Ni alloy; however, the shear strength of the SAC305-0.1Ni was still higher than SAC305. The Ni contributed to finer IMCs layers and interwoven grain structure. The peak shear force in the unaged shear tests and the deviation are shown in Table XVII [88].

TABLE XVII
AVERAGE SHEAR FORCE OF UNAGED SAC305-xNi SOLDER JOINTS
ADAPTED FROM [88].

| Alloy name | Average shear force (gf) | Deviation |
|---|---|---|
| SAC305 | 318.9 | 19.4 |
| SAC305-0.05Ni | 341.3 | 8.9 |
| SAC305-0.1Ni | 335.3 | 8.6 |

### 3.1.3 Improving the Strength of SAC305-0.1Ni by Adding Sb

Wang et al investigated the tensile properties of adding Sb to SAC305 doped with Ni. Though the experiment did not specifically test the shear properties of the alloys, the idea is that the tensile strength data will be similarly relatable to the shear strength the alloys would also have. The intent of this research was to find if the presence of Sb would increase the tensile strength of that alloy over SAC305 and SAC305-0.1Ni. Three different combinations of Sb with SAC305-0.1Ni were tested against SAC305 and SAC305-0.1Ni. The average particle size for Sb and Ni was 18.8 μm and 6.09 μm, respectively. The morphology of the Ni particles was round while the Sb particles exhibit a “lumpy” appearance. The melting temperatures were extracted from a differential scanning calorimetry (DSC) apparatus during thermal analysis. Multiple tests were conducted in this investigation on unaged and aged test articles. Tensile strength testing was conducted on unaged samples. The five solder alloys tested are identified in Table XVIII [89].

TABLE XVIII
COMBINATION OF Ni-Sb DOPED SAC305 ALLOYS
ADAPTED FROM [89].

| Alloy name | Wt% | | | Melting temperature* |
|---|---|---|---|---|
| | SAC305 | Ni | Sb | °C |
| SAC305 | 100 | - | - | 223.7 |
| SAC305-0.1Ni | 99.9 | 0.1 | - | 226.6 |
| SAC305-0.1Ni-1.5Sb | 98.4 | 0.1 | 1.5 | 228.6 |
| SAC305-0.1Ni-2.0Sb | 97.9 | 0.1 | 2.0 | 226.9 |
| SAC305-0.1Ni-2.5Sb | 97.4 | 0.1 | 2.5 | 228.8 |

* melting temperatures obtained from (DSC) apparatus during thermal analysis

The test samples were constructed by using the solder alloys in Table XVIII to solder two high quality, unoxidized copper strips together. The test samples were placed in an AG-X Plus for tensile strength testing. The tensile test was executed at room temperature at a strain speed of 0.2 mm/min. The sample size was 5 test samples. The construction of the test samples is shown in Fig. 3-4 [89].

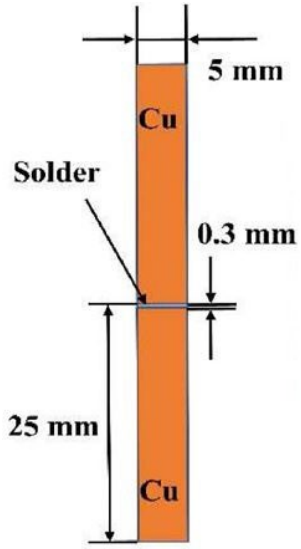


Fig. 3-4: Schematic diagram of tensile test samples.
Source [89].

The results of the experiment demonstrated that the addition of Sb to the SAC305-0.1Ni alloy increased the tensile strength of the solder joint over that of SAC305 and SAC305-0.1Ni. Interestingly though, the tensile strength decreased when the weight percentage of Sb reached 2.5%. The highest tensile strength recorded was 68.59 MPa when testing the SAC305-0.1Ni-2.0Sb alloy. Even though the SAC305-0.1Ni-2.5Sb resulted in a lower tensile strength, it was still 20.81 % higher than SAC305 and 12.51 % higher than SAC305-0.1Ni. The results of the tensile strength test are shown in Fig. 3-5 [89].

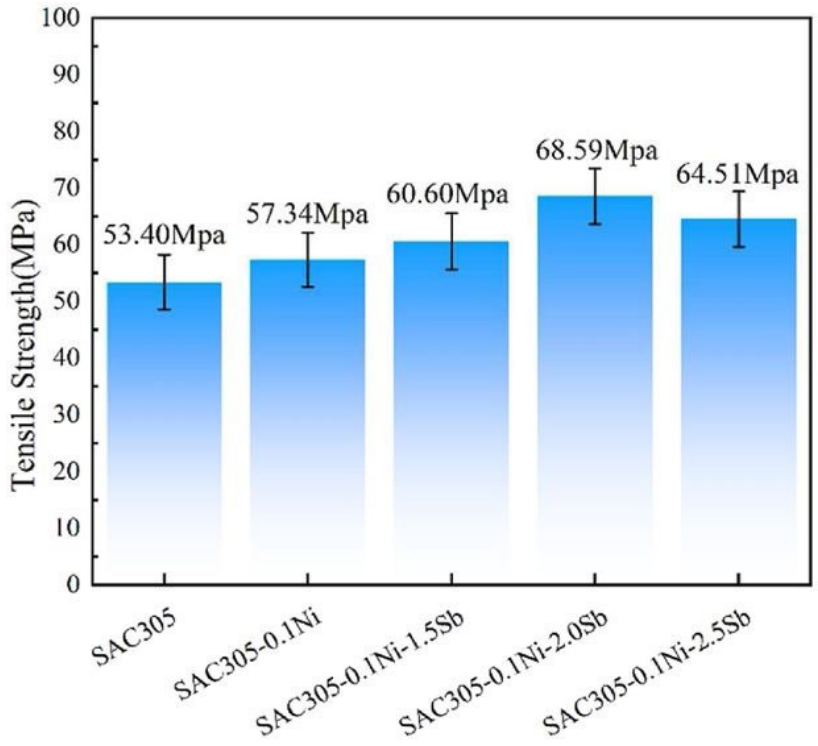


Fig. 3-5: Average tensile strength for SAC305 alloy with Ni and Sb doping. Source [89].

The presence of both Ni and Sb increased the tensile strength over the SAC305 and SAC305-0.1Ni alloys equally through dispersion and solid solution strengthening. The presence of Ni resulted in creating $(Cu,Ni)_6Sn_5$ IMC, but it now with the presence of Sb, the SnSb IMC was

uniformly distributed along the IMC layer thereby refining the microstructure and blocking "dislocation movement." Additionally, the Sb prevented the growth of the IMC layer rendering a much thinner layer which improves tensile strength [89].

### 3.1.4 Bi, Sb, and Ni Effects on SAC305 Strength

Yan et al conducted the same research as Wang but focused on the effects of Bi in the solder alloys. The intent of this research was to find if the presence of Bi, Ni, and Sb would increase the tensile strength of the SAC305 alloy. Three different combinations of Bi with SAC305-0.1Ni-2.0Sb were tested against SAC305. The melting temperatures were extracted from a DSC apparatus during thermal analysis. Multiple tests were conducted in this investigation on unaged and aged test articles. Tensile strength testing was conducted on unaged samples. The four solder alloys tested are identified in Table XIX [90].

TABLE XIX
COMBINATION OF Bi DOPED SAC305-0.1Ni-2.0Sb ALLOYS
ADAPTED FROM [90].

| **Alloy name** | **Wt%** | | | | **Melting temperature*** |
|---|---|---|---|---|---|
| | **SAC305** | **Ni** | **Sb** | **Bi** | **°C** |
| SAC305 | 100 | - | - | - | 226.01 |
| SAC305-0.1Ni-2.0Sb-2.5Bi | 95.40 | 0.1 | 2.0 | 2.5 | 226.06 |
| SAC305-0.1Ni-2.0Sb-3.0Bi | 94.90 | 0.1 | 2.0 | 3.0 | 223.81 |
| SAC305-0.1Ni-2.0Sb-3.5Bi | 94.4 | 0.1 | 2.0 | 3.5 | 229.57 |

* melting temperatures obtained from (DSC) apparatus during thermal analysis

The test samples were constructed the same as Wang's experiment (Fig. 3-4) using the same tensile speed of 0.2 mm/min. Sample size was not indicated. The results of the tensile strength testing are shown in Fig. 3-6 [90].

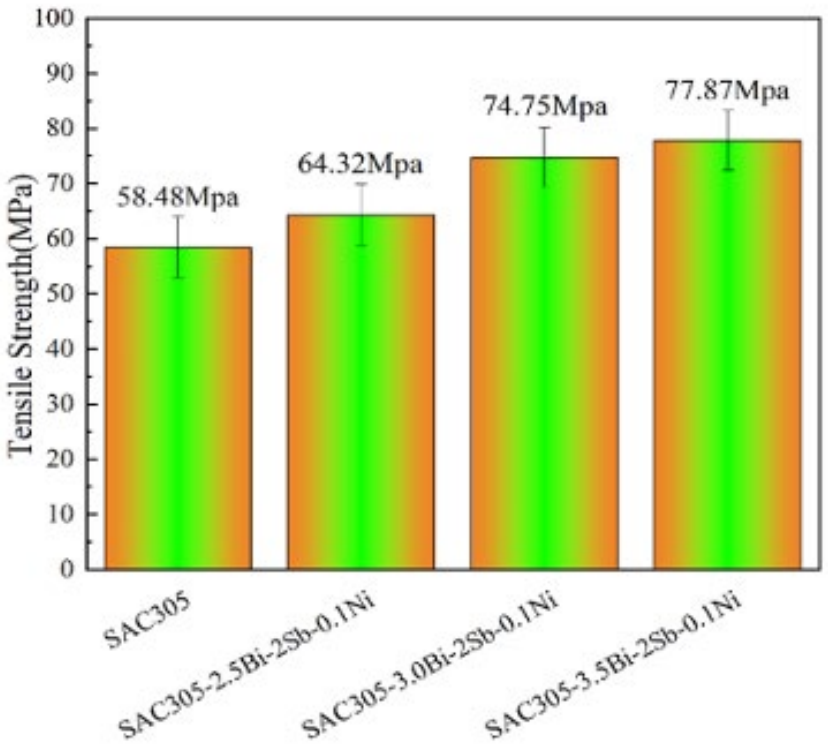


Fig. 3-6: Average tensile strength for SAC305-0.1Ni-2.0Sb alloys doped with Bi. Source [90].

By adding the three elements to the SAC305 alloy, the tensile strength was improved. And by increasing the composition of Bi, the strength was enhanced further. Ni and Bi contributed to the solid solution strengthening and the minimization of the IMC layer due to the formation of $(Cu,Ni)_6Sn_5$ and SnSb IMCs. The attributes of the IMC layers are consistent with the research cited herein that focuses on individual or coupling of Ni, Bi, and Sb with SAC305.

In comparison to the other research, the tensile strength of the SAC305 tested by Yan was slightly higher than the one tested by Wang; intriguingly, the tensile strength of the SAC305-0.1Ni-2.0Sb-2.5Bi tested by Yan was slightly lower than SAC305-0.1Ni-2.0Sb alloy without Bi tested by Wang. But as the composition of Bi increased above 2.5%, the average tensile strength

of the SAC305-Ni-Sb-Bi alloys was much greater than any SAC305 alloy combination with Ni and Sb tested by Wang.

## 3.2 Reliability Testing

### 3.2.1 Fatigue of SAC305 Solder Joints

Abueed et al research the fatigue characteristics of SAC305 solder joints in unaged and aged conditions. The test articles were assembled with FR-4 substrates consisting of 1,080 solder spheres. Each solder sphere measured 30 mil in diameter. The SMT pads had a 22-mil diameter exposed through a SMD design. Each copper pad received an OSP finish. The unaged samples were subjected to three different stress magnitudes with a 0 s dwell utilizing a constant ramp rate of 0.1 mm/s. 7 samples were tested for each stress magnitude. Two parameter Weibull plots were created for the data collected of each cyclic test and shown in Fig. 3-7 [91].

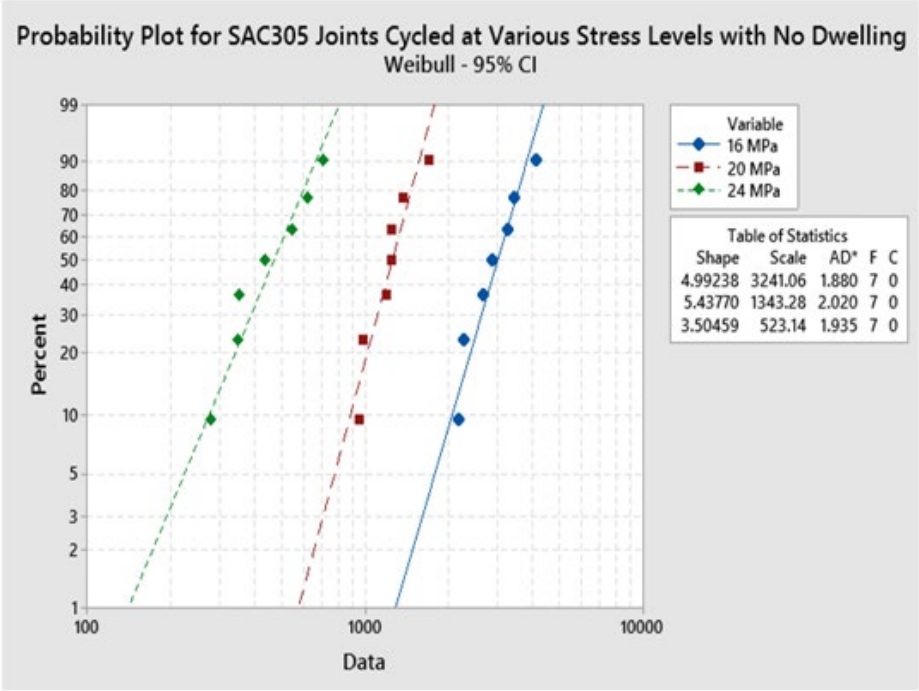


Fig. 3-7: Weibull plots for SAC305 unaged joints at three different fatigue cycles. Source [91].

From the experiment, as the stress magnitude of the cyclic stress increased, reliability significantly decreased. To express the characteristic life (number of cycles) with the associated stress amplitudes, Abueed used a power equation expressed as [91]:

$$N_{63} = C \times P^{-n} \tag{3.1}$$

Where [91]:

- $N_{63}$ is the characteristic life
- $P$ is the stress magnitude
- $C$ is a material constant
- $n$ is the ductility factor, whereas the lower the number; the material behaves more ductile

The power equation relationship for the unaged fatigue test samples is expressed in a log-log graph as shown in Fig. 3-8 [91].

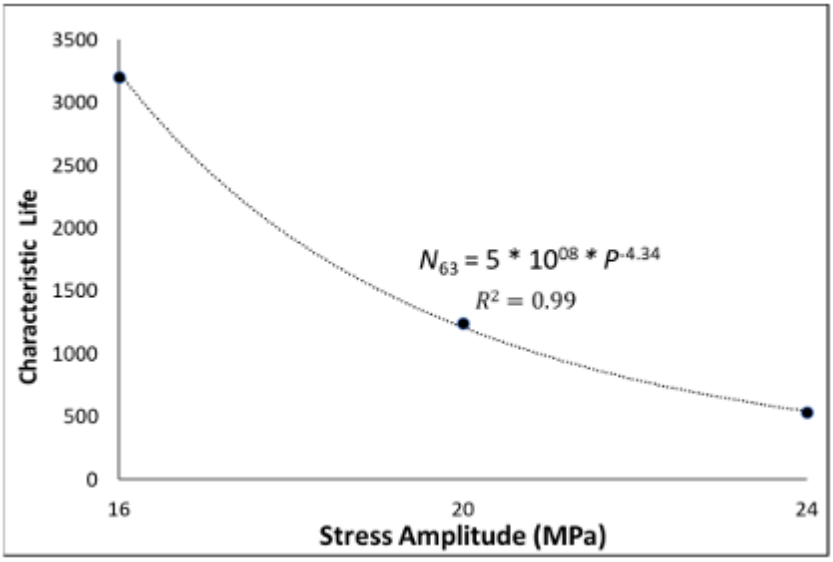


Fig. 3-8: Characteristic life as a function of stress amplitude for unaged SAC305 joints. Source [91].

Athamneh et al conducted a very similar experiment to Abueed. The test articles were constructed the same. Unaged and aged samples were tested. Different aging conditions were stipulated between the two experiments; however, the unaged test conditions were the same. The Two parameter Weibull plots were created for the data collected of each cyclic test and shown in Fig. 3-9 and the power equation to express the characteristic life to the associated stress amplitudes is shown in Fig. 3-10 [92].

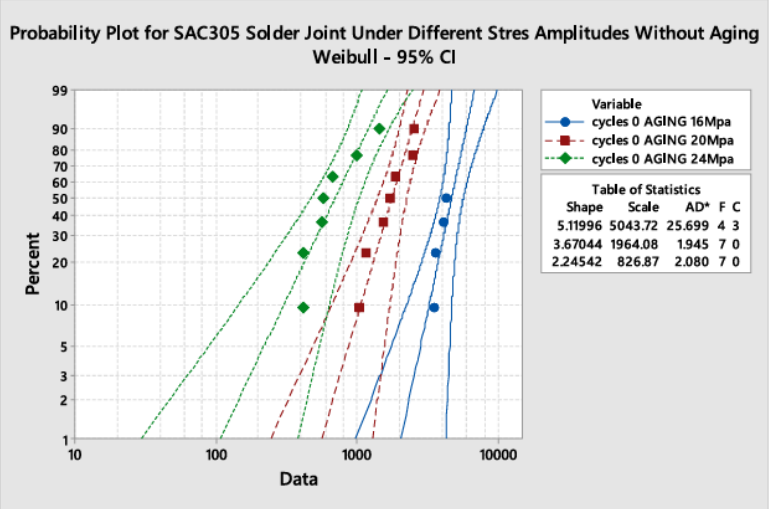


Fig. 3-9: Two parameter Weibull plots for unaged SAC305 joints at different cyclic stress. Source [92].

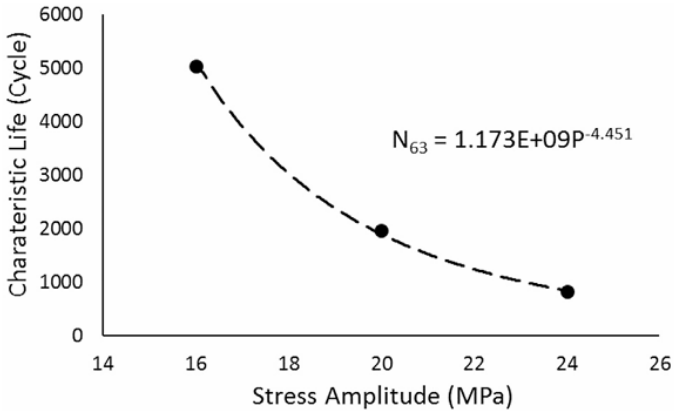


Fig. 3-10: Effects of different shear stress amplitudes on unaged SAC305 characteristic life. Source [92].

The basic relationship between the stress magnitude of the cyclic and reliability documented by Athamneh is the same found by Abueed, but the number of cycles were considerably higher for each stress magnitude.

### 3.2.2 Effects of Bi on SAC Fatigue

Athamneh and Hamasha researched the fatigue benefits of SAC305 by adding Bi to a SAC alloy. The test articles were very similar in nature to previous experiments cited. The test articles were assembled with FR-4 substrates consisting of 1,080 solder spheres. Each solder sphere measured 30 mil in diameter. The SMT pads had a 22-mil diameter exposed through a SMD design. Each copper pad received an OSP finish. Samples were either unaged or aged. The unaged samples were subjected to three different stress magnitudes with a 0 s dwell utilizing a constant ramp rate of 0.1 mm/s. 7 samples were tested for each stress magnitude. The test matrix is shown in Table XX [93].

TABLE XX
FATIGUE TEST MATRIX FOR UNAGED SAC-Q AND SAC305
ADAPTED FROM [93].

| Alloy | Alloy Composition | Stress Level (MPa) | Replicates |
|---|---|---|---|
| SAC305 | Sn–3.0Ag–0.5Cu | 16 | 7 |
| | | 20 | 7 |
| | | 24 | 7 |
| SAC-Q | Sn–3.41Ag–0.51Cu–3.3Bi | 22 | 7 |
| | | 26 | 7 |
| | | 28 | 7 |

Because the presence of Bi renders the SAC alloy more fatigue resistant, the stress magnitudes of the SAC-Q alloy were elevated slightly compared to those of the SAC305. This allowed the SAC-Q fatigue testing failures to occur within a reasonable number of cycles.

The fatigue data was plotted in two-parameter Weibull distributions for each solder alloy. The resulting plots are shown in Fig. 3-11 [93].

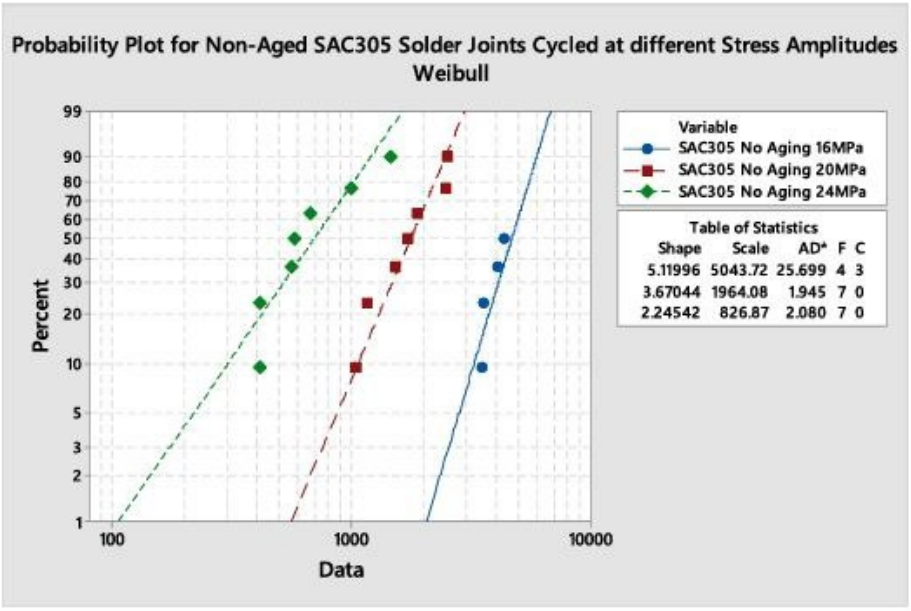


SAC305

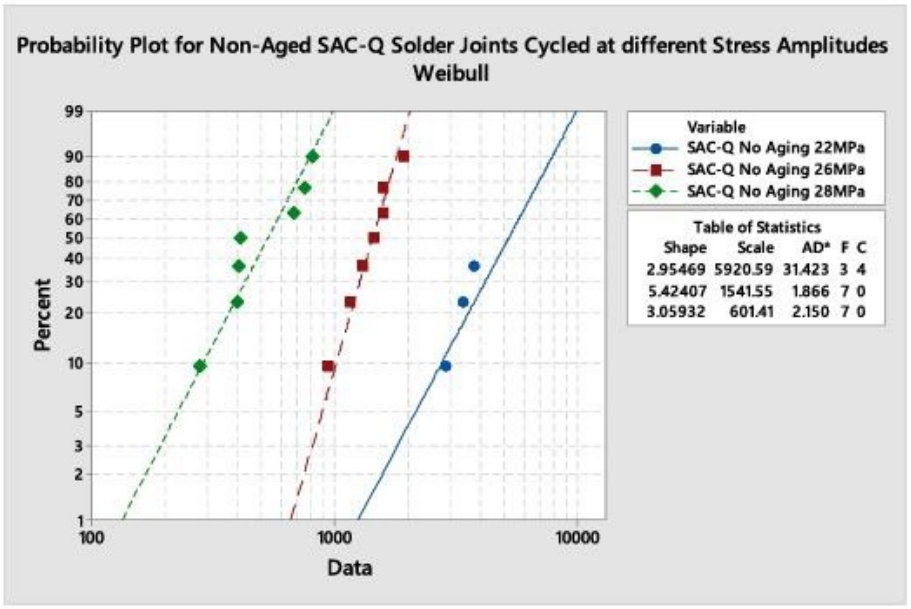


SAC-Q

Fig. 3-11: Two-parameter Weibull plots for unaged SAC305 and SAC-Q fatigue testing. Adapted from [93].

The same power equation used by Abueed was utilized to express the characteristic life versus the associated stress amplitudes for the unaged SAC305 and SAC-Q alloys is shown in Fig 3-12 [93].

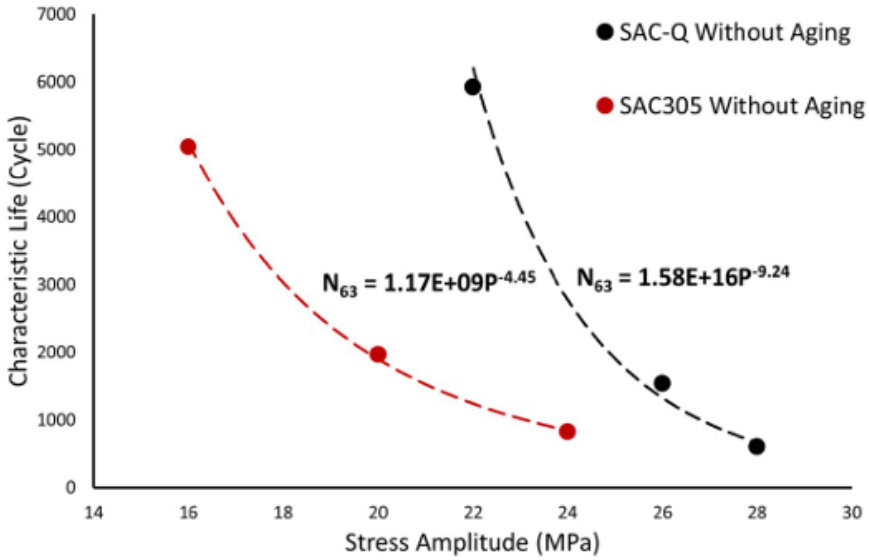


Fig. 3-12: Characteristic life and fatigue stress amplitude for SAC305 and SAC-Q. Source [93].

As Fig. 3-12 demonstrates, the slope of the curve for SAC-Q indicates the alloy behaving more brittle than the SAC305 alloy but able to withstand higher stress amplitudes.

While performing literature review for mechanical fatigue for unaged test article of SAC alloys incorporating minor amounts of Ni and Sb, the results of the search did not provide any references. Most of the research conducted with a SAC alloy having trace amounts of Ni or Sb centered on thermal fatigue and creep. The data captured from thermal fatigue and creep experiments would not be directly related to this research.

### 3.3 Impact of Surface Finishes on SAC alloys

Tony Lentz of the FCT Solder presented technical data at the SMTA International 2018 conference that measured the performance of different surface finishes with lead and lead-free solder paste. Four combinations of solder paste were tested: 1) water-soluble (WS) SN63-37; 2) no-clean (NC) SN63-37; 3) WS SAC305; and 4) NC SAC305. The four solder paste alloys were printed on test samples employing the following surface finishes: 1) HASL; 2) lead-free (LF) HASL; 3) OSP; 4) ENIG; 5) immersion tin (ITin); and 6) immersion silver (ISilver). The test boards were constructed for ball grid arrays (BGA) with 0.4 mm pitch. Solder paste was printed with 5 mil thick stencils with round patterns having 0.50 area ratios (AR). All combinations were evaluated using solder paste inspection (SPI) data in the following categories [94]:

- Printing performance
    - Transfer efficiency for 0.50 area ratio (AR) pattern
    - Coefficient of Variation (TE) in the 0.50 AR pattern
    - Transfer efficiency for 0.4 mm pitch BGAs
    - Coefficient of Variation (TE) in the 0.4 mm BGAs
- Reflow performance
    - Wetting
    - Solder balling
    - Graping (situation where the solder paste does not completely melt and joint together during reflow)
- Voiding performance
    - Void area percentage
    - Large void percentage

The resulting SPI data for each combination of solder paste and surface finish was scored on a scale from 1 to 5 for each of the 9 different categories. A score of 1 indicated that the combination of solder paste and surface finish performed poorly while a score of 5 indicated best performance. Each of the 9 different categories implemented a scoring scale to determine the score. The scores were totaled resulting in a possible maximum score of 45 for each solder paste and surface finish combination. The final scoring results are shown in Table XXI for the NC SAC305 and WS SAC305 solder paste alloys [94].

TABLE XXI
TOTAL SCORES FOR EACH SURFACE FINISH COMBINATION
ADAPTED FROM [94]

| Surface Finish | SAC305 Solder Paste | Print Score (20 max) | Reflow Score (15 max) | Void Score (10 max) | Total (45 max) |
|---|---|---|---|---|---|
| ENIG | WS | 18 | 11 | 5 | 34 |
| | NC | 13 | 11 | 7 | 31 |
| HASL | NC | 13 | 11 | 7 | 31 |
| LF-HASL | NC | 11 | 11 | 9 | 31 |
| OSP | NC | 13 | 7 | 8 | 28 |
| ITin | WS | 17 | 9 | 2 | 28 |
| ITin | NC | 12 | 11 | 4 | 27 |
| HASL | WS | 13 | 10 | 4 | 27 |
| ISilver | WS | 13 | 8 | 6 | 27 |
| ISilver | NC | 9 | 10 | 7 | 26 |
| OSP | WS | 17 | 4 | 2 | 23 |
| LF-HASL | WS | 8 | 11 | 2 | 21 |

Lentz conclude with the following recommendations [94]:

- The NC SAC305 performed better than the WS SAC305 with most surface finishes
- The ENIG worked well for both SAC305 solder paste
- The ISilver performed worse than the other surface finishes for both SAC305 solder paste
- OSP and LF-HASL performed well over a wide range depending on the solder paste applied

Collins et al examined the reliability for three different lead-free solder finishes with SAC 305. The test articles were constructed with 2512 ceramic chip resistors subjected to accelerated temperature cycling (ATC). The PCB substrate was FR-4 material. The assembly of the ceramic chip resistors were designed with a "daisy chain circuit" for monitoring electrical continuity. The temperature cycled between 0 °C and 100 °C with 30-minute dwell times at the extremes. The temperature changed at a rate of 10 °C/min. One population was tested to 2,500 cycles and the other was tested to 8,250 cycles. Failures were established in accordance with the IPC-9701A. ENIG, OSP and immersion silver were the three surface finishes tested. Failure data was fitted to a two-parameter Weibull distribution. The results of the 8,250-cycle population are shown in Table XXII [95].

TABLE XXII
LIFETIME DATA FOR THE SURFACE FINISHES
ADAPTED FROM [95].

| **8,250 Cycles** | | | | |
|---|---|---|---|---|
| **Population** | **% failures** | **Characteristic life (Scale parameter) (η)** (# of thermal cycles) | **Slope Parameter (β)** | **Rho value (*p*)** |
| 36 | 100.0 | 1,719 | 3.4 | 0.97 |
| 36 | 97.2 | 2,248 | 3.1 | 0.94 |
| 26 | 73.0 | 2,713 | 2.9 | 0.94 |
| - The Rho value is a measure of how well the data fits the probability line. It is a value between -1 and 1 | | | | |

Based on the findings, Collins expressed OSP as the best lifetime surface finish for SAC305 with immersion silver being the worst out of the three. Collins cited the excessive void formation occurring during reflow contributing to immersion silver's poor performance.

### 3.4 Effects of Solder Paste Volume on SAC305 Performance

Alakayleh et al performed a very comprehensive study that not only evaluated different solder paste alloys and surface finishes but also different solder paste volumes assembled with a SAC305 solder joint. The test boards were comprised of FR-4 substrates. The boards were constructed to be assembled with Chip Array Ball Grid Arrays (CABGA208) each measuring 15 mm × 15 mm. Only two different surface finishes were examined: 1) OSP; and 2) ENIG. Three different solder paste alloys were used. They are shown in Table XXIII [96].

TABLE XXIII
THREE SOLDER PASTE ALLOYS EXAMINED
ADAPTED FROM [96].

| Solder Paste Alloy | Wt% | | | | |
|---|---|---|---|---|---|
| | Sn | Ag | Cu | Bi | Sb |
| SAC305 | 96.5 | 3.0 | 0.5 | - | - |
| SAC-Bi | 93.2 | 3.0 | 0.8 | 3.0 | - |
| SAC-Bi-Sb | 89.7 | 3.4 | 0.7 | 3.2 | 3.0 |

Three different solder paste printing stencils were designed to provide three different solder paste volumes for the test board assemblies. Each SMT pad with different solder paste thicknesses held an 18 mil SAC305 solder sphere. The stencil thickness and related paste to sphere volume ratio is shown in Table XXIV [96].

TABLE XXIV
SOLDER PASTE VOLUME FOR CABGA208 TEST SAMPLES
ADAPTED FROM [96].

| Paste Volume | Stencil Thickness (mil) | Paste to sphere volume ratio | Aperture diameter (mil) |
|---|---|---|---|
| Low | 4 | 0.1 | 10 |
| Medium | 5 | 0.3 | 15.3 |
| High | 6 | 0.5 | 18 |

The analysis incorporated four different types of SPI data [96]:

- $Ag_3Sn$ particle analysis
- Measuring IMC thickness
- Micro-Vickers hardness testing
- Void analysis

For the number of $Ag_3Sn$ particles formed, as the solder paste volume increased for each solder paste alloy, so the number of $Ag_3Sn$ particles for both surface finishes. Out of the three different solder paste alloys, SAC305 formed the most $Ag_3Sn$ particles for each level of solder paste volume for both surface finishes. Another observation was the size of the $Ag_3Sn$ particles. The size of the particles was large for SAC305-Bi and SAC305-Bi-Sb at a low volume and decreasing in size as the solder paste volume increased. The relative size of the particles in the SAC305 solder paste remained the same regardless of paste volume. Bar charts depicting the results are shown in Fig. 3-13 and Fig. 3-14 [96].

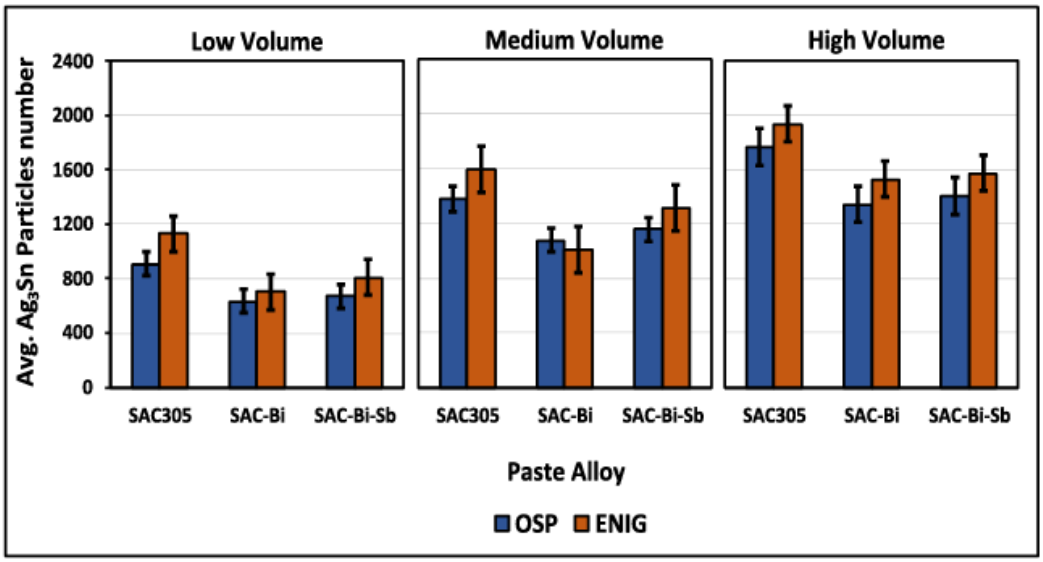


Fig. 3-13: Relationship of number of $Ag_3Sn$ particles to solder paste volume. Source: [96].

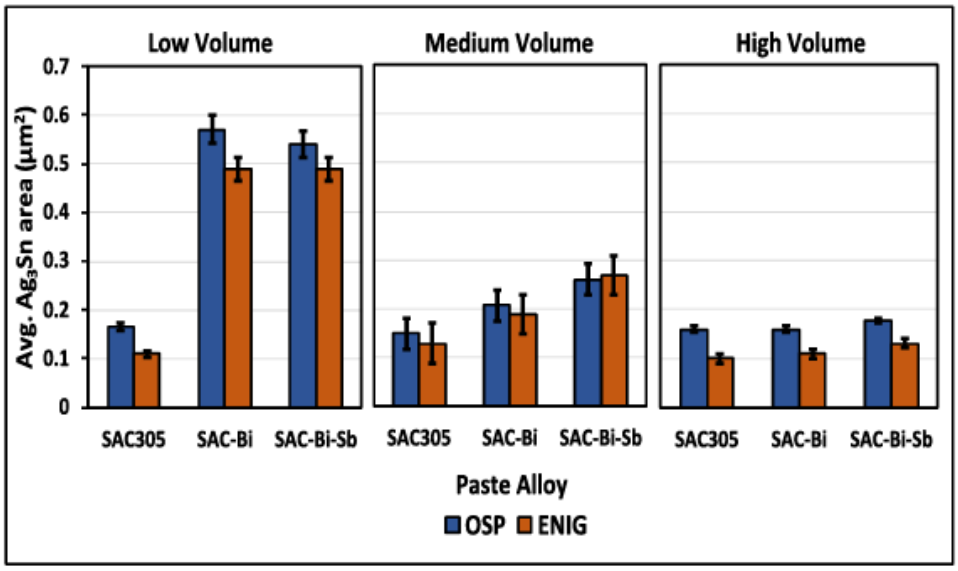


Fig. 3-14: Relationship of average size of $Ag_3Sn$ particle to solder paste volume. Source: [96].

The main effects plots show that the solder paste volume, surface finish and solder paste alloy each had a significant influence on the formation of $Ag_3Sn$ particles as shown in Fig. 3-15 [96].

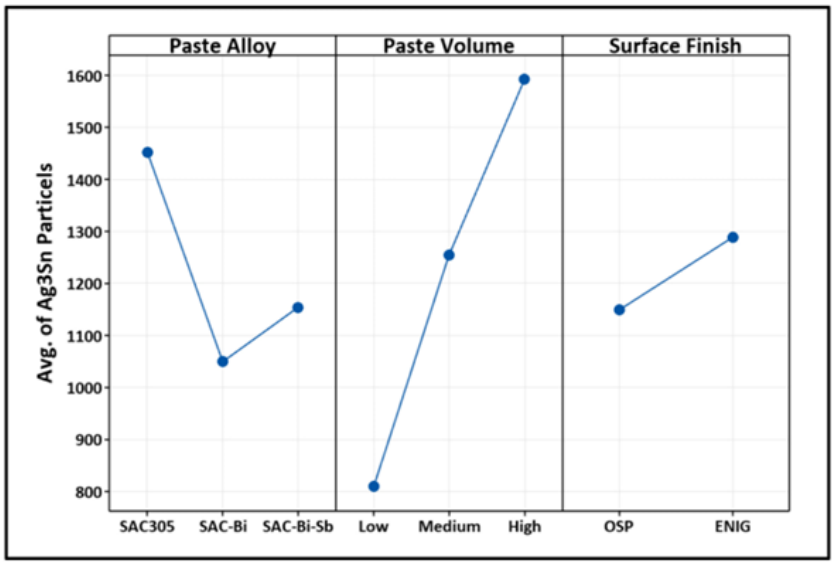


Fig. 3-15: Main effects plots for the average number of $Ag_3Sn$ particles. Source [96].

The main effects plots demonstrate that solder paste volume has a significant effect on the average number of $Ag_3Sn$ particles while the surface finish has a slightly significant effect. The solder paste alloy has a mixed effect. Between SAC305 and SAC-Bi, the main effect plot shows a negative yet very significant effect; however, when evaluating between SAC-Bi and SAC-Bi-Sb, the effect becomes slightly significant with a positive trend [96].

The bar charts for the average IMC thickness for each solder paste alloy and thickness and surface finishes are shown in Fig. 3-16 [96].

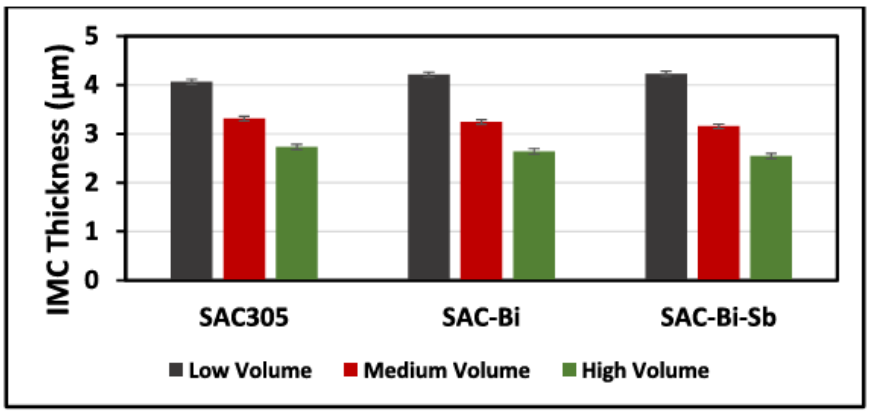


(a) OSP

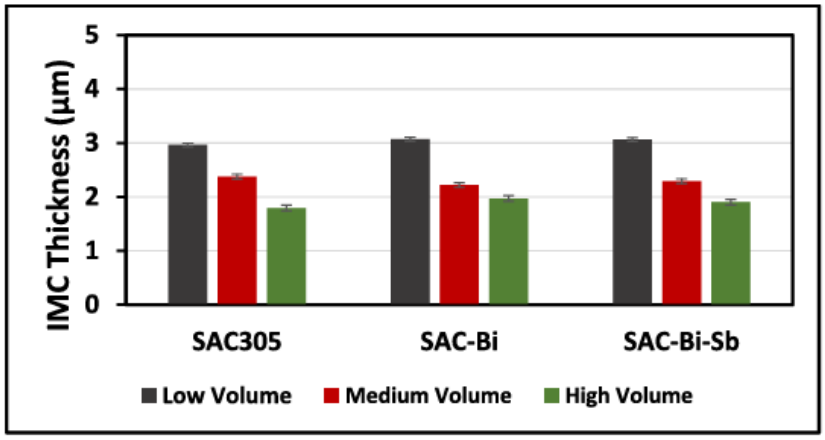


(b) ENIG

Fig. 3-16: The IMC layer thickness of a) OSP and b) ENIG.
Source [96].

From the bar charts it is clear to determine that as the solder paste volume increases, the IMC thickness decreases for all solder paste alloys and surface finishes. To determine the effects of each parameter, the main effect plots for IMC thicknesses are shown in Fig. 3-17 [96].

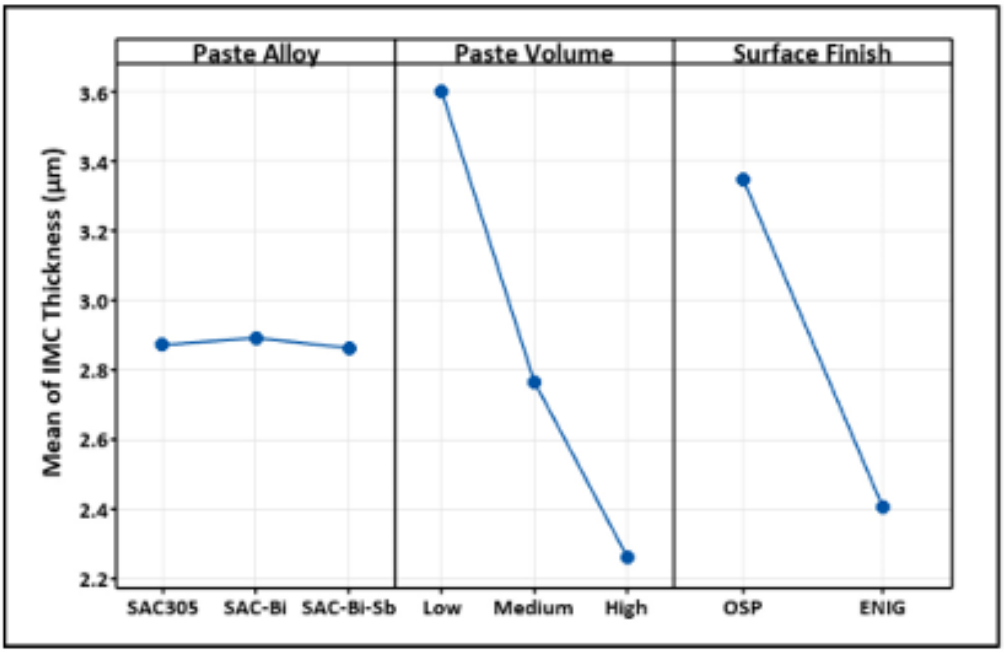


Fig. 3-17: Main effect plots for the average IMC thicknesses.
Source [96].

Taking into account the main effect plots with the bar charts, it becomes obvious to see that the solder paste alloy has little to no effect on the average IMC thickness while the paste volume and surface finish have very significant effects [96].

The average size of the voids that develop in the solder paste was assessed. The determination of the average void size was calculated by totaling the void areas revealed from x-ray images divided by the 104 CABGA208 solder joints examined. The results showed that as the solder paste volume increased, the average size of the voids became larger. This relationship is shown in the bar charts of Fig. 3-18 [96].

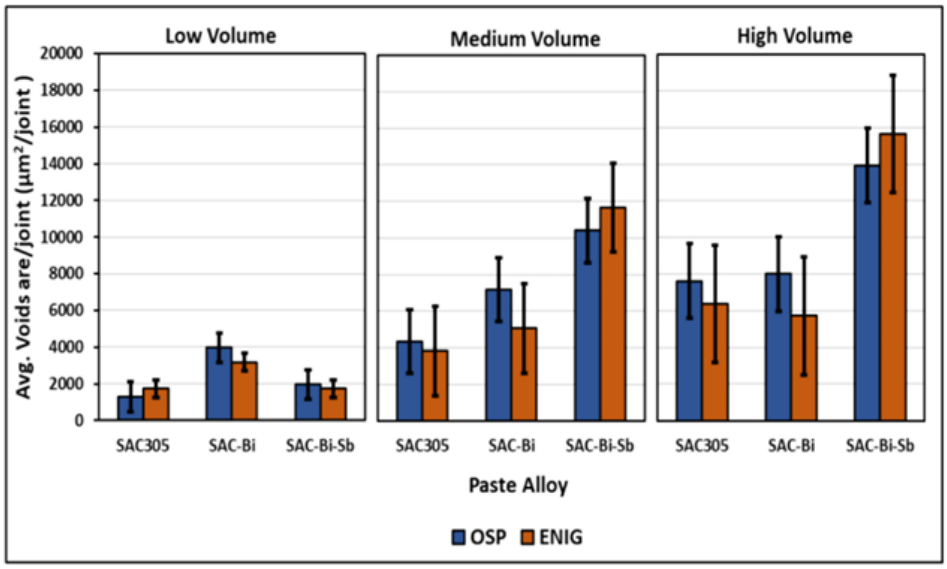


Fig. 3-18: Average void areas of CABGA208 solder joints.
Source [96].

Main effect plots were generated to determine the level of influence of the paste volume and alloy and surface finish. The plots are shown in Fig. 3-19 [96].

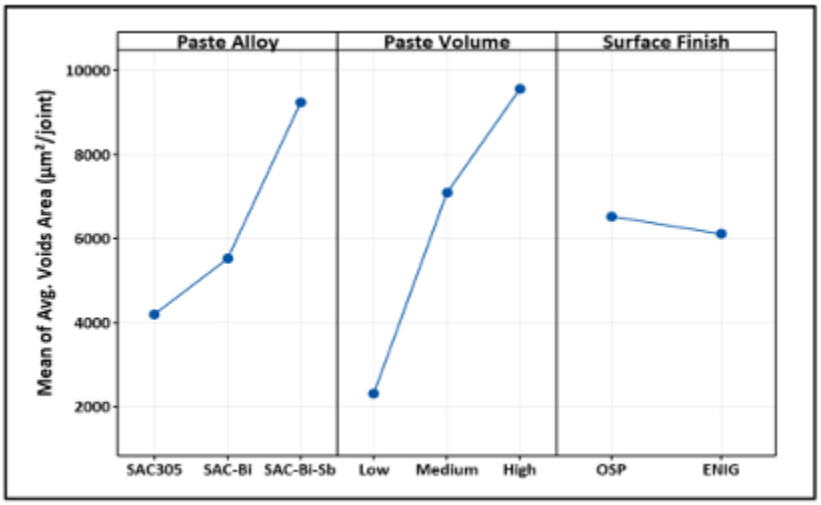


Fig. 3-19: Main effect plots of the mean of the average void area.
Source [96].

The main effect plots reveal a significant to very significant effect of the solder paste volume and alloy on the mean of the average void area with high solder paste volume and SAC-Bi-Sb having the most significant effect. The surface finish has little to no effect on the size of the void area.

## Chapter 4 Sample Preparation and Experimental Methodology

All test single-sided SMT boards are constructed with some common parameters and characteristics. All test boards are composed of a FR-4 substrate. The substrate measures 12 in x 10 in. Each test board contains 1,080 solder spheres. The substrate is scored, or v-cut, into several 10mm x 10mm squares to accommodate mechanical separation. The perimeter squares are void of copper pads. The interior squares contain copper pads. The copper pads are bonded to the FR-4 substrate in SMD configuration. Each interior square is comprised of nine copper pads arranged evenly and equally in a 3 x 3 pattern with a 3 mm pitch between copper pads. A surface finish was applied to each copper pad. Afterwards, solder paste is applied to the finish surfaces using stencils of various thickness. Finally, each copper pad is then soldered with a SAC305 solder sphere. An example of the single-sided SMT boards is shown in Fig. 4-1.

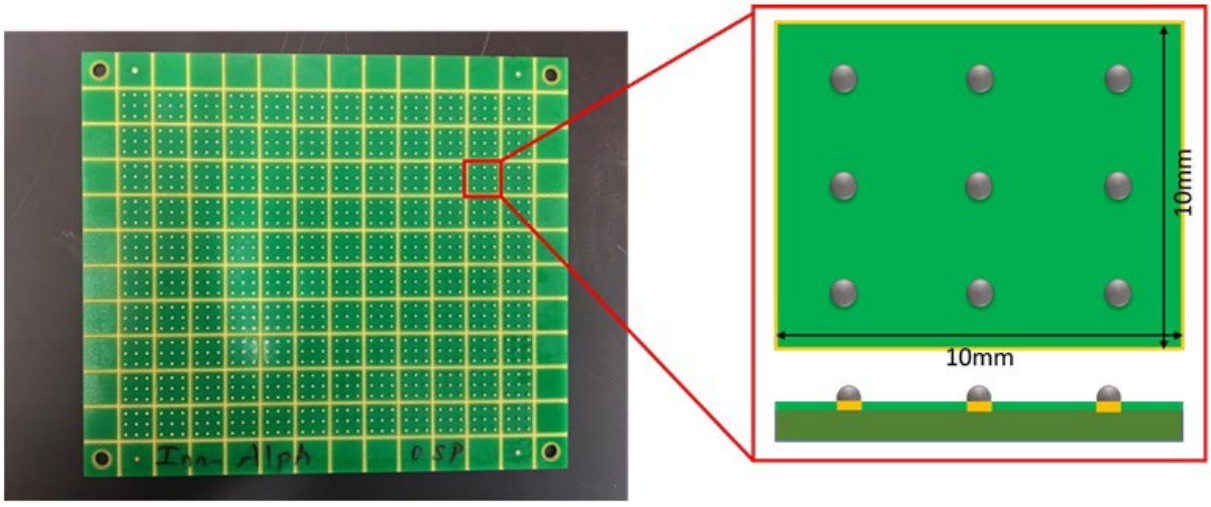


Fig. 4-1: Example of the test SMT boards.
Adapted from [97].

Each copper pad measures 12 mil square while each solder sphere measures 18 mil in diameter. The test articles were mechanically separated from the test boards along the scoring lines into 3

squares by 4 squares samples. Some squares may not contain solder spheres due to their location on the perimeter of the test boards. Photographs for two samples before testing are shown in Fig. 4-2.

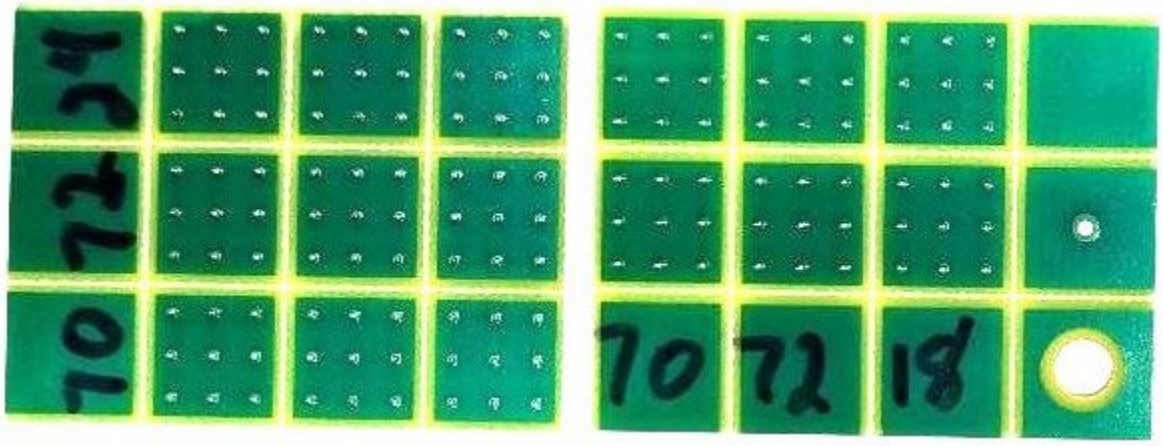


Fig. 4-2: Photo of test samples separated from test boards.

A magnified, orthogonal view of a square with 9 solder spheres is shown in Fig. 4-3.

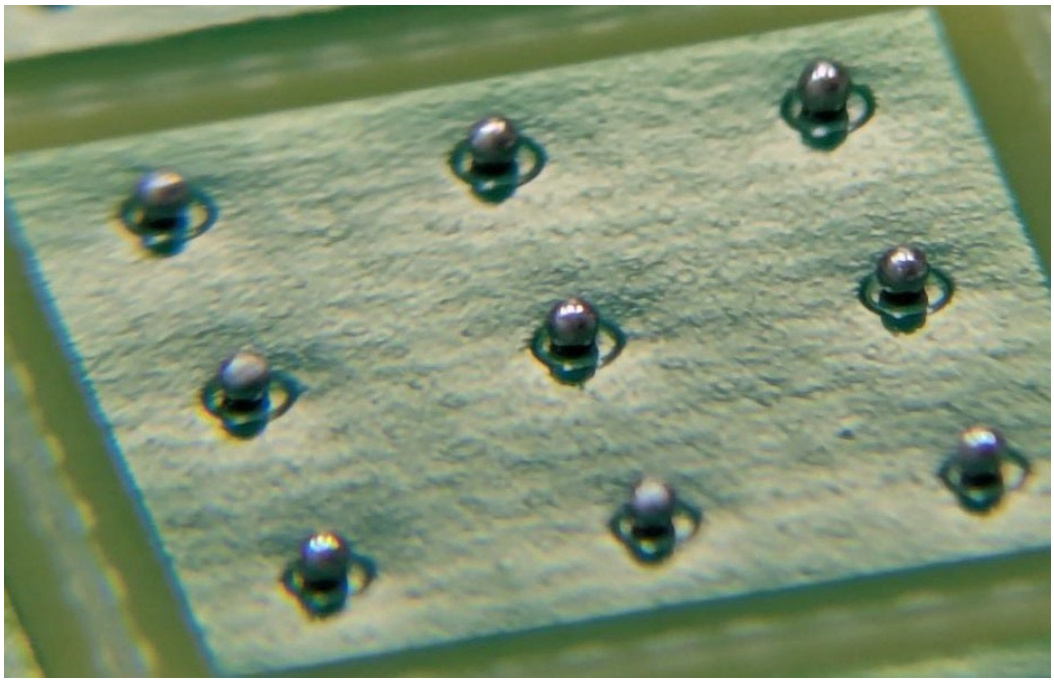

Fig. 4-3: Magnified, orthogonal view of solder spheres on test sample.

## 4.1 Solder Paste and Surface Finishes

As much as the test samples have in common, there are significant differences to which are the focus of the research. Three different solder paste are being evaluated. One solder paste is simply a SAC305 paste of the same configuration as the solder spheres. The remaining two solder paste includes adding Bi, Ni, and Sb to the SAC alloy. The solder paste is supplied by the Senju Metal Industry Co. (SMIC), Ltd. The solder paste alloys are of the exact same composition as those evaluated by Alakayleh in 3.4 of Chapter 3, though the manufacturer was not stated. The names of the solder paste alloys used in the research are covered in Table XXV.

TABLE XXV
SMIC LEAD-FREE SOLDER PASTE ALLOYS TESTED
ADAPTED FROM [98], [99], [100].

| Solder Alloy Name | Alloy composition (wt%) | Melting temp. (°C) | | SMIC Overview |
|---|---|---|---|---|
| | | Solidus | Liquidus | |
| **M705** | Sn-3.0Ag-0.5Cu (SAC305) | 217 | 220 | Pb free standard solder |
| **M758** | Sn-3.0Ag-0.8Cu-3.0Bi-Ni (SAC308-Bi-Ni) | 205 | 215 | Highly joint reliable solder for semiconductor PKG |
| **M794** | Sn-3.4Ag-0.7Cu-3.2Bi-3.0Sb-Ni-x (SAC347-Bi-Sb-Ni-x) | 210 | 221 | Heat & fatigue-resistant alloy for automotive applications |
| x is a proprietary additive(s) known to manipulate grain structure and or intermetallic layer at interface. Several elements have since been targeted by alloy developers to achieve grain morphology variations. These elements may include but may not necessarily be limited to; Ni, In, Co, Fe, As, Ge, La and more. | | | | |

SMIC's M758 and M794 lead-free solder alloys were developed to provide a more heat-fatigue resistant solder alloy beyond that of a standard SAC305. According to SMIC, three different technologies were used to achieve improvements. First, the IMC layer is modified with the addition of Ni which increases the reliability of the bond and increases the strength through

precipitation hardening. This improvement occurs at the micron level. With the addition of Bi and Sb, the solid solution state adds additional strength. This improvement occurs at the atomic level. And finally, by controlling the grain coarsening of Sn, crack propagation is controlled [101]. The increases in shear strength are shown in Fig. 4-4 [102].

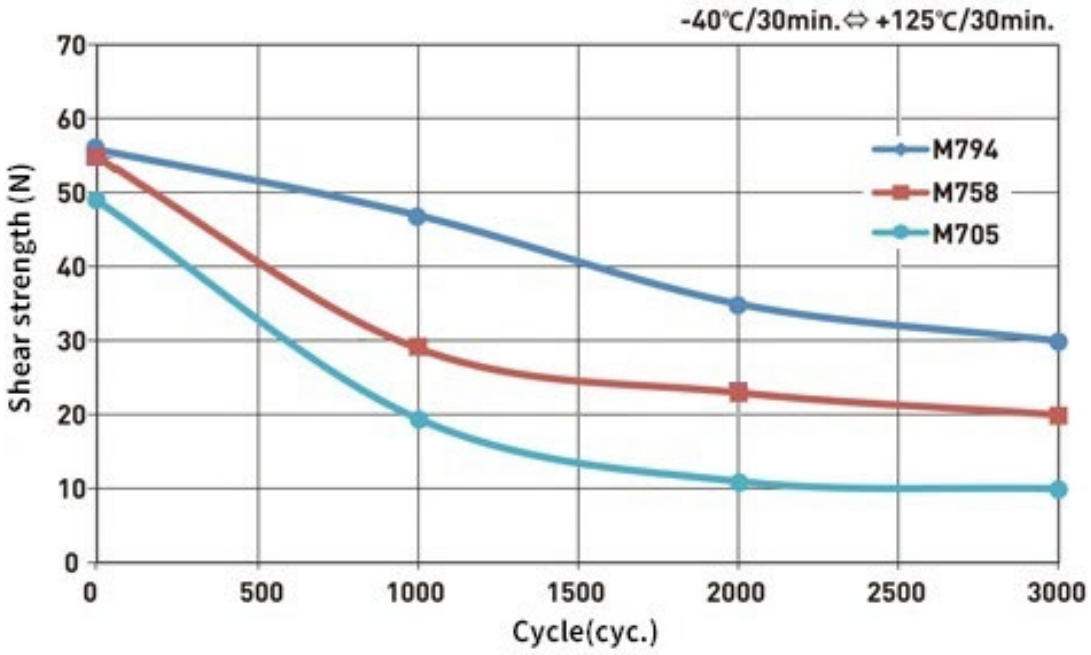


Fig. 4-4: Shear strength comparison of SMIC's lead-free solder alloys.
Adapted from [102].

In addition to the three different solder paste used, three different solder paste volume ratios were selected prior to assembly to be part of the research evaluation. OSP and ENIG where the two types of surface finishes used in conjunction with the three types of solder paste.

## 4.2 Test Board Assembly

The stencils for applying the solder paste are designed and manufactured by StenTech in Dallas, TX. StenTech began manufacturing SMT stencil in 1999. Today, they are one of the most chosen SMT stencil manufacturers in North America [91]. The stencils are fabricated from datum PhD

which is an alloy of stainless steel used explicitly for SMT stencils. Datum PhD is formed from 304 stainless steel that has been cold rolled with very high precision. This delivers stencils with precise thicknesses (solder paste volumes) needed for each SMT pad location. The stencils are laser cut. The laser is a fiber diode laser with a beam thickness of .0008 inch. This makes the aperture wall texture to be very smooth, which improves the release of the solder paste.

Each solder paste stencil is manufactured with 1,080 apertures to coincide with the 1,080 SMT pads on the test boards. All the apertures of the stencil are round with different diameters depending on the thickness of the stencil. The designs of the StenTech stencils are recorded in Appendix A and are summarized in Table XXVI.

TABLE XXVI
STENCIL THICKNESS AND APERTURE SIZE

| STENTECH STENCIL JOB # | STENCIL THICKNESS (mil) | STENCIL APERTURE DIAMETER (mil) |
|---|---|---|
| **1184433** | 4 | 10.0 |
| **1184434** | 5 | 15.3 |
| **1184435** | 6 | 18.0 |

The stencils were shipped to Universal Instruments at their Conklin, NY facility for assembling the test boards. Universal Instruments procures test board substrates (which includes the base FR-4 material, the SMT pads, and the solder mask) from their list of approved suppliers. Upon receipt of the substrates, the exposed surfaces of all the SMT pads with a SMD configuration measured 12 mil square. Universal Instruments began the assembly process by applying the three different SMIC's solder paste to the boards using three stencils, each with a different thickness and aperture diameter, representing the desired paste volume. The solder paste printing was performed by their DEK Galaxy SMT stencil printer shown in Fig. 4-5.


Fig. 4-5: Universal Industries' DEK Galaxy SMT stencil printer.

Following the solder paste printing, 18-mil solder spheres composed of SAC305 were populated on the test boards. The test boards were then passed through a Centurion 10-zone reflow oven for final assembly. The Centurion used is pictured in Fig. 4-6.


Fig. 4-6: Universal Industries' Centurion 10-zone reflow oven.

All combinations of the test boards were subjected to the same reflow profile. The reflow profile data is captured in Appendix B and summarized in a graph in Fig. 4-7.

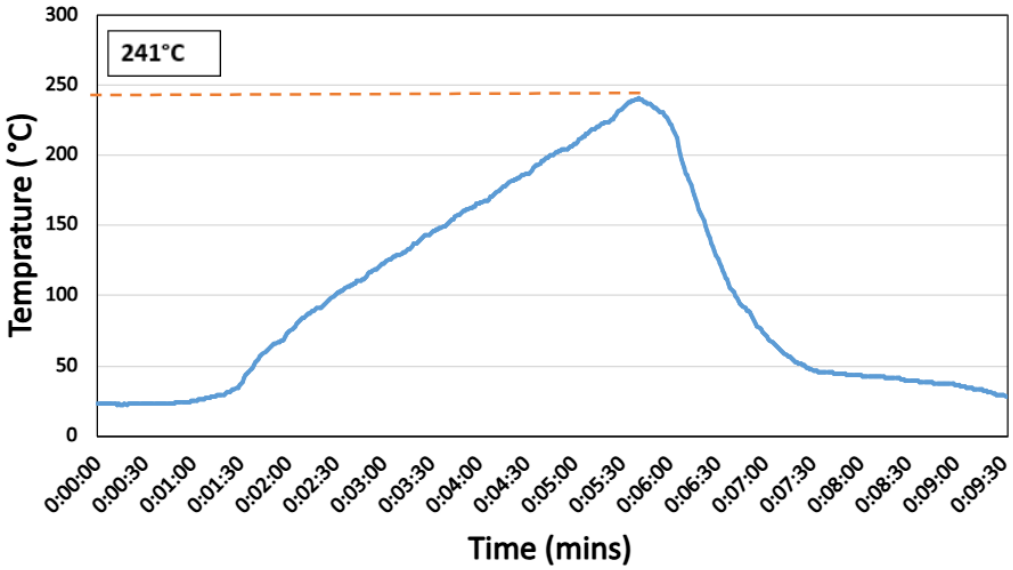


Fig. 4-7: Centurion reflow profile for assembling test boards.

In total, thirty-seven test boards were assembled with the three different SMIC solder paste alloys, three different solder paste volume ratios, and two different surface finishes. All the test boards were serialized. This helps to reduce errors when selecting the correct test sample composed of a particular solder paste and volume. The samples were inspected for any assembly defects before being shipped. The test boards were received at Auburn University on June 14, 2023. All test boards were inventoried/accounted and visually inspected for any obvious defect that may occur during shipping. The test boards were kept in a climate-controlled room at standard room temperature until needed for testing. The test boards with specific configurations are shown in Table XXVII.

TABLE XXVII
TEST BOARD SERIAL NUMBERS

| Solder Sphere | Paste Model Number | Surface Finish | % Solder Paste Volume of Total Solder Joint | Stencil Thickness | Sample1 Barcode | Sample2 Barcode |
|---|---|---|---|---|---|---|
| SAC305 (18 mil) | M705-GRN360-K2-V Type 4 | OSP | 0.1 | 4 mil | 707215 | 707216 |
| | | | 0.3 | 5 mil | 707217 | 707218 |
| | | | 0.5 | 6 mil | 707219 | 707220 |
| | | ENIG | 0.1 | 4 mil | 707233 | 707234 |
| | | | 0.3 | 5 mil | 707235 | 707236 |
| | | | 0.5 | 6 mil | 707237 | 707238 |
| | M758-GLV-HF Type4 | OSP | 0.1 | 4 mil | 707221 | 707222 |
| | | | 0.3 | 5 mil | 707223 | 707224 |
| | | | 0.5 | 6 mil | 707225 | 707226 |
| | | ENIG | 0.1 | 4 mil | 707239 | 707240 |
| | | | 0.3 | 5 mil | 707241 | 707242 |
| | | | 0.5 | 6 mil | 707243 | 707244 |
| | M794-GRN360-K1-V8 Type 4 | OSP | 0.1 | 4 mil | 707227 | 707228 |
| | | | 0.3 | 5 mil | 707229 | 707230 |
| | | | 0.5 | 6 mil | 707231 | 707232 |
| | | ENIG | 0.1 | 4 mil | 707245 | 707246 |
| | | | 0.3 | 5 mil | 707247 | 707248 |
| | | | 0.5 | 6 mil | 707249 | 707250 |
| | M705-GRN360-K2-V Type 4 | OSP | 0.1 | 4 mil | PST409087 | |

SMIC's solder paste model numbers are broken down into 4 parts:

$$\underset{1}{\underline{\text{M705}}} - \underset{2}{\underline{\text{GRN360}}} - \underset{3}{\underline{\text{K2}}} - \underset{4}{\underline{\text{V}}}$$

- 1 – solder paste alloy
- 2 – flux classification
- 3 – viscosity range (for GRN360 only)
- 4 – version (if needed)

A breakdown of the SMIC's solder paste model numbers under test is shown in Table XXVIII.

TABLE XXVIII
BREAKDOWN OF SMIC'S SOLDER PASTE MODEL NUMBERS

| | |
|---|---|
| **Solder Alloy** | M705, M758, M794, . . . . . |
| **Flux Classification** | GRN360 (original): No Clean, ROL1<br>GLV-HF: No Clean, ROL0<br>GRN360 (V4/V8): No Clean, ROL0 |
| **Viscosity**<br>(for GRN360 only) | K1: Lower Viscosity Range (EU mostly)<br>K2: Middle (most common)<br>K3: Higher (rare) |
| **Version**<br>(if needed) | V: Origin<br>V4: 4th Generation<br>V8: 8th Generation |

The Type 4 designation refers to the powder grain size. The Type 4 designation is classified in the IPC standard, J-STD-005B, Requirements for Soldering Pastes. The powder grain size of Type 4 is covered in Section 2.3.2 of Chapter 2 in Table XI.

### 4.3 Testing Equipment and Setup

The shear and fatigue testing will be instrumented by using an Instron 5948 high precision materials testing system. The testing system has the load capacity range to apply test loads less than 2 mN and up to 2 kN. The machine is equipped to implement displacements at the micro-level by utilizing a digital linear actuator drive with fully variable speed control. The servoelectric actuator is accompanied by a 20 nm axial resolution linear encoder. It has a testing speed range from 0.001 to 1500 mm/min. The actual test system and component description is shown in Fig. 4-8.

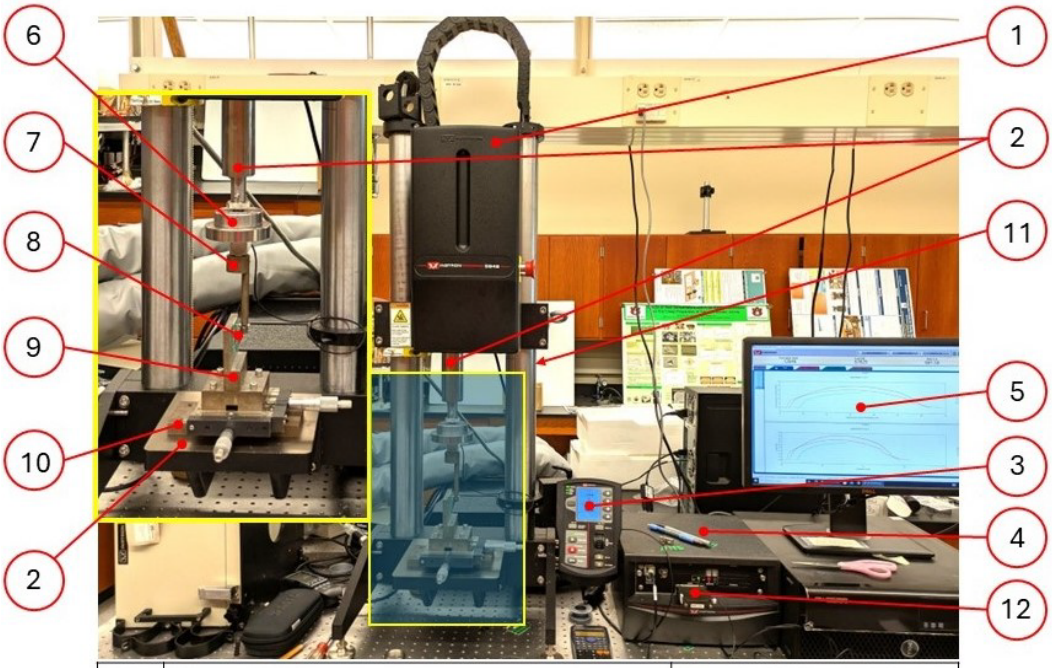


| # | Description | Model #/Serial # |
|---|---|---|
| 1 | MicroTester | Instron 5948 |
| 2 | Actuator (MicroTester) | Instron 5948 |
| 3 | Control panel | Instron A620-840<br>s/n OW51304186 |
| 4 | 5900 Controller | Instron OP620-315 |
| 5 | Computer monitor (shear testing) | |
| 6 | Static load cell; ± 50 N | Instron 2530-437<br>s/n 128346 |
| 7 | Custom tool for shearing/fatiguing solder spheres | |
| 8 | Test article under test | |
| 9 | Custom tool fixture for mounting test article | |
| 10 | Linear (xy) translation stage (w/ two micrometer heads; Range: 0-25mm; Graduations: 0.01mm) | Model XYT-25;<br>2x Mitutoyo 150-801 |
| 11 | Column (load frame) | Instron 5948B12691 |
| 12 | Connector (static load cell) | |

Fig. 4-8: Instron 5948 MicroTester system's components and descriptions.

The load frame consists of a base beam with two columns. At the top of the two columns is a crosshead with two clamping bolts on each side. The actuator mounts to the crosshead. The crosshead can be repositioned up and down along the columns to account for different grips and specimen lengths. A yellow safety collar is positioned underneath the crosshead on one of the columns. The control panel mounted on the side of the load frame allows control of the actuator without the need for software interface. The load cell mounts to the actuator and provides mounting for the tool needed to perform the shear and fatigue loading of the solder joints. The load cell connects electrically to the 5900 controller module. The 5900 controller module is the primary part of the Instron 5948 system that communicates to the computer. The controller contains sensor conditioning cards for the load cell and transfers data between the load cell and the computer. The load frame also connects to the 5900 controller module via the control panel. Information from the control panel such as extension and load are communicated to the computer and the Bluehill software application.

Instron's Bluehill 3 Testing Software is their top-of-the-line material and component testing software application. It can be used for testing plastics, composites, metal, elastomers, adhesives, textiles, and other materials. Each test method within the software application provides the ability to test tension, compression, flexure, fatigue, and creep. The software application, when executing a test, manipulates the actuator on the load frame via the computer's connection with the 5900 controller then through the control panel. The current version utilized with the Instron 5948 system is v3.25. The start screen of the Bluehill 3 application is shown in Fig. 4-9.

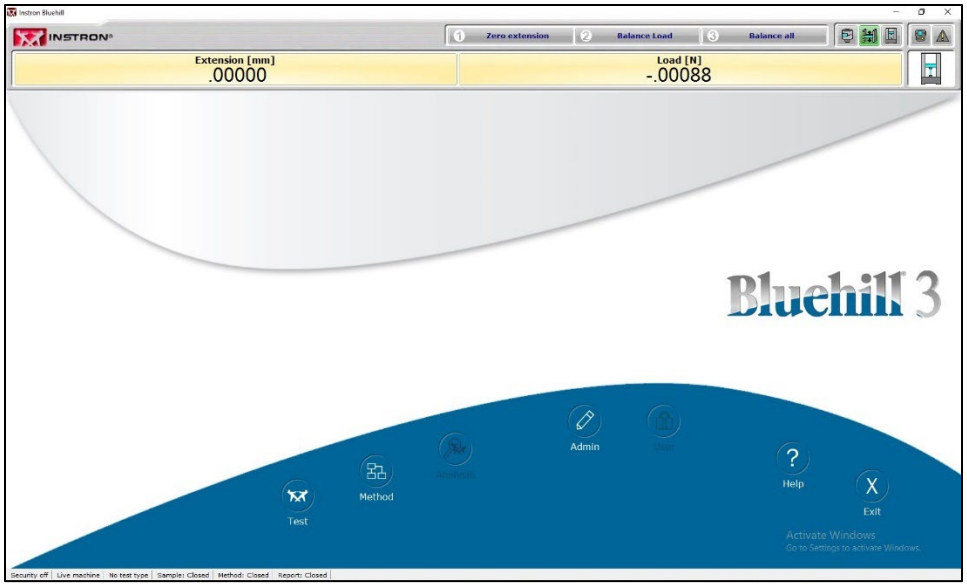


Fig. 4-9: Bluehill 3 v3.25 start-up screen.

The test sample is adhered to the tool fixture by using an instant adhesive. A test sample mounted on the custom tool fixture with the shear tool (coupled to the load cell) in position to apply a load to a solder joint is shown in Fig. 4-10.

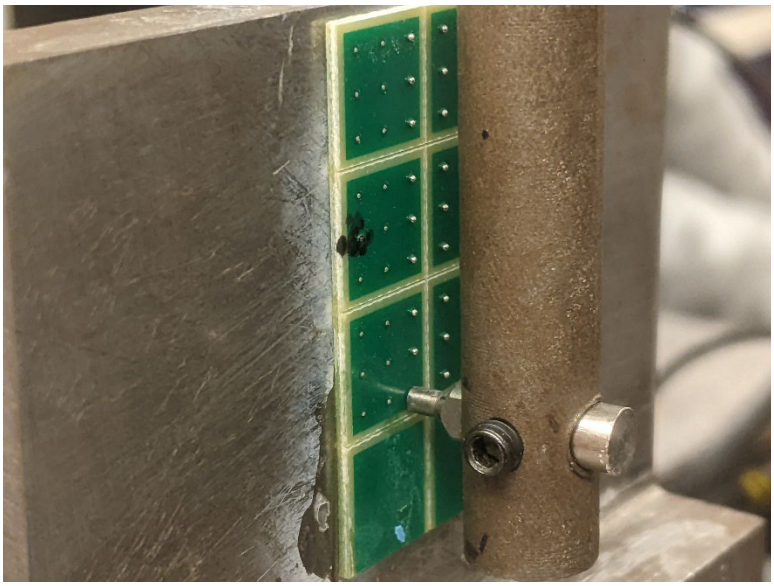

Fig. 4-10: Actual test article subjected to a loading test.

The assembly of the substrate was modeled to illustrate the SMD construction around the SMT pad. The opening in the solder mask exposing the SMT pad is illustrated in Fig. 4-11.

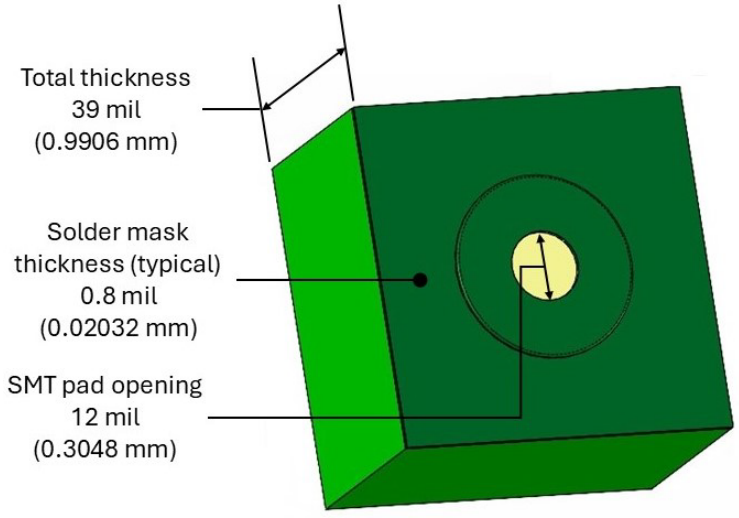


Fig. 4-11: Isometric view of the model of the SMT pad with SMD.

A model was also created of the testing apparatus to illustrate the placement of the shear tool around the solder sphere for shear and fatigue testing. The illustrations for the test articles with 4 mil and 5 mil thick solder paste are shown in Fig. 4-12.

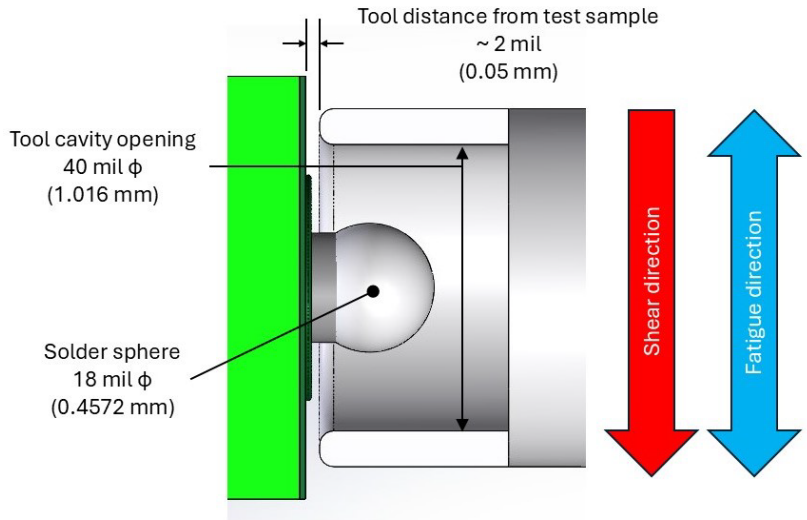


Fig. 4-12: Test setup illustrating the shear tool distance from test article.

## 4.4 Proposed Test Plan

### 4.4.1 Study I

The objective of this study is to examine SMIC's suggested shear strength improvements of M758 and M794 alloys over the standard SAC305 (M705) alloy. It will also evaluate the significance of changing the solder paste volume regarding shear strength. The test samples will have an OSP surface finish. The test samples were not aged. They will be tested in an as-received condition. There are 4 different strain rate levels that will be conducted for each solder paste and solder paste thickness configuration. Table XXIX summarizes the shear testing plan.

TABLE XXIX
SHEAR TEST MATRIX FOR STUDY I

| Test Board Serial Number of Test Sample | Configuration | Strain Rate Level ($sec^{-1}$) | Replicates |
|---|---|---|---|
| 707215 | 4 mil thick M705 solder paste OSP | 0.001 | 7 |
| | | 0.01 | 7 |
| | | 0.1 | 7 |
| | | 1 | 7 |
| 707221 | 4 mil thick M758 solder paste OSP | 0.001 | 7 |
| | | 0.01 | 7 |
| | | 0.1 | 7 |
| | | 1 | 7 |
| 707227 | 4 mil thick M794 solder paste OSP | 0.001 | 7 |
| | | 0.01 | 7 |
| | | 0.1 | 7 |
| | | 1 | 7 |
| 707218 | 5 mil thick M705 solder paste OSP | 0.001 | 7 |
| | | 0.01 | 7 |
| | | 0.1 | 7 |
| | | 1 | 7 |
| 707224 | 5 mil thick M758 solder paste OSP | 0.001 | 7 |
| | | 0.01 | 7 |
| | | 0.1 | 7 |
| | | 1 | 7 |
| 707230 | 5 mil thick M794 solder paste OSP | 0.001 | 7 |
| | | 0.01 | 7 |
| | | 0.1 | 7 |
| | | 1 | 7 |

The shear strength is recorded in .05 second increments for the 1 and 0.1 strain rates and .10 second increments for the 0.01 and 0.001 strain rates. For each strain rate test, the Instron applies the load until the solder joint completely fails. Since the solder joints are a very ductile material, the yield strength isn't easily identifiable. A 0.2 % offset yield strength would need to be implemented to estimate that value, whereas the ultimate strength is very distinguishable. So, from the data collected, the ultimate strength will be averaged and plotted in individual value plots against the different solder paste and solder paste volumes. The ultimate strengths of the solder pastes and associated volumes will then be plotted against each of the four strain rates.

The data in determining the ultimate strengths will then be used to perform an analysis of variance (ANOVA). From the ANOVA, main effects plots will be generated to evaluate the changes in the means of the shear strength associated with the different solder pastes and volumes and the different strain rates to determine their influence on the means. Interaction plots will be constructed to show if there is any interaction between the solder pastes and volumes and strain rates and to what degree. Finally, the ultimate shear strengths will be plotted as a fitted function of strain rates to evaluate the behaviors against the different solder pastes and volumes.

### 4.4.2 Study II

The objective of this study is to evaluate the reliability (fatigue strength) of M758 and M794 alloys over the standard SAC305 (M705) alloy. The evaluation will be conducted with test articles assembled with 4 mil thick solder paste. The test samples will have an OSP surface finish. The test samples were not aged. They will be tested in an as-received condition. There are 3 different cyclic shear stress levels that will be conducted for each solder paste configuration. Table XXX summarizes the fatigue strength testing plan.

TABLE XXX
FATIGUE TEST MATRIX FOR STUDY II

| Test Board Serial Number of Test Sample | Configuration | Stress Level (MPa) | Replicates |
|---|---|---|---|
| 707215 | 4 mil thick M705 solder paste OSP | 16 | 7 |
| | | 20 | 7 |
| | | 24 | 7 |
| 707221 | 4 mil thick M758 solder paste OSP | 16 | 7 |
| | | 20 | 7 |
| | | 24 | 7 |
| 707227 | 4 mil thick M794 solder paste OSP | 16 | 7 |
| | | 20 | 7 |
| | | 24 | 7 |

Weibull distribution will be used to analysis the reliability of the different solder paste joints. The testing will start at time zero which will reduce the distribution to a 2-parameter Weibull model. The number of cycles that each solder joint sustains before failure will serve for the continuous variable of time. Weibull probability plots of the three different solder joints will be produced in log-log graphs to show characteristic fatigue life of those joints under the three different stress amplitudes. This analysis will provide the shape and scale parameters for each combination of cyclic stress levels and solder paste alloys.

In addition, each solder paste joint will be fitted for to a function that plots the characteristic life (number of cycles) and the associated stress amplitudes in a log-log graph. This will provide the ability to estimate the number of cycles the solder paste joint could sustain if subjected to a given cyclic stress amplitude. Finally, the characteristic life and B10 life will be summarized in bar charts.

### 4.4.3 Study III

The objective of this study is to further examine the shear and fatigue strengths of M758 and M794 alloys over the standard SAC305 (M705) alloy. The test of this study uses test samples having an ENIG surface finish as opposed to OSP. The results will be compared to those captured in Study I. The test samples were not aged. They will be tested in an as-received condition. The four different strain rate levels and three different fatigue stress levels will be repeated for each test sample constructed with ENIG surface finishes. Table XXXI and Table XXXII summarize the shear and fatigue testing plans.

TABLE XXXI
SHEAR TEST MATRIX FOR STUDY III

| Test Board Serial Number of Test Sample | Configuration | Strain Rate Level ($sec^{-1}$) | Replicates |
|---|---|---|---|
| 707233 | 4 mil thick M705 solder paste ENIG | 0.001 | 7 |
| | | 0.01 | 7 |
| | | 0.1 | 7 |
| | | 1 | 7 |
| 707239 | 4 mil thick M758 solder paste ENIG | 0.001 | 7 |
| | | 0.01 | 7 |
| | | 0.1 | 7 |
| | | 1 | 7 |
| 707245 | 4 mil thick M794 solder paste ENIG | 0.001 | 7 |
| | | 0.01 | 7 |
| | | 0.1 | 7 |
| | | 1 | 7 |

TABLE XXXII
FATIGUE TEST MATRIX FOR STUDY III

| Test Board Serial Number of Test Sample | Configuration | Stress Level (MPa) | Replicates |
|---|---|---|---|
| 707233 | 4 mil thick M705 solder paste ENIG | 16 | 7 |
| | | 20 | 7 |
| | | 24 | 7 |
| 707239 | 4 mil thick M758 solder paste ENIG | 16 | 7 |
| | | 20 | 7 |
| | | 24 | 7 |
| 707245 | 4 mil thick M794 solder paste ENIG | 16 | 7 |
| | | 20 | 7 |
| | | 24 | 7 |

The results of this study will be a combination of the outputs from Study I and II. With the solder paste thickness being tested at 4 mil, the ultimate strength will be averaged and plotted in individual value plots against the different solder paste tested at 4 mil thick and surface finishes (OSP and ENIG). The ultimate strengths of the solder pastes and associated surface finishes will then be plotted against each of the four strain rates.

The data in determining the ultimate strengths will then be used to perform an analysis of variance (ANOVA). From the ANOVA, main effects plots will be generated to evaluate the changes in the means of the shear strength associated with the different solder paste at 4 mil thick, surface finishes and the different strain rates to determine their influence on the means. Interaction plots will be constructed to show if there is any interaction between the solder pastes, surface finishes and strain rates and to what degree. Finally, the ultimate shear strengths will be plotted as a fitted function of strain rates to evaluate the behaviors against the different solder pastes and surface finishes.

Weibull distribution will again be used to analysis the reliability of the different solder paste joints. Weibull probability plots of the three different solder joints and associated surface finishes will be produced in log-log graphs to show characteristic fatigue life of those joints under the three different stress amplitudes. This analysis will provide the shape and scale parameters for each combination of cyclic stress levels, solder paste alloys, and surface finishes.

In addition, each solder paste joint and associated surface finish will be fitted for to a function that plots the characteristic life (number of cycles) and the associated stress amplitudes in a log-log graph. This will provide the ability to estimate the number of cycles that a particular solder paste joint/surface finish combination could sustain if subjected to a given cyclic stress amplitude. Finally, the characteristic life and B10 life will be summarized in bar charts.

## Chapter 5 Effect of Solder Paste on the Shear Properties of SAC305 Solder Joints

Most of the publications sited in Chapter 2 covering mechanical properties of solder alloys focused on the normal (or tensile) stress strain relationship. In researching literature and experiments specifically concerning the use of Ni, Bi, and Sb with SAC305 solder alloy, the results of the search found it was a mix of tensile and shear testing that was performed. Since Chapter 2 did not elaborate on the relationship between shear stress and strain, it becomes important to expound on the shear stress strain relationship and the governing equations used in the research being presented.

The shear testing conducted will be a direct shear (or simple shear). This simply states that the shear is caused by the "direct action" of the force being applied. The type of shear is termed a single shear where the shear force is equal to the force (*F*) applied as shown in Fig. 5-1 [13].

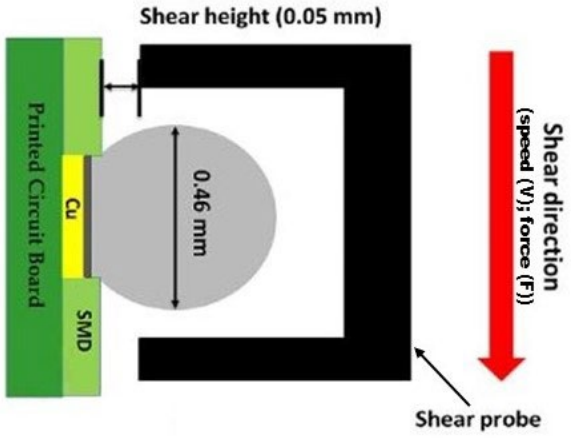


Fig. 5-1: Illustration of single direct shear.
Adapted from [86].

The average shear stress of a single direct shear can be calculated as shown in Equation 5.1 [13].

$$\tau_{avg} = \frac{F}{A} \tag{5.1}$$

The strain and rate of strain, borrowed from fluid mechanics, can be calculated as shown in Equation 5.2 [103].

$$\gamma = \frac{V}{shear\ height};\ \dot{\gamma} = \frac{d\gamma}{dt} \tag{5.2}$$

Therefore, the shear speed and shear height used for the experiment can be used to calculate the actual strain rates for all four levels of Study I and III as shown in Table XXXIII.

TABLE XXXIII
STUDY I & III – ACTUAL STRAIN RATE LEVELS

| **Proposed Strain Rate Level ($sec^{-1}$)** | **Shear speed (mm/sec)** | **Shear height (mm)** | **Actual Strain Rate Level (sec-1)** |
|---|---|---|---|
| 0.001 | 0.00018288 | 0.05 | 0.0036576 (~0.004) |
| 0.01 | 0.0018288 | 0.05 | 0.036576 (~0.04) |
| 0.1 | 0.018288 | 0.05 | 0.36576 (~0.4) |
| 1 | 0.18288 | 0.05 | 3.6576 (~4.0) |

Table XXXIV shows the date that each test of this study was conducted. All experiments were conducted at room temperature.

TABLE XXXIV
DATES OF STUDY I TESTS

| **Test Board Serial Number of Test Sample** | **Configuration** | **Strain Rate Level ($sec^{-1}$)** | **Test Date** | **Days After Receipt** |
|---|---|---|---|---|
| 707215 | M705 solder paste, 4 mil, OSP | 0.01 and 0.001 | 7/18/2023 | 34 |
| | | 1 and 0.1 | 7/17/2023 | 33 |
| 707221 | M758 solder paste, 4 mil, OSP | 0.01 and 0.001 | 7/19/2023 | 35 |
| | | 1 and 0.1 | 7/18/2023 | 34 |
| 707227 | M794 solder paste, 4 mil, OSP | All | 7/20/2023 | 36 |
| 707218 | M705 solder paste, 5 mil, OSP | All | 3/10/2025 | 635 |
| 707224 | M758 solder paste, 5 mil, OSP | All | 3/11/2025 | 636 |
| 707230 | M794 solder paste, 5 mil, OSP | All | 3/11/2025 | 636 |

Fig. 5-2 shows the results of shear testing unaged test articles with SAC305 solder spheres combined with M705 solder paste at 4 mil thick with an OSP surface finish under all four different strain rates.

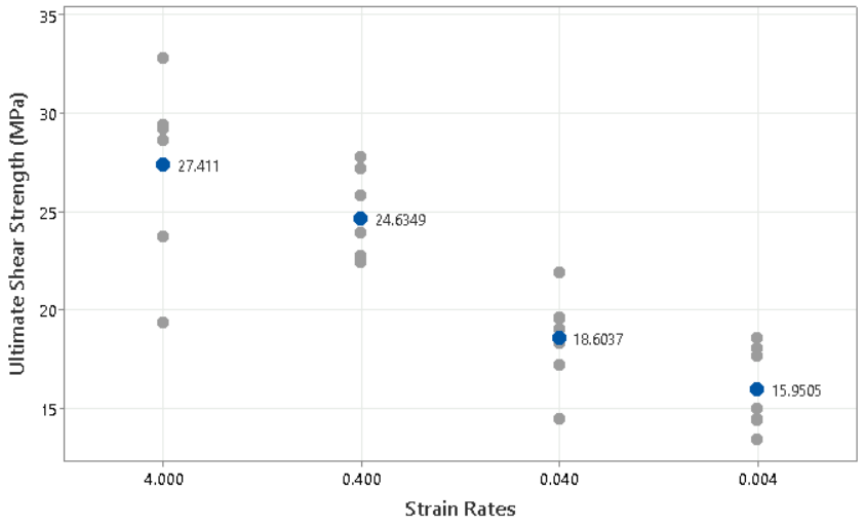


Fig. 5-2: Study I - Individual value and mean plot for M705: 4 mil, OSP.

Fig. 5-3 and 5-4 show the results of shear testing unaged SAC305 solder spheres with M758 and M794 solder pastes at 4 mil thick with an OSP surface finish under all four different strain rates.

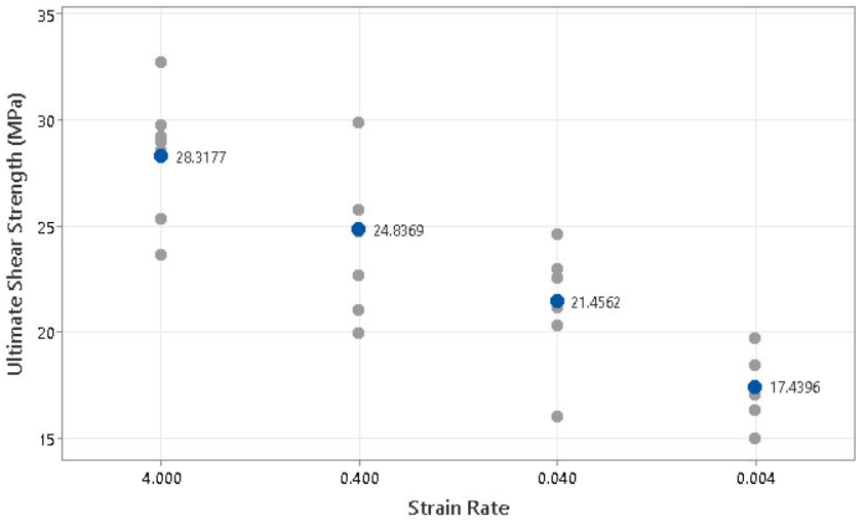


Fig. 5-3: Study I - Individual value and mean plot for M758: 4 mil, OSP.

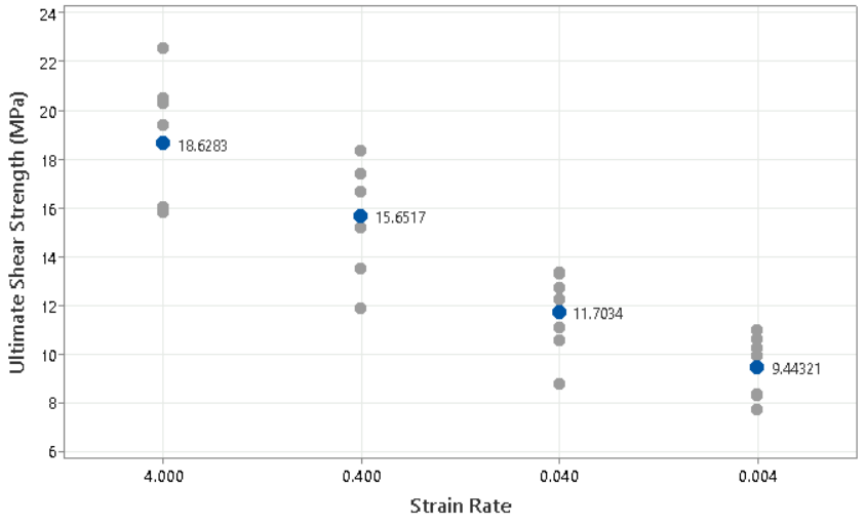


Fig. 5-4: Study I - Individual value and mean plot for M794: 4 mil, OSP.

Looking at the results of shear testing the three different solder paste alloys at a thickness of 4 mil, it shows that the M758 alloy performs slightly better than the M705 (SAC305) alloy. However, the M794 alloy performed significantly less than the M758, and more noticeably, the M705 alloy. Tensile strength testing by Wang covered in 3.1.3 of Chapter 3 provided evidence that increasing the percentage of Sb from 2.0% to 2.5%, while maintaining the concentration of Ni, lowered the tensile strength of the SAC305-Ni-Sb alloy. In addition, Yan tensile strength testing covered in 3.1.4 of Chapter 3 demonstrated that maintaining Sb at 2.0% while increasing Bi of a SAC305-Bi-Sb-Ni alloy increased the tensile strength of the alloy. Taking these experiments into account, there was an expectation that M794 may perform lower than M758 being that M794 alloy contains 3.0% Sb, but the delta between the average ultimate shear stresses was more than anticipated. In addition, the performance of M794 being lower than M705 was not expected.  Also, M794 has an additional element in the alloy whose identity and concentration are proprietary which may contribute to the poor performance.

Another observation was that the ultimate shear stress for each solder paste alloy decreased as the strain rate slowed. This observation was to be expected. Fig. 5-5 compares all three solder

paste alloys' average ultimate stresses tested at 4 mil thickness with OSP surface finish for all four different strain rates.

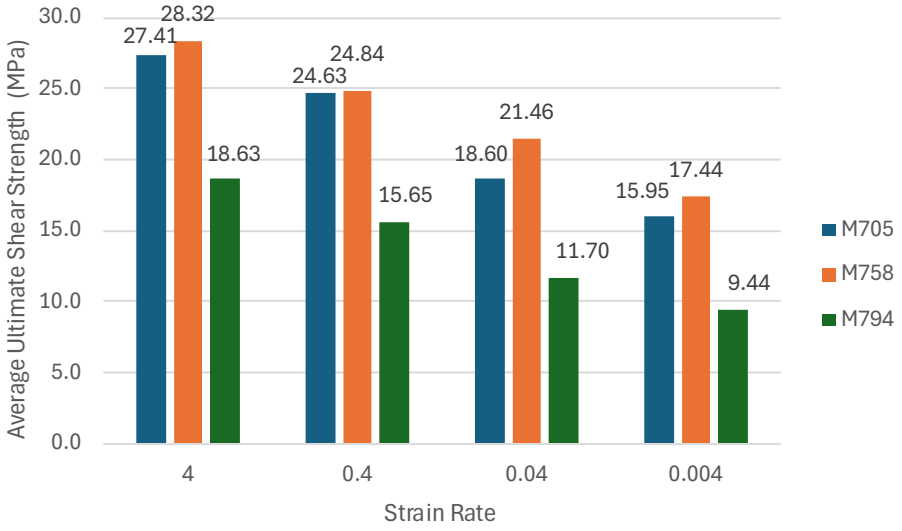


Fig. 5-5: Study I - average ultimate shear strength: 4 mil, OSP.

Fig. 5-6 shows the observations of all three solder paste alloys tested to 5 mil thicknesses for all four strain rates.

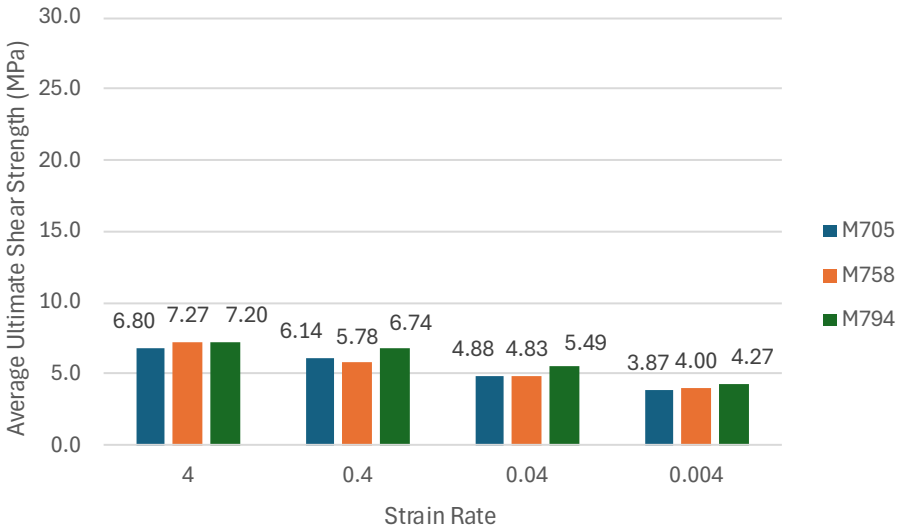


Fig. 5-6: Study I - average ultimate shear strength: 5 mil, OSP.

Testing the three different solder paste alloys at a higher thickness resulted in the average ultimate strength decreasing for all three alloys. By increasing the solder paste thickness from 4 mil to 5 mil for M705 and M758, it resulted in the average ultimate strength decreasing by a factor of 4 while the M794 decreased by a factor slightly higher than 2.

Alakayleh indicated in 3.4 of Chapter 3 that for these specific solder paste alloys the IMC thicknesses and average $Ag_3Sn$ area (with the exception of SAC305 solder paste remaining relatively unchanged) decreases as the volume increase but also pointing out that the number of the $Ag_3Sn$ particles and average void area increased as the volume increased. For SAC305, SAC-Bi and SAC-Bi-Sb evaluated by Alakayleh, the number of $Ag_3Sb$ particles increased by approximately 50%, 60%, and 65% respectively between 4 mil and 5 mil thicknesses. This can be expected due to the higher volume of solder paste contributing a higher weighted percentage of Ag. The most noticable was that the average void area per solder joint increased approximately by a factor of 2, 0.4, and 4.5 respectively between 4 mil and 5 mil thicknesses [96]. Ismail indicated that coarsening and growing of $Ag_3Sn$ particles will reduce the mechanical strength of a solder joint. The growth and coarsening of $Ag_3Sn$ particles will also contribute to the creation of additional voids and cracks [79].

Though the articles tested with 5 mil solder paste thickness were not thermally aged, they were aged. The solder joints with 5 mil thick solder paste were tested over 630 days after receipt from the manufacturer and 600 days after testing the units with 4 mil thick solder paste. With the awareness that increasing the solder paste volume of these particular alloys creates additional $Ag_3Sn$ particulars and increases the average void area, the 600 days could have led to modifications taking place in the microstructure; thereby, negatively affecting the ultimate strength of the 5 mil thick solder joints. These can leading factors in why the average ultimate

strength of the solder paste alloys at 5 mil thick results were substantibly lower than those at 4 mil thick.

The average ultimate shear strength trended downward as the strain rate increased for all three solder paste alloys, but surprisingly different from the 4 mil thick samples, the M794 had the highest average ultimate shear strength compared to the M705 and M758 for the 5 mil thick samples. Without the benefits of having SEM images to further investigate the probable causes to attribute to M794 having a higher ultimates strength, the reasoning can only be theorized. With the additions of Bi, Sb, Ni, and the unknown element providing the expected solution and dispersion hardening, this would have offset the impact of $Ag_3Sn$ coarsening thereby retaining a higher strength over the M705 and M758 alloys.

The main effects plot for the different solder paste alloy, solder paste thickness and strain rate were plotted against the average ultimate strength as shown in Fig. 5-7.

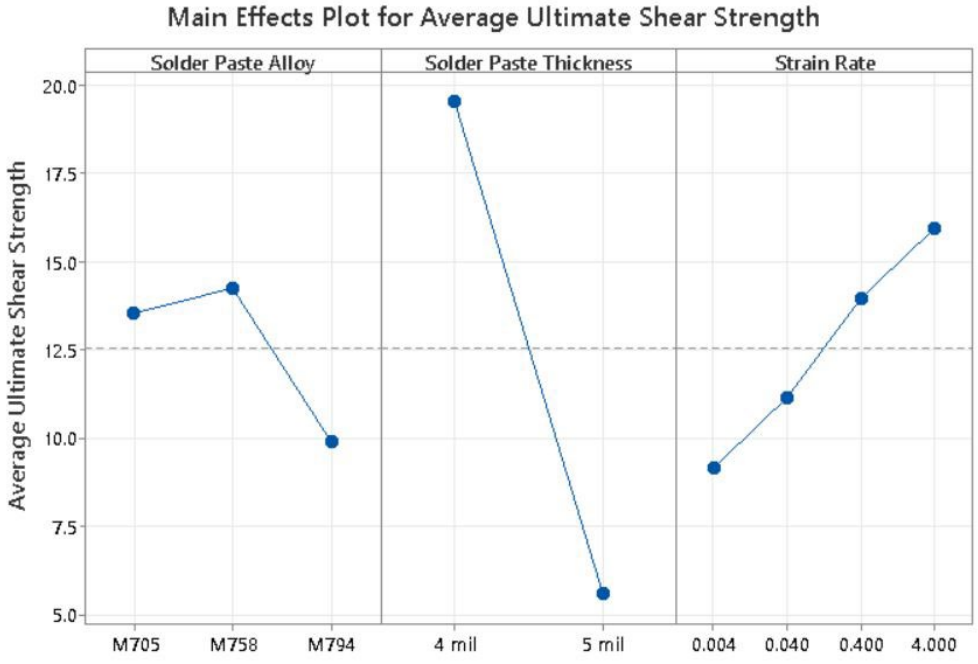


Fig. 5-7: Study I - main effects plot for solder paste alloy/thickness and strain rate.

The main effects plot clearly shows that the solder paste thickness greatly affects the average ultimate shear strength. As known, the main effects plot confirms that the slower the strain rate, the lower the ultimate shear strength. There's not much difference between M705 and M758 solder paste alloys; conversely, the use of M794 has a significant negative affect on the ultimate shear strength.

The interaction between the solder paste alloys and thicknesses at the different strain rates is shown in the interaction plot of Fig. 5-8.

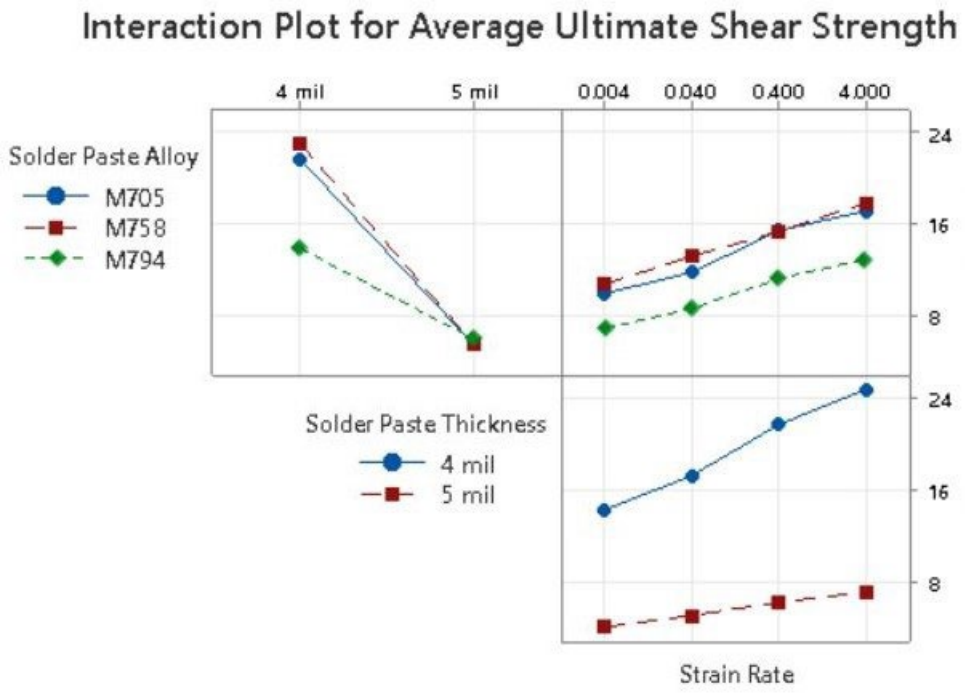


Fig. 5-8: Study I – interaction plot of solder paste alloy/thickness and strain rate.

The interaction plot shows that there is effectively no interaction between the solder paste alloys and strain rate in determining ultimate shear strength. There is an interaction between the solder paste alloys and their thickness. The interaction plot hints that there may be a slight interaction between the solder paste thickness and strain rate.

The relationship between strain rate and average ultimate shear strength are plotted in log-log graphs to "remove" the skewness and provide a linear relationship between the two. From the log-log linear relationship, a power function will be extracted to easily show a percentage change or multiplicative constant between the two parameters for a given solder paste alloy. The log-log graphs for the 4 mil and 5 mil thick solder paste test samples are shown in Fig. 5-9 and 5-10.

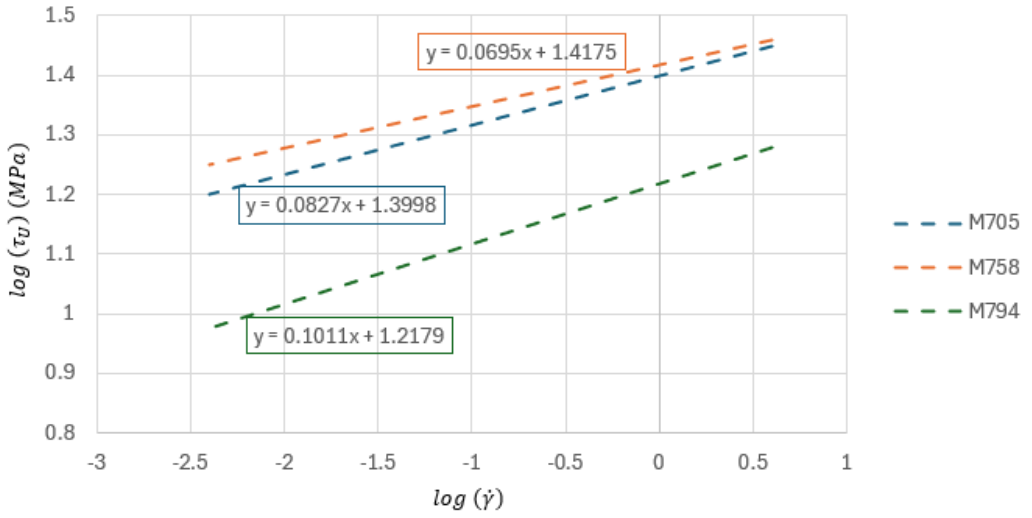


Fig. 5-9: Study I – log-log graph of strain rate and ultimate shear strength: 4 mil, OSP.

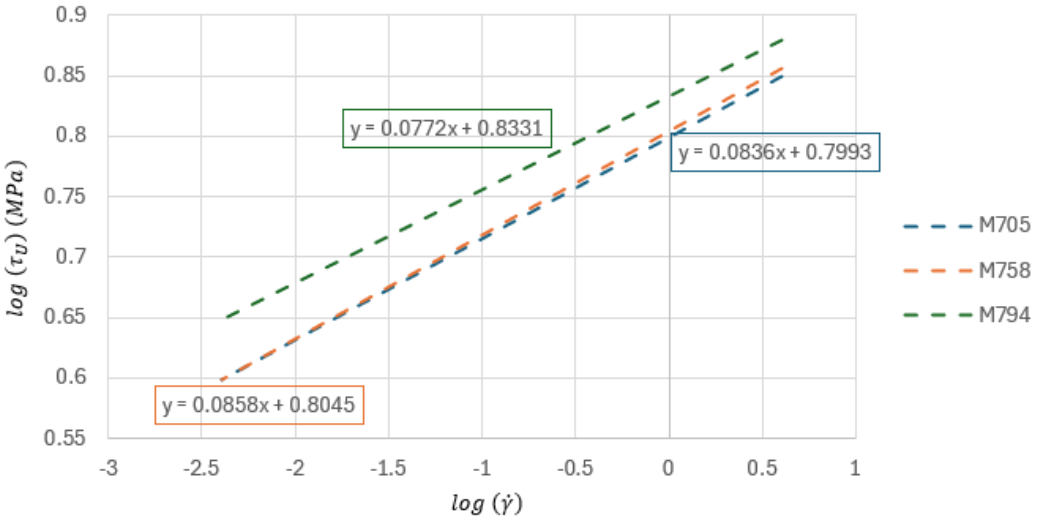


Fig. 5-10: Study I – log-log graph of strain rate and ultimate shear strength: 5 mil, OSP.

From the linear relationships identified in the log-log graphs, the power functions for each combination of solder paste alloy, solder paste thickness, and strain rate are shown in Table XXXV.

TABLE XXXV
STUDY I – POWER FUNCTIONS FOR USS

| Solder Paste Alloy | Solder Paste Thickness (w/ OSP) | Average Ultimate Shear Strength |
|---|---|---|
| **M705** | 4 mil | $25.11\dot{\gamma}^{0.0827}$ |
| | 5 mil | $6.30\dot{\gamma}^{0.0836}$ |
| **M758** | 4 mil | $26.15\dot{\gamma}^{0.0695}$ |
| | 5 mil | $6.38\dot{\gamma}^{0.0858}$ |
| **M794** | 4 mil | $16.52\dot{\gamma}^{0.1011}$ |
| | 5 mil | $6.81\dot{\gamma}^{.0772}$ |

Fatigue testing was conducted without any dwell at room temperature thereby eliminating or reducing the effects of creep on the test samples. The shear speed for the fatigue tests was set at 0.1 mm/sec with 10,000 cycles established as a test stop should a broken solder joint wedge itself between the shear tool and test board to prompt continue execution of the test. Test data is recorded for the time (sec), extension (mm), load (gf), tensile stress (MPa), and cycle count. The data retrieved is used to generate Weibull probability plots to estimate characteristic fatigue life of the solder joints. The characteristic life (number of cycles) can be compared and modeled with the stress amplitudes to provide behavioral characteristics for reliability comparison between the three different solder paste alloys.

The load for each cyclic fatigue test is established in units of grams-force and presented in Table XXXVI.

TABLE XXXVI
INSTRON SETTING FOR ALL FATIGUE TESTING

| | | Load | | | | | |
|---|---|---|---|---|---|---|---|
| 12 mil, circular SMT pad (m) | SMT Pad area ($m^2$) | 16 MPa test (N) | Instron setting (gf) | 20 MPa test (N) | Instron setting (gf) | 24 MPa test (N) | Instron setting (gf) |
| $3.048x10^{-3}$ | $7.297x10^{-8}$ | 1.168 | 119.05 | 1.459 | 148.81 | 1.751 | 178.57 |

Table XXXVII shows the date that each test of this study was conducted. All experiments were conducted at room temperature.

TABLE XXXVII
DATES OF STUDY II TESTS

| Test Board Serial Number of Test Sample | Configuration | Stress Level (MPa) | Test Date | Days After Receipt |
|---|---|---|---|---|
| 707215 | M705 solder paste, 4 mil, OSP | 16 | 9/18/2023 | 96 |
| | | 20 and 24 | 9/19/2023 | 97 |
| 707221 | M758 solder paste, 4 mil, OSP | 16 (3 samples) | 9/19/2023 | 97 |
| | | 16 (4 samples), 20 and 24 | 9/20/2023 | 98 |
| 707227 | M794 solder paste, 4 mil, OSP | All | 9/21/2023 | 99 |

Fig. 6-1 shows the two-parameter Weibull probability plot for M705 with 4 mil thick solder paste and OSP surface finish for all three fatigue stress amplitude tests along with calculated estimates for the shape and scale parameters.

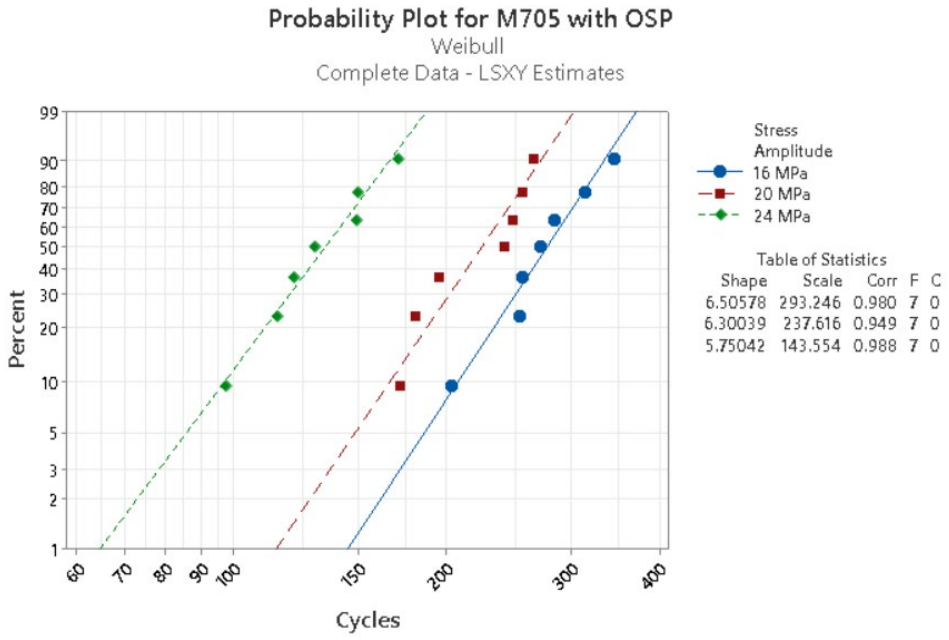


Fig. 6-1: Two-parameter Weibull probability plot for M705: 4 mil, OSP.

Fig. 6-2 and 6-3 provide the same plots for M758 and M794.

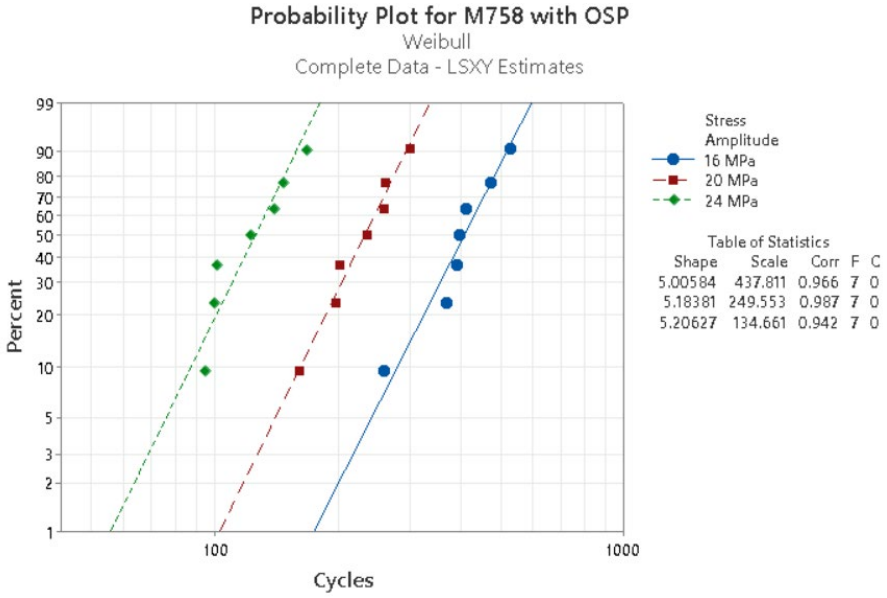


Fig. 6-2: Two-parameter Weibull probability plot for M758: 4 mil, OSP.

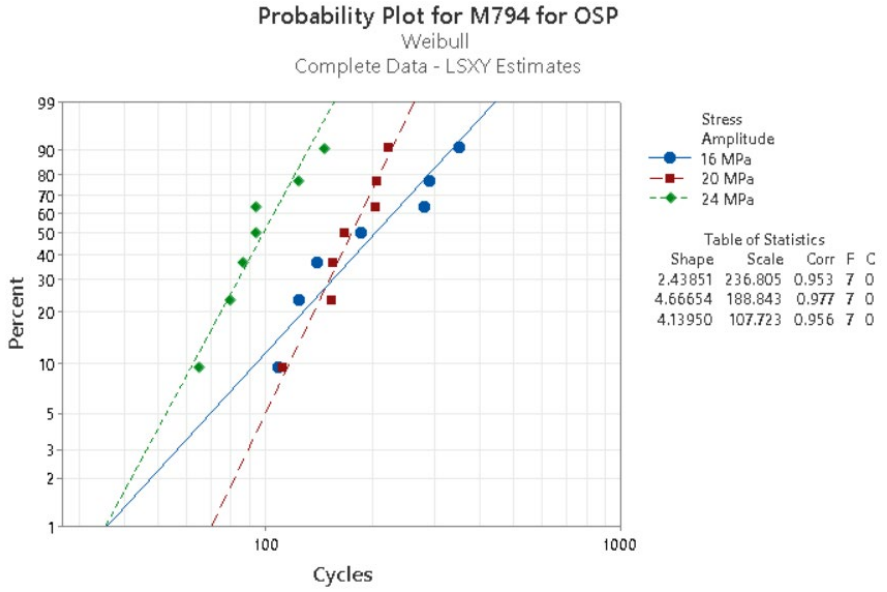


Fig. 6-3: Two-parameter Weibull probability plot for M794: 4 mil, OSP.

For the most part, each solder paste alloy indicates that the solder joint becomes less reliable as the fatigue stress amplitude is increased. The correlation coefficients for all are very close to 1 (all are 0.94 or higher), suggesting that there is a strong linear relationship in the plots. There is a

distinction to be noted in the M794 solder past alloy. For 16 and 20 MPa probability plots were below 30%, the solder joint is more reliable when subjected to a 20 MPa stress amplitude than when subjected to the lower 16 MPa load. For each cyclic load, the solder paste alloys are compared in Fig. 6-3 through 6-5.

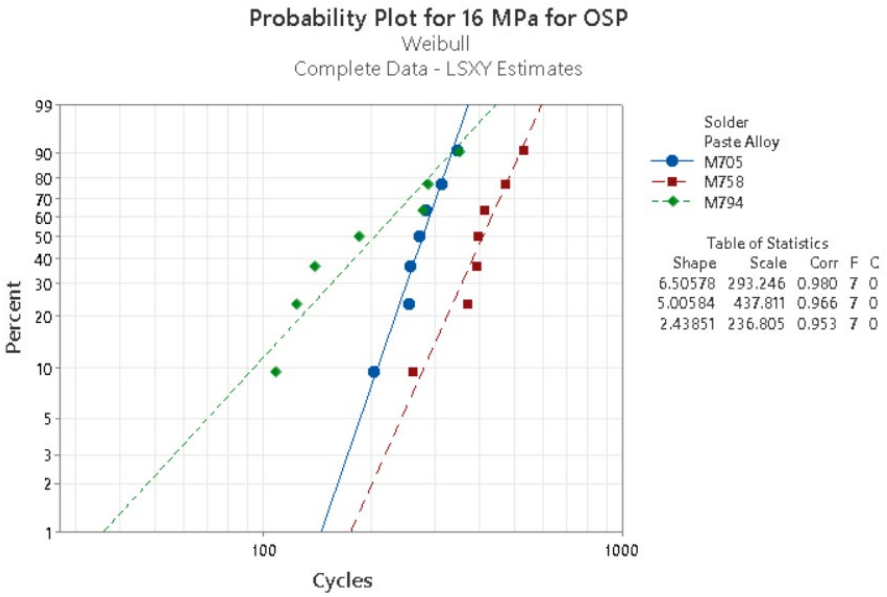


Fig. 6-4: Two-parameter Weibull probability plot for 16 MPa load: 4 mil, OSP.

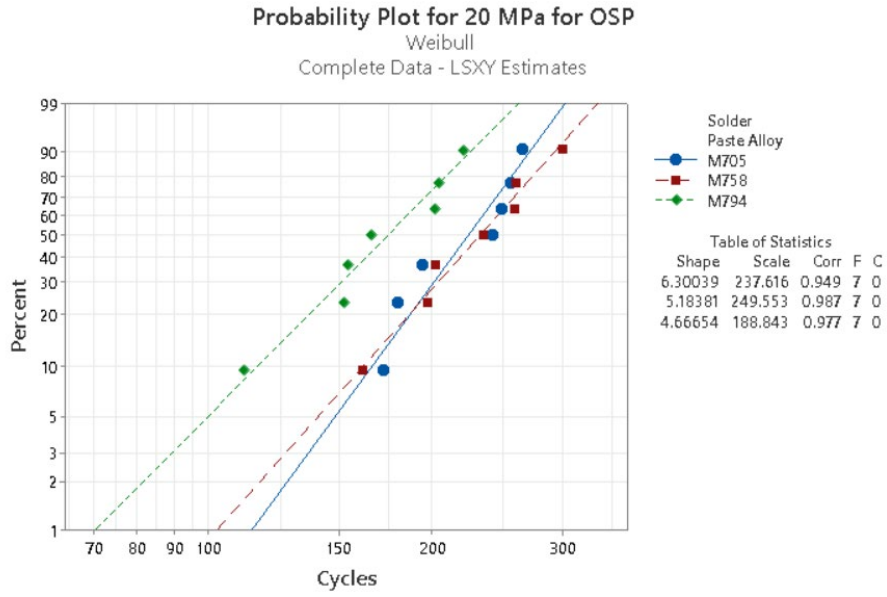


Fig. 6-5: Two-parameter Weibull probability plot for 20 MPa: 4 mil, OSP.

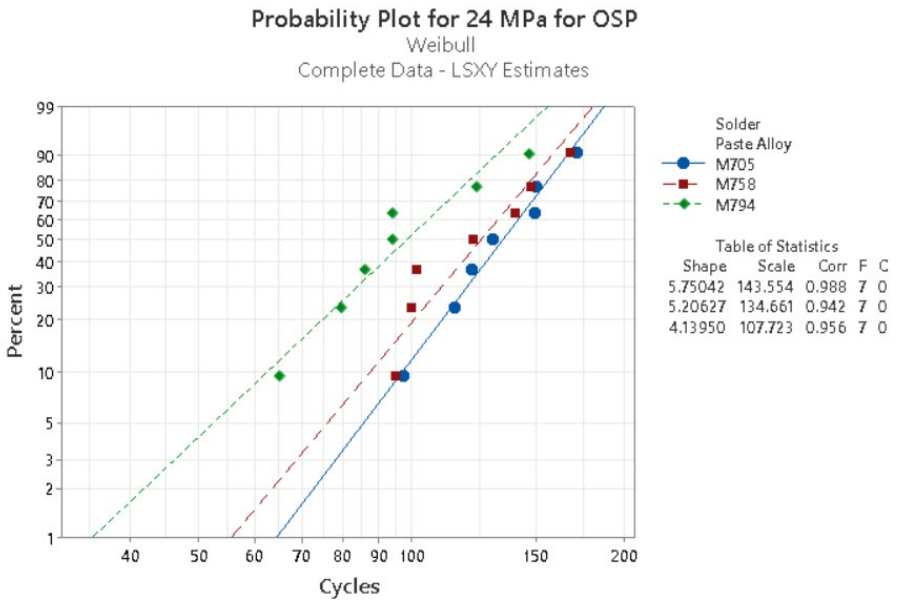


Fig. 6-6: Two-parameter Weibull probability plot for 24 MPa: 4 mil, OSP.

From the Weibull probability plots for each fatigue test, the M758 is clearly better at the 16 MPa cyclic load. The 20 MPa Weibull probability plots show mixed results between M758 and M705 depending on the level of reliability that is being evaluated or of interest. The M705 seems to edge out the M758 at the higher, 24 MPa cyclic load.

The characteristic life is the point in a Weibull distribution where the probability of failure becomes independent of all the parameters that model the distribution. It is set at 63.2 % which captures the moment when failures are expected [104]. The B10 expresses the percentile of product life where 10 % of the products fail. By taking the shape and scale parameters from the Weibull probability plots, the characteristic life and B10 life of each of the solder paste alloys can be easily compared. Bar charts providing the comparison are shown in Fig. 6-7 and 6-8.

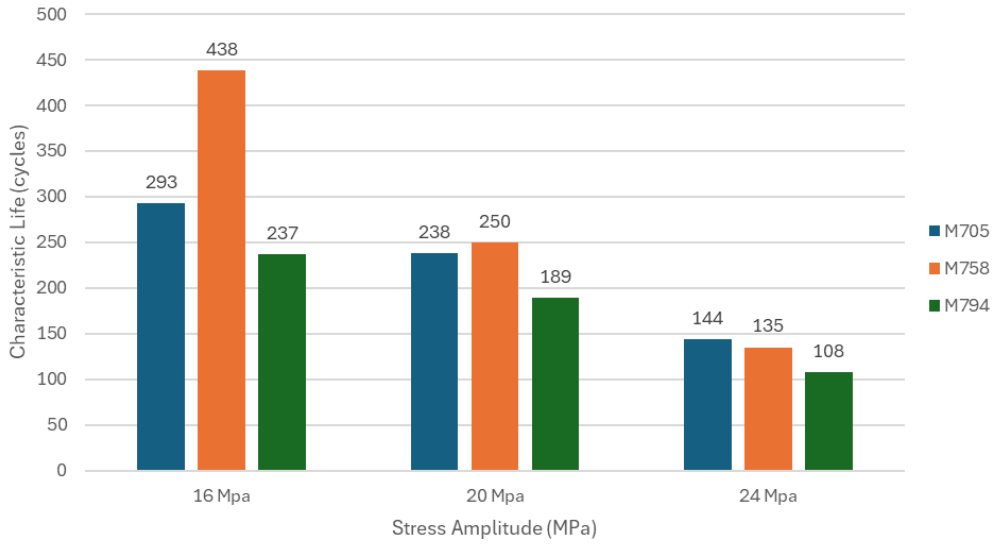


Fig. 6-7: Characteristic life comparison between solder paste alloys: 4 mil, OSP.

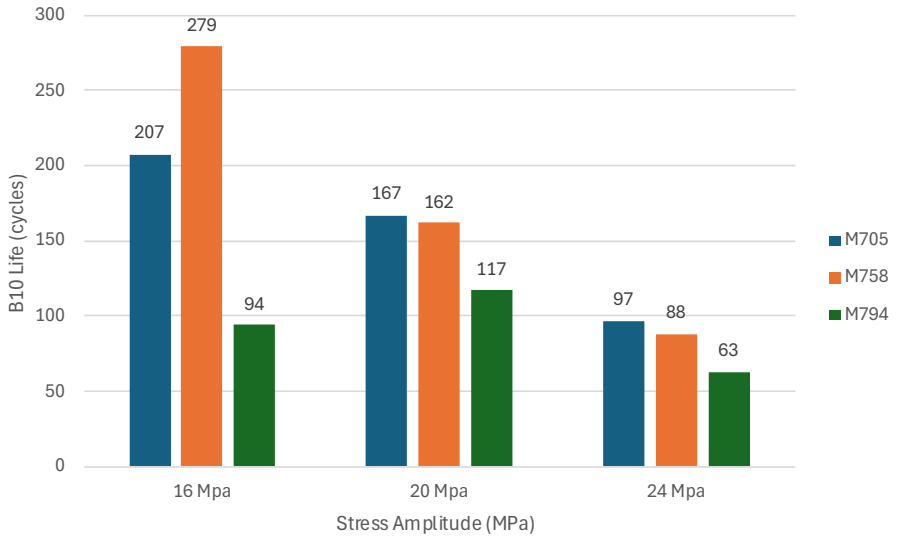


Fig. 6-8: B10 life comparison between solder paste alloys: 4 mil, OSP.

The M758 solder paste alloy outperformed the M705 and M794 for the 16 MPa and 20 MPa stress cycles. For the 16 MPa cyclic load, the M758 characteristic life is 49 % better than M705 and 85 % better than M794. For the 20 MPa cyclic load, the M758 characteristic life is 5 %

better than M705 and 32 % better than M794. There was a significant decrease in the ratios of M758 characteristic life going from 16 MPa to 20 MPa compared to the other two. Conversely, M705 edges out M758 for the 24 MPa cyclic load being 7 % better than M758 and 33 % better than M794. For the most part, the B10 characteristic lifes show a similar relationship between the solder paste alloys with the except of the 20 MPa comparison. With the characteristic lifes being close for the 20 MPa fatigue test, M705 edges out M758 with a slight higher B10 life due to the shape parameter being slightly higher.

Using Equation (3.1), the characteristic life can be modeled in a power expression as shown in Fig. 6-9.

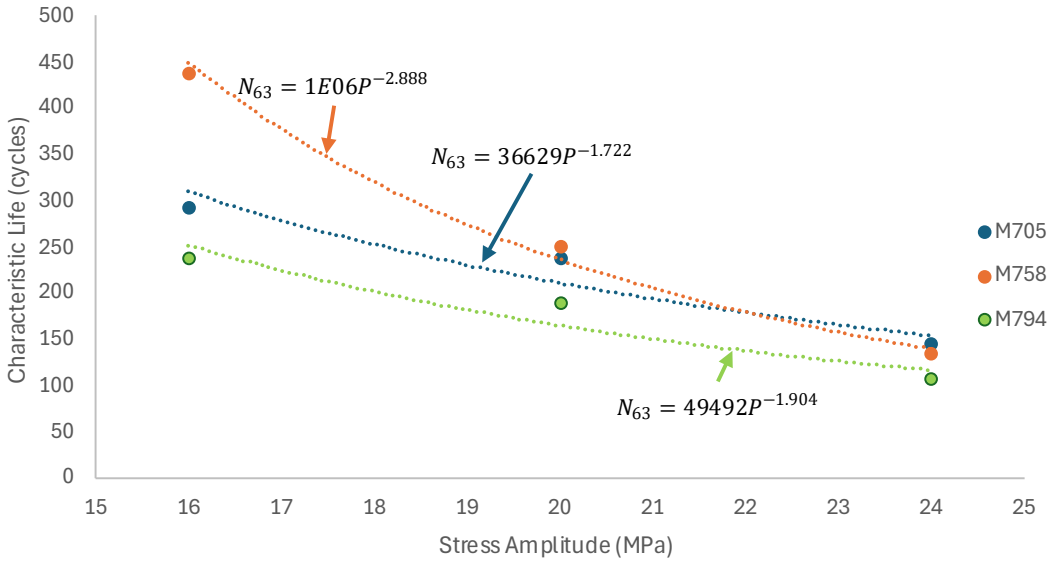


Fig. 6-9: Study II – characteristic life vs stress amplitude: 4 mil, OSP.

The material constants also provide insight into the behavior of the solder paste alloys as the stress amplitude is decreased below 16 MPa. The M758 has the highest of all three until reaching

the final cyclic load. In comparing the M705 to M794, the M794 has a higher material constant than the M705. At the 16 MPa stress amplitude, the M705 has a higher characteristic life than the M794 but as the stress amplitude approaches zero, at some point, the M794 would have a higher characteristics life than the M705. The exponent, ductility factor, indicates that the M758 behavior is more brittle than the M705 and M794. This is easily verified visually also due to the slope of the M758 plot is higher than the slope of the M705 and M794 curves. Note at the 24 MPa stress level that the characteristic life of M758 drops below M705. As the stress amplitude is increased past 24 MPa, the brittle behavior of M758 would suggest the characteristic life may drop below the M794.

Table XXXVIII shows the date that each test of this study was conducted. All experiments were conducted at room temperature.

TABLE XXXVIII
DATES OF STUDY III TESTS

| **Test Board Serial Number of Test Sample** | **Configuration** | **Strain Rate Level ($sec^{-1}$)** | **Test Date** | **Days After Receipt** |
|---|---|---|---|---|
| 707233 | M705 solder paste, 4 mil, ENIG | 0.001 | 8/8/2023 | 55 |
| | | 1, 0.1, and 0.01 | 8/7/2023 | 54 |
| 707239 | M758 solder paste, 4 mil, ENIG | 0.01 and 0.001 | 8/9/2023 | 56 |
| | | 1 and 0.1 | 8/8/2023 | 55 |
| 707245 | M794 solder paste, 4 mil, ENIG | 0.001 | 8/11/2023 | 58 |
| | | 1, 0.1, and 0.01 | 8/10/2023 | 57 |
| **Test Board Serial Number of Test Sample** | **Configuration** | **Stress Level (MPa)** | **Test Date** | **Days After Receipt** |
| 707233 | M705 solder paste, 4 mil, ENIG | All | 11/6/2023 | 145 |
| 707239 | M758 solder paste, 4 mil, ENIG | All | 11/7/2023 | 146 |
| 707245 | M794 solder paste, 4 mil, ENIG | All | 11/8/2023 | 147 |

Fig. 7-1 shows the results of shear testing unaged test articles with SAC305 solder spheres combined with M705 solder paste at 4 mil thick with an ENIG surface finish under all four different strain rates.

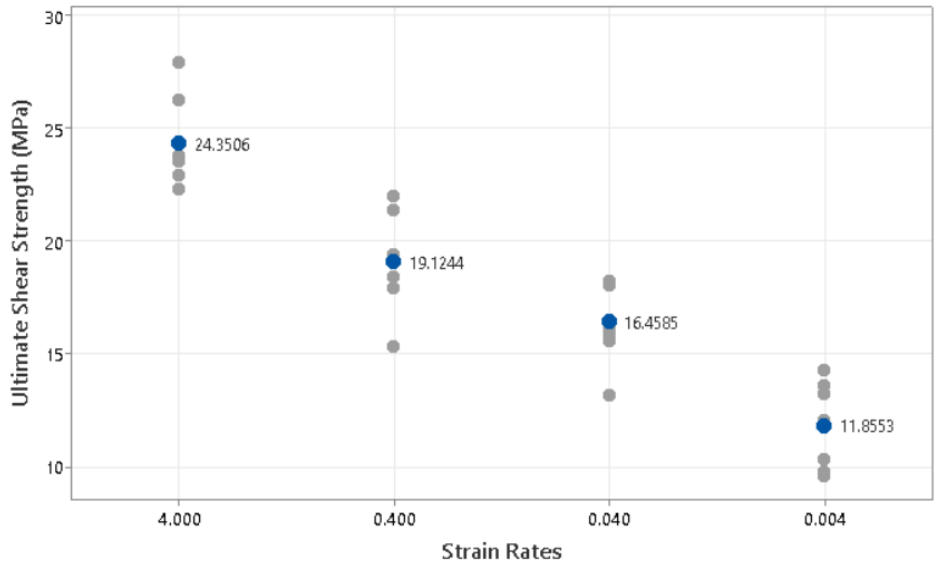


Fig. 7-1: Study III - Individual value and mean plot for M705: 4 mil, ENIG.

Fig. 7-2 and 7-3 show the results of shear testing unaged SAC305 solder spheres with M758 and M794 solder pastes at 4 mil thick with an ENIG surface finish under all four different strain rates.

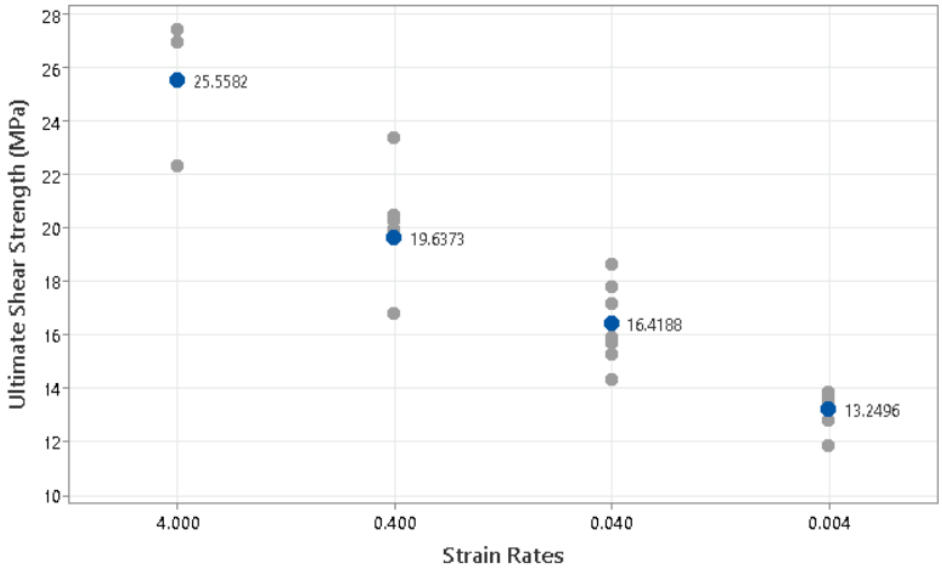


Fig. 7-2: Study III - Individual value and mean plot for M758: 4 mil, ENIG.

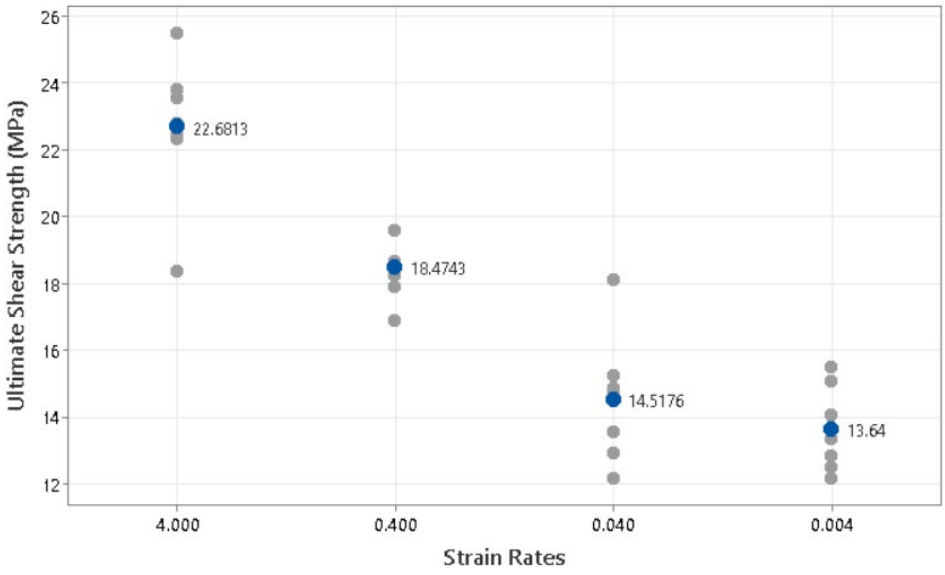


Fig. 7-3: Study III - Individual value and mean plot for M794: 4 mil, ENIG.

Looking at the results of shear testing the three different solder paste alloys at a thickness of 4 mil with an ENIG surface finish, it shows that all three exhibited very similar results for each of the four different strain rates. Fig. 7-4 provides a better view of comparing all three solder paste alloys' average ultimate stresses tested at 4 mil thickness with ENIG surface finish for all four different strain rates.

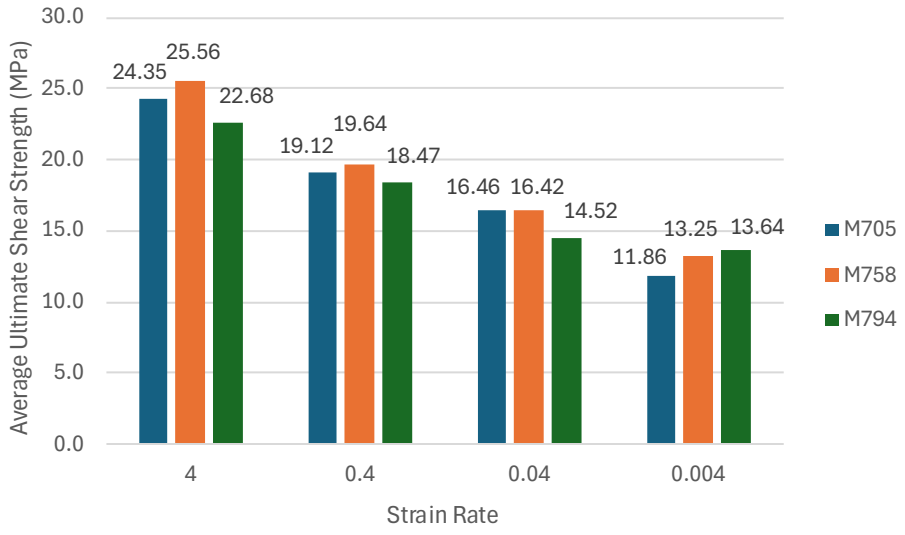


Fig. 7-4: Study III - average ultimate shear strength: 4 mil, ENIG.

Testing the three different solder paste alloys at the same thickness with two different surface finishes (OSP and ENIG) resulted in the average ultimate strength being very close for all three alloys. Table XXXIX compares the average ultimate shear strength between the two surface finishes for all three solder paste alloys at 4 mil thicknesses.

TABLE XXXIX
AVERAGE USS BETWEEN OSP AND ENIG: 4 MIL

| **Strain Rate Level ($sec^{-1}$)** | **M705** Average Ultimate Shear Strength (MPa) | **M758** Average Ultimate Shear Strength (MPa) | **M749** Average Ultimate Shear Strength (MPa) |
|---|---|---|---|
| 4 | 27.41100 (OSP) | 28.31768 (OSP) | 18.62832 (OSP) |
| | 24.35058 (ENIG) | 25.55823 (ENIG) | 22.68134 (ENIG) |
| 0.4 | 24.63490 (OSP) | 24.83687 (OSP) | 15.65174 (OSP) |
| | 19.12442 (ENIG) | 19.63731 (ENIG) | 18.47433 (ENIG) |
| 0.04 | 18.60369 (OSP) | 21.45623 (OSP) | 11.70344 (OSP) |
| | 16.45854 (ENIG) | 16.41877 (ENIG) | 14.51759 (ENIG) |
| 0.004 | 15.95055 (OSP) | 17.43963 (OSP) | 9.44321 (OSP) |
| | 11.85528 (ENIG) | 13.24957 (ENIG) | 13.64004 (ENIG) |

Alakayleh indicated in 3.4 of Chapter 3 that for these specific solder paste alloys the average number of $Ag_3Sn$ particles decreases with the use of OSP over ENIG. In contrast, the use of OSP has a significant effect on increasing the means of the IMC thickness and the Micro-Vicker hardness of the solder joint over the use of ENIG. The is also a slight increase of the mean of the average void area with the use of OSP over ENIG [96]. Knowing that as the IMC layer increases, the solder joint becomes more brittle, this adds to accepting the higher USS for the OSP over ENIG for the M705 and M758 alloys. The M794 stands out as the lone except to this behavior. The ratios of the USS from the OSP to ENIG surface finishes were very consistant. The ratio for

the M705 and M758 ranged from 1.1 to 1.3 for all four strain rates. The ratios for M794 ranged from 0.69 to 0.85. This matches Lentz's analysis in 3.3 of Chapter 3 for ENIG and no clean OSP being closely. Lentz rated ENIG (water soluable and no clean) slightly higher than OSP no clean for printing, wetting, and void suppression which contributes to the expectations seen in the behavior of M794. The OSP solder joints were tested approximately 30 days after receipt; the ENIG solder joints were tested approximately 60 days after receipt.

The main effects plot for the different solder paste alloy, solder paste thickness and strain rate were plotted against the average ultimate strength as shown in Fig. 7-5.

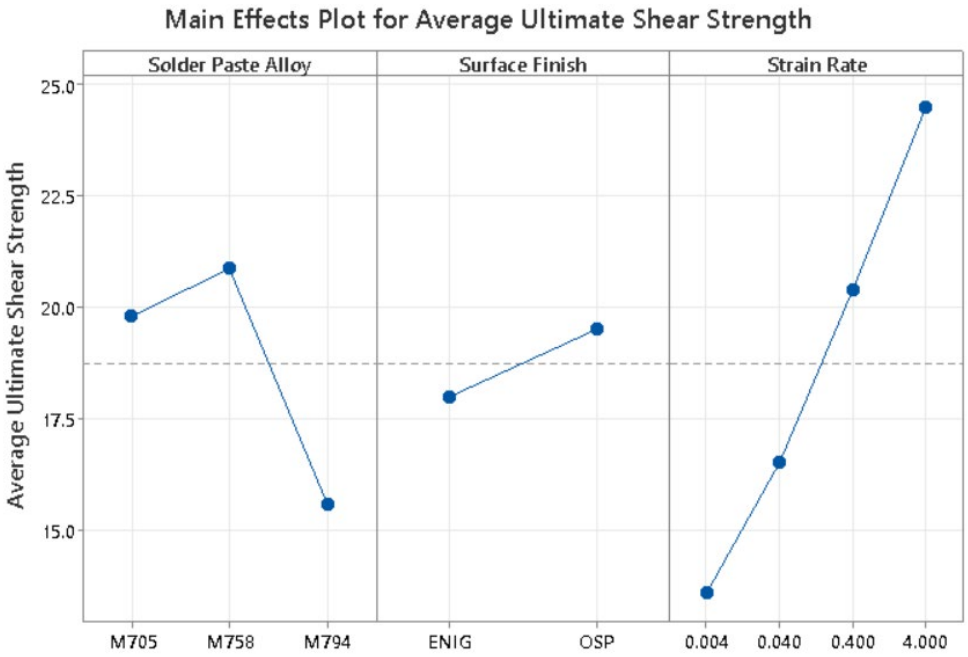


Fig. 7-5: Study III - main effects plot for solder paste alloy/thickness and strain rate.

The main effects plot confirms that the slower the strain rate, the lower the ultimate shear strength. There's not much difference between M705 and M758 solder paste alloys; conversely, the use of M794 has a significant negative affect on the ultimate shear strength. These two plots mirrors what was discovered in Study I with OSP surface finishes and 4 mil thick solder paste.

The main effect plot of the surface finish suggest that OSP has a stronger effect on the average USS as demonstrated in Table XXXIX.

The interaction between the solder paste alloys and surface finishes at the different strain rates is shown in the interaction plot of Fig. 7-6.

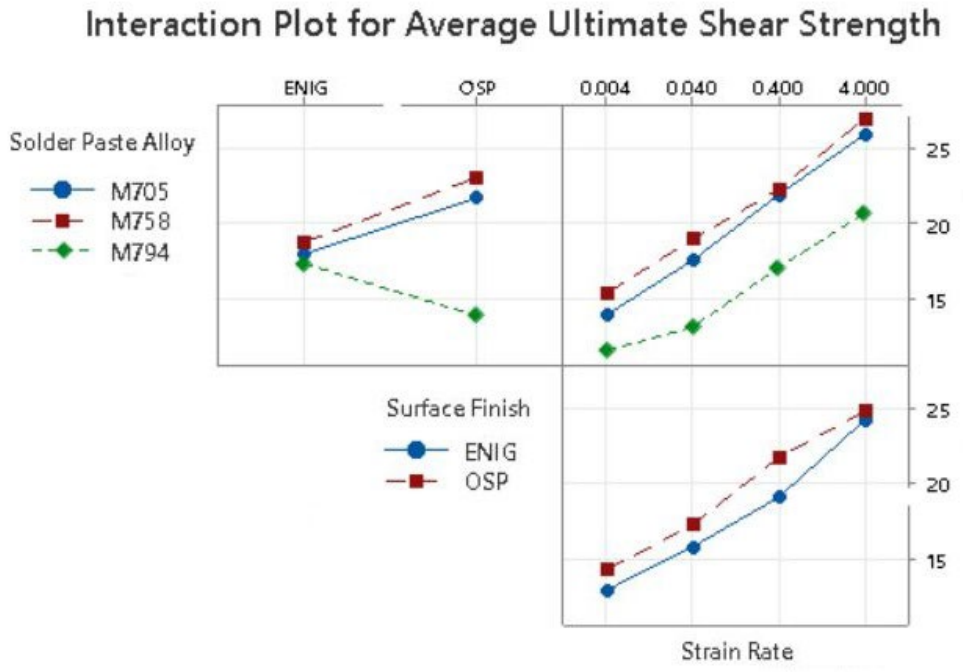


Fig. 7-6: Study III – Interaction plot of solder paste alloy/thickness and strain rate.

The interaction plot shows that there is effectively no interaction between the solder paste alloys and strain rate in determining ultimate shear strength. There may be an interaction between the solder paste alloys and surface finishes. The interaction plot also indicates that there is no interaction between the surface finishes and strain rate.

The relationship between strain rate and average ultimate shear strength are plotted in log-log graphs to “remove” the skewness and provide a linear relationship between the two. From the log-log linear relationship, a power function will be extracted to easily show a percentage change

or multiplicative constant between the two parameters for a given solder paste alloy. The log-log graphs for the 4 mil thick solder paste test samples are shown in Fig. 7-7.

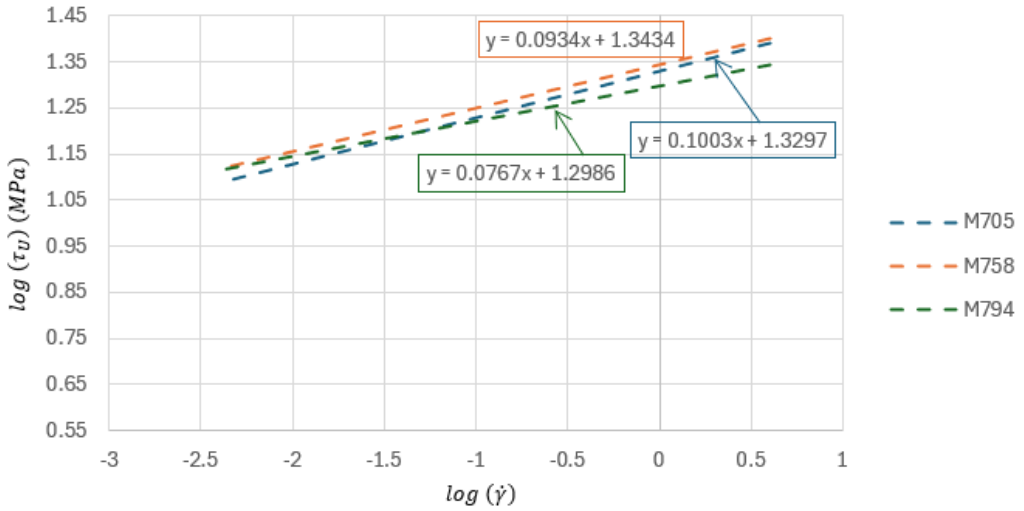


Fig. 7-7: Study III – log-log graph of strain rate and ultimate shear strength: 4 mil, ENIG.

From the linear relationships identified in the log-log graphs, the power functions for each combination of solder paste alloy and strain rate are shown in Table XL.

TABLE XL
STUDY III – POWER FUNCTIONS FOR USS

| Solder Paste Alloy | Solder Paste Thickness (w/ ENIG) | Average Ultimate Shear Strength |
|---|---|---|
| **M705** | 4 mil | $21.36\dot{\gamma}^{0.1003}$ |
| **M758** | 4 mil | $22.05\dot{\gamma}^{0.0934}$ |
| **M794** | 4 mil | $19.89\dot{\gamma}^{0.0767}$ |

Fig. 7-8 shows the two-parameter Weibull probability plot for M705 with 4 mil thick solder paste and ENIG surface finish for all three fatigue stress amplitude tests along with calculated estimates for the shape and scale parameters.

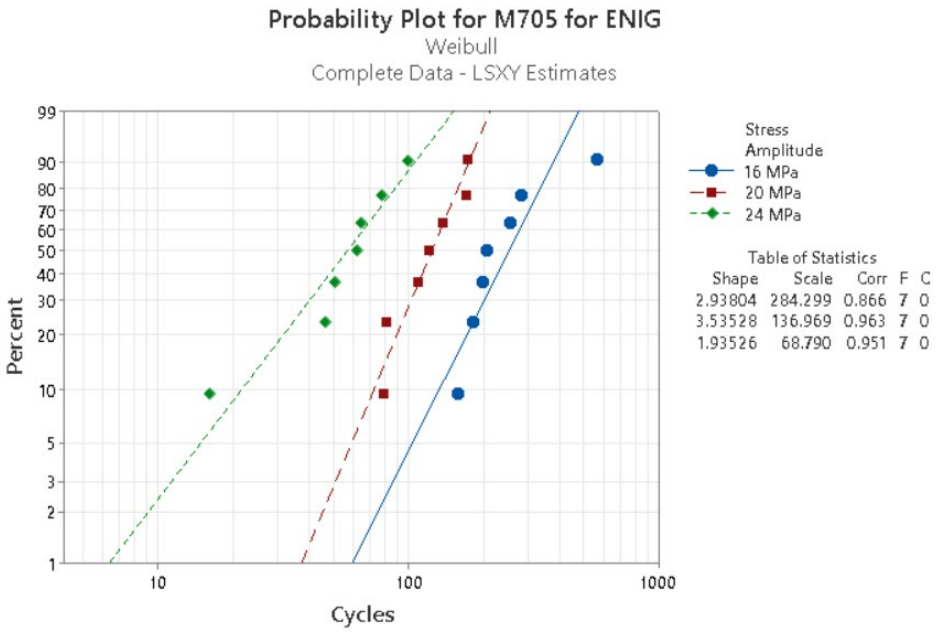


Fig. 7-8: Two-parameter Weibull probability plot for M705: 4 mil, ENIG.

Fig. 7-9 and 7-10 provide the same plots for M758 and M794.

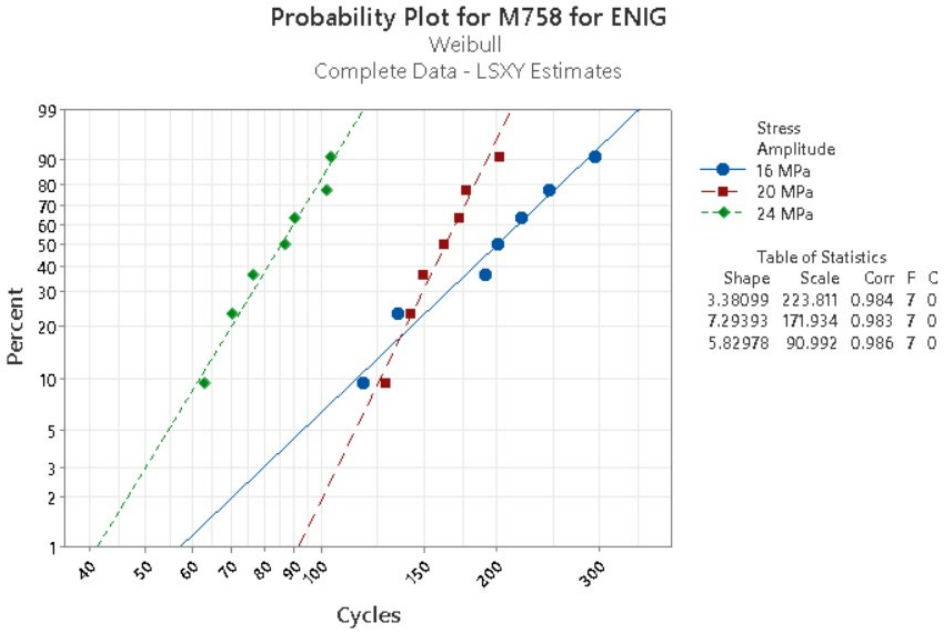


Fig. 7-9: Two-parameter Weibull probability plot for M758: 4 mil, ENIG.

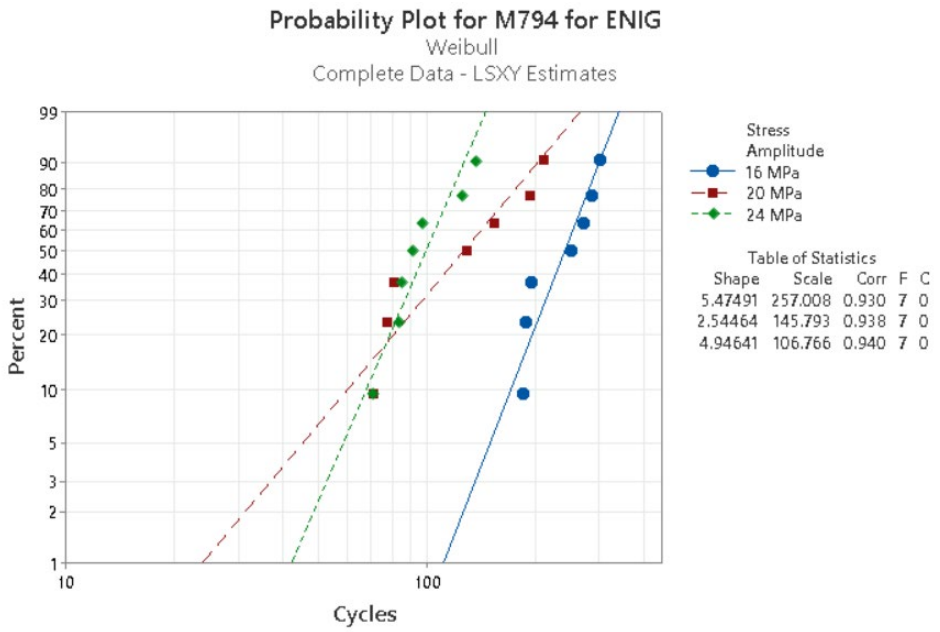


Fig. 7-10: Two-parameter Weibull probability plot for M794: 4 mil, ENIG.

The behavior of the M705 solder paste with ENIG is similar to its behavior with OSP. The behavior of the M758 solder paste with ENIG differs from its OSP application. Instead of distinct and separate Weibull probability plots as shown with OSP, the 16 MPa and 20 MPa probability plots intersect with the ENIG application. The M794 performance switched. With the OSP, the 16 MPa and 20 MPa interested leaving the 24 MPa isolated while with the ENIG, the 20 MPa and 24 MPa probability plots overlapped leaving the 16 MPa remote from the other plots. The correlation coefficients for all are very close to 1 (all are 0.93 or higher) with M705, 16 MPa probability plot being the lone outlier. Generally, all probability plots suggest a linear relationship.

For each cyclic load, the solder paste alloys are compared in Fig. 7-11 through 7-13.

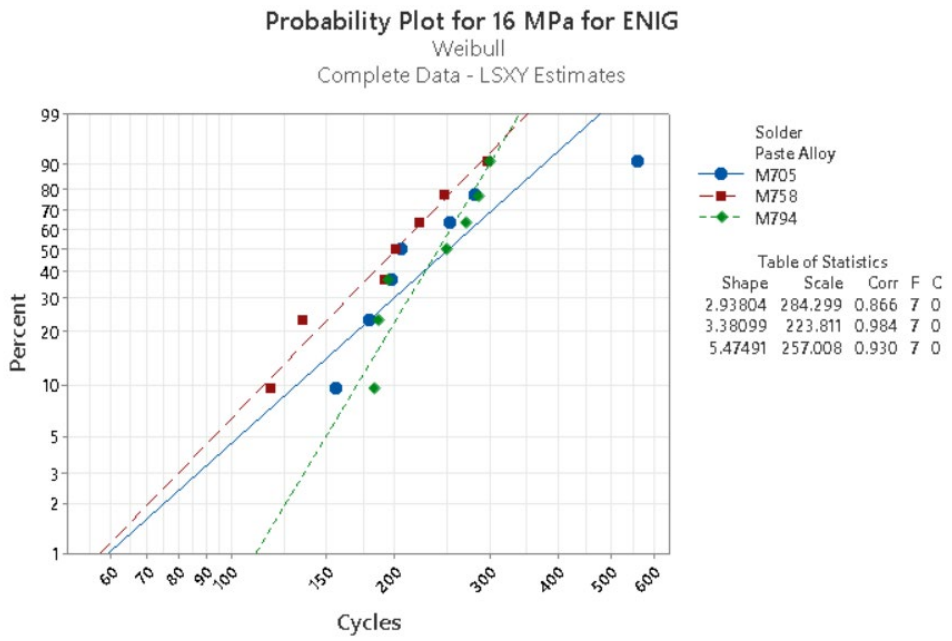


Fig. 7-11: Two-parameter Weibull probability plot for 16 MPa load: 4 mil, ENIG.

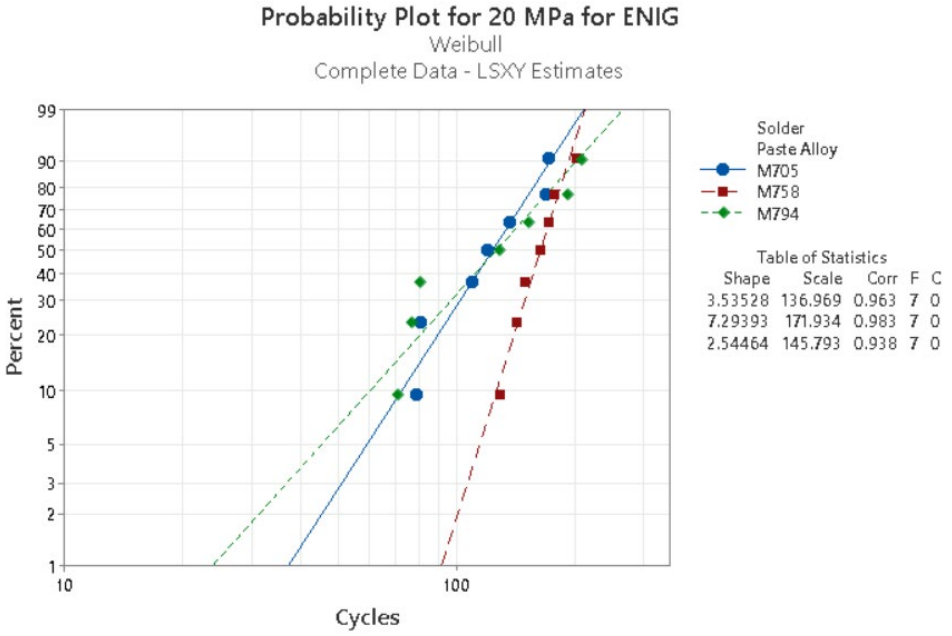


Fig. 7-12: Two-parameter Weibull probability plot for 20 MPa: 4 mil, ENIG.

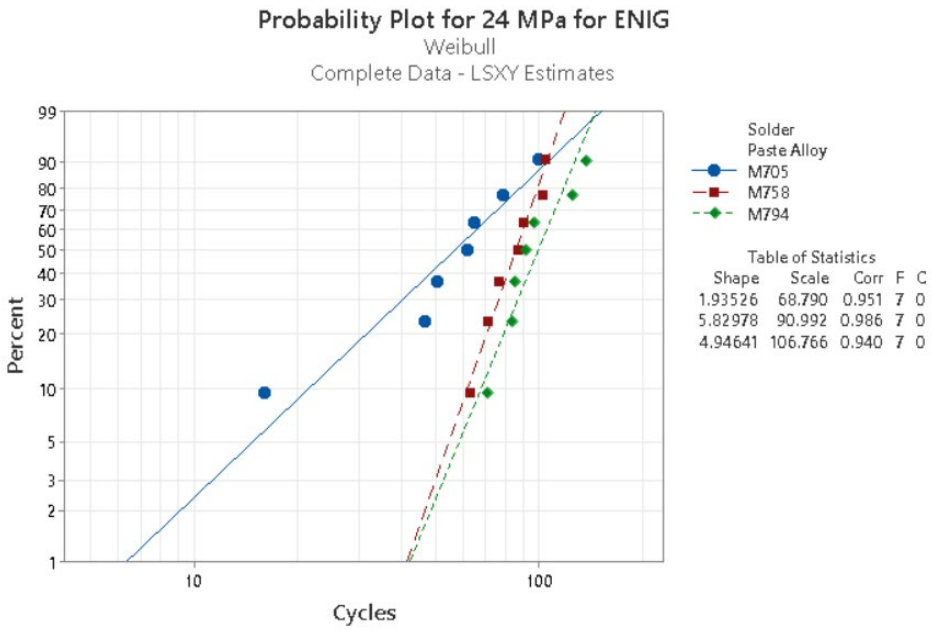


Fig. 7-13: Two-parameter Weibull probability plot for 24 MPa: 4 mil, ENIG.

From the Weibull probability plots for each fatigue test, there are multiple crossings of the probability plots for the solder paste alloys. The best or preferred alloy is not as clear. It would be dependent on the reliability being examined or desired. The characteristic life will provide a specific examination between the alloys that should add clarity to the reliability performance of each. Bar charts comparing the characteristic life and B10 life are shown in Fig. 7-14 and 7-15.

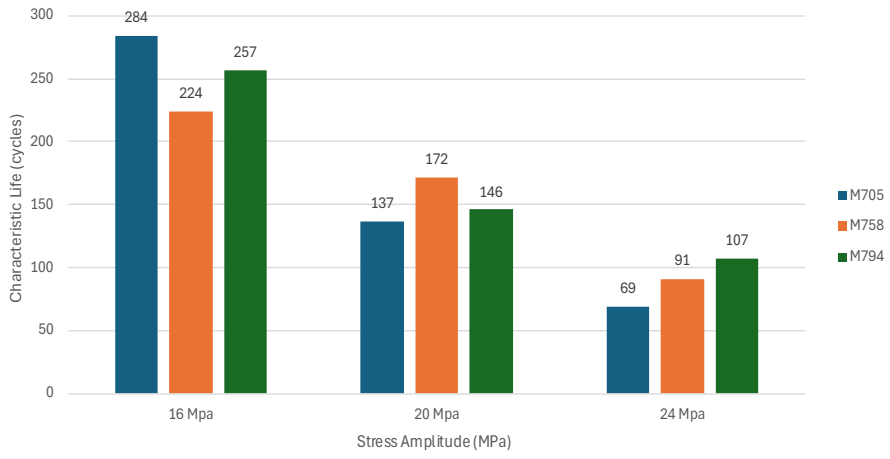


Fig. 7-14: Characteristic life comparison between solder paste alloys: 4 mil, ENIG.

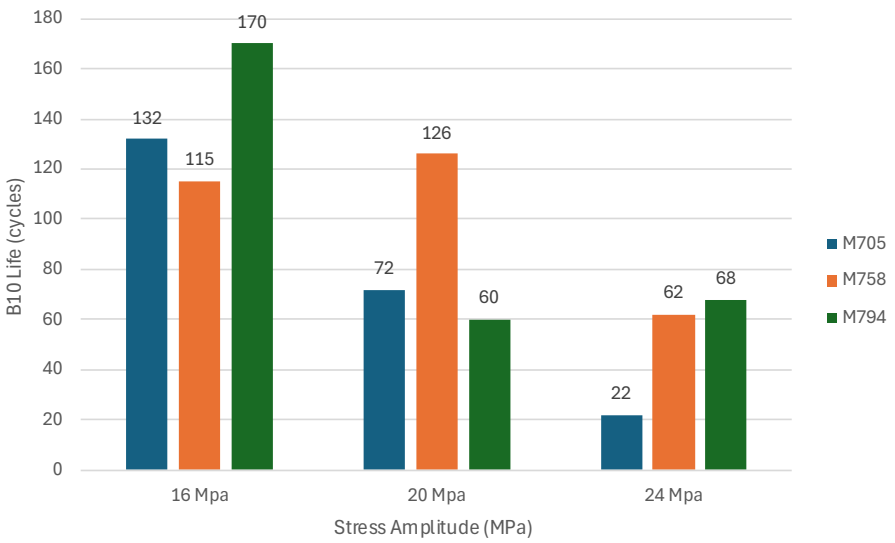


Fig. 7-15: B10 life comparison between solder paste alloys: 4 mil, ENIG.

The M705 solder paste alloy outperformed the M705 and M794 for the 16 MPa stress cycle. For the 16 MPa cyclic load, the M705 characteristic life is 26 % better than M758 and 11 % better than M794. For the 20 MPa cyclic load, the M758 is clearly better than the other two. The M758 characteristic life is 26 % better than M705 and 18 % better than M794. Finally for the 24 MPa cyclic load, the M794 has the higher characteristic life. It is 18 % better than M758 and 55 % better than M705.

Due the the multiple crossings of the Weibull probability plots, the B10 characteristic lifes shows a significant change in the comparisons. For the 16 MPa cyclic load, the M794, as opposed to the M705, exhibits a much higher B10 characteristic life (29 % higher than M705, 48 % higher than M758). The M758, which has the higher characteristic life at the 20 MPa cyclic load, has a much higher B10 life at the same load by much greater margins. It is 75 % higher than M705 and 110 % higher than M794. For the 24 MPa, the M794 has still the better B10 life but the B10 life of the M758 and M705 changed in opposite directions. The M794 B10 life is 210 % better than the M705 (wider margin than the characteristic life); however, only 10 % higher than M758.

Using Equation (3.1), the characteristic life can be modeled in a power expression as shown in Fig. 7-16.

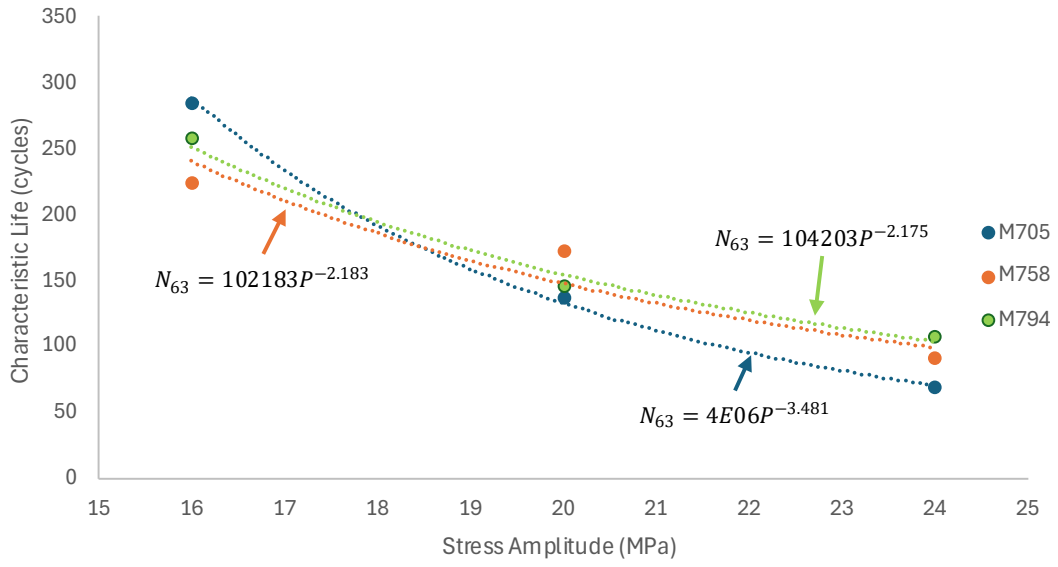


Fig. 7-16: Study II – characteristic life vs stress amplitude: 4 mil, ENIG.

The material constants also provide insight into the behavior of the solder paste alloys as the stress amplitude is decreased below 16 MPa. The M705 has the highest of all three starting with the 16 MPa cyclic load. The M705 (with ENIG) also has the higher material constant as opposed to the M758 with OSP. Conversely, when the cyclic load reaches and surpasses 18 MPa, the characteristic life of M705 drops below the other two. The material constants for M758 and M794 are very close with M794 having the highest one of the two. The exponent, ductility factor, indicates that the M705 behavior is more brittle than the M758 and M794. This is easily verified visually also due to the slope of the M705 plot is higher than the slope of the M758 and M794 curves. With close material constants and equivalent ductility factors, it is presumed that M794 with ENIG will always have a higher characteristic life for most (if not all) cyclic loads.

To finish, each solder paste alloy will be evaluated onto itself for the two surface finishes. The Weibull probability plots for the 16 MPa and 24 MPa cyclic loads are shown for M705 in Fig. 7-17 and 7-18.

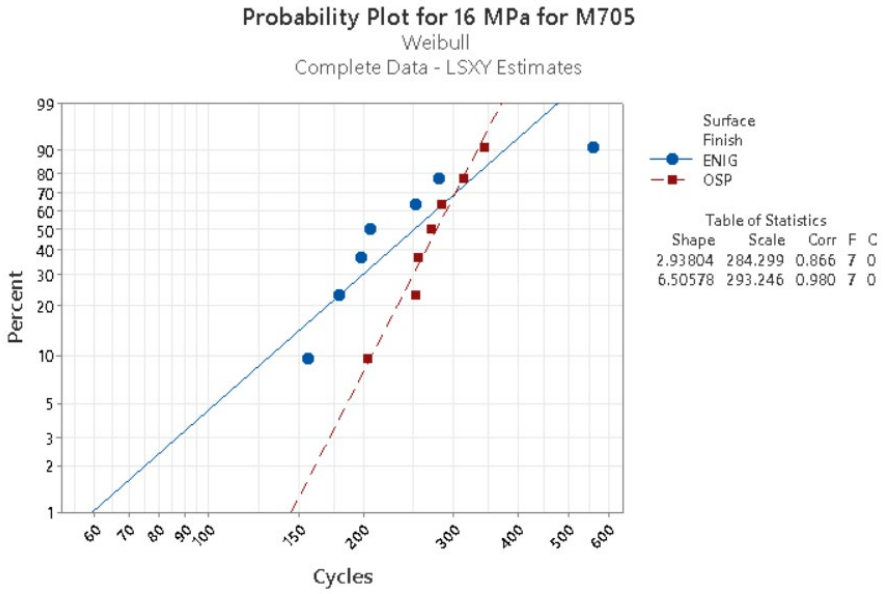


Fig. 7-17: Two-parameter Weibull probability plot: M705, 16 MPa, 4 mil, OSP, ENIG.

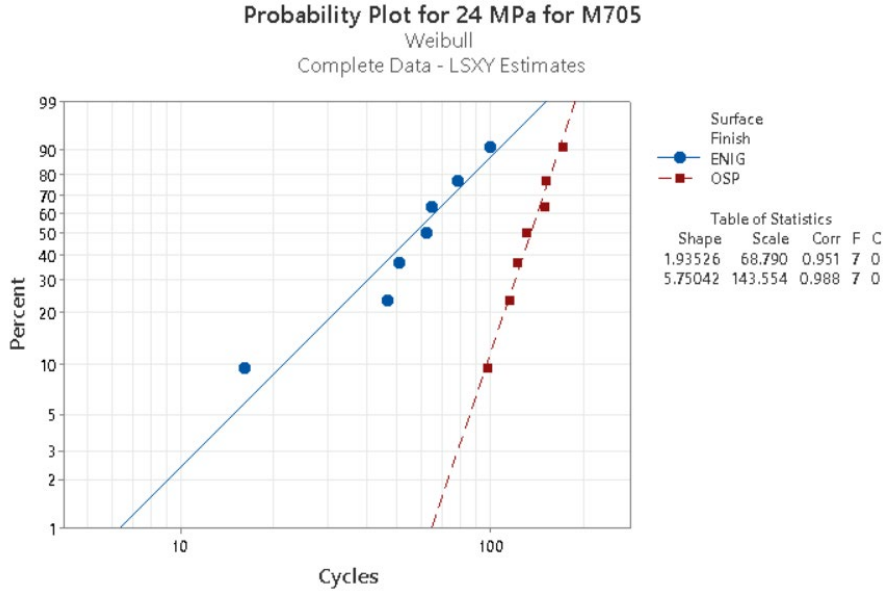


Fig. 7-18: Two-parameter Weibull probability plot: M705, 24 MPa, 4 mil, OSP, ENIG.

The Weibull probability plots for the 16 MPa and 24 MPa cyclic loads are shown for M758 in Fig. 7-19 and 7-20.

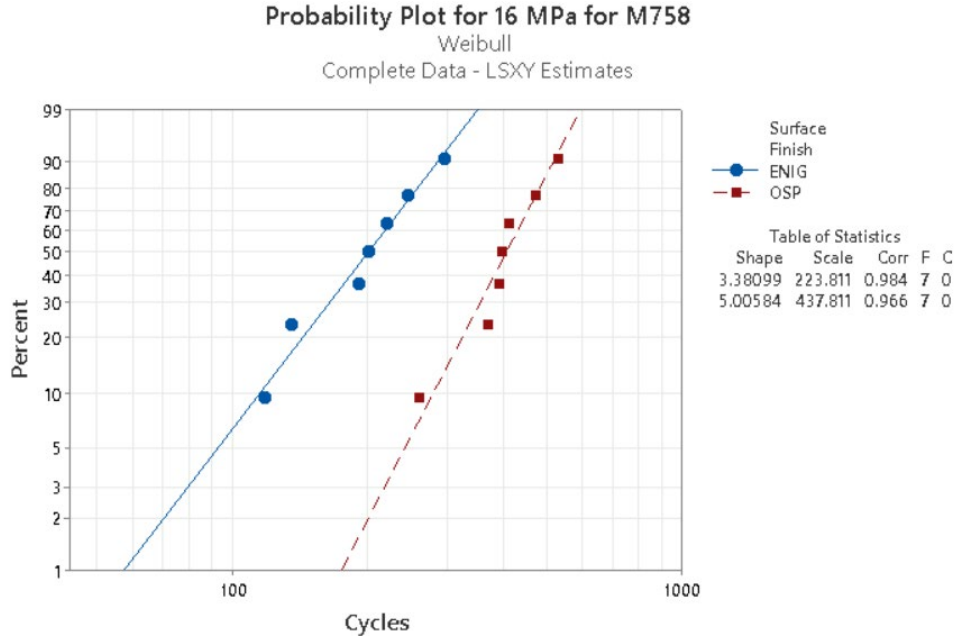


Fig. 7-19: Two-parameter Weibull probability plot: M758, 16 MPa, 4 mil, OSP, ENIG.

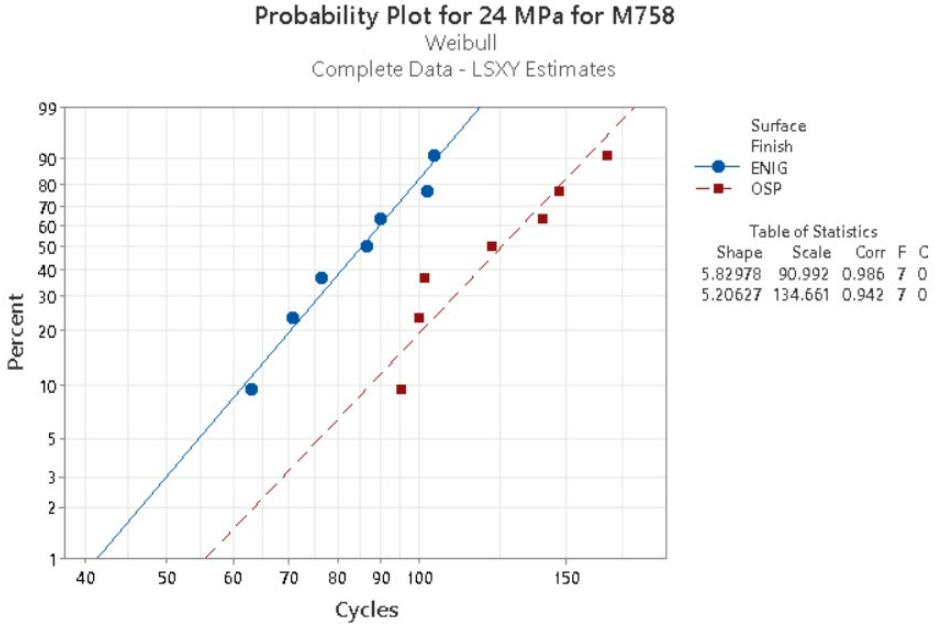


Fig. 7-20: Two-parameter Weibull probability plot: M758, 24 MPa, 4 mil, OSP, ENIG.

The Weibull probability plots for the 16 MPa and 24 MPa cyclic loads are shown for M794 in Fig. 7-21 and 7-22.

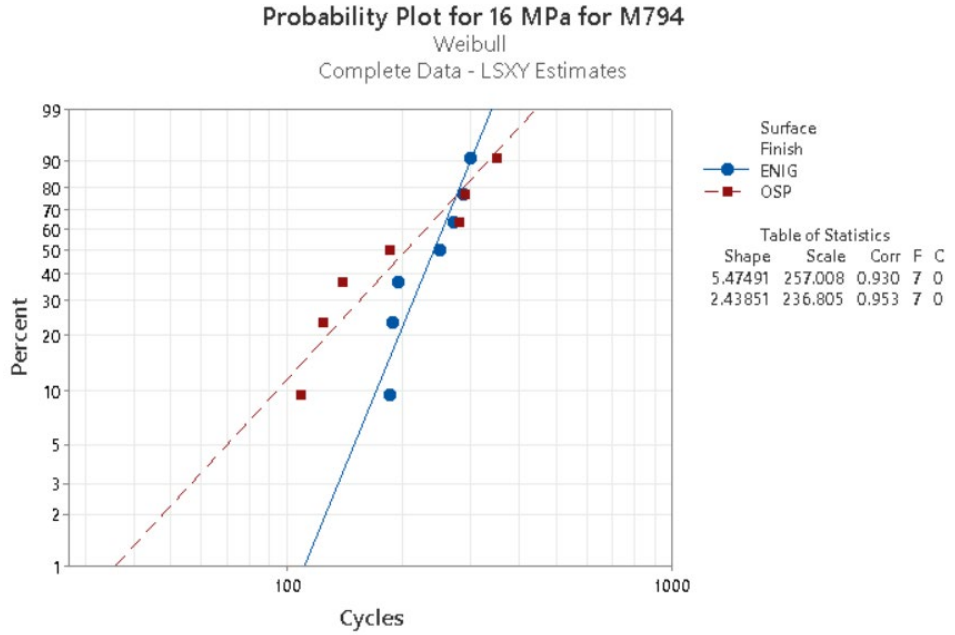


Fig. 7-21: Two-parameter Weibull probability plot: M794, 16 MPa, 4 mil, OSP, ENIG.

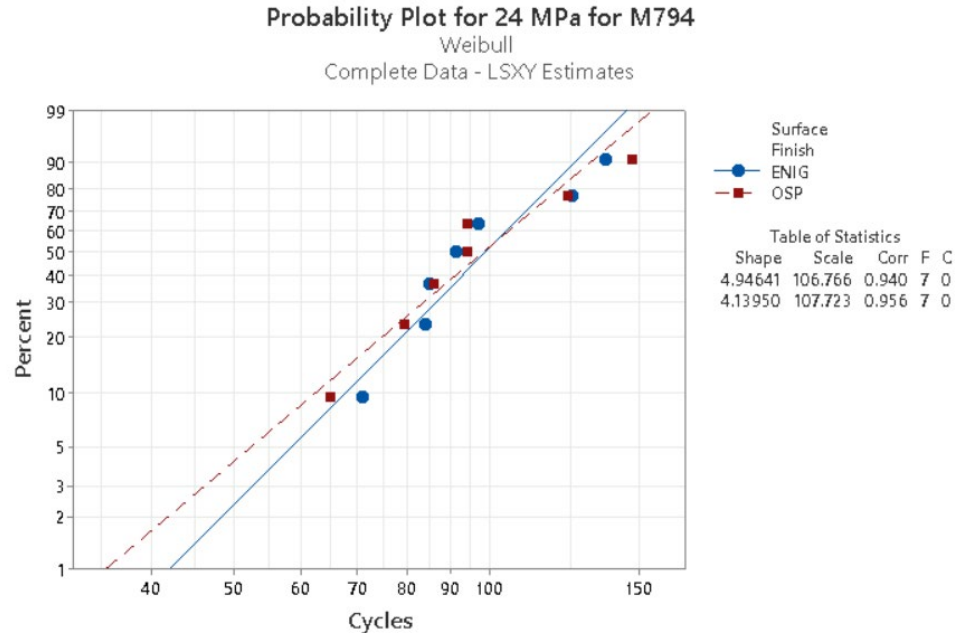


Fig. 7-22: Two-parameter Weibull probability plot: M794, 24 MPa, 4 mil, OSP, ENIG.

The Weibull probability plots for M705 at the 16 MPa cyclic for the OSP and ENIG surface finishes intersect but probability plots distance themselves when subjected to the higher, 24 MPa cyclic load. Using Equation (3.1) to plot the characteristic life against the stress amplitudes, the model provides additional understanding. The characteristic life of M705 with OSP and ENIG surface finishes is shown in Fig. 7-23.

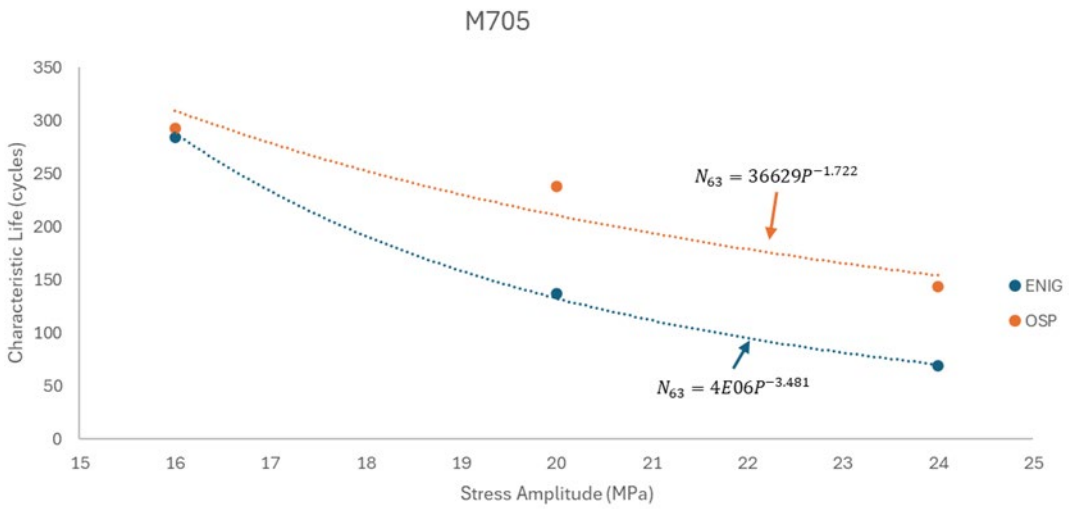


Fig. 7-23: Characteristic life of M705: 4 mil thick.

From the characteristic life plot of M705, the behavior of the solder paste alloy with OSP and ENIG surface finishes is made sharper. M705 paired with an ENIG surface finish has a higher material constant and a higher ductility factor. This pairing is more brittle than M705 paired with an OSP surface finish. As the cyclic load drops below 16 MPa, the two curves would cross and the M705/ENIG pair would render a higher characteristic life. But as the cyclic stress amplitude increases further from 16 MPa, the M705/OSP pair provides the higher characteristic life and continues to distance itself from the M705/ENIG pairing.

The Weibull probability plots for M758 at the 16 MPa cyclic for the OSP and ENIG surface finishes intersect are a good distance apart but when subjected to the higher, 24 MPa cyclic load, the probability plots move closer toward each other. Using Equation (3.1) to plot the characteristic life against the stress amplitudes, the model provides additional understanding. The characteristic life of M758 with OSP and ENIG surface finishes is shown in Fig. 7-24.

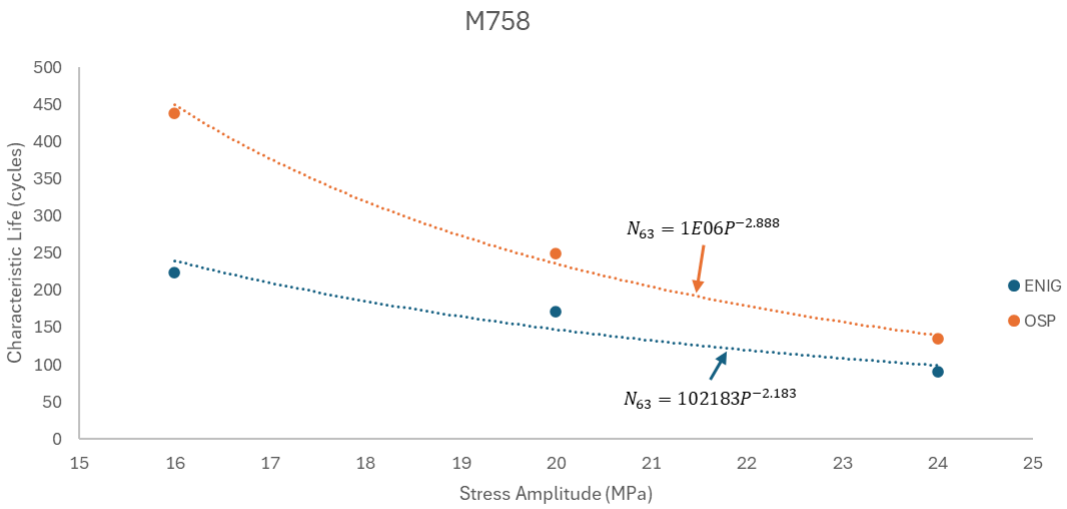


Fig. 7-24: Characteristic life of M758: 4 mil thick.

From the characteristic life plot, the M758 behavior is very opposite from the behavior of M705. In this case, M758 paired with an OSP surface finish has a higher material constant and a higher ductility factor. This pairing is more brittle than M758 paired with an ENIG surface finish. As the cyclic load drops below 24 MPa, the two curves continue to separate with the M758/OSP pair providing the higher characteristic life as the cyclic load continues to drop. But as the cyclic stress amplitude increases further from 24 MPa, both curves continue to converge and cross at some higher stress amplitude past 24 MPa leaving neither combination more reliable than the other.

The Weibull probability plots for M794 at the 16 MPa cyclic for the OSP and ENIG surface finishes intersect are a good distance apart but when subjected to the higher, 24 MPa cyclic load, the probability plots move closer toward each other. Using Equation (3.1) to plot the characteristic life against the stress amplitudes, the model provides additional understanding. The characteristic life of M794 with OSP and ENIG surface finishes is shown in Fig. 7-25.

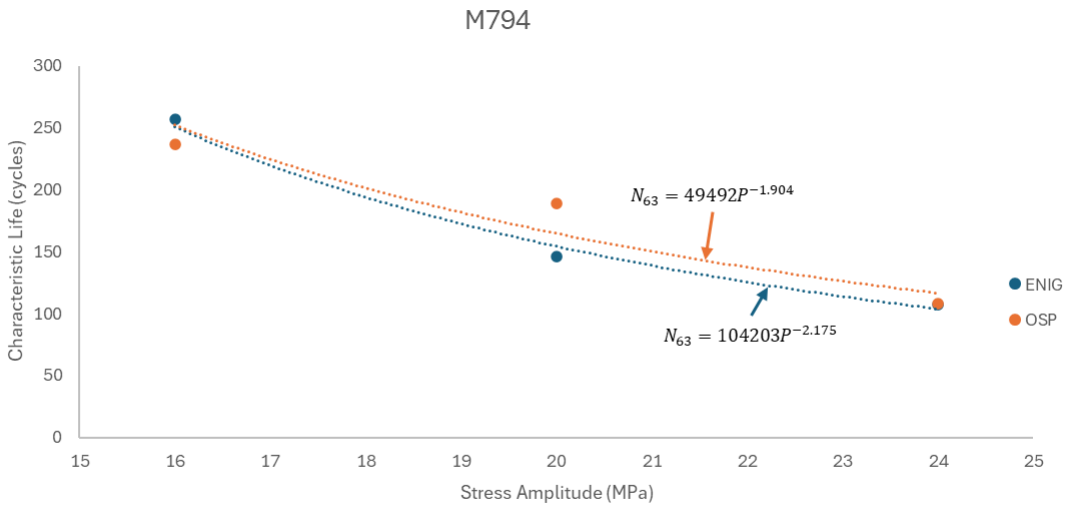


Fig. 7-25: Characteristic life of M794: 4 mil thick.

From the characteristic life plot, the M794 behavior is very opposite from the behavior of M705 and M758. The pairing with an OSP surface finish or an ENIG surface finish has very little effect on the reliability of the solder paste alloy. The material constant of the M794/ENIG pair is a little more than double the material constant of the M794/OSP pair. The curves cross at or near the 16 MPa stress amplitude. As cyclic stress drops from 16 MPa, the M794/ENIG pair would provide higher reliability. The ductility factors for each curve are very close in proximity. With the ductility factors matched with their respective material constants, it depicts both combinations with the same level of ductile behavior and characteristic life as cyclic stress increases far past 16 MPa.

## Chapter 8 Results and Conclusions.

For ultimate shear strengths at 4 mil thickness, the M758 solder paste alloy provides the highest level of performance over the M705 and M794 regardless of surface finish and strain rate as shown in Table XXXIX. It is also noted that M758's ultimate shear strength is only fractionally better than the USS of M705 for either surface finish or strain rate. The M794 solder paste alloy was the weakest of the three for both surface finish and strain rate combinations. Individually, the M758 and M705 performed better when combined with an OSP surface finish while the M794 produced higher USS results with an ENIG surface finish. The shear results for the M705 (SAC305) and M758 (SAC308-Bi-Ni) did not reach the percentage difference in magnitude documented by Belhadi in Section 3.1.1 of Chapter 3 for SAC305 and SAC-3Bi. The main difference between Belhadi's experiment and the results obtained here is that the different solder alloys tested here were only in the paste and not the entire solder joint which would suggest fractional improvement.

The ultimate shear strengths at 5 mil thickness were unexpected. Adding an additional mil thickness of the same solder paste alloys tested at 4 mil resulted in a substantial reduction in the USS for all the alloys. There were no significant outliers of the calculated means within the sample sizes. The USS of all the 5 mil thick sample sizes range from 2.90686 MPa to 8.66639 MPa. Simply put, there were no individually tested 5 mil thick solder paste, solder joint that tested higher than 8.66 MPa for USS. The introduction of human error was assessed but would have to have been replicated 84 consecutive times (3 alloys, 4 strain rates, 7 replicates) over two days. This did not seem plausible. The Bluehill test controls for shear testing were the exact same test controls used for the test articles assembled with the 4 mil thick option. Errors made during the production and assembly of the test articles were identified as a root cause for the results

being low but there was no way of investigating the validity. A request was sent to SMIC to evaluate the assembly (reflow) and test data. Furthermore, fatigue testing of test articles assembled with 5 mil thick solder paste was not part of this examination so, additional test data was not available to help determine if error(s) were committed. For example, if fatigue testing of the 5 mil thick solder paste joints produced noticeably low cycle counts, it would help validate the execution of the shear tests. The 5 mil thick test samples were tested 600+ days after being received (not counting the days after final assembly, packaging, and shipping). If this is a factor, it would be unsettling to discover the drastic drop in shear strength performance of the solder joints considering the test samples were not subjected to accelerated aging conditions.

Fatigue testing was performed only with 4 mil thick solder paste test articles constructed with OSP and ENIG surface finishes. In determining the choice solder paste alloy and surface finish combination is not as straight forward because the judgement is dependent on the intended operational environment and the desired reliability of the end item. The desire is to have the highest reliability for a given environment. Table XLI shows the best performing solder paste and surface finish combination for B10 life based on the data collected.

TABLE XLI
MOST RELIABLE SOLDER PASTE SOLUTION

| **Cyclic Stress Amplitude** | **Best Solution (90 % reliability)** |
|---|---|
| **< 16 MPa** | M758 with OSP |
| **16 – 20 MPa** | M758 with OSP |
| **20 – 24 MPa** | M705 with OSP |
| **> 24 MPa** | M705 with OSP |

All solder paste alloys performed better when paired with an OSP surface finish. Individually, the M758 performed the best overall when assembled to a OSP surface finish. The M758

combined with an OSP surface finish responded with more brittle behavior than when assembled with ENIG. The M705 combined with an ENIG surface finish responded with a more brittle behavior than with assembled to with OSP. The M794 response was essentially unchanged when assembled to either the ENIG or OSP surface finished copper pad.

Further analysis could support determining the behavior of the solder paste combinations. The data produced from testing could be used to extrapolate the plastic strain and shear energy of the solder joint under fatigue testing. Since the experiments are of the low cycle fatigue failure, utilizing the Coffin-Mason expression in Equation (2.24) can help in understanding the effects of the plastic strain on the responses captured.

Another model not mentioned in Chapter 2 is the shear energy model. The model, utilizing a power expression like the Coffin-Mason expression, estimates the failure from fatigue from the hysteresis energy loops. The energy transferred to the solder joint in a fatigue cycle is mathematically equal to the "non-recoverable work." This energy is calculated by adding all the products of the peaks of the irreversible displacements by the forces acting on the solder joint. This model focuses on the premise that breakage will happen when the "work" is centered in the weakest area of the solder joint reaches a specific value when cracking initiates [105].

Cross-section views and top views of unaltered and tested solder paste joint would provide supplementary evidence to better analysis the results obtained. By using a scanning electron microscope (SEM) and cross-polarized microscope (CPM), the composition before and after testing can be visually assessed. Unaltered examination of the 5-mil thick solder paste joints would provide visual indication of voids, cracks, or other defects that were pre-existing that would point to the low shear strengths collected. The photographs of unaltered and tested solder paste joints would provide indication of the IMC compositions and layers to help verify proper

bonding and attesting to the brittle or ductile behavior witnessed. Future research needs to be conducted on the advantages and disadvantages of the difference in solder paste volume. Based on the limited data retrieved and the analyses provided, it would be safe to determine the findings of changing solder paste thickness as inconclusive.

## References


[1] J. Pearce, "Solders Technology Roadmap 2015: Tomorrow's Solders," ITRI Ltd, Hertfordshire, UK, 2015.

[2] G. M. Freedman, "Soldering Fundamentals," in *Printed Circuits Handbook*, 7th ed., C. F. Coombs, Jr. and H. T. Holden, Eds., New York, NY: McGraw Hill Eduction, 2016, pp. 969-975.

[3] J. S. Hwang, "Solder Technologies for Electronic Packaging and Assembly," in *Electronic Packaging and Interconnection Handbook*, 4th ed., C. A. Harper, Ed., New York, NY: McGraw-Hill, 2005, pp. 5.1-5.116.

[4] G. M. Freedman, "Solder Fluxes," in *Printed Circuits Handbook*, 7th ed., C. F. Coombs, Jr. and H. T. Holden, Eds., New York, NY: McGraw-Hill Education, 2016, pp. 997-1013.

[5] H. T. Holden, "Assembly Processes," in *Printed Circuits Handbook*, 7th ed., C. F. Coombs, Jr. and H. T. Holden, Eds., New York, NT: McGraw-Hill Eduction, 2016, pp. 887-934.

[6] *Picture 2. Component Leads and Pad dimensions.* [Art]. PCB 3D, 2010-2021. Accessed: Oct 13, 2023. Available: https://www.pcb-3d.com/tutorials/how-to-calculate-pth-hole-and-pad-diameter-sizes-according-to-ipc-7251-ipc-2222-and-ipc-2221-standards/.

[7] *Surface Mount Technology (SMT).* [Art]. Sino Voltaics, 2023. Accessed: Oct 23, 2023. Available: https://sinovoltaics.com/learning-center/inverters/surface-mount-technology/.

[8] R. P. Prasad, Surface Mount Technology: Principles and Practice, 2nd ed., Boston, MA: Chapman and Hall, 1997.

[9] G. M. Freedman, "Soldering Techniques," in *Printed Circuits Handbook*, 7th ed., C. F. Coombs, Jr. and H. T. Holden, Eds., New York, NY: McGraw-Hill Education, 2016, pp. 1015-1073.

[10] M. N. Tamin and N. M. Shaffiar, Solder Joint Reliability Assessment: Finite Element Simulation Methodology (Advanced Structured Materials (37)), Cham: Springer, 2014.

[11] *Ductile Brittle and Plastic Material Stress Strain Curve Comparison.* [Art]. SMLease Design, Accessed: Oct 27, 2023. Available: https://www.smlease.com/entries/mechanical-design-basics/stress-strain-curve-diagram/.

[12] J. H. Lau and N.-C. Lee, Assembly and Reliability of Lead-Free Solder Joints, Gateway East: Springer, 2020.

[13] R. C. Hibbeler, Mechanics of Materials, Upper Saddle River, NJ: Pearson Prentice Hall, 2008.

[14] *Stress-strain curve of a ductile material.* [Art]. ScienceABC, 2023. Accessed: Nov 15, 2023. Available: https://www.scienceabc.com/innovation/what-is-the-stress-strain-curve.html.

[15] G. M. Freedman, "Soldering Materials and Metallurgy," in *Printed Circuits Handbook*, 7th ed., C. F. Coombs, Jr. and H. T. Holden, Eds., New York, NY: McGrall Hill Education, 2016, pp. 977-996.

[16] D. J. Gunton and G. A. Saunders, "The Young's modulus and Poisson's ratio for Arsonic, Antimony and Bismuth," *Journal of Materials Science,* vol. 7, pp. 1061-1068, 1972.

[17] R. M. Christensen, "FailureCriteria," 21 October 2012. [Online]. Available: https://www.failurecriteria.com/physicalductilit.html. [Accessed 20 November 2023].

[18] R. G. Budynas, Advanced Strength and Applied Stress Analysis, Boston, MA: McGraw Hill, 1999.

[19] J. H. L. Pang, Lead Free Solder: Mechanics and Reliability, New York, NY: Springer, 2012.

[20] INFORM, Inc, "Electric Appliance Recycling in Japan," INFORM, Inc, New York, 2003.

[21] H. Ma and J. C. Suhling, "A Review of Mechanical Properties of Lead-Free Solders for Electronic Packaging," *Journal of Materials Science,* vol. 44, pp. 1141-1158, 27 January 2009.

[22] D. E. Sullivan, "Recycled Cell Phones - A Treasure Trove of Valuable Metals," U.S. Geological Survey, Denver, 2006.

[23] N. Jiang, L. Zhang, Z.-Q. Liu, L. Sun, W.-M. Long, P. He, M.-Y. Xiong and M. Zhao, "Reliability Issues of Lead-Free Solder Joints in Electronic Devices," *Sci Technol Adv Mater,* vol. 20, no. 1, pp. 876-901, 11 July 2019.

[24] S. Cheng, C.-M. Huang and M. Pecht, "A Review of Lead-Free Solders for Electronics Applications," *Microelectronics Reliability,* vol. 75, pp. 77-95, 2017.

[25] *Requirements for Electronic Grade Solder Alloys and Fluxed and Non-Fluxed Solid Solders for Electronic Soldering Applications,* IPC J-STD-006C, 2013.

[26] *Requirements for Electronic Grade Solder Alloys and Fluxed and Non-Fluxed Solid Solders for Electronic Soldering Applications,* IPC J-STD-006C-AM1, 2017.

[27] "How Much Does a Solder Cost," solderingrepair.com, 12 September 2023. [Online]. Available: https://solderingrepair.com/how-much-does-a-solder-cost/. [Accessed 15 January 2024].

[28] M. Ahmad and M. Brillhart, "Component-To-PWB Reliability: Estimating Solder Joint Reliability and the Impact of Lead-Free Solders," in *Printed Circuits Handbook*, 7th ed., C. F. Coombs, Jr. and H. T. Holden, Eds., New York, NY: McGraw-Hill Education, 2016, pp. 1401-1435.

[29] L. W. Ritchey, "Physical Characteristics of the PCB," in *Printed Circuits Handbook*, 7 ed., C. F. Coombs, Jr. and H. T. Holden, Eds., New York, NY: McGraw Hill Education, 2016, pp. 365-372.

[30] S. R. Shaw, "Rigid and Flexible Printed Circuit Board Technology," in *Electronic Packaging and Interconnection Handbook*, C. A. Harper, Ed., New York, New York: McGraw-Hill, 2005, pp. 9.1-9.88.

[31] *Difference between Single Layer PCB and Double Layer PCB.* [Art]. The Engineering Knowledge, 2019. Accessed: March 5, 2024. Available: https://www.theengineeringknowledge.com/single-sided-pcb-board/.

[32] *Cross-sectional view of a generic structure of a Printed Circuit Board (PCB).* [Art]. Micromachines, 2022.

[33] Chris, "Surface Mount Technology Introduction: Process, Types & Principle," 14 November 2022. [Online]. Available: https://jamindopcba.com/surface-mount-technology/. [Accessed 30 January 2024].

[34] Sasmita, "electronicspost.com," 6 July 2018. [Online]. Available: https://electronicspost.com/types-of-pcb/. [Accessed 17 March 2024].

[35] E. Kelley and D. Trobough, "Introduction to Base Material," in *Printed Circuits Handbook*, 7th ed., C. F. Coombs, Jr. and H. T. Holden, Eds., New York, NY: McGraw Hill Education, 2016, pp. 171-196.

[36] E. Kelley and D. Trobough, "The Impact of Lead-Free Assembly on Base Material," in *Printed Circuits Handbook*, 7th ed., C. F. Coombs, Jr and H. T. Holden, Eds., New York, NY: McGraw Hill Education, 2016, pp. 273-292.

[37] E. Kelley and D. Trobough, "Properties of Base Material," in *Printed Circuits Handbook*, 7th ed., C. F. Coombs, Jr. and H. T. Holden, Eds., New York, NY: McGraw Hill Education, 2016, pp. 225-240.

[38] E. Kelley and D. Trobough, "Selecting Base Materials," in *Printed Circuits Handbook*, 7th ed., C. F. Coombs, Jr. and H. T. Holden, Eds., New York, NY: McGraw Hill Education, 2016, pp. 293-316.

[39] Appendix C, "Important Properties for Designing with Plastics," in *Handbook of Plastics, Elastomers, and Composites*, 3rd ed., C. A. Harper, Ed., New York, NY: McGraw Hill, 1996, pp. C.1-C.72.

[40] W. Li, "Ceramic PCB: A Game-Changer in Electronics Manufacturing," Moko Technology, 14 June 2023. [Online]. Available: https://www.mokotechnology.com/ceramic-pcb/. [Accessed 18 June 2024].

[41] RayMingPCB, "Metal PCB Materials Differences: Aluminum vs. Copper Core vs. Iron Based," RayMing Technologies, 2024. [Online]. Available: https://www.raypcb.com/3-base-material-for-metal-core-pcb/. [Accessed 07 June 2024].

[42] M. P. Smith, P. V. Cavallaro, J. D. O'Donnell, N. A. Valm, E. A. Warner and N. Gencarelle, "Mechanical Characterization of Thermally Insulated Composites," in *the ASME 2022 International Mechanical Engineering Congress and Exposition (IMECE2022-95165)*, Columbus, OH, USA, Oct. 30 - Nov. 3, 2022.

[43] F. Czerwinski, "Thermal Stability of Aluminum Alloys," *Materials,* vol. 13(15), no. 3441, 4 August 2020.

[44] O. Shepelev, S. Kenig and H. Dodiuk, "Nanotechnology-Based Thermosets," in *Handbook of Thermoset Plastics*, 4th ed., H. Dodiuk, Ed., Cambridge, MA: Elsevier, 2022, pp. 833-890.

[45] O. Guillon, W. Rheinheimer and M. Bram, "A Perspective on Emerging and Future Sintering Technologies of Ceramic Materials," *Advanced Engineering Materials,* vol. 25, no. 18, September 2023.

[46] H. T. Chiu, S. H. Chiu, R. E. Jeng and J. S. Chung, "A Study of the Combustion and Fire-Retardance Behaviour of Unsaturated Polyester/Phenolic Resins Blends," *Polymer Degradation and Stability,* vol. 70, no. 3, pp. 505-514, 2000.

[47] O. Mathieu, "Choosing Among Ceramic Substrates for Power Circuits," EETech Group, LLC, 13 September 2017. [Online]. Available: https://eepower.com/technical-articles/choosing-among-ceramic-substrates-for-power-circuits/#. [Accessed 06 June 2024].

[48] M. Li and S. J. Zinkle, "Physical and Mechanical Properties of Copper and Copper Alloys," in *Comprehensive Nuclear Materials*, vol. 4, R. J. M. Konings, T. R. Allen, R. E. Stoller and S. Yamanaka, Eds., Waltham, MA: Elsevier, 2012, pp. 667-690.

[49] "Aluminum Oxidation: Process, Prevention, and Solutions," Okdor, 2 February 2024. [Online]. Available: https://okdor.com/aluminum-oxidation/. [Accessed 16 July 2024].

[50] U. Waseem, "PCB Material: A Comprehensive Guide to Understanding and Choosing the Right Materials," Wevolver, 28 September 2023. [Online]. Available: https://www.wevolver.com/article/pcb-material. [Accessed 17 July 2024].

[51] A. Pizzi and C. C. Ibeh, "Phenol-Formaldehyde Resins," in *Handbook of Thermoset Plastics*, 4th ed., H. Dodiuk, Ed., Cambridge, MA: Elsevier, 2022, pp. 13-40.

[52] K. Pielichowski, J. Njuguna and T. M. Majka, Thermal Degradation of Polymeric Materials, Cambridge, MA: Elsevier, 2023.

[53] J. S. Sallo, "Resins," in *Printed Circuit Board Materials Handbook*, M. W. Jawitz, Ed., New York, NY: McGraw-Hill, 1997, pp. 6.1-6.15.

[54] *Solder Mask Defined and Non-Solder Mask Defined in PAD.* [Art]. Digikey, 2018. Accessed: July 23, 2024. Available: https://forum.digikey.com/t/solder-mask-defined-and-non-solder-mask-defined-in-pad/2069.

[55] R. Schetty, "Lead-Free Finishes for Printed Circuit Boards and Components," in *Handbook of Lead-Free Solder Technology for Microelectronic Assemblies*, K. J. Puttlitz and K. A. Stalter, Eds., New York, NY: Marcel Dekker, Inc., 2004, pp. 431-464.

[56] D. A. Vaughan, "Solder Mask," in *Printed Circuits Handbook*, 7th ed., C. F. Coombs, Jr. and H. T. Holden, Eds., New York, NY: McGraw-Hill Education, 2016, pp. 771-788.

[57] *Solder Adherence of SMD and NSMD BGA Pads.* [Art]. MacroFab, 2016. Accessed: July 25, 2024. Available: https://www.macrofab.com/blog/bga-pad-creation-smd-nsmd/.

[58] *Isometric view of BGA Pad Styles.* [Art]. MacroFab, 2016. Accessed: July 25, 2024. Available: https://www.macrofab.com/blog/bga-pad-creation-smd-nsmd/.

[59] C. Cohn, "Packaging and Interconnection of Integrated Circuits," in *Electronic Packaging and Interconnection Handbook*, 4th ed., C. A. Harper, Ed., New York, NY: McGraw-Hill, 2005, pp. 6.1-6.96.

[60] G. Milad, "Printed Circuit Board Surface Finishes," in *Printed Circuits Handbook*, 7th ed., C. F. Coombs, Jr. and H. T. Holden, Eds., New York, NY: McGraw-Hill Education, 2016, pp. 755-770.

[61] G. C. Munie and L. J. Turbini, "Fluxes and Cleaning," in *Printed Circuits Handbook*, 7th ed., C. F. Coombs, Jr. and H. T. Holden, Eds., New York, NY: McGraw-Hill Education, 2016, pp. 957-968.

[62] M. E. Fine, "Physical Basis for Mechanical Properties of Solders," in *Handbook of Lead-Free Solder Technology for Microelectronic Assemblies*, K. J. Puttlitz and K. A. Stalter, Eds., New York, NY: Marcel Dekker, Inc, 2004, pp. 211-238.

[63] Mineral Commodity Summaries, "U.S. Geological Survey (USGS) Publications Warehouse," January 2024. [Online]. Available: https://pubs.usgs.gov/periodicals/mcs2024. [Accessed 6 August 2024].

[64] "dailymetalprice.com," [Online]. Available: https://www.dailymetalprice.com/metalprices.php. [Accessed 6 August 2024].

[65] "argusmedia.com," [Online]. Available: https://www.argusmedia.com/metals-platform/priceindex. [Accessed 6 August 2024].

[66] D. Suraski, "A Study of Antimony in Solder," AIM Solder, New York.

[67] L. J. Turbini and D. Bernier, "Environmental Impact of Lead and Alternatives in Electronics," in *Handbook of Lead-Free Solder Technology for Microelectronic Assemblies*, K. J. Puttlitz and K. A. Stalter, Eds., New York, NY: Marcel Dekker, Inc, 2004, pp. 83-114.

[68] *Requirements for Soldering Fluxes,* IPC J-STD-004D, 2023.

[69] *Requirements for Solder Paste,* IPC J-STD-005B, 2024.

[70] W. Ramberg and W. R. Osgood, "Description of Stress-Strain Curves by Three Parameters," National Advisory Committee for Aeronautics, Washington, DC, Technical Note No. 902, 1943.

[71] R. J. Sanford, Principles of Fracture Mechanics, Upper Saddle River, NJ: Prentice Hall, 2003.

[72] E. J. Cotts, R. Kinyanjui, R. Chromik, A. Zribi and P. Borgesen, "Formation of Intermetallic Compounds at Pb-Sn/Metal and Lead-Free/Metal Interfaces in Solder Joints," in *Handbook of Lead-Free Solder Technology for Microelectronic Assemblies*, K. J. Puttlitz and K. A. Stalter, Eds., New York, NY: Marcel Dekker, Inc., 2004, pp. 465-494.

[73] G. Milad and D. Gudeczauskas, Artists, *EPMA analysis of DIG with SAC alloy soldering 1000 hrs at 150 °C.* [Art]. Uyemura International Corporation, 2024. Accessed: September 9, 2024. Available: https://www.uyemura.com/articles/solder-joint-reliability-of-gold-surface-finishes-ENIG-ENEPIG-DIG.html.

[74] M. Ahmad and M. Brillhart, "Component-to-PWB Reliability: The Impact of Design Variables and Lead Free," in *Printed Circuits Handbook*, 7th ed., C. F. Coombs, Jr. and H. T. Holden, Eds., New York, NY: McGraw-Hill Education, 2016, pp. 1347-1374.

[75] U. Waseem, "Understanding the ENIG Finish: a Comprehensive Guide," Wevolver, 31 October 2023. [Online]. Available: https://www.wevolver.com/article/understanding-the-enig-finish-a-comprehensive-guide. [Accessed 9 September 2024].

[76] M.-S. Kang, Y.-J. Jeon, D.-S. Kim and Y.-E. Shin, "Degradation Characteristics and $Ni_3Sn_4$ IMC Growth by a Thermal Shock Test in SAC305 Solder Joints of MLCCs Applied in Automotive Electronics," *International Journal of Precision Engineering and Manufacturing,* vol. 17, no. 4, pp. 445-452, April 2016.

[77] M. I. I. Ramli, M. A. A. M. Salleh, M. M. A. B. Abdullah, N. S. M. Z. Zaimi, A. V. Sandu, P. Vizureanu, A. Rylski and S. F. M. Amli, "Formation and Growth of Intermetallic Compounds in Lead-Free Solder Joints: A Review," *Materials,* vol. 15, no. 1451, pp. 1-20, 15 February 2022.

[78] C. Shen, Z. Hai, C. Zhao, J. Zhang, M. J. Bozack, J. C. Suhling and J. L. Evans, "Reliability Analysis of Aging in Joint Microstructures for Sn-Ag-Cu Solder Joints during Thermal Cycling," in *International Technical Conference and Exhibition on Packaging*

*and Integration of Electronic and Photonic Microsystems (InterPACK)*, San Francisco, CA, 2015.

[79] Ismail, Norliza, Yusoff, Wan Yusmawati Wan, Amat, Azuraida, Manaf, Nor Azlian Abdul and Ahmad, Nurazlin, "A Review of Extreme Condition Effects on Solder Joint Reliability: Understanding Failure Mechanisms," *Defence Technology,* vol. 41, pp. 134-158, November 2024.

[80] A. A. Primavera, "Electronics Assembly and the Impact of Lead-Free Materials," in *Handbook of Lead-Free Solder Technology for Microelectronic Assemblies*, K. J. Puttlitz and K. A. Stalter, Eds., New York, NY: Marcel Dekker, Inc., 2004, pp. 495-568.

[81] T. Yasmin, M. Sadiq and M. I. Khan, "Effect of Lanthanum Doping on the Microstructure Evolution and Intermetallic Compound (IMC) Growth during Thermal Aging of SAC305 Solder Alloy," *Journal of Material Sciences & Engineering,* vol. 3, no. 2, 2014.

[82] J.-P. Clech, "Lead-Free Solder Joint Reliability: Fundamentals and Design-For-Reliability Rules," in *Printed Circuits Handbook*, 7th ed., C. F. Coombs, Jr. and H. T. Holden, Eds., New York, NY: McGraw-Hill Education, 2016, pp. 1375-1400.

[83] K. C. Kapur and M. Pecht, Reliability Engineering, Hoboken, NJ: John Wiley % Sons, 2014.

[84] B. Illowsky and S. Dean, Introductory Statistics 2e, N/A: Independently Published, 2023.

[85] A. N. O'Connor, M. Modarres and A. Mosleh, Probability Distributions Used in Reliability Engineering, College Park, MD: Center for Reliability Engineering University of Maryland, 2016.

[86] M. E. A. Belhadi, S. Hamasha and A. Alahmer, "Effect of Bi Content and Aging on Solder Joint Shear Properties Considering Strain Rate," *Microelectronics Reliability,* vol. 146, no. 115020, July 2023.

[87] C. Fleshman, W.-Y. Chen, T.-T. Chou, J.-H. Huang and J.-G. Duh, "The Variation of Grain Structure and the Enhancement of Shear Strength in SAC305-0.1Ni/OSP Cu Solder Joint," vol. 189, pp. 76-79, 1 March 2017.

[88] C. Fleshman, R.-w. Song and J.-G. Duh, "Improving Shear Test Performance of SAC305/OSP Cu Solder Joints by Modifying Microstructure With Minor Ni Doping Before and After Aging," *Materials Chemistry and Physics,* vol. 245, no. 122761, 15 April 2020.

[89] B. Wang, J. Yan, J. Liu, J. Zhao and L. Zhao, "Ni and Sb Improve the Microstructure, Mechanical Properties, and Solder Joint Reliability of Sn-3.0Ag-0.5Cu Alloy," *Vacuum,* vol. 231, no. 113782, January 2025.

[90] J. Yan, B. Wang, J. Zhao, L. Zhao, R. Guo and J. Sheng, "Improvement of Heat Aging Resistance and Tensile Strength of SAC305/Cu Solder Joints by Multi-Element Microalloying," *Intermetallics,* vol. 173, no. 108428, October 2024.

[91] M. Abueed, R. A. Athamneh, M. Tanash and S. Hamasha, "The Reliability of SAC305 Individual Solder Joints During Creep-Fatigue Conditions at Room Temperature," *Crystals,* vol. 12(9), no. 1306, 2022.

[92] R. A. Athamneh, D. B. Hani, H. Ali and S. Hamasha, "Reliability Modeling for Aged SAC305 Solder Joints Cycled in Accelerated Shear Fatigue Test," *Microelectronics Reliability,* vol. 104, no. 113507, 2020.

[93] R. A. Athamneh and S. Hamasha, "Fatigue Behavior of SAC-Bi and SAC305 Solder Joint With Aging," *IEEE Transactions on Components, Packaging and Manufacturing Technology,* vol. 10, no. 4, pp. 611-620, April 2020.

[94] T. Lentz, "How Does Surface Finish Affect Solder Paste Performance?," in *SMTA International 2018*, 2018.

[95] M. N. Collins, J. Punch and R. Coyle, "Surface Finish Effect on Reliability of SAC 305 Soldered Chip Resistors," *Soldering & Surface Mount Technology,* vol. 24, no. 4, pp. 240-248, 14 September 2012.

[96] A. Alakayleh, S. Hamasha and A. Alahmer, "The Impact of Paste Alloy, Paste Volume, and Surface Finish on Solder Joint," *Microelectronics Reliabililty,* vol. 160, no. 115457, September 2024.

[97] S. Su, "Reliability of Doped SnAgCu Solder Alloys with Various Surface Finishes Under Realistic Service Conditions," Ph.D. dissertation, Dept. Industrial and Systems Eng., Auburn Univ., Auburn, AL, USA, 2019.

[98] "List of Solder Alloys," [Online]. Available: senju.com/en/products/ecosolder/alloy_form/. [Accessed 3 March 2025].

[99] "SMIC Lead Free Solder Catalogue," Senju Metal Industry Co., Tokyo, Japan, 2020.

[100] "SMIC Lead-Free Solder Preforms Catalogue," Senju Metal Industry Co., Tokyo, Japan, 2020.

[101] "M58/M758/M731 - Solder Alloy Material with Excellent Thermal Fatigue Resistance," Senju Metal Industry Co., [Online]. Available: www.senju.com/en/products/ecosolder/alloy/alloy_tec.php. [Accessed 4 March 2025].

[102] *M758/M794.* [Art]. Senju Metal Industry Co., Accessed: March 4, 2025. Available: https://cn.senju.com/cn/products/ecosolder/alloy/alloy_tec.php.

[103] M. R. Lindeburg, Mechanical Engineering Reference Manual for the PE Exam, 11th ed., Belmont, CA: Professional Publications, Inc., 2001.

[104] "Understanding Weibull Analysis," PTC Inc., [Online]. Available: https://support.ptc.com/help/wrr/r12.0.2.0/en/index.html#page/wrr/PractitionersGuide/UnderstandingWeibullAnalysis.html. [Accessed 2 October 2025].

[105] "Chapter 3: Solder Joint Reliability Assessment," Virginia Tech, [Online]. Available: https://vtechworks.lib.vt.edu/server/api/core/bitstreams/94e13bf9-f58b-4782-b157-e99a9e063218/content. [Accessed 12 October 2025].

[106] "Who We Are," StenTech, 2025. [Online]. Available: https://www.stentech.com/company/who-we-are. [Accessed 10 March 2025].

# Appendices

# Appendix A:
# Stencil Design Documents

29X29

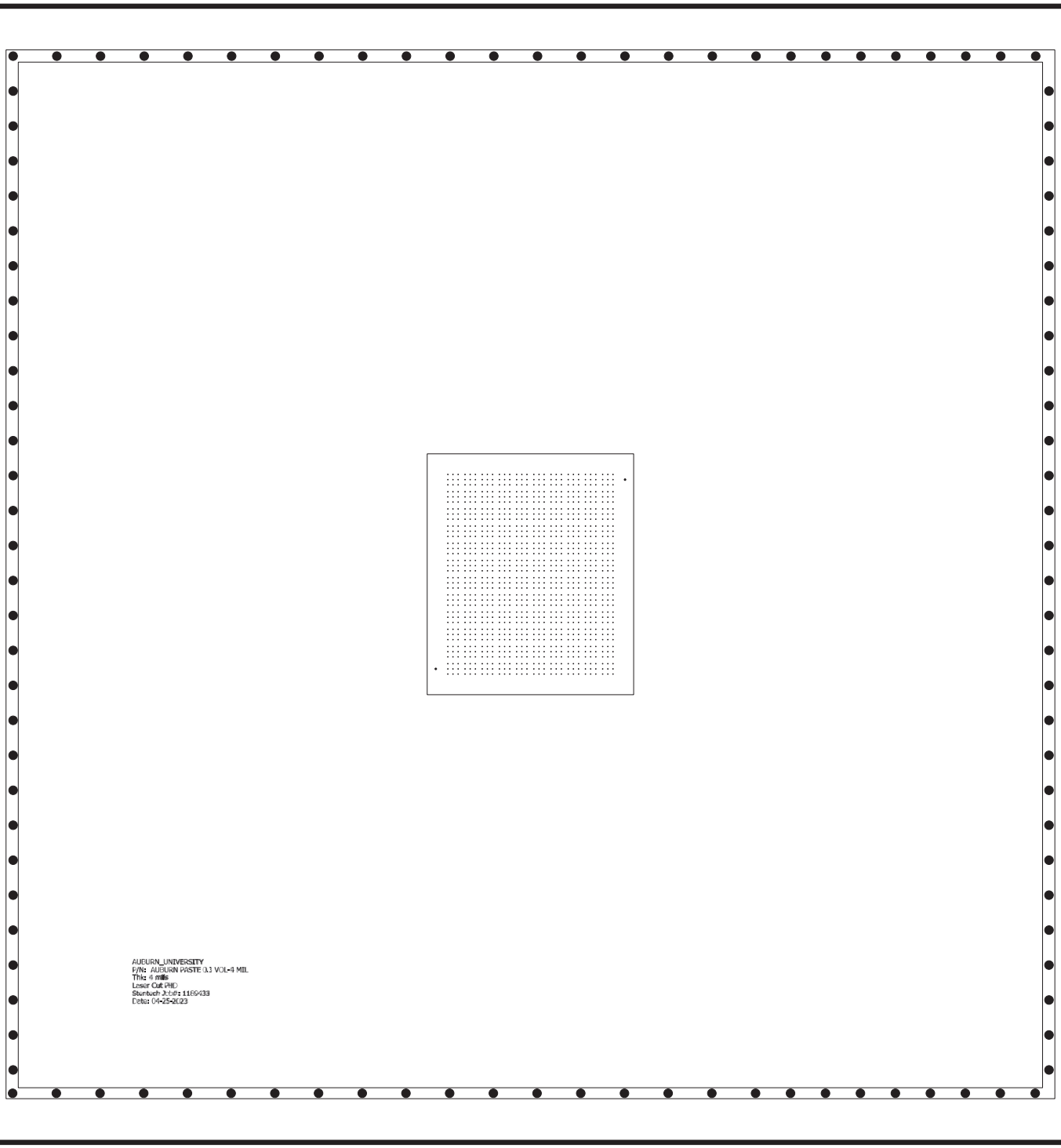


29X29

| | | | | | |
|---|---|---|---|---|---|
| STENTECH<br>EXPERTISE YOU CAN TRUST<br>WWW.STENTECH.COM<br>Job # 1189433 | CUSTOMER: AUBURN_UNIVERSITY | | ENGINEERED BY: VGER | REVIEWED BY: | |
| | P/N: AUBURN PASTE 0.1 VOL-4MILS | | LEAD FREE: No | # OF APERTURES: 1000 | |
| | FRAME: 29X29_TUDE | DATE: 04-25-2023 | MIN. AREA RATIO: 0.157 | # OF FIDUCIALS: 2 | D-CODE: 13 |
| | THICKNESS: 4 mils | MATERIAL: Stainless PHD | PASTE VOLUME: 0.000346 Cu In | MIN. APERTURE: 10.0x10.0 mils | MIN. PITCH: 110.1 mils |
| | PROCESS: Laser Cut | OFFSET: Centered | LIBRARY: AUBURN_UNIVERSITY | | |
| | COATING: None | | SHAPE SET: NO_EDITS | | |

29X29

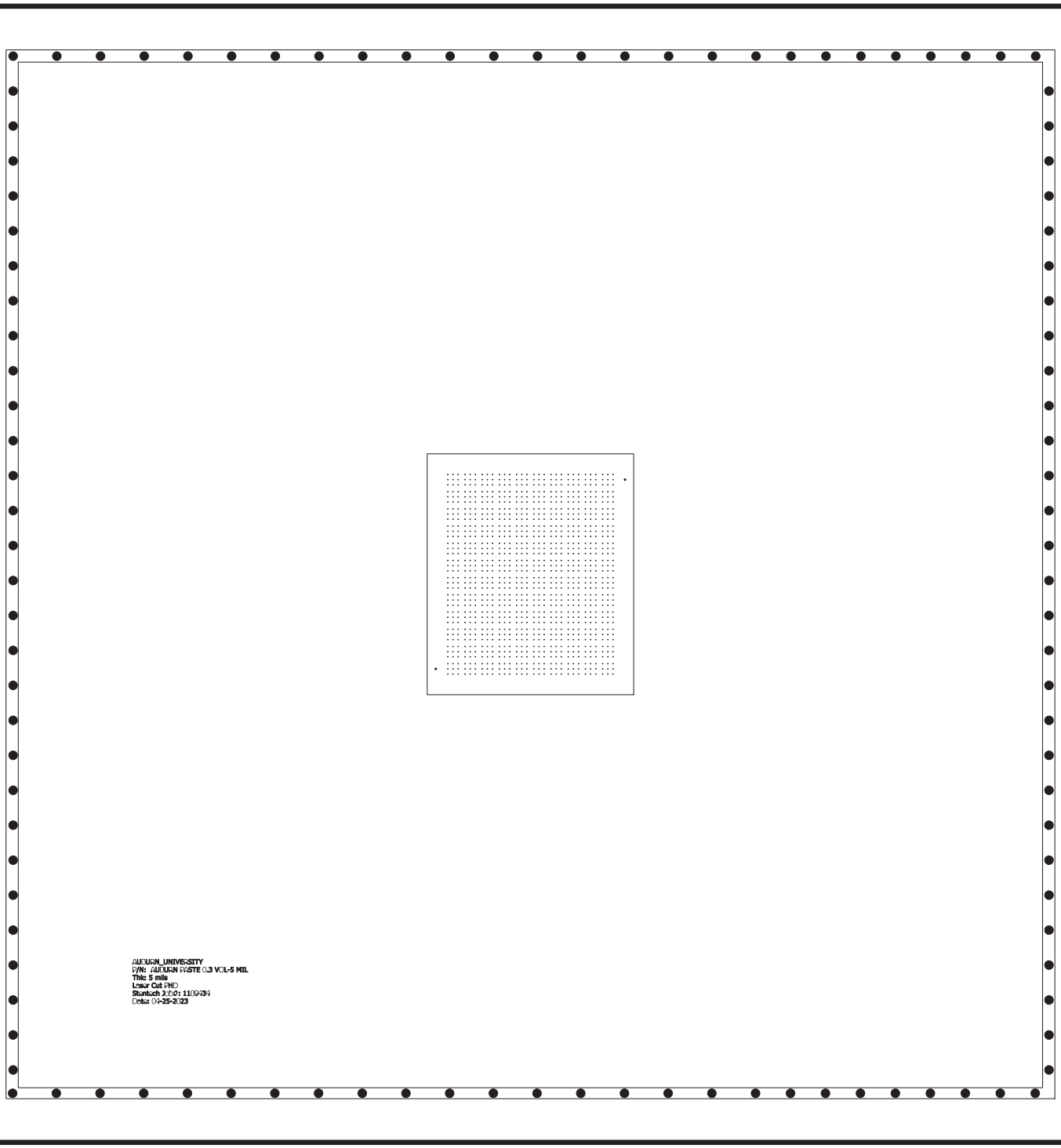


29X29

| | | | | | |
|---|---|---|---|---|---|
| STENTECH EXPERTISE YOU CAN TRUST WWW.STENTECH.COM Job # 1189434 | CUSTOMER: AUBURN_UNIVERSITY | | ENGINEERED BY: LNSM | REVIEWED BY: | |
| | P/N: AUBURN PASTE 0.3 VOL-5 MIL | | LEAD FREE: No | # OF APERTURES: 1000 | |
| | FRAME: 29X29_TUDE | DATE: 04-25-2023 | MIN. AREA RATIO: 0.765 | # OF FIDUCIALS: 2 | D-CODE: 13 |
| | THICKNESS: 5 mils | MATERIAL: Stainless PHD | PASTE VOLUME: 0.000993 Cu In | MIN. APERTURE: 15.3x15.3 mils | MIN. PITCH: 19.1 mils |
| | PROCESS: Laser Cut | OFFSET: Centered | LIBRARY: AUBURN_UNIVERSITY | | |
| | COATING: None | | SHAPE SET: NO_EDITS | | |

29X29

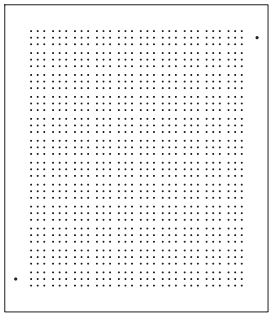

AUBURN_UNIVERSITY
P/N: AUBURN PASTE 0.5 VOL-5MILS
Thk: 5 mils
Stentech Job#: 1189435
TOP SIDE
LASER CUT PHD
Date: 04-25-2023

SQUEEGEE VIEW
PROCESS FLOW

29X29

| | | | | |
|---|---|---|---|---|
| STENTECH<br>EXPERTISE YOU CAN TRUST<br>WWW.STENTECH.COM<br>Job # 1189435 | CUSTOMER: AUBURN_UNIVERSITY | | ENGINEERED BY: VGER | REVIEWED BY: |
| | P/N: AUBURN PASTE 0.5 VOL-5MILS | | LEAD FREE: No | # OF APERTURES: 1000 |
| | FRAME: 29X29_TUDE | DATE: 04-25-2023 | MIN. AREA RATIO: 0.750 | # OF FIDUCIALS: 2 D-CODE: 13 |
| | THICKNESS: 5 mils | MATERIAL: Stainless PHD | PASTE VOLUME: 0.001648 Cu In | MIN. APERTURE: 10.0x10.0 mils MIN. PITCH: 11.1 mils |
| | PROCESS: Laser Cut | OFFSET: Centered | LIBRARY: AUBURN_UNIVERSITY | |
| | COATING: None | | SHAPE SET: NO_EDITS | |

**Appendix B**
**Temperature Data for Test Board Reflow Profile**

| SAC305 Reflow profile | | | | | |
|---|---|---|---|---|---|
| Time | Temp (°C) | Time | Temp (°C) | Time | Temp (°C) |
| 0:00:00 | 23 | 0:00:39 | 23 | 0:01:18 | 29 |
| 0:00:01 | 23 | 0:00:40 | 23 | 0:01:19 | 29 |
| 0:00:02 | 23 | 0:00:41 | 23 | 0:01:20 | 30 |
| 0:00:03 | 23 | 0:00:42 | 23 | 0:01:21 | 31 |
| 0:00:04 | 23 | 0:00:43 | 23 | 0:01:22 | 31 |
| 0:00:05 | 23 | 0:00:44 | 23 | 0:01:23 | 31 |
| 0:00:06 | 23 | 0:00:45 | 23 | 0:01:24 | 32 |
| 0:00:07 | 23 | 0:00:46 | 23 | 0:01:25 | 33 |
| 0:00:08 | 23 | 0:00:47 | 23 | 0:01:26 | 33 |
| 0:00:09 | 23 | 0:00:48 | 23 | 0:01:27 | 34 |
| 0:00:10 | 23 | 0:00:49 | 24 | 0:01:28 | 34 |
| 0:00:11 | 23 | 0:00:50 | 24 | 0:01:29 | 36 |
| 0:00:12 | 22 | 0:00:51 | 24 | 0:01:30 | 37 |
| 0:00:13 | 23 | 0:00:52 | 24 | 0:01:31 | 38 |
| 0:00:14 | 22 | 0:00:53 | 24 | 0:01:32 | 41 |
| 0:00:15 | 22 | 0:00:54 | 24 | 0:01:33 | 43 |
| 0:00:16 | 22 | 0:00:55 | 24 | 0:01:34 | 44 |
| 0:00:17 | 23 | 0:00:56 | 24 | 0:01:35 | 46 |
| 0:00:18 | 22 | 0:00:57 | 24 | 0:01:36 | 48 |
| 0:00:19 | 23 | 0:00:58 | 24 | 0:01:37 | 49 |
| 0:00:20 | 23 | 0:00:59 | 25 | 0:01:38 | 51 |
| 0:00:21 | 23 | 0:01:00 | 25 | 0:01:39 | 53 |
| 0:00:22 | 23 | 0:01:01 | 25 | 0:01:40 | 54 |
| 0:00:23 | 23 | 0:01:02 | 25 | 0:01:41 | 55 |
| 0:00:24 | 23 | 0:01:03 | 26 | 0:01:42 | 57 |
| 0:00:25 | 23 | 0:01:04 | 26 | 0:01:43 | 58 |
| 0:00:26 | 23 | 0:01:05 | 26 | 0:01:44 | 59 |
| 0:00:27 | 23 | 0:01:06 | 26 | 0:01:45 | 60 |
| 0:00:28 | 23 | 0:01:07 | 26 | 0:01:46 | 61 |
| 0:00:29 | 23 | 0:01:08 | 27 | 0:01:47 | 62 |
| 0:00:30 | 23 | 0:01:09 | 27 | 0:01:48 | 63 |
| 0:00:31 | 23 | 0:01:10 | 27 | 0:01:49 | 64 |
| 0:00:32 | 23 | 0:01:11 | 28 | 0:01:50 | 65 |
| 0:00:33 | 23 | 0:01:12 | 28 | 0:01:51 | 66 |
| 0:00:34 | 23 | 0:01:13 | 28 | 0:01:52 | 66 |
| 0:00:35 | 23 | 0:01:14 | 28 | 0:01:53 | 67 |
| 0:00:36 | 23 | 0:01:15 | 29 | 0:01:54 | 67 |
| 0:00:37 | 23 | 0:01:16 | 29 | 0:01:55 | 68 |
| 0:00:38 | 23 | 0:01:17 | 29 | 0:01:56 | 68 |

| SAC305 Reflow profile | | | | | |
|---|---|---|---|---|---|
| Time | Temp (°C) | Time | Temp (°C) | Time | Temp (°C) |
| 0:01:57 | 69 | 0:02:36 | 106 | 0:03:15 | 133 |
| 0:01:58 | 71 | 0:02:37 | 107 | 0:03:16 | 133 |
| 0:01:59 | 73 | 0:02:38 | 107 | 0:03:17 | 134 |
| 0:02:00 | 74 | 0:02:39 | 108 | 0:03:18 | 135 |
| 0:02:01 | 75 | 0:02:40 | 108 | 0:03:19 | 137 |
| 0:02:02 | 76 | 0:02:41 | 109 | 0:03:20 | 137 |
| 0:02:03 | 77 | 0:02:42 | 109 | 0:03:21 | 138 |
| 0:02:04 | 78 | 0:02:43 | 111 | 0:03:22 | 139 |
| 0:02:05 | 80 | 0:02:44 | 111 | 0:03:23 | 140 |
| 0:02:06 | 81 | 0:02:45 | 111 | 0:03:24 | 141 |
| 0:02:07 | 82 | 0:02:46 | 112 | 0:03:25 | 142 |
| 0:02:08 | 83 | 0:02:47 | 112 | 0:03:26 | 143 |
| 0:02:09 | 84 | 0:02:48 | 113 | 0:03:27 | 143 |
| 0:02:10 | 84 | 0:02:49 | 114 | 0:03:28 | 143 |
| 0:02:11 | 86 | 0:02:50 | 116 | 0:03:29 | 144 |
| 0:02:12 | 87 | 0:02:51 | 117 | 0:03:30 | 145 |
| 0:02:13 | 87 | 0:02:52 | 117 | 0:03:31 | 146 |
| 0:02:14 | 88 | 0:02:53 | 118 | 0:03:32 | 146 |
| 0:02:15 | 89 | 0:02:54 | 119 | 0:03:33 | 147 |
| 0:02:16 | 89 | 0:02:55 | 119 | 0:03:34 | 147 |
| 0:02:17 | 90 | 0:02:56 | 120 | 0:03:35 | 148 |
| 0:02:18 | 91 | 0:02:57 | 121 | 0:03:36 | 148 |
| 0:02:19 | 91 | 0:02:58 | 122 | 0:03:37 | 149 |
| 0:02:20 | 91 | 0:02:59 | 123 | 0:03:38 | 149 |
| 0:02:21 | 92 | 0:03:00 | 123 | 0:03:39 | 150 |
| 0:02:22 | 93 | 0:03:01 | 124 | 0:03:40 | 151 |
| 0:02:23 | 94 | 0:03:02 | 125 | 0:03:41 | 152 |
| 0:02:24 | 95 | 0:03:03 | 126 | 0:03:42 | 153 |
| 0:02:25 | 96 | 0:03:04 | 126 | 0:03:43 | 154 |
| 0:02:26 | 97 | 0:03:05 | 127 | 0:03:44 | 154 |
| 0:02:27 | 98 | 0:03:06 | 128 | 0:03:45 | 156 |
| 0:02:28 | 99 | 0:03:07 | 128 | 0:03:46 | 157 |
| 0:02:29 | 100 | 0:03:08 | 129 | 0:03:47 | 157 |
| 0:02:30 | 101 | 0:03:09 | 129 | 0:03:48 | 158 |
| 0:02:31 | 102 | 0:03:10 | 129 | 0:03:49 | 159 |
| 0:02:32 | 102 | 0:03:11 | 130 | 0:03:50 | 160 |
| 0:02:33 | 103 | 0:03:12 | 131 | 0:03:51 | 161 |
| 0:02:34 | 104 | 0:03:13 | 131 | 0:03:52 | 162 |
| 0:02:35 | 105 | 0:03:14 | 132 | 0:03:53 | 162 |

| SAC305 Reflow profile | | | | | |
|---|---|---|---|---|---|
| Time | Temp (°C) | Time | Temp (°C) | Time | Temp (°C) |
| 0:03:54 | 163 | 0:04:33 | 189 | 0:05:12 | 219 |
| 0:03:55 | 163 | 0:04:34 | 191 | 0:05:13 | 220 |
| 0:03:56 | 164 | 0:04:35 | 192 | 0:05:14 | 221 |
| 0:03:57 | 164 | 0:04:36 | 193 | 0:05:15 | 221 |
| 0:03:58 | 166 | 0:04:37 | 193 | 0:05:16 | 222 |
| 0:03:59 | 166 | 0:04:38 | 194 | 0:05:17 | 223 |
| 0:04:00 | 166 | 0:04:39 | 196 | 0:05:18 | 223 |
| 0:04:01 | 167 | 0:04:40 | 196 | 0:05:19 | 224 |
| 0:04:02 | 167 | 0:04:41 | 197 | 0:05:20 | 224 |
| 0:04:03 | 168 | 0:04:42 | 198 | 0:05:21 | 224 |
| 0:04:04 | 168 | 0:04:43 | 198 | 0:05:22 | 225 |
| 0:04:05 | 168 | 0:04:44 | 199 | 0:05:23 | 226 |
| 0:04:06 | 169 | 0:04:45 | 200 | 0:05:24 | 226 |
| 0:04:07 | 171 | 0:04:46 | 200 | 0:05:25 | 228 |
| 0:04:08 | 171 | 0:04:47 | 201 | 0:05:26 | 229 |
| 0:04:09 | 172 | 0:04:48 | 202 | 0:05:27 | 231 |
| 0:04:10 | 173 | 0:04:49 | 202 | 0:05:28 | 232 |
| 0:04:11 | 174 | 0:04:50 | 203 | 0:05:29 | 233 |
| 0:04:12 | 175 | 0:04:51 | 203 | 0:05:30 | 234 |
| 0:04:13 | 176 | 0:04:52 | 204 | 0:05:31 | 235 |
| 0:04:14 | 177 | 0:04:53 | 204 | 0:05:32 | 236 |
| 0:04:15 | 178 | 0:04:54 | 204 | 0:05:33 | 237 |
| 0:04:16 | 178 | 0:04:55 | 204 | 0:05:34 | 238 |
| 0:04:17 | 179 | 0:04:56 | 205 | 0:05:35 | 238 |
| 0:04:18 | 180 | 0:04:57 | 206 | 0:05:36 | 239 |
| 0:04:19 | 181 | 0:04:58 | 206 | 0:05:37 | 239 |
| 0:04:20 | 182 | 0:04:59 | 207 | 0:05:38 | 240 |
| 0:04:21 | 182 | 0:05:00 | 208 | 0:05:39 | 240 |
| 0:04:22 | 183 | 0:05:01 | 208 | 0:05:40 | 241 |
| 0:04:23 | 183 | 0:05:02 | 209 | 0:05:41 | 240 |
| 0:04:24 | 184 | 0:05:03 | 211 | 0:05:42 | 240 |
| 0:04:25 | 184 | 0:05:04 | 212 | 0:05:43 | 239 |
| 0:04:26 | 185 | 0:05:05 | 213 | 0:05:44 | 238 |
| 0:04:27 | 186 | 0:05:06 | 213 | 0:05:45 | 238 |
| 0:04:28 | 186 | 0:05:07 | 215 | 0:05:46 | 237 |
| 0:04:29 | 187 | 0:05:08 | 215 | 0:05:47 | 237 |
| 0:04:30 | 187 | 0:05:09 | 216 | 0:05:48 | 236 |
| 0:04:31 | 187 | 0:05:10 | 217 | 0:05:49 | 235 |
| 0:04:32 | 188 | 0:05:11 | 218 | 0:05:50 | 234 |

| SAC305 Reflow profile | | | | | |
|---|---|---|---|---|---|
| Time | Temp (°C) | Time | Temp (°C) | Time | Temp (°C) |
| 0:05:51 | 234 | 0:06:30 | 126 | 0:07:09 | 62 |
| 0:05:52 | 233 | 0:06:31 | 123 | 0:07:10 | 61 |
| 0:05:53 | 232 | 0:06:32 | 121 | 0:07:11 | 60 |
| 0:05:54 | 231 | 0:06:33 | 118 | 0:07:12 | 59 |
| 0:05:55 | 231 | 0:06:34 | 116 | 0:07:13 | 58 |
| 0:05:56 | 229 | 0:06:35 | 113 | 0:07:14 | 57 |
| 0:05:57 | 228 | 0:06:36 | 112 | 0:07:15 | 57 |
| 0:05:58 | 227 | 0:06:37 | 109 | 0:07:16 | 56 |
| 0:05:59 | 225 | 0:06:38 | 106 | 0:07:17 | 55 |
| 0:06:00 | 223 | 0:06:39 | 104 | 0:07:18 | 54 |
| 0:06:01 | 222 | 0:06:40 | 102 | 0:07:19 | 53 |
| 0:06:02 | 219 | 0:06:41 | 99 | 0:07:20 | 53 |
| 0:06:03 | 216 | 0:06:42 | 98 | 0:07:21 | 52 |
| 0:06:04 | 212 | 0:06:43 | 96 | 0:07:22 | 52 |
| 0:06:05 | 206 | 0:06:44 | 94 | 0:07:23 | 51 |
| 0:06:06 | 201 | 0:06:45 | 93 | 0:07:24 | 51 |
| 0:06:07 | 197 | 0:06:46 | 92 | 0:07:25 | 50 |
| 0:06:08 | 194 | 0:06:47 | 91 | 0:07:26 | 49 |
| 0:06:09 | 191 | 0:06:48 | 89 | 0:07:27 | 49 |
| 0:06:10 | 187 | 0:06:49 | 89 | 0:07:28 | 48 |
| 0:06:11 | 186 | 0:06:50 | 88 | 0:07:29 | 48 |
| 0:06:12 | 183 | 0:06:51 | 86 | 0:07:30 | 47 |
| 0:06:13 | 179 | 0:06:52 | 84 | 0:07:31 | 47 |
| 0:06:14 | 175 | 0:06:53 | 82 | 0:07:32 | 47 |
| 0:06:15 | 172 | 0:06:54 | 80 | 0:07:33 | 46 |
| 0:06:16 | 169 | 0:06:55 | 78 | 0:07:34 | 46 |
| 0:06:17 | 166 | 0:06:56 | 77 | 0:07:35 | 46 |
| 0:06:18 | 162 | 0:06:57 | 76 | 0:07:36 | 46 |
| 0:06:19 | 159 | 0:06:58 | 74 | 0:07:37 | 46 |
| 0:06:20 | 157 | 0:06:59 | 73 | 0:07:38 | 45 |
| 0:06:21 | 153 | 0:07:00 | 72 | 0:07:39 | 45 |
| 0:06:22 | 149 | 0:07:01 | 71 | 0:07:40 | 45 |
| 0:06:23 | 146 | 0:07:02 | 69 | 0:07:41 | 45 |
| 0:06:24 | 143 | 0:07:03 | 68 | 0:07:42 | 45 |
| 0:06:25 | 141 | 0:07:04 | 67 | 0:07:43 | 44 |
| 0:06:26 | 137 | 0:07:05 | 66 | 0:07:44 | 44 |
| 0:06:27 | 135 | 0:07:06 | 65 | 0:07:45 | 44 |
| 0:06:28 | 132 | 0:07:07 | 64 | 0:07:46 | 44 |
| 0:06:29 | 129 | 0:07:08 | 63 | 0:07:47 | 44 |

| SAC305 Reflow profile | | | | | |
|---|---|---|---|---|---|
| Time | Temp (°C) | Time | Temp (°C) | Time | Temp (°C) |
| 0:07:48 | 44 | 0:08:27 | 40 | 0:09:06 | 34 |
| 0:07:49 | 44 | 0:08:28 | 39 | 0:09:07 | 34 |
| 0:07:50 | 44 | 0:08:29 | 39 | 0:09:08 | 34 |
| 0:07:51 | 43 | 0:08:30 | 39 | 0:09:09 | 34 |
| 0:07:52 | 43 | 0:08:31 | 39 | 0:09:10 | 34 |
| 0:07:53 | 43 | 0:08:32 | 39 | 0:09:11 | 33 |
| 0:07:54 | 43 | 0:08:33 | 39 | 0:09:12 | 33 |
| 0:07:55 | 43 | 0:08:34 | 39 | 0:09:13 | 33 |
| 0:07:56 | 43 | 0:08:35 | 39 | 0:09:14 | 33 |
| 0:07:57 | 43 | 0:08:36 | 39 | 0:09:15 | 33 |
| 0:07:58 | 43 | 0:08:37 | 38 | 0:09:16 | 33 |
| 0:07:59 | 43 | 0:08:38 | 38 | 0:09:17 | 32 |
| 0:08:00 | 43 | 0:08:39 | 38 | 0:09:18 | 32 |
| 0:08:01 | 42 | 0:08:40 | 38 | 0:09:19 | 32 |
| 0:08:02 | 42 | 0:08:41 | 38 | 0:09:20 | 31 |
| 0:08:03 | 42 | 0:08:42 | 38 | 0:09:21 | 31 |
| 0:08:04 | 42 | 0:08:43 | 38 | 0:09:22 | 31 |
| 0:08:05 | 42 | 0:08:44 | 38 | 0:09:23 | 30 |
| 0:08:06 | 42 | 0:08:45 | 38 | 0:09:24 | 30 |
| 0:08:07 | 42 | 0:08:46 | 37 | 0:09:25 | 29 |
| 0:08:08 | 42 | 0:08:47 | 37 | 0:09:26 | 29 |
| 0:08:09 | 42 | 0:08:48 | 37 | 0:09:27 | 29 |
| 0:08:10 | 42 | 0:08:49 | 37 | 0:09:28 | 29 |
| 0:08:11 | 42 | 0:08:50 | 37 | 0:09:29 | 29 |
| 0:08:12 | 42 | 0:08:51 | 37 | 0:09:30 | 29 |
| 0:08:13 | 42 | 0:08:52 | 37 | 0:09:31 | 28 |
| 0:08:14 | 42 | 0:08:53 | 37 | 0:09:32 | 28 |
| 0:08:15 | 41 | 0:08:54 | 37 | | |
| 0:08:16 | 41 | 0:08:55 | 37 | | |
| 0:08:17 | 41 | 0:08:56 | 37 | | |
| 0:08:18 | 41 | 0:08:57 | 37 | | |
| 0:08:19 | 41 | 0:08:58 | 37 | | |
| 0:08:20 | 41 | 0:08:59 | 36 | | |
| 0:08:21 | 41 | 0:09:00 | 36 | | |
| 0:08:22 | 41 | 0:09:01 | 36 | | |
| 0:08:23 | 41 | 0:09:02 | 36 | | |
| 0:08:24 | 41 | 0:09:03 | 35 | | |
| 0:08:25 | 40 | 0:09:04 | 35 | | |
| 0:08:26 | 40 | 0:09:05 | 35 | | |